Vulnerability of U.S. Water Supply to Shortage

A Technical Document Supporting the Forest Service 2010 RPA Assessment

Romano Foti, Jorge A. Ramirez, and Thomas C. Brown

Foti, Romano; Ramirez, Jorge A.; Brown, Thomas C. 2012. **Vulnerability of U.S. water supply to shortage: a technical document supporting the Forest Service 2010 RPA Assessment**. Gen. Tech. Rep. RMRS-GTR-295. Fort Collins, CO: U.S. Department of Agriculture, Forest Service, Rocky Mountain Research Station. 147 p.

Abstract: Comparison of projected future water demand and supply across the conterminous United States indicates that, due to improving efficiency in water use, expected increases in population and economic activity do not by themselves pose a serious threat of large-scale water shortages. However, climate change can increase water demand and decrease water supply to the extent that, barring major adaptation efforts, substantial future water shortages are likely, especially in the larger Southwest. Because further global temperature increases are probably unavoidable, adaptation will be essential in the areas of greatest increase in projected probability of shortage.

Keywords: vulnerability, water supply, water demand, water yield, climate change

Authors

Romano Foti, Princeton University, New Jersey

Jorge A. Ramirez, Colorado State University, Fort Collins, Colorado

Thomas C. Brown, U.S. Department of Agriculture, Forest Service, Rocky Mountain Research Station, Fort Collins, Colorado

You may order additional copies of this publication by sending your mailing information in label form through one of the following media. Please specify the publication title and number.

Publishing Services

Telephone	(970) 498-1392
FAX	(970) 498-1122
E-mail	rschneider@fs.fed.us
Web site	http://www.fs.fed.us/rmrs
Mailing Address	Publications Distribution Rocky Mountain Research Station 240 West Prospect Road Fort Collins, CO 80526

Summary

The likelihood of future water shortages depends on how water supply compares with demands for water use. Comparison of supply and demand within a probabilistic framework yields an estimate of the probability of shortage and thus a measure of the vulnerability of the water supply system. This comparison was performed for current conditions and for several possible future conditions reflecting alternative socio-economic scenarios and climatic projections. Examining alternative futures provides a measure of the extent to which serious future risks of water shortage must be anticipated.

Water supply was quantified by first estimating freshwater input as precipitation minus evapotranspiration for each point in a grid covering the study area. These water inputs were then allocated to major river basins and made available to meet basic in-stream flow requirements, satisfy off-stream demands including those from downstream basins or those reached by trans-basin diversions, and add to reservoir storage. Off-stream demands were estimated as threshold quantities of desired water use based on extending past trends in water use under the assumption that water supply would be no more constraining to future water withdrawals than in the recent past. Modeling water supply and demand in this way does not provide a forecast of future shortage levels. Rather, it provides a projection of the degree to which water shortages would occur in the absence of adaptation measures to either increase supply or decrease demand.

On a per capita basis, aggregate water withdrawal in the United States has been dropping since at least 1985. This reduction has occurred largely because of changes in the irrigation, thermoelectric, and industrial water use sectors. In the West, agricultural acreage has been decreasing and water withdrawal efficiency has been improving. Water withdrawal per kilowatt hour produced at thermoelectric plants has been steadily dropping as production has moved to more water-efficient plant types. And industrial water use has been dropping as industrial capacity has moved overseas and water recycling has become more common at remaining plants.

Despite the reductions in per-capita water withdrawal, total U.S. withdrawal rose from 1985 to 2000, largely in response to population growth of roughly 2.7 million persons per year. However, the most recent data show a drop in total withdrawals, attributable to large reductions in irrigation and industrial withdrawals plus a slowing of the increase in domestic and public withdrawals.

In the absence of future climate change, per-capita withdrawals are projected to continue dropping and total water withdrawals are projected to drop for several decades and then rise moderately. However, future climate change will increase water use for agricultural irrigation and landscape maintenance in response to rising plant water requirements, and at thermoelectric plants to accommodate rising electricity demands for space cooling. Including these effects, per-capita withdrawals are projected to drop only moderately for the next few decades and then level off as the effects of climate change become greater, and total withdrawals are projected to rise nearly continuously into the future. Projected withdrawals differ across the global emissions scenarios examined, especially in the latter decades of the century.

Although precipitation is projected to increase in much of the United States with future climate change, in most locations that additional precipitation will merely accommodate rising evapotranspiration demand in response to temperature increases. Where the effect of rising evapotranspiration exceeds the effect of increasing precipitation, and where precipitation actually declines, as is likely in parts of the Southwest, water yields are projected to decline. For the United States as a whole, the declines are substantial, exceeding 30% of current levels by 2080 for some scenarios examined.

Vulnerability was defined as the probability of shortage, that is, of off-stream demand exceeding supply. Demand and supply were modeled on an annual basis for 98 river basins covering the coterminous United States called Assessment Sub-Regions (ASRs). Current levels of inter-ASR diversion were accounted for, as were existing reservoir storage capacity and basic in-stream flow needs. Only renewable sources of supply were considered; thus, lowering of groundwater tables was not considered a source of supply.

Only a few ASRs currently show a probability of shortage above 0.1. However, the probabilities tend to rise in the future and are projected to reach 1.0 in some ASRs. Vulnerability is greatest in arid and semiarid areas of the U.S.—including the Southwest, parts of California, and the central and southern Great Plains—where current conditions are already precarious. In some cases, important reservoirs are left with little or no water. Although the detailed results differ depending on which scenario is simulated and which climate model is used, the general finding of increasing and substantial vulnerability in the larger Southwest holds true in all cases. Of course, even in ASRs with no annual vulnerability, shortages may occur in sub-ASR (e.g., upstream) locations or during certain seasons.

The gradually increasing future vulnerability results from the effect of increasing population on water demand, and of climate change on both water supply and water demand. In about one-half of the ASRs where vulnerability is projected to increase, decreases in water yield, and thus in water supply, have a greater effect on vulnerability than do increases in water demand, whereas in the other ASRs the reverse is true.

The projected levels of vulnerability in some ASRs are clearly untenable, indicating that adaptation will be essential. Adaptation options that are likely to be considered include groundwater mining (while supplies last), reductions in in-stream flows, water transfers, water conservation beyond the levels assumed here, alterations of reservoir operating rules and other water management agreements, population shifts, and, in selected locations, increases in water storage and diversion capacity.

Contents

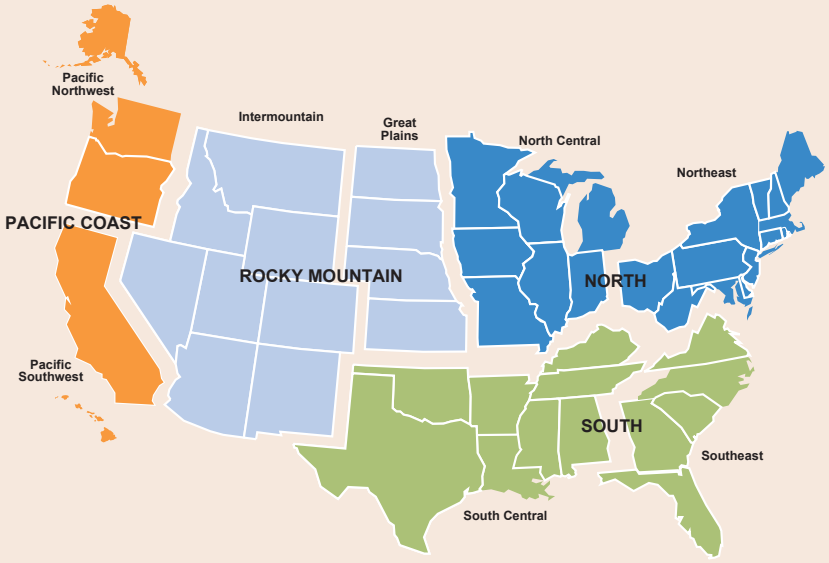

Chapter 1: Introduction

Off-stream water use in the United States increased over 10-fold during the Twentieth Century in response to tremendous population and economic growth (Brown 2000). Although water use efficiency has improved in the last few decades as a result of technological advances, environmental controls, and increasing scarcity, rising population and incomes are both putting enhanced pressure on water supplies and increasing calls to protect stream water quality and maintain habitat for endangered aquatic species (Gillilan and Brown 1997). Complicating the picture, climatic change is increasing hydrologic uncertainty. Taken together, these forces are making careful water management ever more important. A realistic broad-scale understanding of the vulnerability of the United States water supply system to shortage should be a component of any attempt to define the magnitude of the threat and is essential in determining appropriate mitigation and adaptation measures.

This study is one of several assessments, commonly known as the Resources Planning Act (RPA) assessments, performed every ten years pursuant to the Renewable Resources Planning Act of 1974 (public law 93-378) (U.S. Department of Agriculture, Forest Service 2012). Many different aspects of water resources could have been covered in this assessment, but available resources require us to focus on a subset. For this iteration of the assessment, we concentrate on water quantity rather than water quality and on renewable water sources, thereby ignoring groundwater mining. Further, given the time-step of our analysis, we do not address flooding. Although limited, this assessment of prospective shortages of renewable water sources nevertheless requires a comprehensive look at water supply and water demand across the United States.

1.1 Vulnerability

The vulnerability of a system is a function of its ability to respond to (i.e., cope with, adapt to) inherently variable stressors. In this study, given the uncertainty characterizing both the stressors and the capacity to withstand them, we quantify vulnerability within a probabilistic framework. In particular, we estimate vulnerability as the probability that a critical system threshold, itself a function of both the capacity and the stressors of the system, will be crossed (Kochendorfer and Ramirez 1996). In the context of the United States water supply system, that threshold is reached when water demand exceeds supply.

Vulnerability was assessed on an annual basis for three different possible scenarios of future socioeconomic and climatic conditions, with the climatic conditions of each scenario projected by three different global climate models, providing nine different sets of future conditions and related estimates of vulnerability. The nine different sets of future conditions are called alternative “futures” herein.

In assessing vulnerability, we are not attempting to show how water allocation will actually change in response to population growth and climate change. Rather, we aim to show where and to what extent water shortages would occur if populations grew and the

climate changed as expected but water allocation infrastructure, laws, and established trends in water use rates did not change. The results indicate where adaptation to changing circumstances will be most essential.[1]

1.2 Spatial Scale of Analysis

We estimate water yield on a fine-scale grid, but supply and demand and thus the vulnerability of water supply to shortage are necessarily estimated by river basin. Supply and demand are estimated for each of 98 basins, called Assessment Sub-regions (ASRs), which together make up the 18 Water Resource Regions (WRRs) of the 48 contiguous states of the United States. The analysis is restricted to the contiguous states because climatic data needed to downscale global climate model (GCM) predictions of climate variables were not available for Alaska and Hawaii. WRRs were defined by the Water Resources Council (1968) in its First National Water Assessment and are now widely used in reporting about large-scale water issues (Table 1.1, Figure 1.1). ASRs were originally delineated by the Water Resources Council (1978) for its Second National Water Assessment. Estimates for ASRs can be aggregated to obtain estimates for the WRRs (Table 1.2, Figure 1.1).

WRRs are large enough to reveal underlying water use trends that might be difficult to discern for smaller areas that may be overly sensitive to data inaccuracies or unusual localized perturbations but are too large for most water resource planning exercises, especially those seeking to compare demand and supply. ASRs allow analysis of some large regional differences within WRRs, yet are generally large enough to support the use of county-level data important in analyzing water demand. ASRs are tracked with a four-digit code (Table 1.2) and are either the same as or aggregations of the standard four-digit basins.[2]

Table 1.1. Water resource regions (WRRs).

WRR		Area ($km^2/10^3$)	Outlows to
1	New England	166	Atlantic Ocean and Canada
2	Mid-Atlantic	291	Atlantic Ocean
3	South Atlantic-Gulf	716	Atlantic Ocean
4	Great Lakes	452	Great Lakes
5	Ohio	422	WRR 8
6	Tennessee	106	WRR 5
7	Upper Mississippi	492	WRR 8
8	Lower Mississippi	272	Gulf of Mexico
9	Souris-Red-Rainy	154	Canada
10	Missouri	1323	WRR 7
11	Arkansas-White-Red	642	WRR 8
12	Texas-Gulf	471	Gulf of Mexico
13	Rio Grande	343	Gulf of Mexico
14	Upper Colorado	294	WRR 14
15	Lower Colorado	363	Gulf of California
16	Great Basin	367	Closed basin
17	Pacific Northwest	718	Pacific Ocean
18	California	417	Pacific Ocean

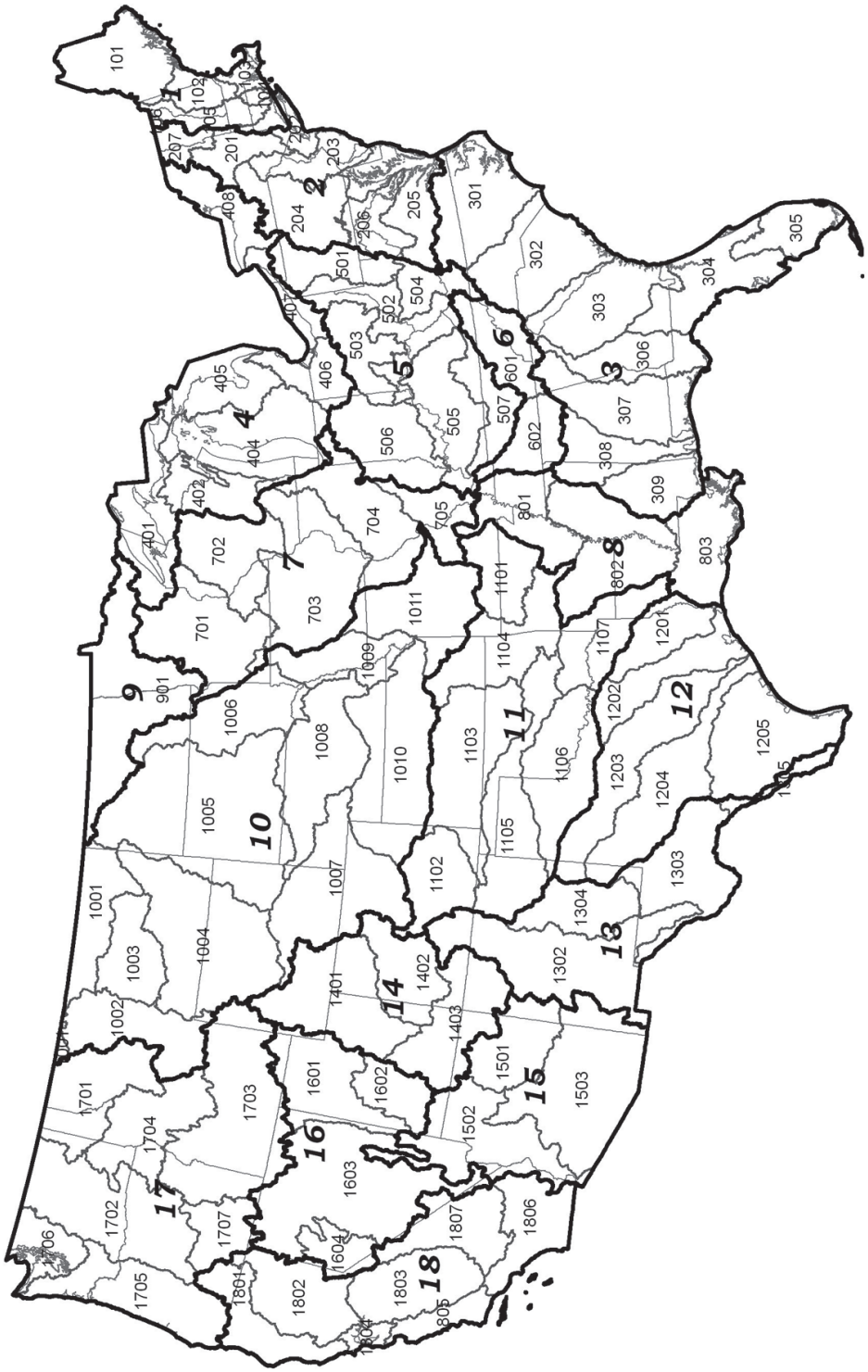

Figure 1.1. WRRs and ASRs.

Table 1.2. Assessment sub-regions (ASRs).

ASR	WRC name	Area (km^2)	Outlows to
101	Northern Maine	79,380	Atlantic Ocean
102	Saco-Merrimack	23,755	Atlantic Ocean
103	Massachusetts-Rhode Island Coastal	11,105	Atlantic Ocean
104	Housatonic-Thames	11,699	Atlantic Ocean
105	Connecticut River	28,913	Atlantic Ocean
106	St. Francois	1,522	Canada
201	Upper Hudson	32,937	202
202	Lower Hudson-Long Island-North NJ	12,696	Atlantic Ocean
203	Delaware	38,258	Atlantic Ocean
204	Susquehanna	71,208	Chesapeake Bay, Atlantic Ocean
205	Upper and Lower Chesapeake	60,453	Chesapeake Bay, Atlantic Ocean
206	Potomac	36,751	Chesapeake Bay, Atlantic Ocean
207	Richelieu	19,824	Canada
301	Roanoke-Cape Fear	98,446	Atlantic Ocean
302	Pee Dee-Edisto	108,293	Atlantic Ocean
303	Savannah-St. Marys	94,520	Atlantic Ocean
304	St. Johns-Suwannee	84,875	Atlantic Ocean, Gulf of Mexico
305	Southern Florida	42,599	Atlantic Ocean, Gulf of Mexico
306	Apalachicola	61,606	Gulf of Mexico
307	Alabama-Choctawhatchee	95,927	Gulf of Mexico
308	Mobile - Tombigbee	55,719	Gulf of Mexico
309	Pascagoula Pearl	51,395	Gulf of Mexico
401	Lake Superior	43,902	Lake Superior
402	Northwestern Lake Michigan	48,394	Lake Michigan
404	Eastern & Southwestern Lake Michigan	68,099	Lake Michigan
405	Lake Huron	42,136	Lake Huron
406	St. Clair-Western Lake Eire	40,821	Lake Eire
407	Eastern Lake Erie	15,620	Lake Eire
408	Lake Ontario	46,319	Lake Ontario
501	Ohio Headwaters	49,385	502
502	Upper Ohio-Big Sandy	73,154	505
503	Muskingum-Skioto-Miami	51,614	501
504	Kanawha	31,692	501
505	Kentucky-Licking-Green-Ohio	84,163	801
506	Wabash	85,340	505
507	Cumberland	46,429	505
601	Upper Tennessee	58,141	602
602	Lower Tennessee	47,731	505
701	Mississippi Headwaters	115,964	702
702	Black Root-Chippewa-Wisconsin	83,452	703
703	Rock-Mississippi-Des Moines	147,431	704
704	Salt-Sny-Illinois	100,684	705
705	Lower Upper Mississippi	44,160	801
801	Hatchie-Mississippi-St. Francis	72,315	802
802	Yazoo-Mississippi-Ouachita	121,744	803
803	Mississippi Delta	67,949	Gulf of Mexico
901	Souris-Red-Rainy	153,942	Canada
1001	Missouri-Milk-Saskatchewan	68,295	1005
1002	Missouri-Marias	87,786	1003
1003	Missouri-Musselshell	60,762	1001

(continued)

Table 1.2. (Continued)

ASR	WRC name	Area (km^2)	Outlows to
1004	Yellowstone	181,533	1005
1005	Western Dakotas	255,602	1006
1006	Eastern Dakotas	92,199	1009
1007	North and South Platte	143,214	1008
1008	Niobrara-Platte-Loup	115,182	1009
1009	Middle Missouri	59,396	1011
1010	Kansas	155,718	1011
1011	Lower Missouri	103,566	705
1101	Upper White	57,877	801
1102	Upper Arkansas	64,596	1103
1103	Arkansas-Cimmaron	128,070	1104
1104	Lower Arkansas	94,846	801
1105	Canadian	122,607	1104
1106	Red - Washita	102,504	1107
1107	Red-Sulphur	71,641	802
1201	Sabine-Neches	51,292	Gulf of Mexico
1202	Trinity-Galvaston Bay	65,548	Gulf of Mexico
1203	Brazos	118,229	Gulf of Mexico
1204	Colorado (Texas)	114,232	Gulf of Mexico
1205	Neches-Texas Coastal	115,387	Gulf of Mexico
1302	Upper & Middle Rio Grande	164,443	1303
1303	Rio Grande - Pecos	101,479	1305
1304	Upper Pecos	61,166	1303
1305	Lower Rio Grande	16,179	Gulf of Mexico
1401	Green-White-Yampa	126,004	1403
1402	Colorado-Gunnison	67,969	1403
1403	Colorado-San Juan	99,938	1502
1501	Little Colorado	70,090	1502
1502	Lower Colorado Mainstem	122,863	Mexico
1503	Gila	169,794	1502
1601	Bear-Great Salt Lake	94,157	Closed
1602	Sevier Lake	42,285	Closed
1603	Humboldt-Tonopah Desert	197,830	Closed
1604	Central Lahontan	32,872	Closed
1701	Clark Fork-Kootenai	94,001	1702
1702	Upper / Middle Columbia	151,062	1705
1703	Upper / Central Snake	188,705	1704
1704	Lower Snake	90,727	1702
1705	Coast-Lower Columbia	104,524	Pacific Ocean
1706	Puget Sound	36,782	Pacific Ocean
1707	Oregon closed basin	45,088	Closed
1801	Klamath-Northern Coastal	64,799	Pacific Ocean
1802	Sacramento-Lahontan	83,980	San Francisco Bay
1803	San Joaquin-Tulare	83,208	San Francisco Bay
1804	San Francisco Bay	10,546	Pacific Ocean
1805	Central California Coastal	29,680	Pacific Ocean
1806	Southern California Coastal	70,287	Pacific Ocean
1807	Lahontan-South	73,283	Closed

1.3 Temporal Scale of Analysis

The Renewable Resources Planning Act specifies that the decennial assessments will project demand and supply 50 years into the future, which in this case would be to 2060. However, because the potential effects of climate change on water supply and demand become more significant in the latter half of the century (Solomon and others 2009), we extend this assessment beyond 2060.

Water yield was estimated for each year through 2090 based on annual estimates of key hydrologic drivers, principally temperature and precipitation. Water demand to 2090 was estimated at five-year intervals in accordance with the U.S. Geological Survey (USGS) schedule for estimating water withdrawal; interpolation was then used to provide annual estimates of demand. Simulations of annual water allocation over the period 1953-2090 allowed computation of estimates of vulnerability for five 20-year time periods: the current period is represented by the average across years 1986-2005, and the future is represented by four periods centered at years 2020, 2040, 2060, and 2080.

1.4 Water Supply and Demand

Water is a mobile resource. It can be used to meet local demands, moved to satisfy needs elsewhere, or stored for future use. It follows that the amount of water available at a certain time and location is not simply the water naturally available at that location. Rather, the water supply of a river basin depends on a complex network of natural and artificial water conveyances, reservoirs, environmental requirements, and consumptive use demands.

Water supply, the amount of water available to meet consumptive use demands, in an ASR was quantified on an annual basis as water yield plus inflow from upstream, subjected to the effect of management via reservoir storage, in-stream flow requirements, and trans-basin diversions.[3] The components of supply were estimated as follows:

- Assuming that natural water storage (the sum of natural surface and subsurface storage) does not change annually, water yield of a basin is the sum of annual surface and groundwater runoff. Water yield was estimated for each 5x5 km cell in the United States as the difference between precipitation and actual evapotranspiration. Water yield estimates were then summed across cells within a basin.

- Reservoir storage capacity was determined at the ASR level by aggregating storage capacities of natural and man-made impoundments.

- In-stream flow requirements, which refer to the flows required to ensure minimum flows for ecosystems, recreation, hydropower, etc., were determined for each ASR as a fraction of its average annual inflow.

- Trans-ASR diversions, which represent water diverted from one ASR to another as the result of legal agreements between the jurisdictions involved, were computed by analyzing available data on inter-basin diversions and aggregating the results by ASR.

Water demand, equal to desired consumptive use, was determined for each ASR as a threshold amount of water use based on historical records of water withdrawals and consumptive use proportions and on projections of water use drivers and rates of withdrawal per unit of a driver. Estimation of future demands involves both deterministic and stochastic (climate dependent) components. Note that "demand" as used here does not refer to an economic demand function but rather simply to the quantity of water that would be used if water use drivers and withdrawal rates were to occur as projected. This approach is in keeping with our objective of determining when and where changes in water demand (and supply) will be necessary.

1.5 Water Allocation and Routing

Water basins, such as ASRs, can be connected to each other by both natural and artificial links. Natural links are determined by the river network, which routes water downstream. Artificial links rely on canals, pipelines, and other built conveyances that move water across basin boundaries contrary to the natural flow path. When both types of links are considered, the United States is found to consist of three main networks of ASRs containing in total 83 ASRs. Most of the remaining 15 ASRs are found along the coasts and discharge directly to the oceans.

Water allocation within each network was simulated using a water routing model that relies on specified priorities that determine the order in which different water uses are satisfied. The probability of a water shortage in each ASR is thus determined within each network by following the specified priorities—in light of reservoir storage capacities, in-stream flow requirements, and other conditions or constraints—in an attempt to satisfy water demands given the available water supply.

Chapter 2: Future Climatic and Socio-economic Projections

2.1 Overview

Estimating future vulnerability of U.S. water supply to shortage requires projections of water supply and demand. Climate directly affects both supply and demand. In addition, population and economic conditions directly affect demand. Because future climate, population, and economic conditions are uncertain and may take a variety of paths, we project supply and demand for alternative scenarios of future conditions. Further, climatic conditions under each scenario are projected using three different global climate models. The resulting set of nine different possible futures provides a range of estimates of demand and supply, and therefore of vulnerability. The mixture of results offers a rough indication of the uncertainty about future conditions.

2.2 Future Socio-Economic Scenarios

The increasing globalization of the world economy and the possibility of substantial climatic change have created considerable uncertainty about future U.S. water supply and demand. One way to capture this uncertainty, adopted by the Intergovernmental Panel on Climate Change (IPCC), is to examine various possible future scenarios. As a starting point for the RPA assessments, three scenarios—A1B, A2, and B2—each based on a different storyline, were chosen from the IPCC set (Nakicenovic and others 2000).

The IPCC scenarios are internally consistent possible global futures that differ in many ways having to do with fertility rate, technological change, international trade, income growth, and energy development. Most importantly for this and the other RPA assessments, the scenarios specify alternative future population and income levels, with implications for climatic variables that can be modeled using GCMs and spatial downscaling methods. The scenarios thus capture a range of potential futures that may substantially affect future water supply and demand in the United States.

Of the three scenarios, the A2 scenario is the most extreme and the B2 scenario is the least extreme in terms of resulting atmospheric CO_2 concentration. For example, year 2100 CO_2 concentrations are 856 ppm with the A2 scenario and 621 ppm for the B2 scenario, with the A1B scenario falling roughly midway between these extremes at 717 ppm (Table 2.1). However, it is important to note that the CO_2 concentrations of these scenarios do not differ greatly until later in the Twenty-First Century. The CO_2 concentrations of the A2 and A1B scenarios are very similar in 2060 (572 and 580 ppm, respectively), although the B2 concentration begins diverging from the other two in about 2020 (and is 504 ppm in 2060). One must extend the purview of the study beyond 2060 to observe the greatest differences in the scenarios and their impacts.

Table 2.1. Atmospheric CO_2 concentrations and global mean temperature changes of the IPCC scenarios.

	A1B-AIM		A2-ASF		B2-MESSAGE	
	CO_2 [a]	ΔT [b]	CO_2	ΔT	CO2	ΔT
1970	325		325		325	
1980	337		337		337	
1990	353		353		353	
2000	369	0.2	369	0.2	369	0.2
2010	391	0.5	390	0.4	388	na
2020	420	0.7	417	0.7	408	na
2030	454	1.0	451	0.9	429	na
2040	491	1.4	490	1.2	453	na
2050	532	1.7	532	1.5	478	na
2060	572	2.0	580	1.9	504	na
2070	611	2.2	635	2.3	531	na
2080	649	2.4	698	2.8	559	na
2090	685	2.6	771	3.2	589	na
2100	717	2.8	856	3.6	621	2.4

[a] In ppm. Source: http://www.ipcc-data.org/ddc_co2.html, reference model runs.
[b] Multi-model °C change from 1980-1999 mean. Source: http://www.ipcc.ch/pdf/assesment-report/ar4/syr/ar4_syr_spm.pdf. Decadal changes were not listed for the B2 scenario.

As with CO_2 concentration, global temperature differences among the scenarios are relatively small until the latter half of the Twenty-First Century. The multi-model projected global average surface warming projected by 2060 (relative to 1980-1999) are about 2 °C for the A1B scenario and 1.9 °C for the A2 scenario (a 2060 estimate for the B2 scenario was not available) (Table 2.1). However, by 2100 the surface warmings of the B2, A1B, and A2 scenarios are projected to be 2.4 °C, 2.8 °C, and 3.6 °C, respectively.

The population and economic projections of the IPCC scenarios do not use the most recent U.S. Census or economic data, and thus are somewhat dated. The IPCC projections were updated for the 2010 RPA assessments based on more recent information for the U.S. (USDA Forest Service 2012) (Table 2.2). The population projections for the RPA assessment A1B scenario incorporate the 2000 census and presume a continuation of past levels of growth in U.S. population, and the A2 and B2 scenario populations were determined in relation to the revised A1B scenario by maintaining the relative population differences among the original IPCC scenarios. Scenario A2 expects a higher population growth rate than the A1B scenario, and the B2 scenario expects a lower growth rate (Figure 2.1). Scenario A1B expects much higher economic growth in the United States than do the other two scenarios (Figure 2.2). Further details about the projections of population and income are found in Chapter 5.

Table 2.2. Scenarios of future conditions in the United States.

	A1B	A2	B2
Population growth	Medium	High	Low
Economic growth	High	Low-medium	Low
Temperature increase	Medium	High	Low

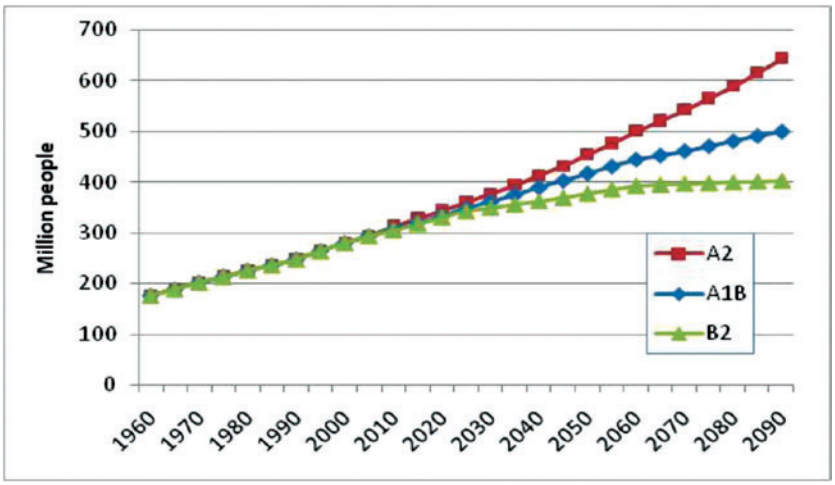

Figure 2.1. Past and projected U.S. population.

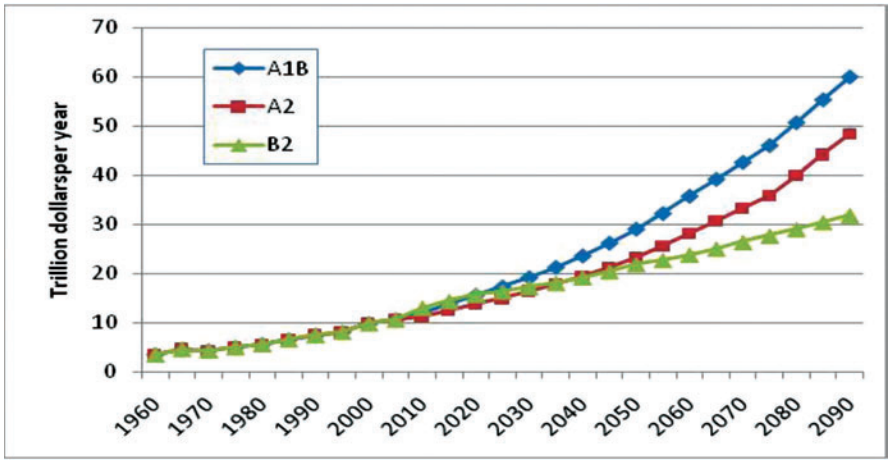

Figure 2.2. Past and projected total annual personal income of the United States, in 2006 dollars.

2.3 Future Climate: Global Climate Models

The A1B and A2 scenarios were used in combination with the following GCMs:

- Canadian Centre for Climate Modeling and Analysis Coupled Global Climate Model, Version 3.1, Medium Resolution (hereafter CGCM);
- Australian Commonwealth Scientific and Industrial Research Organization Mark 3.5 Climate System Model (hereafter CSIRO); and
- Japanese Centre for Climate System Research Model for Interdisciplinary Research on Climate, Version 3.2, Medium Resolution (hereafter MIROC).

The B2 scenario was used in combination with three other climate models:

- Canadian Centre model CGCM2 (hereafter also CGCM),
- Australian Commonwealth model CSIRO-Mk2 (hereafter also CSIRO), and
- United Kingdom Met Office Hadley climate model (HADN) (Table 2.3). See Joyce and others (2011) for details.

Table 2.3. Alternative futures (scenario-GCM combinations).

A1B	A2	B2
CGCM31 MR	CGCM31 MR	CGCM2 MR
CSIROMK35	CSIROMK35	CSIROMK2 filtered
MIROC32 MR	MIROC32 MR	HADCM3

Monthly estimates of precipitation and temperature were available from all GCMs for the period 2001-2100 at the 5 arc minute grid level for the United States (Joyce and others 2011, in press). The specific variables were precipitation in millimeters and mean daily minimum and maximum air temperatures in degrees Celsius.

The use of these distinct and well-established GCMs ensured that the downscaled scenarios met the IPCC criteria for selecting scenarios for climate change impact studies, including: (1) consistency of regional scenarios with global projections; (2) physical congruence across climate variables; and (3) applicability to impact assessment, which is facilitated by the downscaled data being reported as change factors that can be referenced to locally observed climate data.

2.3.1 Downscaling and Bias Removal

The spatial resolution of GCM output is too large to support most river basin studies, and thus the GCM results needed to be downscaled for use with the ASRs. Further, GCM output commonly contains a bias, which is recognized by comparing the GCM estimates for a past period with field-based measurements for the same period. Downscaling and bias correction of the GCM data occurred in two steps. The first step, performed by Joyce and others (in press), involved downscaling the raw GCM simulations from their original spatial resolutions to the 5 arc minute scale (roughly a 10-km grid) and adjusting for bias using 30 years of historical data. The second step, performed by the authors of this report, consisted of further downscaling the data to match the 5-km grid resolution of this study for water yield estimation and removing residual bias using data for eight recent years.

The first step began with converting the monthly values from the GCM datasets to monthly change factors (also called deltas) using the means of the simulated monthly values for the 30-year period 1961-1990 as the baseline. In the case of temperature variables (monthly mean daily minimum and maximum air temperature), the change factors were computed as the arithmetic difference between the monthly value and the corresponding 30-year mean (1961-1990) of the same temperature variable for that month. For monthly precipitation, the change factor was the ratio of the GCM-based monthly value to the 1961-1990 mean for that month.

The change factors were then interpolated using the ANUSPLIN software (McKenney and others 2006; Price and others 2006) to create time series for the period over which the GCM simulations were carried out, extending to 2100. ANUSPLIN produced a fitted spline "surface" equation for each monthly variable, which was then used to downscale the change factor of that monthly variable to the 10-km grid scale. Finally, the bias was removed by superimposing the downscaled change factor onto the historical average for that variable with the historical estimates taken from the PRISM (Parameter-elevation Regressions on Independent Slopes) dataset (Daly and others 1994).

For temperature (T), for example, the downscaling and bias correction procedure was as follows, where Y indicates a year from 2001 to 2090, j indicates month, G indicates GCM estimates, H indicates historical data, and Δ signifies the delta:

- Compute deltas at GCM scale: $\Delta T_{G,Y,j} = T_{G,Y,j} - T_{G,1961-90,j}$
- Use the ANUSPLIN model to downscale the deltas to 10-km grid
- Compute final values at 10-km scale: $T'_{G,Y,j} = T_{H,1961-90,j} + \Delta T_{G,Y,j}$

For more detail, see Joyce and others (2011).

In the second step, the 10-km data were further downscaled, using simple spatial interpolation, to match our 5x5 km water yield grid. Then, the data were further adjusted using the most recent observations of T and P available from PRISM for years 2001-2008. The adjustment (δ) was computed as the difference between the 2001-2008 averages predicted by the GCMs and the observed averages from the PRISM data. For example, we calculated temperature as follows:

- Compute difference: $\delta T_{G,j} = T_{G,2001-08,j} - T_{H,2001-08,j}$
- Remove difference: $T''_{G,Y,j} = T'_{G,Y,j} - \delta T_{G,j}$

This adjustment had a significant impact on potential evapotranspiration computed from the estimates of T.[4]

As mentioned, only temperature and precipitation were downscaled from GCM output (Joyce and others 2011, in press). The lack of net radiation, wind speed, and vapor pressure data precluded application of the widely used Penman method for computing potential evapotranspiration. Thus, potential evapotranspiration, in mm per day, was computed from the downscaled and bias-adjusted estimates using a modification of Penman's equation by Linacre (1977):

$$ETp = \left[500\left(T'+0.006\,h\right)/\left(100-A\right)+15\left(T'-Td\right)\right]/\left(80-T'\right) \quad (2.1)$$

where *T', h*, *Td*, and *A* represent, respectively, monthly mean temperature in degrees Celsius, elevation in meters, mean monthly dew point temperature in degrees Celsius, and latitude in degrees. Because dew point temperature was not available in the downscaled GCM data, Linacre's suggested approximation of *T'−Td* is used:

$$T' - Td = 0.0023h + 0.37T' + 0.53R + 0.35Rann - 10.9\ ^{\circ}\mathrm{C} \quad (2.2)$$

where *Rann* is mean temperature of the hottest month minus mean temperature of the coldest month, and *R* is mean daily range in temperature. For past years, dew point temperature was available from the PRISM dataset. Note that relying solely on temperature data could result in an overestimate of potential evapotranspiration, at least in some areas, thereby producing overestimates of water demand and underestimates of water yield, and thus overestimates of projected shortages. This possibility should be investigated in future research.

2.3.2 Future Precipitation

Average annual precipitation in the United States is projected to change from 77 cm in 2005 to from 63 to 80 cm in 2060 (Figure 2.3). The 2005 point in Figure 2.3 represents a mean for the period 2001-2010, and the other four points are 20-year means centered at those years. Aggregate precipitation changes little over time for most futures (Figure 2.3).

Looking at aggregate U.S. precipitation masks regional differences. For example, with the A1B-CGCM future, mean precipitation is projected to consistently increase in most of the Northeast and Texas and decrease in the West (Figure C1). Besides this large-scale behavior, however, coherent patterns of changes in precipitation with the A1B-CGCM future are not easily identifiable.

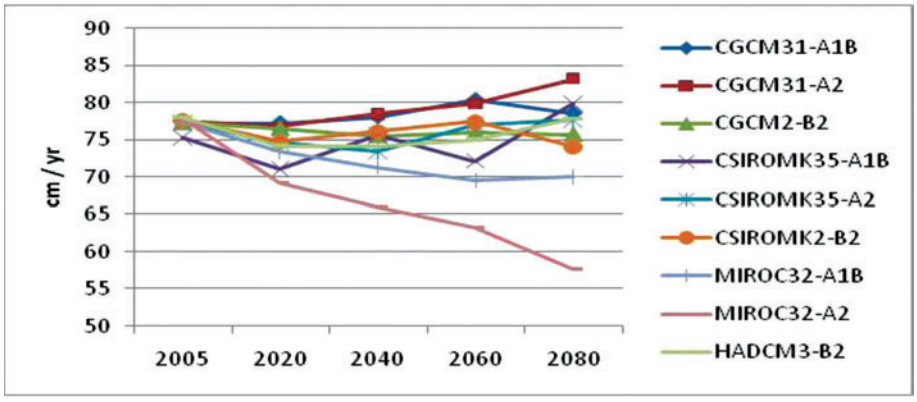

Figure 2.3. Nine projections of mean annual U.S. precipitation.

The variation in precipitation found among alternative futures at the aggregate scale (Figure 2.3) is also apparent at the ASR scale, as is seen by comparing the maps shown in Figures C1-C9 (Appendix C). Although all futures show precipitation increasing in the Northeast, there is little agreement elsewhere. Some consistent trends, however, are identifiable for specific futures, as seen in the following examples: for A2-CGCM, an increase is projected in the North and decrease is projected in the South; for B2-CGCM, a decrease is projected in the Central United States and in the Southwest; for CSIRO, a decrease is projected in the Southeast for the A1B scenario and in the Southeast and Northeast for the A2 and B2 scenarios; and for MIROC, a large decrease is projected in the Southeast, and decreases are projected everywhere else except in the Northeast. In a few cases, precipitation is not expected to monotonically increase (or decrease) throughout the century, but rather alternate from periods of increase to periods of decrease. This is expected to happen in the southern East Coast for A1B-CGCM, in the central Great Plains for A2-GCMC, in the southern Great Plains for A1B-CSIRO, and in Texas and eastern California for B2-HADN. For more on future precipitation, see Figures C1-C9 (Appendix C), Joyce and others (2011, in press).

2.3.3 Future Potential Evapotranspiration

Future potential evapotranspiration is tied to temperature, which is projected to rise in all nine futures. Average (the midpoint between minimum and maximum temperature) annual temperature is projected to rise from 11.8 °C in 2005 to from 13.5 to 15.0 °C in 2060 depending on the future (Figure 2.4). Annual average potential evapotranspiration, therefore, is projected to rise as well from 3.5 mm/d in 2005 to from 4.0 to 4.6 mm/d in 2060 (Figure 2.5).

Spatial distributions of potential evapotranspiration changes for the nine futures are presented in Figures C10-C18 (Appendix C). Instances of projected decrease are limited to scattered areas and isolated periods, the most evident of which is the East Coast and eastern Great Plains for B2-CGCM in 2020.

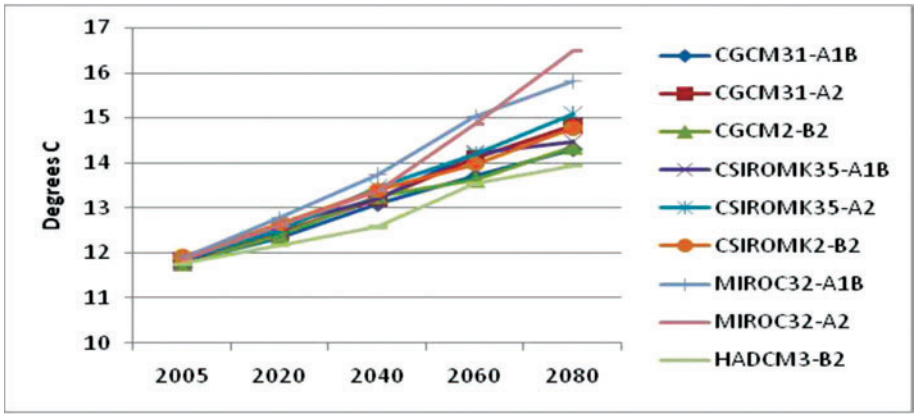

Figure 2.4. Nine projections of mean annual U.S. temperature.

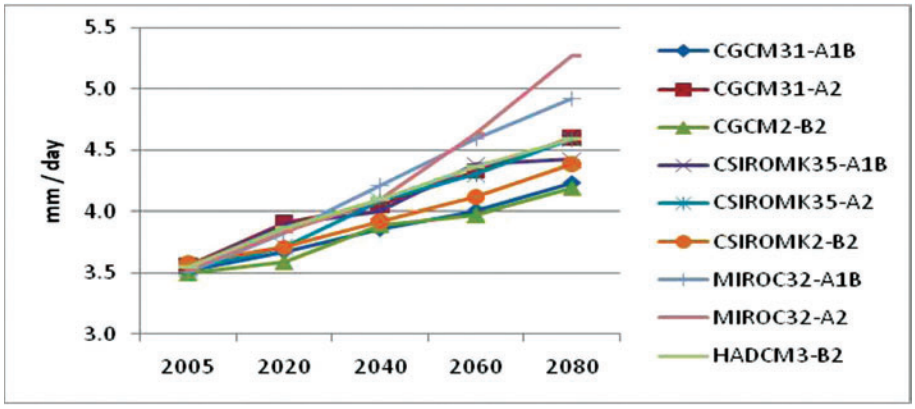

Figure 2.5. Nine projections of mean annual potential U.S. evapotranspiration.

The projections from the MIROC model are the most extreme, with increases in average U.S. potential evapotranspiration that exceed 30% by 2060. The MIROC and CSIRO models project large increases in the Southeast, especially for the A2 scenario. Changes projected by the CGCM model are less dramatic than those of the other two models; increases of 15.8%, 25.9%, and 14.1% are projected for the A1B, A2, and B2 scenarios, respectively, by 2060. However, for the Colorado River Basin, the CGCM model projects increases in potential evapotranspiration of 21.1%, 25.1%, and 18.3%, respectively.

Chapter 3: Water Yield

3.1 Overview

Water supply begins with water yield. To estimate water yield, we adopted a water balance model proposed by Eagleson (1978a). Eagleson's model is a mechanistic representation of the water dynamics occurring across the soil-atmosphere interface as a result of a stochastic climatic input. Input to the model includes soil hydraulic properties and characteristics of rainfall events, with climate represented by the probability distributions functions (PDFs) of precipitation and potential evapotranspiration. The model generates PDFs of water fluxes (actual evapotranspiration, surface runoff, and groundwater runoff) as output.

The water balance model was calibrated using historical streamflow records (for years 1953-2005) and then applied to all locations in the United States under current and potential future climatic conditions, providing estimates for future years 2006-2090. Since the model is a lumped representation of the annual water balance, we subdivided the U.S. territory into a study grid (of 5x5 km cells) and estimated water fluxes in each cell.

In the following sections, we describe the water balance model, the area of analysis and parameters of the model, the model calibration procedure, model input for future climatic and socio-economic scenarios, and the resulting water yield projections.

3.2 Problem Formulation

Eagleson's model is a one-dimensional representation of soil moisture dynamics as forced by a stochastic climate (Eagleson 1978a-g). The model describes the relationships between annual amounts of precipitation, runoff, infiltration, and evapotranspiration as a function of volumetric soil moisture and soil and vegetation characteristics. The description is physically based and only accounts for processes operating in the vertical direction, across the soil-atmosphere interface.

The water balance equation for the control volume (Figure 3.1) is as follows:

$$\int_0^t \left\{ i(t) - e_T(t) - \frac{\partial}{\partial t}\left[V_{ss}(t) - V_{sg}(t) \right] \right\} \cdot dt = \int_0^t \left[r_s(t) + r_g(t) \right] \cdot dt \qquad (3.1)$$

where $i(t)$, $e_T(t)$, $V_{ss}(t)$, $V_{sg}(t)$, $r_s(t)$, and $r_g(t)$, are, respectively, storm intensity, the evapotranspiration rate, volume of water storage on the surface, volume of water storage below the surface, surface runoff rate, and the groundwater runoff rate. Snow, ice, and movements of soil moisture as vapor are not considered.

Integration of equation 3.1 is very complex for several reasons: (1) climatic forcing (i.e., precipitation and potential evapotranspiration) is stochastic, (2) all terms in the equation depend on the soil moisture content, which is difficult to evaluate or measure; and (3) integration requires that carryover storage be evaluated. In order to obtain an analytical solution to the water balance equation, it is assumed that the system is in equilibrium with the climate at its mean value. This implies that the long-term mean amount of moisture storage (above

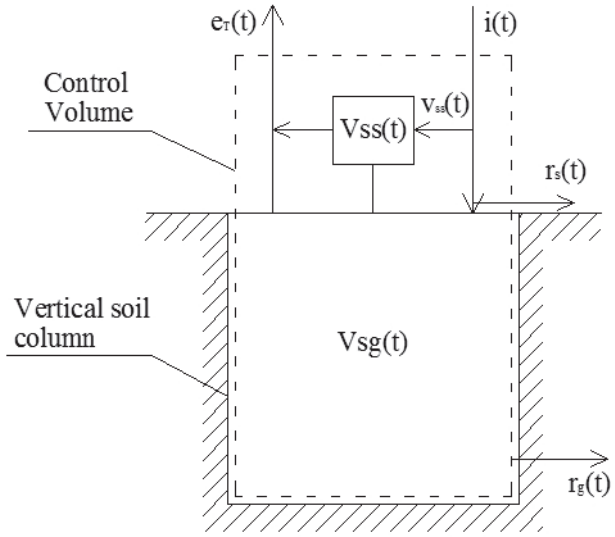

Figure 3.1. Control volume, input, and output fluxes relative to Eagleson annual water balance model.

and below the surface) is constant, thereby avoiding the need to compute carryover storage.[5] Taking the expectation of equation 3.1 under the assumption that the system is in equilibrium with the climate leads to:

$$E\left[P_A\right] - E\left[E_{T_A}\right] = E\left[R_{s_A}\right] + E\left[R_{g_A}\right] \tag{3.2}$$

where $E[P_A]$, $E[E_{T_A}]$, $E[R_{s_A}]$, and $E[R_{g_A}]$, are, respectively, the expected annual precipitation, the expected annual actual evapotranspiration, the expected annual surface runoff, and the expected annual groundwater runoff. Because of the equilibrium assumption, the terms for the changes in surface and groundwater storage do not appear in equation 3.2.

Each of the water balance terms in equation 3.2 is a function of soil moisture, the characteristics of the stochastic precipitation input, the rate of potential evapotranspiration, the physical properties of the soil (e.g., porosity, intrinsic permeability, pore disconnectedness), and the properties of the vegetation (transpiration potential and fractional vegetation cover).

3.2.1 Model Structure and Assumptions

The physical system is represented as a dynamic soil moisture process with stochastic precipitation and potential evapotranspiration inputs. Output is a set of annual values of the other components of the water balance.

The arriving precipitation events are assumed to occur as Poisson-distributed rectangular pulses (Figure 3.2). This simplification enables representation of the precipitation process with a few easily treatable parameters. Storm intensity and storm duration are assumed to be independent and exponentially distributed, while storm depth is assumed to be gamma distributed.

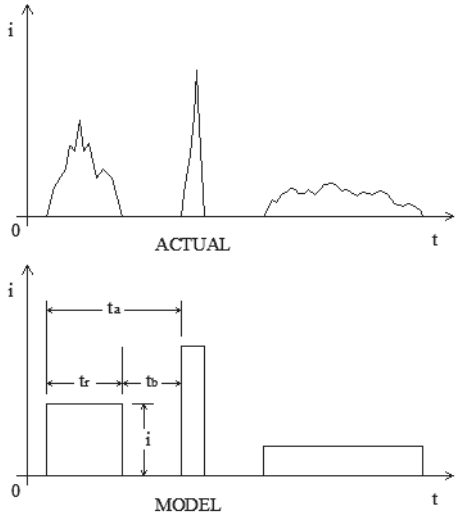

Figure 3.2. Comparison between the actual behavior of rainfall and the one modeled for this analysis. The x-axis reports time, and the y-axis reports rain intensity. The parameters t_a, t_r, and t_b represent, respectively, the inter-arrival time, storm duration, and time between two storms.

The soil is assumed to be homogeneous and characterized by a vegetative coverage operating in equilibrium with its environment in an unstressed state. Soil moisture dynamics are captured through a simplified version of the concentration-dependent diffusion equation (Phillip 1969), while the soil properties are based on the Brooks-Corey model (Brooks and Corey 1966).

The solution of the water balance equation in the form equation 3.2 or an equivalent formulation implies knowledge of all the relevant water fluxes. As mentioned before, water fluxes can be expressed as analytical functions of soil moisture content, here defined as the relative soil saturation and a small number of climate, vegetation, and soil parameters. Relative soil saturation is given as:

$$s = \frac{\theta_t - \theta_r}{n_t - \theta_r} \tag{3.3}$$

where θ_t, θ_r, and n_t are, respectively, the total volumetric water content of the soil, the residual volumetric soil water content, and the soil porosity.

Under the assumption of a stationary system, the solution of equation 3.2 is obtained under the constraint of uniform soil moisture content in a semi-infinite soil column. To solve the balance equation, Eagleson (1978a-g) proposed using a single value of the soil moisture concentration, s_0, that can be defined as a "temporal mean of the spatial average" (Figure 3.3).

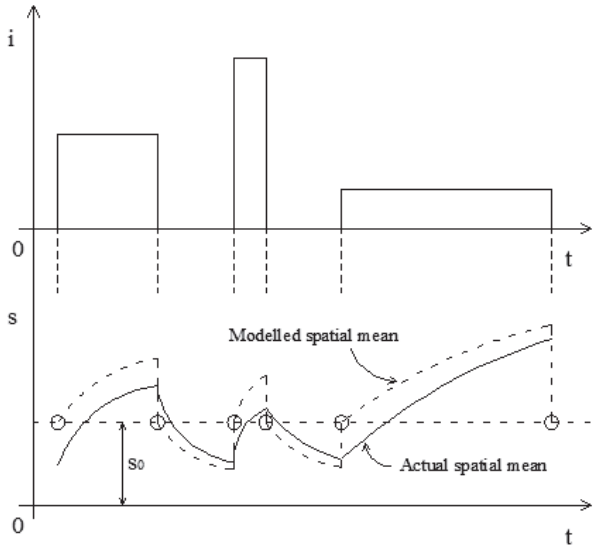

Figure 3.3. Spatial mean of soil moisture content. Comparison between the actual behavior of the soil moisture concentration and the simplified model adopted in the analysis.

With soil and climate parameters fixed for the given control volume, the water balance equation is essentially a function of the following two unknowns: the average soil moisture content, s_0, and the vegetation fractional coverage, M. However, for each set of soil and climate parameters, there is more than a unique set of s_0 and M that satisfies equation 3.2 and closes the water balance. In this framework, we further assume that vegetation operates, in the long term, under conditions of minimum stress. As suggested by Eagleson (1978g), this implies that equation 3.2 will be solved for the set of s_0 and M under which soil moisture content is maximized.

3.3 Area of Analysis and Data

The United States was subdivided into a 5x5 km grid and mapped using the Clarke 1866 Albers projection, producing a study grid of 630 rows and 994 columns. The water balance model requires the input of soil, precipitation, and vegetation properties for each cell of the study grid, as well as the climatic forcing PDFs (Table 3.1).

The following subsections describe the collected soil and climatic datasets and the adaptation of the available datasets to the study grid.

3.3.1 Soil Hydraulic Parameters

The VEMAP soil dataset (Kittel and others 1995, 1996) was used as the preferred source of parameters for describing soil hydraulic characteristics. The dataset contains 18 parameters for the 0-50 cm and the 50-150 cm soil layers, including bulk density and texture (i.e., percentages of sand, silt, and clay).

Table 3.1. Parameter and inputs of the water balance model.

Soil hydraulic parameters	
n	Total porosity
m	Pore size distribution index
$\Psi(1)$	Saturated matric potential
$K(1)$	Saturated hydraulic conductivity
c	Pore disconnectedness index
d	Diffusivity index
h_0	Surface retention capacity
Precipitation parameters (long-term storm statistics)	
t_r	Mean storm duration
t_b	Mean time between storms
t_a	Mean inter-arrival time
m_i	Mean storm intensity
m_h	Mean storm depth
m_n	Mean number of storms per year
m_{Pa}	Mean annual precipitation
τ	Mean rainy season duration
k	Parameter of the gamma distribution of storm depth
Vegetation parameters	
k_v	Plant transpiration efficiency
Climatic input (forcing of the water balance)	
Joint PDF of annual precipitation and annual potential evapotranspiration	

Using the standard assumption that mineral density is 2.65 g/cm^3, bulk density, ρ, from the VEMAP data was converted to total porosity as follows:

$$n = 1 - \frac{\rho}{2.65} \tag{3.4}$$

Pore size distribution, m, residual water content, ξ, and saturated matric potential, $\Psi(1)$, were estimated using multiple linear regression relating them to the percentages of clay, silt, and sand based on the 11 USDA textural classes (Kochendorfer 2005). Regression results are listed in Table 3.2.

Table 3.2. Results of multivariate linear regression of Brooks and Corey parameters (Abu Rizaiza 1991; Kochendorfer 2005).

		Coefficients		
Parameter	**Intercept**	**%Sand**	**%Clay**	**R^2**
ξ	-0.0295	0.00076	0.00201	0.831
$\Psi(1)$	14.6	-0.09340	0.45400	0.893
m	0.202	0.00329	-0.00318	0.868

Hydraulic conductivity was estimated following the equation derived by Brutsaert (1967):

$$K(1) = a \cdot \left(\frac{n - \xi}{\psi(1)} \right)^2 \cdot \frac{m^2}{(m+1) \cdot (m+2)} \tag{3.5}$$

where the coefficient a equals 35 cm^3/s (Kochendorfer 2005).

The pore disconnectedness index, c, and the diffusivity index, d, were evaluated as follows:

$$c = \frac{(2+3m)}{m} \tag{3.6}$$

$$d = c - \frac{1}{m} - 1 \tag{3.7}$$

The VEMAP data are provided on a 0.5x0.5 degree grid covering the United States. That grid contains 115 columns and 48 rows, whereas our study grid contains 994 columns and 630 rows. In order to extend the results obtained at the VEMAP database resolution to our study grid, the following two-step procedure was used: (1) each cell of our grid falling at the center point of a VEMAP cell was assigned the values of that VEMAP cell; (2) remaining cells were filled by weighting the nine nearest cells of the VEMAP database according to their inverse distance squared.

3.3.2 Long-Term Storm Statistics

Long-term means of hourly storm statistics, characterizing the Poisson arrival precipitation model, were estimated for stations available in the National Climatic Data Center (NCDC) hourly dataset (available at www.ncdc.noaa.gov/oa/climate/climatedata.html). Estimates for the stations were then extended to the United States at the 5x5-km spatial resolution.

A total of 5264 hourly data gages were available from the NCDC dataset. The NCDC gages, however, are spatially and temporally heterogeneous—more numerous in densely populated regions of the United States and more scarce in desert and mountain areas (Figure 3.4). Record length was also extremely variable, ranging from 1 to 53 years (Figure 3.5).

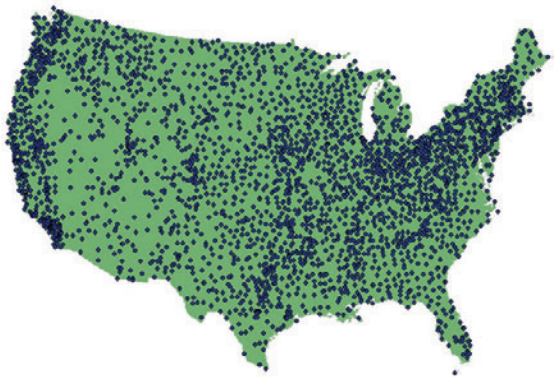

Figure 3.4. Spatial distribution of NCDC stations providing hourly datasets of precipitation.

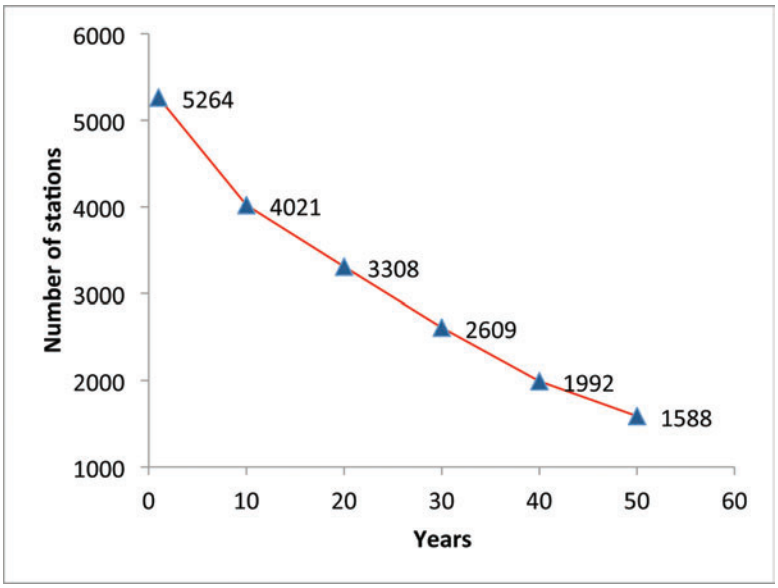

Figure 3.5. Number of NCDC stations providing hourly data of precipitation as a function of record length.

Furthermore, many of the NCDC stations have large amounts of missing or unreliable data (the latter being records that, according to the NCDC, did not pass an extreme value threshold test). Because we evaluated the storm statistics by analyzing the sequences of storms as they occurred in time, a large amount of missing data could not be tolerated because they alter dramatically the shape of such sequence, potentially leading to large errors.

Of the 5264 stations available, 2088 were eventually selected for further use. We included only those stations with at least 30 years of hourly precipitation records with no more than 25% of the data missing. No correction was performed on the extreme values, principally because of the lack of specific information on which to base a correction.

Using the complete record of each included station, the following long-term storm statistics were evaluated: mean storm duration, t_r; mean time between storms, t_b; mean storm inter-arrival time, t_a; mean storm intensity, m_i; mean storm depth, m_h; mean number of storms per year, m_n; mean annual precipitation, m_{Pa}; mean rainy season duration, τ; and the parameter of the gamma distribution of storm depth, k.

In agreement with Eagleson's model (Eagleson 1978a, 1978b), storm sequences are treated as a series of rectangular pulses. Thus, the total precipitation of a given event was obtained by summing hourly precipitation amounts over the duration of the event. Rainfall intensity was computed as the total precipitation during an event divided by the event's duration.

Characterizing storms as rectangular pulses allows precipitation to be represented, in statistical terms, by a few easily measurable parameters. Each single storm and inter-storm period may be completely described by the time of arrival of the storm, the storm intensity, the

inter-storm time, and the storm duration. In this approach, storm intensity and duration are assumed to be independent and exponentially distributed (Eagleson 1978b), whereas the sequence of storms is assumed to be Poisson-distributed.

If storm events are extracted from the precipitation records under the assumption that a single hour with no precipitation is sufficient to separate events, the resulting sequence of events typically is not Poisson-distributed. The lack of a Poisson distribution indicates that some raw storms are not really independent of each other, suggesting that the time period being used to separate discrete rain events is too short and some contiguous rain periods should be considered as part of the same rainy event rather than as independent events.

To address this issue, the raw sequences of precipitation data were processed following the procedure outlined by Restrepo-Posada and Eagleson (1982). This procedure requires determining the minimum rainless time span between two rain events that needs to elapse for the events to be considered as separate storms. To this aim, each raw sequence of rain events was subjected to the condition of being first-order Poissonian, that is, to have the mean of inter-arrival time equal to its standard deviation. The procedure uses the ratio of the standard deviation to the mean (that is, the coefficient of variation) of storm event inter-arrival time as the criterion for determining when a first-order Poisson distribution is achieved. The coefficient of variation is computed first from the original precipitation sequence, where a single rainless hour is used to separate rainfall events. If the resulting coefficient of variation is greater than 1, the minimum rainless time span between storms is increased to two hours, such that events separated by only a rainless period of one hour are merged together. The process continues, increasing the time between storms by one hour each iteration, until the coefficient of variation of the resulting sequence is as close as possible to 1. The final sequence of storms is then used to evaluate all of the long-term storm statistics for the given station.

3.3.2.1 Spatial extension of storm statistics

To extend the station storm statistics to the full 5x5 km grid of the United States, we used a regionalization procedure that relies on regressing storm statistics on total precipitation. Ordinary kriging and simple inverse distance methods were not considered because they do not take into account factors that may deeply influence storm statistics, such as elevation or total precipitation. Grid cells containing a selected NCDC station were assigned the storm statistics (storm depth, duration, inter-arrival time, time between storms, etc.) of that station. For each cell without a station, separately for each storm statistic, the statistic was regressed on average precipitation, with the cases for the regression being the stations falling within a circular region of 100-km radius centered at the cell. The regressions were then used to estimate the values of the storm statistics of the cells (Figure 3.6). Weighted linear regression was used, with the weights being proportional to the square of the inverse of the distance between the station and the cell of interest. The values of total precipitation at the station points were taken from the PRISM dataset (Daly and others 1994).

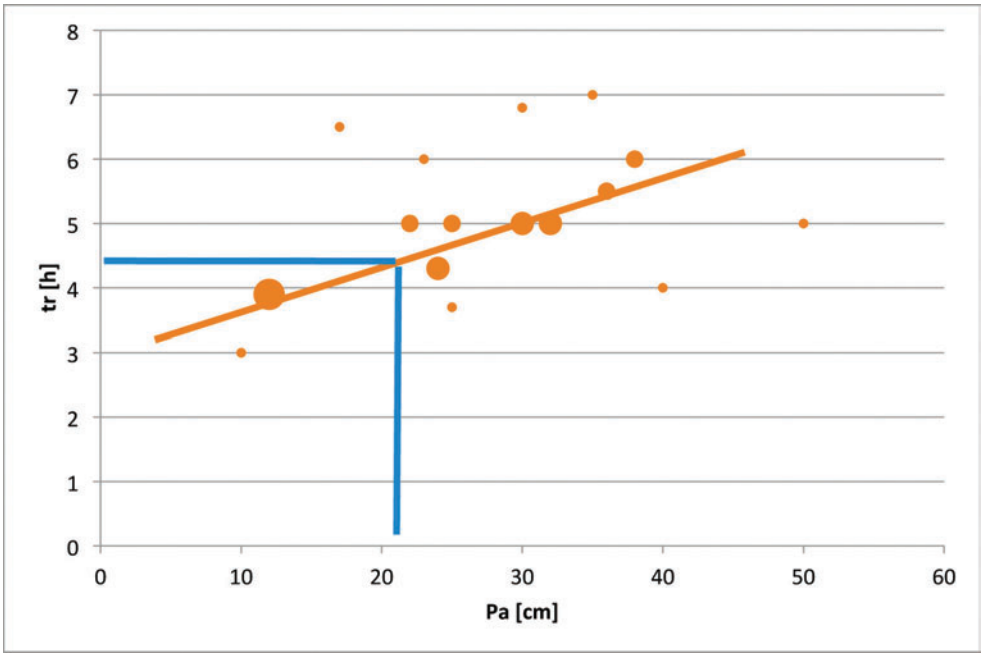

Figure 3.6. Sketch of weighted linear regression used to evaluate storm statistics (in this case, storm duration) at 5x5 km resolution. Orange dots represent stations located near the cell under analysis. Dot size represents the weight given to the station in the regression, the weight being inversely proportional to the station's distance from the cell of interest. The orange line is the regression line as estimated by the weighted linear regression. Blue lines represent the procedure to estimate the value of the storm statistic of interest (in this case storm duration) for the cell considered from its value of precipitation as extracted from PRISM dataset at the 5x5 km spatial resolution.

3.3.3 Vegetation Parameters

Application of Eagleson's water balance model requires specification of only one vegetation parameter, plant transpiration efficiency, k_v, which is defined as the ratio between potential evaporation from bare soil and potential transpiration from vegetated soil under a condition of unlimited water supply. As described in section 3.4, we use this parameter as a primary knob for model calibration. Therefore, for each cell of the study grid, k_v was estimated in a way that allows modeled fluxes to match observed ones.

3.3.4 Climatic Variables (forcing of the water balance)

Annual joint PDFs of precipitation and potential evapotranspiration were needed for the annual implementation of Eagleson's model; it is from these that it is possible to determine the PDFs of the water fluxes. Annual historical values for precipitation and for minimum, maximum, and dew point temperature were taken from the PRISM database (Daly and others 1994) at the 5x5-km resolution. Those datasets were mapped using the Clarke 1866 Albers projection in order to match our existing dataset format.

Historical values for potential evapotranspiration were derived according to equation 2.1.

3.4 Model Calibration

The goal of water balance model calibration was to reproduce observed natural water yield as closely as possible, not only in terms of long-term mean annual yield but also in terms of annual streamflow. The model was calibrated by minimizing the mean squared error between modeled water yield and estimates of historical natural streamflow. Three different historical streamflow datasets were used:

- 42-year series of annual streamflow records for 655 relatively unmodified test basins across the United States (Hobbins and others 2001; Slack and Landwehr 1992);
- reconstructed natural streamflow estimates for years 1906-2006 for a set of watersheds in the Colorado River Basin, provided by the U.S. Bureau of Reclamation (USBR); and
- 30-year average reconstructed natural streamflow for the eight-digit basins of the United States estimated by the USGS (Krug and others 1989).

Calibration was performed at the basin level (either a test basin or eight-digit basin), which required running the water yield model at the basin level. The parameters needed to run the model at the basin level were estimated by averaging parameter values across all 5x5-km cells within a basin.

Recall that the water yield model provides estimates of total natural water yield, equal to the sum of surface and subsurface yield. The calibration process is subject to errors if measured or reconstructed natural flows used for calibration do not accurately capture the sum of surface and subsurface flow that would naturally leave the basin, be it a test basin or eight-digit basin. Such error can occur where some of the water yield leaves the basin beneath surface, so that it is not captured at the stream gauge measuring basin outflow. It may also occur if withdrawals within the basin are not accounted for. Further, additional error can be caused at the annual time step by annual fluctuation in the amount of water stored as groundwater.

3.4.1 Model Calibration Over the 655 Test Basins

The 655 test basins were given first priority for model calibration; eight-digit basin data were used for calibration only outside of the boundaries of the test basins. The test basins were preferred because they are relatively unaffected by human intervention, such that streamflow is a fairly accurate estimate of natural water yield, thereby avoiding the need for natural flow reconstruction. For each of the test basins, a 42-year (1953-1994) sequence of annual streamflow data was used to calibrate the model, allowing us to compare predictions and observations on a year-by-year basis.[6]

Given that the water yield model represents a first order expansion around an equilibrium solution (Eagleson 1978f), calibrating the model on a mean annual basis (that is, comparing observed and predicted mean annual yield) theoretically would be sufficient to obtain an acceptable year-by-year fit. However, because of the limitations previously discussed, especially the possibility of annual changes in stored water that go unnoticed, a year-by-year

calibration may produce an improved fit. As seen in the following two subsections, where a mean annual calibration did not produce acceptable results, we tested a year-by-year calibration.

The approaches described in the next two sections, one based on the plant transpiration efficiency factor of the Eagleson model and the other based on a comparison of modeled and measured water yield, were developed to calibrate the model for areas within the 655 test basins. Each basin was individually calibrated using the procedure that produced the better result.

3.4.1.1 Calibration based on plant transpiration efficiency

Adjustment of plant transpiration efficiency (k_v in the water balance model) was selected a priori as the principal calibration approach. Although in principle the model could have been calibrated by adjusting any other model parameter or set of parameters, plant transpiration efficiency was the only parameter for which we had neither a direct measurement nor any reliable approximation available at the large scale. Further, we sought to avoid use of sophisticated multivariate methods of calibration because of the complexities involved with using such methods over large spatial scales with many calibration sites, and because we hoped to keep the approach as tractable as possible. A simple bisection method—a mathematical solution-finding method that repeatedly bisects an interval and then selects for further processing a subinterval in which the solution must lie—was implemented in order to calculate at the basin level the single value of k_v that allowed a perfect match between average modeled water yield and observed average streamflow. [7]

In order to prevent the calibration procedure from converging to a solution through infeasible values of k_v, we constrained k_v to fall within a fixed range. Although the literature suggests a range for k_v as broad as 0.4-2.6 (Eagleson 1978d), values at the upper end of that range often were found to lead to numeric instability of the model. To avoid such instability, we constrained k_v to range from 0.4 to 1.5.

For a large majority of the test basins, a value for k_v within the range 0.4-1.5 was found that allowed mean predicted annual yield to equal the 42-year average measured streamflow (Figure 3.7). In these cases, annual water yields were calculated by running the model with k_v set at the determined level and using annual values of precipitation and evapotranspiration as model inputs. Results were then compared with the observed traces of streamflow (Figure 3.8).

The year-by-year calibration option was examined when an acceptable mean annual value of k_v was not obtained. This option allowed k_v to vary year-by-year in relation to precipitation fluctuations. Allowing k_v to vary annually with precipitation (essentially, allowing plant transpiration to vary) reflects short-term plant adaptability to climatic conditions. The procedure consisted of the following steps:

- Find a set of 42 annual values of k_v that allows modeled water yield to match the observed streamflow each year.
- Linearly regress the annual values of k_v on annual precipitation of the basin.

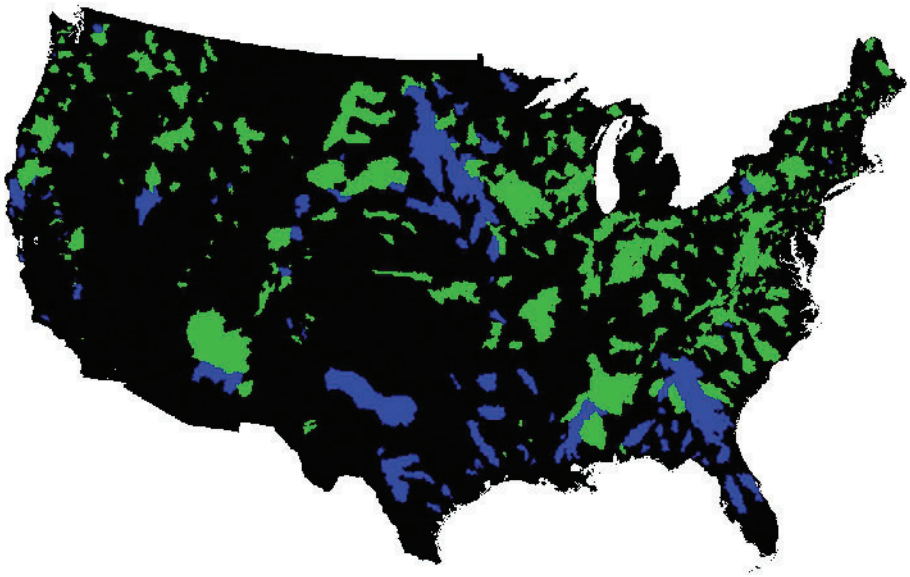

Figure 3.7. Test basins shown in green are those where a perfect match between average observed streamflow and mean simulated yield was achieved by changing the transpiration efficiency (k_v) only. Test basins in blue are those where a match was not possible by changing only k_v.

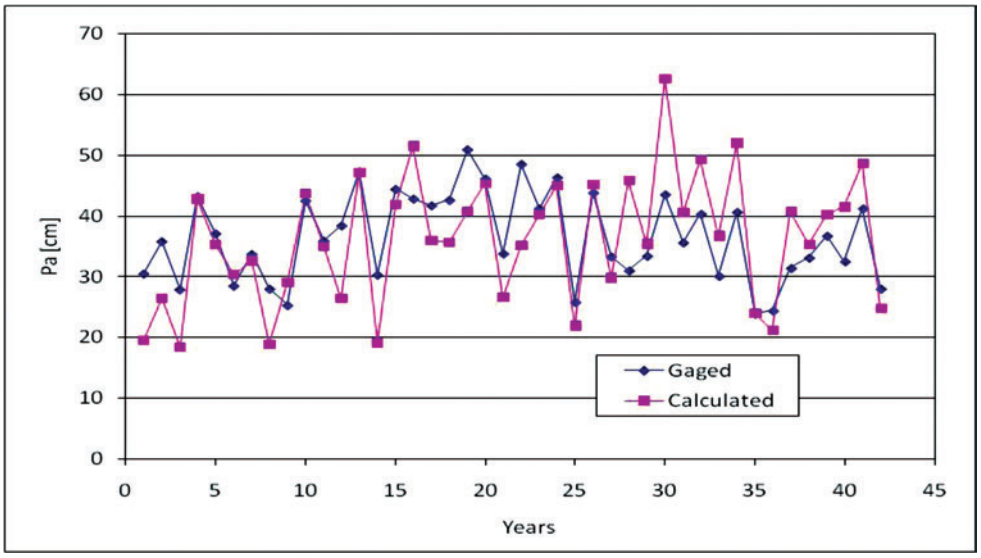

Figure 3.8. 42-year sequence of calculated yield and measured streamflow for test basin 411. The estimated sequence is obtained by using a value for plant transpiration efficiency that led to convergence between mean annual estimated yield and mean annual measured streamflow.

- Calculate water fluxes in a given year i using the value of $(k_v)_i = a+b \cdot (P_A)_i$, where (P_A) is precipitation in year i, and a and b are the coefficients of the linear regression of k_v on P_A and k_v, as illustrated in Figure 3.9.

We adopted the year-by-year k_v calibration procedure if it improved the fit of the model. Compare Figure 3.10 with Figure 3.8 for an example of the improvement achieved using an annually varying k_v for calibration. The year-by-year calibration produced a better match between observed streamflow and modeled yield for a considerable number of basins (Figure 3.11).

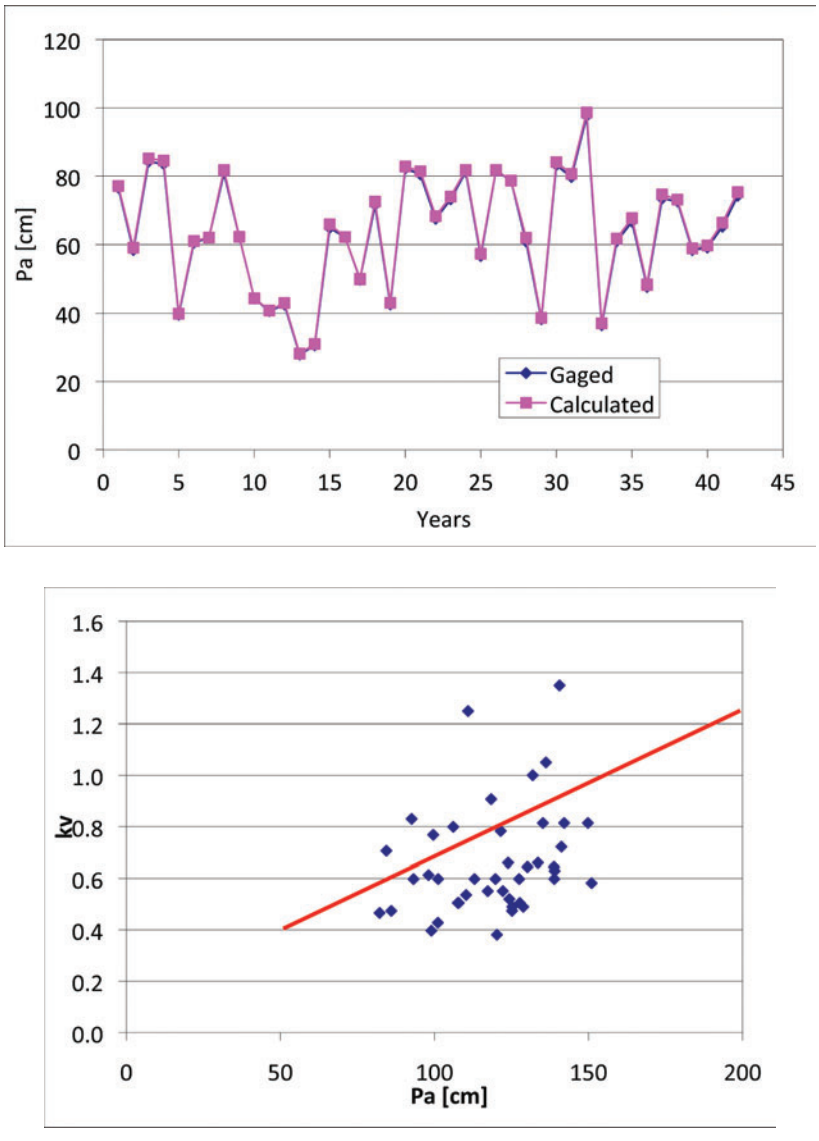

Figure 3.9. Calibration of test basin 21. Top: 42-year sequence of calculated yield and measured streamflow, with the calibration based on 42 annual estimates of k_v. Bottom: annual values of k_v that guarantee a perfect match between measured and calculated yield versus annual measured precipitation, also showing the linear regression line resulting from regressing k_v on precipitation.

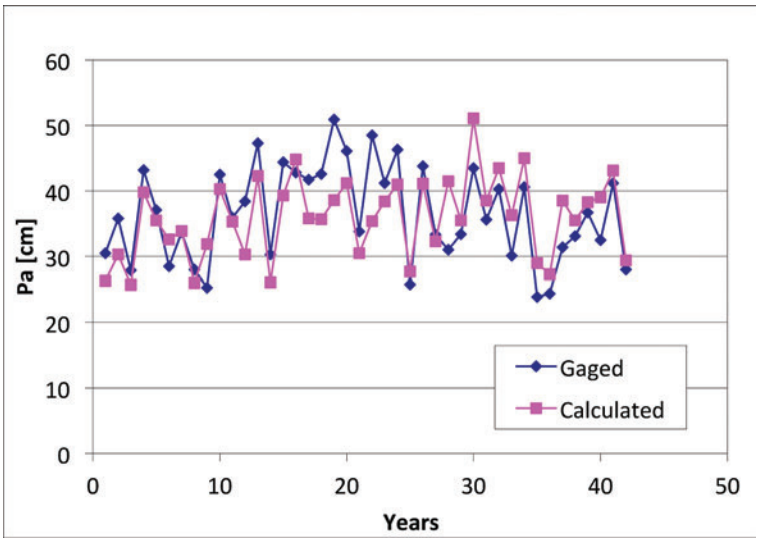

Figure 3.10. 42-year sequence of calculated yield and measured streamflow for test basin 411. The estimated sequence is obtained by using a variable plant transpiration efficiency factor as obtained from the regressive procedure.

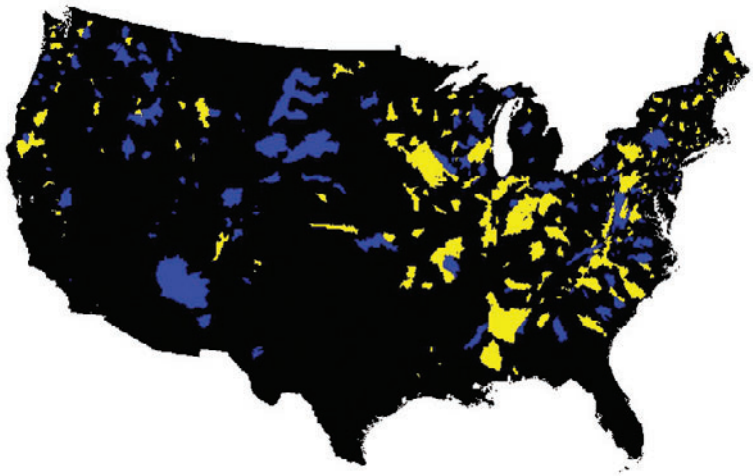

Figure 3.11. Test basins where convergence of mean annual estimates was achieved using k_v (those shown in green in Figure 3.7) are shown here in blue or yellow. Those shown in blue are basins where a yearly variable k_v leads to a better match between model yield and observed streamflow. Yellow indicates basins where keeping k_v constant (and equal to the value obtained in step 1 of calibration process) lead to a better fit with the observed streamflow sequence (in terms of 42-year MSE).

3.4.1.2 Calibration based on effective water yield

For basins where the k_v calibration procedures previously described did not allow modeled fluxes to match historical observations, an alternative approach was used that relied on computation of the ratio of modeled to observed streamflow. For this approach, the transpiration efficiency factor (k_v) was set to 1 (such that plant potential transpiration equals potential evaporation). With k_v set to 1, all fluxes were computed and the ratio between modeled mean annual yield and mean measured streamflow, *YS*, was calculated as follows:

$$YS = \frac{\left(\overline{Y_A}\right)_{MODELED}}{\left(\overline{Streamflow}\right)_{OBSERVED}} \tag{3.8}$$

YS then was used to scale each year's modeled total yield. The effective water yield for year *i*, $(Y_A)_{iEFF}$, was then calculated as:

$$\left(Y_A\right)_{i\,EFF} = \left(Y_A\right)_{i\,MODELED} \cdot \frac{1}{YS} \tag{3.9}$$

See Figure 3.12 for an example of the application of this procedure.

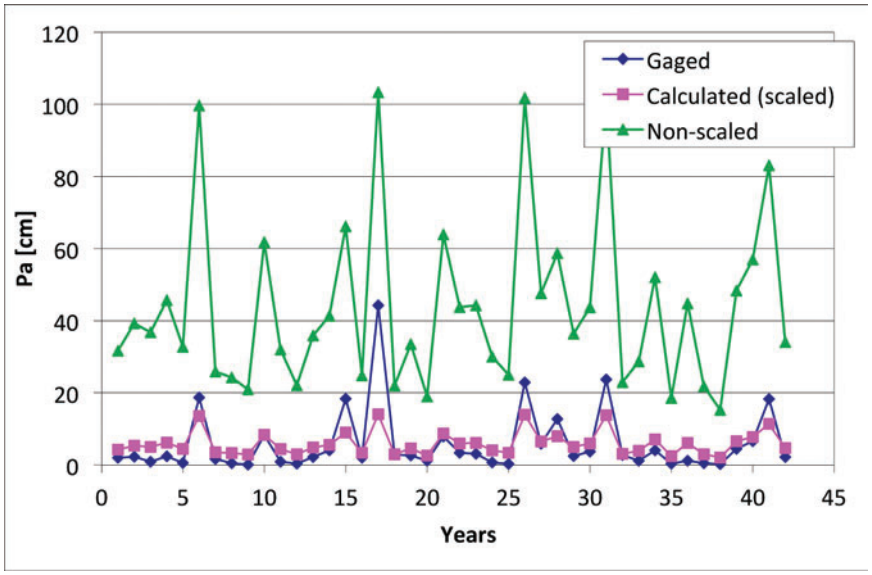

Figure 3.12. 42-year sequence of calculated yield and measured streamflow for test basin 566, showing measured streamflow (blue), calculated un-scaled yield (green), and effective (calculated and scaled) yield per equation 3.9 (pink).

As was done with the k_v approach to calibration, to improve the year-by-year fit of the yield traces and better capture the annual variability of the observed streamflow, we investigated the possibility of allowing *YS* to vary annually in relation to precipitation. An optimal scaling value was determined by ensuring that both the long-term mean yield (that is, the yield predicted by the model if precipitation and potential evapotranspiration are set at their mean annual values) and the 42-year average yield (that is, the average of the 42 annual estimates of yield, each obtained with the annual values of precipitation and potential evapotranspiration) converged to the mean observed streamflow. In summary, this procedure consisted of finding the value of η in equation 3.10 that leads to the sequence of scaled values of *YS* at year *i*, $(YS^*)_i$, that satisfies the aforementioned condition:

$$\left(YS^*\right)_i = \frac{\left[\left(P_A\right)_i - m_{PA}\right]\cdot \eta + m_{PA}}{m_{PA}} \cdot YS \tag{3.10}$$

When this procedure was successful, that is, when it improved the fit between observations and simulations, effective water yield in the given basin in year *i* was calculated as:

$$\left(Y_A\right)_{i\,EFF} = \left(Y_A\right)_{i\,MODELED} \cdot \frac{1}{\left(YS\right)_i} \tag{3.11}$$

For an example of the improvement achieved by allowing YS to vary with precipitation—that is, using in each year *i* the value of $(YS^*)_i$ that is calculated based on actual precipitation $(P_A)_i$—compare Figure 3.13 with Figure 3.12. This annualized procedure improved the fit for many test basins (Figure 3.14).

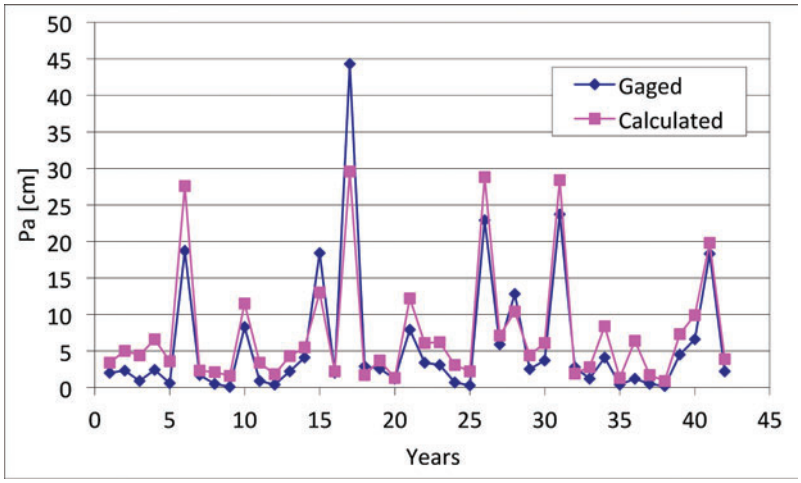

Figure 3.13. 42-year sequence of calculated yield and measured streamflow for test basin 566, showing measured streamflow (blue) and calculated yield (pink). Yield is calculated by scaling each year's prediction of annual yield by a factor equal to the ratio of the ratio mean estimated yield to average measured streamflow (*YS*) times the actual value of precipitation.

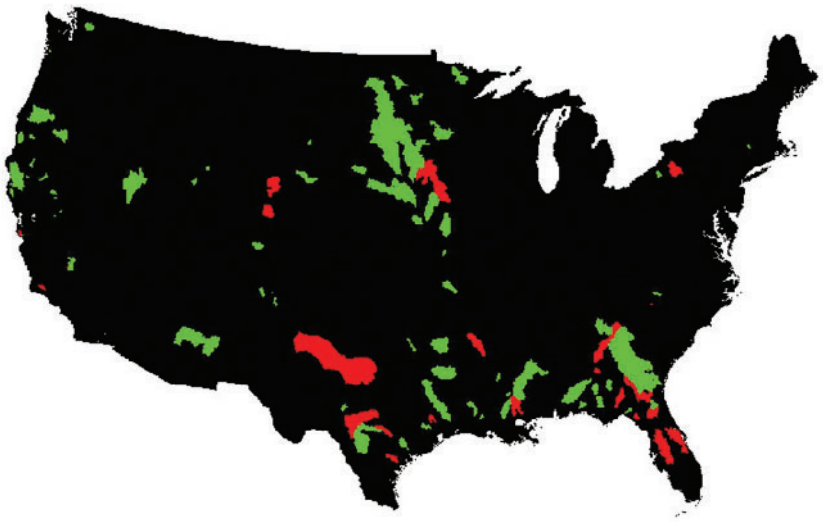

Figure 3.14. Basins in red are those where a yearly variable scaling factor leads to a better match between modeled yield and measured streamflow (for basins where convergence was not achieved using only the k_y claibration procedure). Green indicates basins where a better match between model and observations was found by keeping the scaling factor constant from year to year.

As apparent in Figure 3.15 and Figure 3.16, the largest absolute errors between estimated water yield and observed streamflow occur in the eastern and far western United States, with smaller errors in the Interior West and Great Plains. However, examining relative as opposed to absolute errors reveals a different pattern, with many areas of the central and southern United States having errors comparable in magnitude to the average yield.

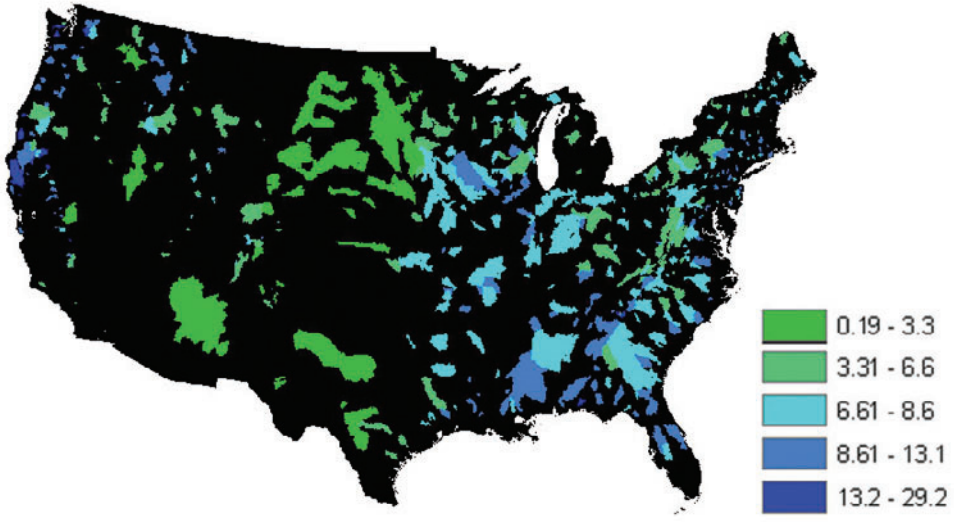

Figure 3.15. Square root of the mean squared error between modeled water yield and measured streamflow (MSE) for the test basins (cm).

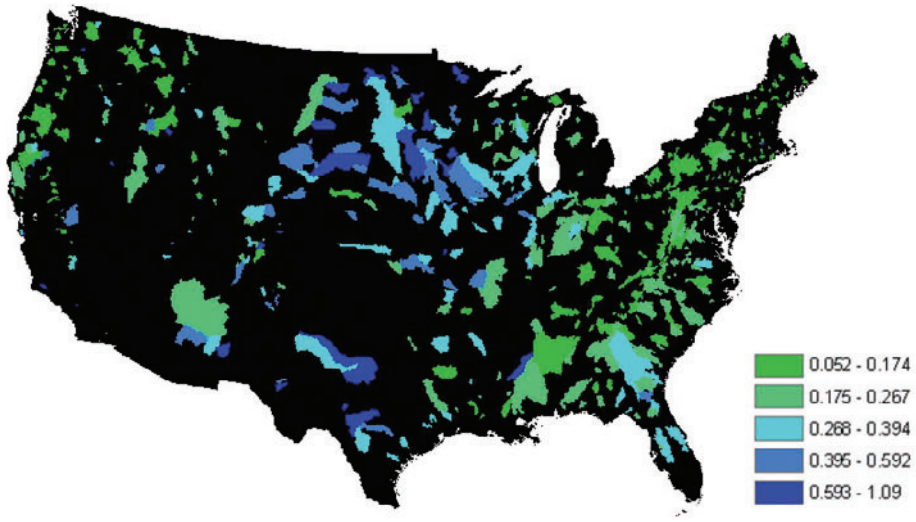

Figure 3.16. Ratio of the square root of MSE to average streamflow for the tests basins.

3.4.2 Calibration by Eight-Digit Basin

In areas where no test basins were present, the model was calibrated using 30-year (1951-1980) average reconstructed natural flows estimated by the USGS for the eight-digit basins of the United States (Krug and others 1989) (Figure 3.17). In addition, for the Colorado River Basin the eight-digit basin flows were used in combination with reconstructed natural flows estimated by the USBR. Of the USBR flow estimates, we used data for years 1953-2004.

The natural flow estimates from the USBR were considered more reliable than the eight-digit basin averages from the USGS for the same area. Some of the flows from the USBR refer to stations with drainage areas considerably larger than the typical eight-digit basin (Figure 3.18). Where USBR flow estimates were available for a catchment that included more than one eight-digit basin, the interior eight-digit basin averages were scaled in such a way that the aggregate streamflow across the interior basins matched the USBR average for the catchment. The scale factor, ξ, was obtained as follows:

$$\xi = \frac{\overline{Streamflow}_{USBR} \cdot A_{USBR}}{\sum \left(\overline{Streamflow}_{8DB} \cdot A_{8DB} \right)_i} \tag{3.12}$$

where $\overline{Streamflow}_{USBR}$, A_{USBR}, $\overline{Streamflow}_{8DB}$, and A_{8DB} are, respectively, the average observed streamflow for the USBR catchment, the area of the USBR catchment, the average streamflow, and the area of each of the eight-digit basins contained within the USBR catchment. Calibration was then performed at the eight-digit basin scale by matching the modeled yield with a corrected eight-digit basin streamflow, $\overline{Streamflow}^{*}_{8DB}$, obtained as follows:

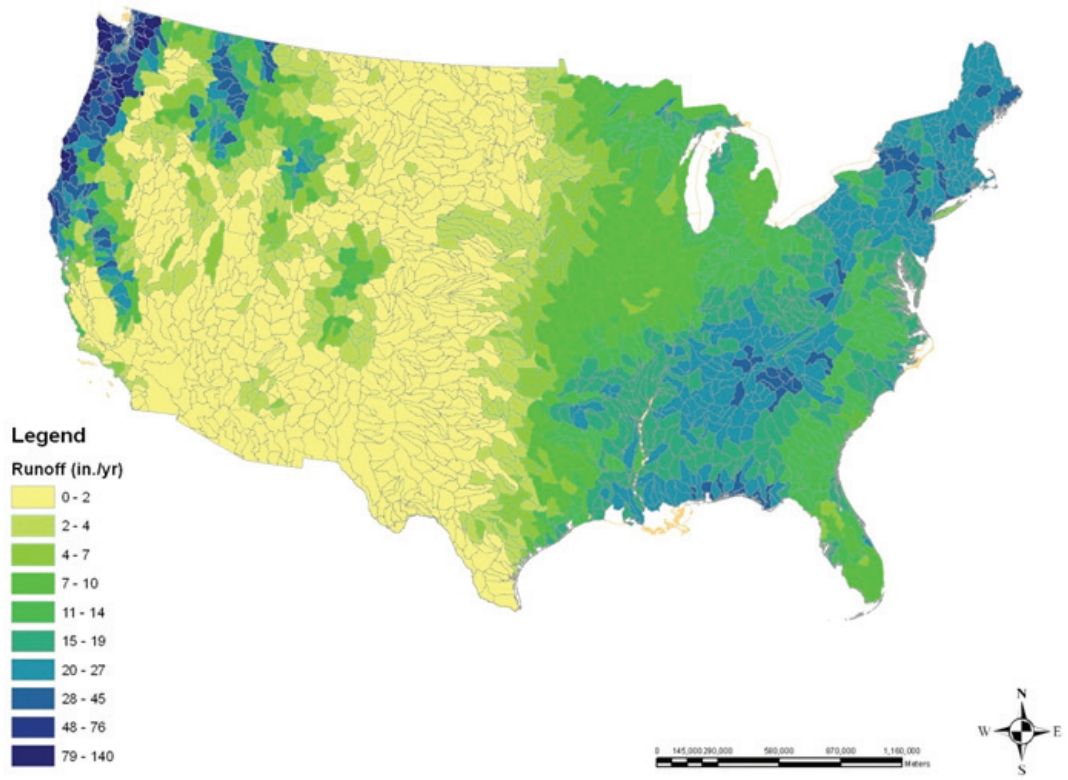

Figure 3.17. USGS average runoff at the eight-digit basin level.

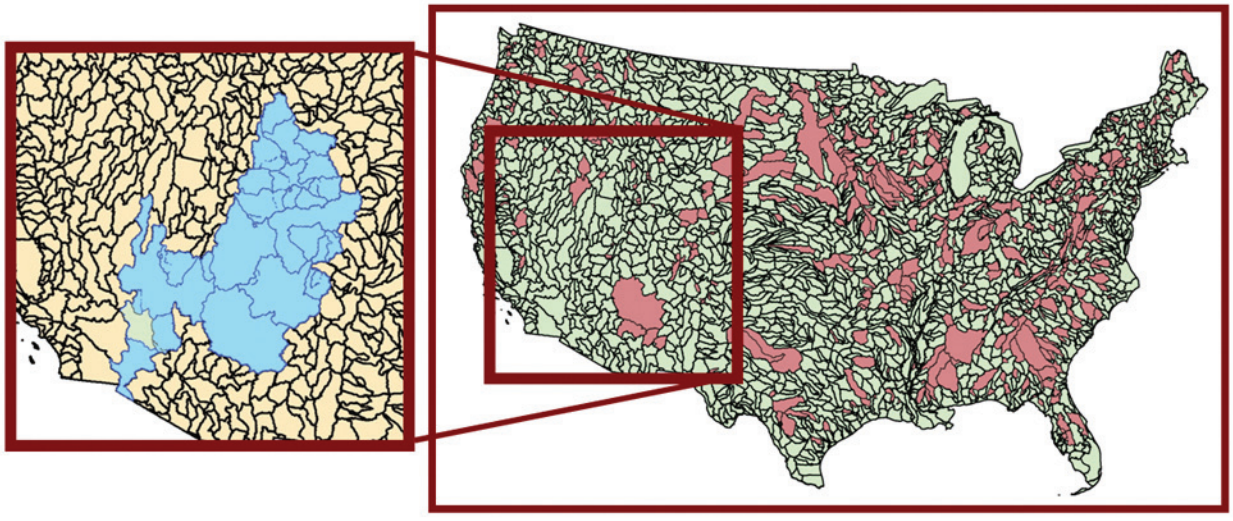

Figure 3.18. Map of the 655 test basins (red) and eight-digit basins (green) with zoom of the Colorado River Basin showing watersheds for which data were from the USBR (light blue).

$$\overline{Streamflow}^{*}_{8DB} = \xi \cdot \overline{Streamflow}_{8DB} \quad (3.13)$$

This procedure guarantees that global simulated yields match the observed streamflow at the scale of the USBR catchments and, simultaneously, that the lower scale variability at the eight-digit basin is preserved.

Calibration over the eight-digit basins, or over the eight-digit basins in combination with the USBR streamflow records, was then performed following the approach described previously for the test basins, except for the year-by-year regressions, which were not used with the eight-digit basins.

During the calibration over the eight-digit basins, we found some instances where the eight-digit basin estimated streamflow exceeded the mean precipitation calculated from the PRISM dataset, which questions the reliability of some records. Since we considered the PRISM information to be more reliable than the information on streamflow at the eight-digit basins, we constrained the streamflow of each eight-digit basin to be bounded between 0.02 and 0.97 times the PRISM precipitation. The choice of the range was dictated by the analysis of the 655 test basins (our most reliable source of streamflow records), where 0.02 and 0.97 were respectively the lowest and the highest runoff ratio observed.

3.5 Extension of Calibrated Parameters to the United States

Once calibration was performed for the entire study area, the model could be applied at the 5x5-km or any larger spatial scale. To apply the model at the 5x5-km scale, each cell was assigned the values of k_v or *YS* that allowed convergence between average observed streamflow and mean modeled water yield for the basin (either test basin or eight-digit basin) to which the cell belonged. Ultimately, we found that applying the model at the 5x5-km resolution for all nine alternative futures was computationally too time consuming to be practicable. Therefore, we used the model at the grid cell level only to estimate the average mean annual yield (Figure 3.19) for comparison with the USGS mean annual runoff estimates (Figure 3.17). Estimation of annual historical water yield and future water yield based on climatic and socio-economic projections was instead performed at the eight-digit basin scale.

3.6 Model Input Parameters for Future Climatic Scenarios

Application of the model to predict future water yield required estimates of model input parameters for future years. As previously explained, input parameters of the model include the soil hydraulic properties, vegetation properties (essentially vegetation transpiration efficiency, k_v), and storm statistics.

With varying levels of confidence, we assumed that future levels of these parameters would equal past levels. Regarding the soil hydraulic properties, this assumption is easily accepted, as the parameters are representative of soil texture and composition, which are unlikely to change over this century. Somewhat less easily accepted, but still, in our judgment, reasonable, is the assumption that the plant coefficient k_v will remain constant over the time horizon, as it ideally represents the result of the plant evolutionary adaptation to the environment.

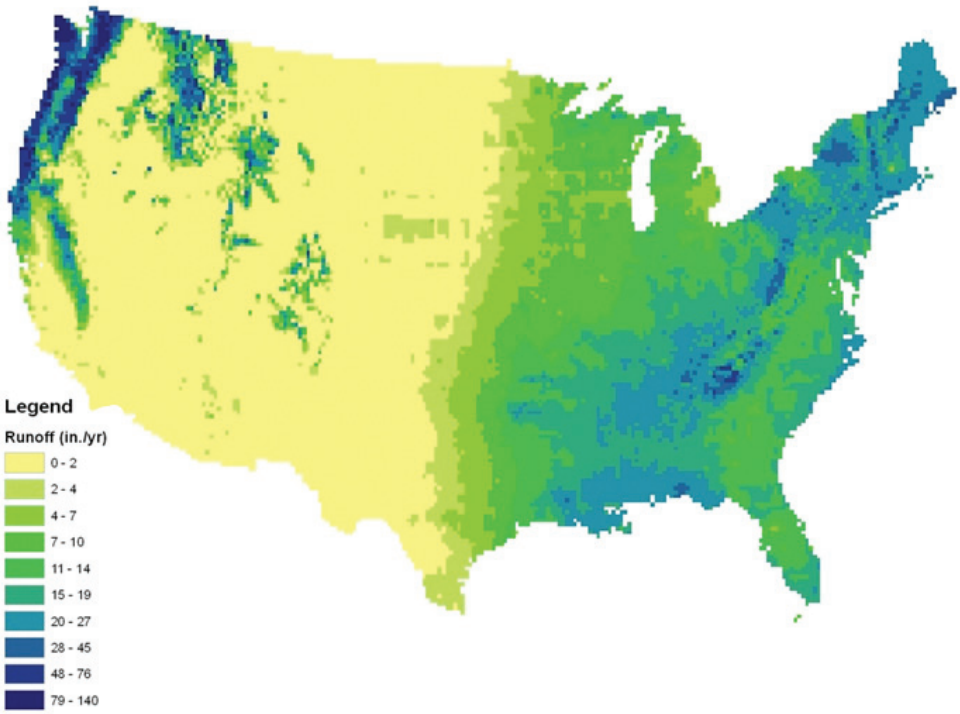

Figure 3.19. Modeled average runoff for the study grid.

On the other hand, storm characteristics may be expected to change as the climate changes. Our estimation of storm statistics based on past weather data relied on the assumption of a stationary climate, which is an assumption that will be increasingly untenable if the climate changes as indicated by current global climate models. Estimation of storm statistics for the future, however, is constrained by the fact that their estimation relies on hourly precipitation data. As described above, hourly data were available for past years, but estimates of future precipitation were available only at the monthly time step. Therefore, to reflect future climatic conditions, changes in the values of storm statistics would need to be inferred from changes in monthly climatic data. Because of the magnitude of uncertainty that would be introduced by such inference, we decided to apply the current storm statistics to future water yield estimation.[8]

In summary, projection of water yield for future climatic and socio-economic scenarios was based on the water yield model as forced by the future predicted PDFs for precipitation and potential evapotranspiration but employing historical soil, vegetation, and storm parameters.

3.7 Future Water Yield

Projections for precipitation and temperatures (and therefore potential evapotranspiration) for the nine alternative futures were used in the water balance model to estimate future traces of water yield for the period 2006-2090. Because the changes in projected water yield are the direct result of the changes in precipitation and potential evapotranspiration rates, some of the trends of future yield can easily be anticipated. The overall picture, in fact, shows water yield decreasing throughout the Twenty-First Century (Figure 3.20). The "current" point represents a mean for the period 1986-2005, and the other points are 20-year means centered at the years shown. Using the CGCM model, for example, decreases in mean annual yield across the United States of 15.8%, 21.7%, and 17.2% are expected by 2060 with the A1B, A2, and B2 scenarios, respectively.

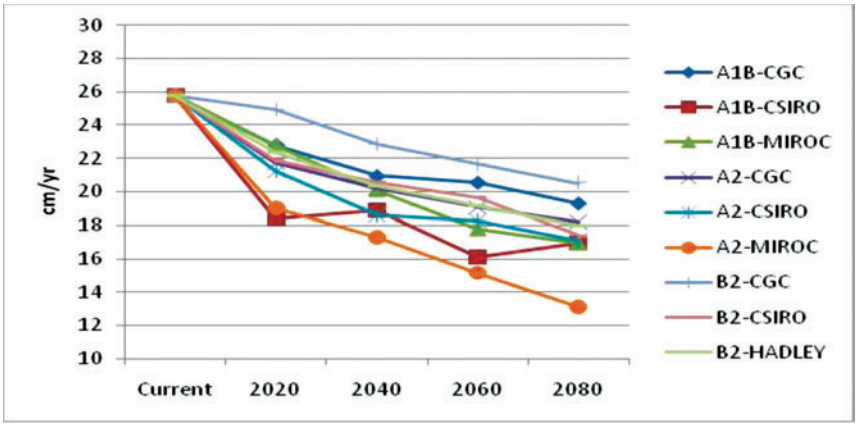

Figure 3.20. Nine projections of mean annual U.S. water yield.

Maps of future water yield for the nine alternative futures are provided in Figures 3.21-3.29 and confirm the overall decrease seen in Figure 3.20. In general, the magnitude of the decrease is larger in the eastern United States, although areas of the central and western United States are expected to experience the largest percentage decreases. Besides the case of the northern East Coast and noticeably in the East for the B2-CSIRO case, increases in yield are often localized in small areas and only occur for a few of the alternative futures.

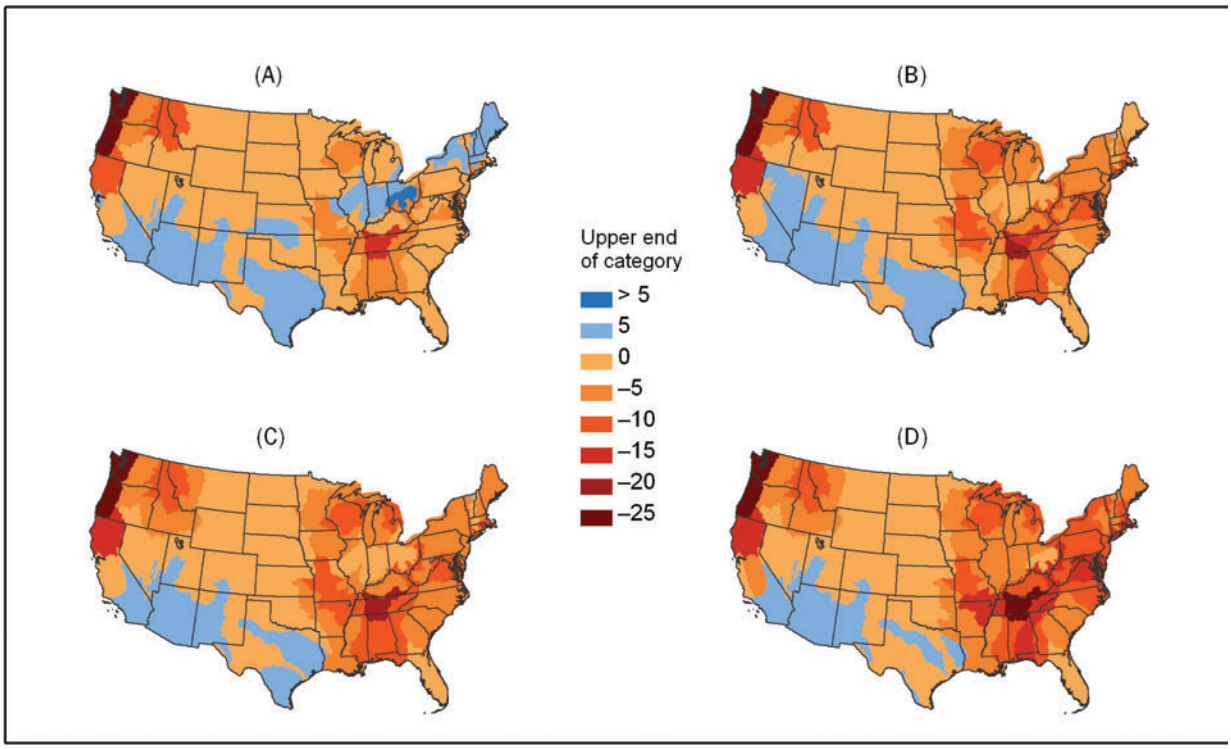

Figure 3.21. Change from current conditions in mean water yield (cm/yr) with the A1B-CGCM future for: (A) 2020; (B) 2040; (C) 2060; (D) 2080.

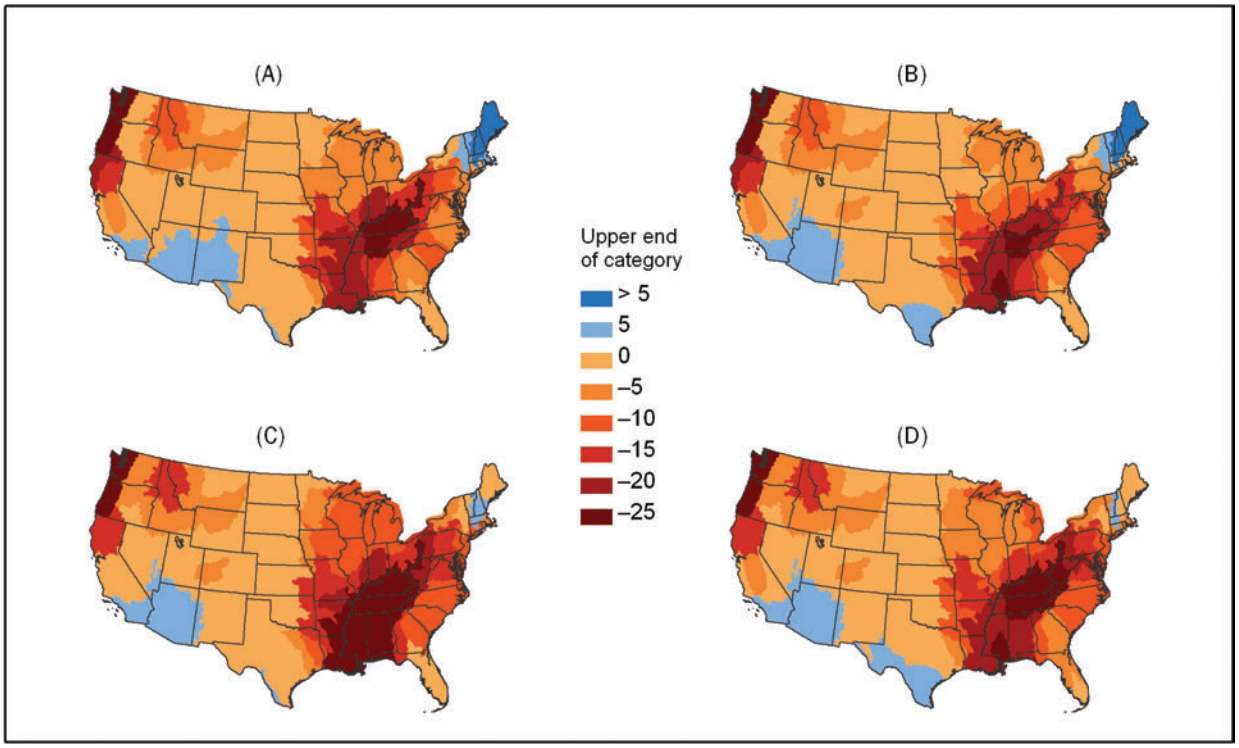

Figure 3.22. Change from current conditions in mean water yield (cm/yr) with the A1B-CSIRO future for: (A) 2020; (B) 2040; (C) 2060; (D) 2080.

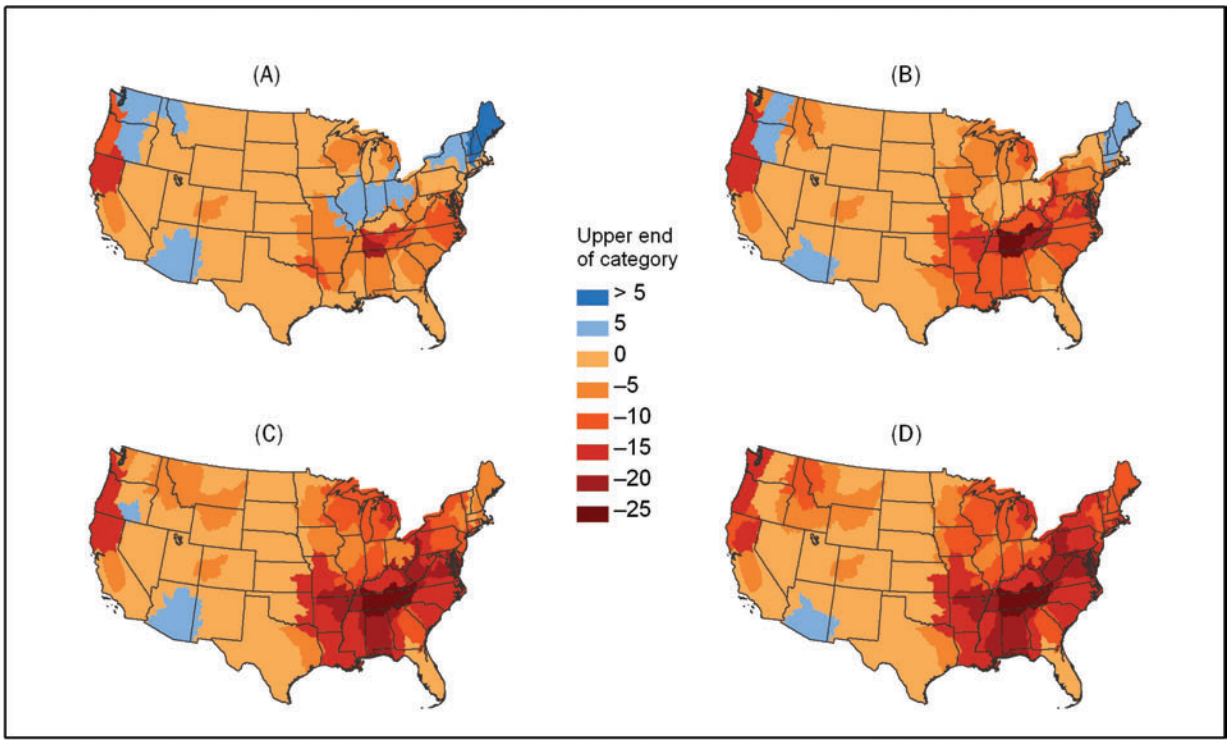

Figure 3.23. Change from current conditions in mean water yield (cm/yr) with the A1B-MIROC future for: (A) 2020; (B) 2040; (C) 2060; (D) 2080.

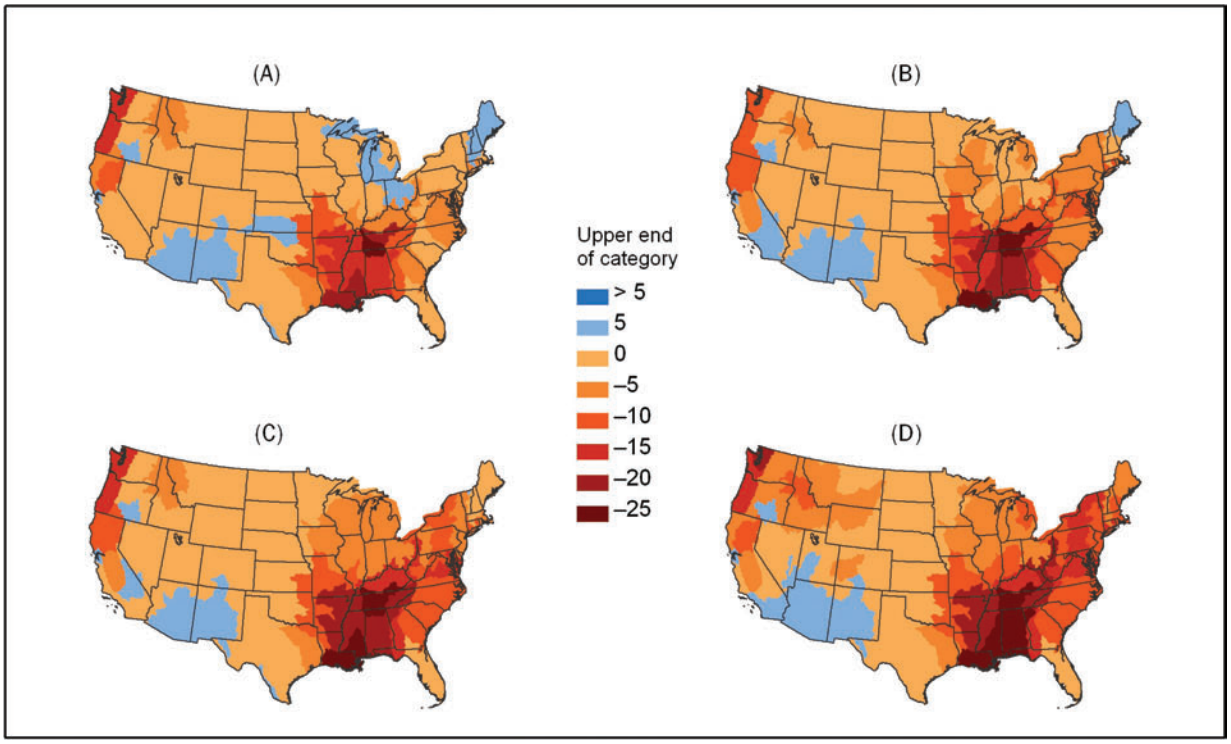

Figure 3.24. Change from current conditions in mean water yield (cm/yr) with the A2-CGCM future for: (A) 2020; (B) 2040; (C) 2060; (D) 2080.

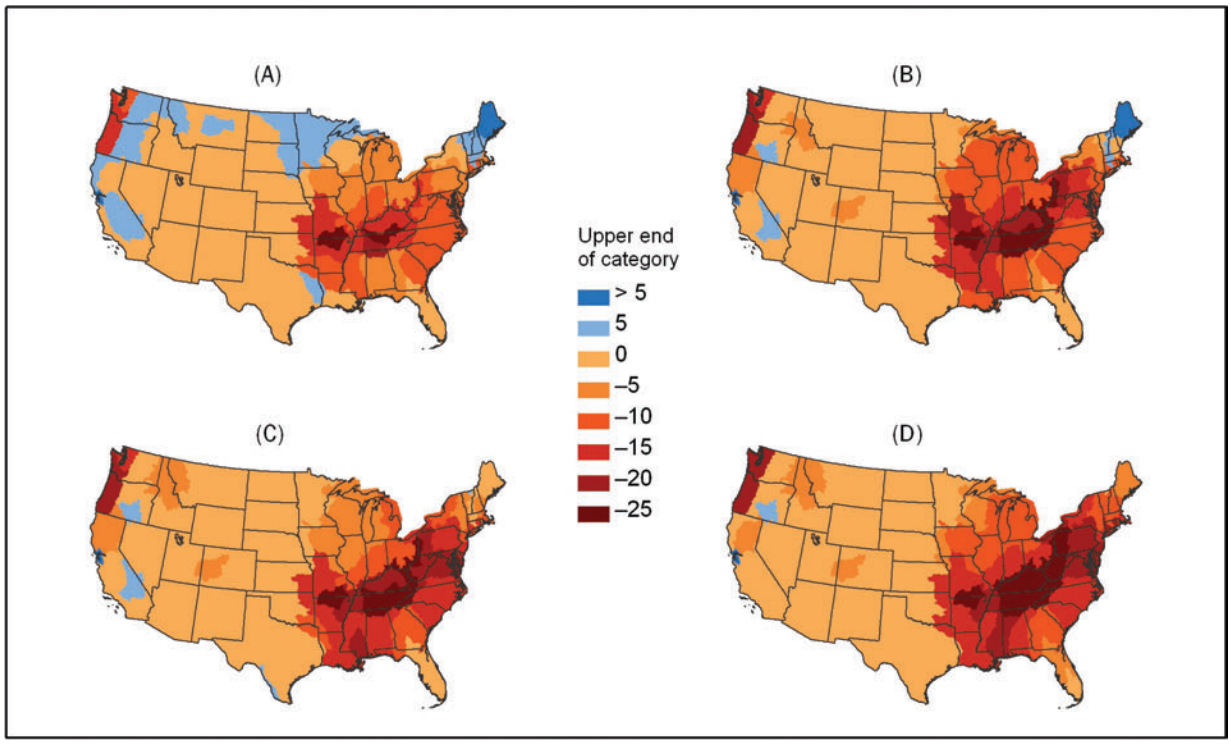

Figure 3.25. Change from current conditions in mean water yield (cm/yr) with the A2-CSIRO future for: (A) 2020; (B) 2040; (C) 2060; (D) 2080.

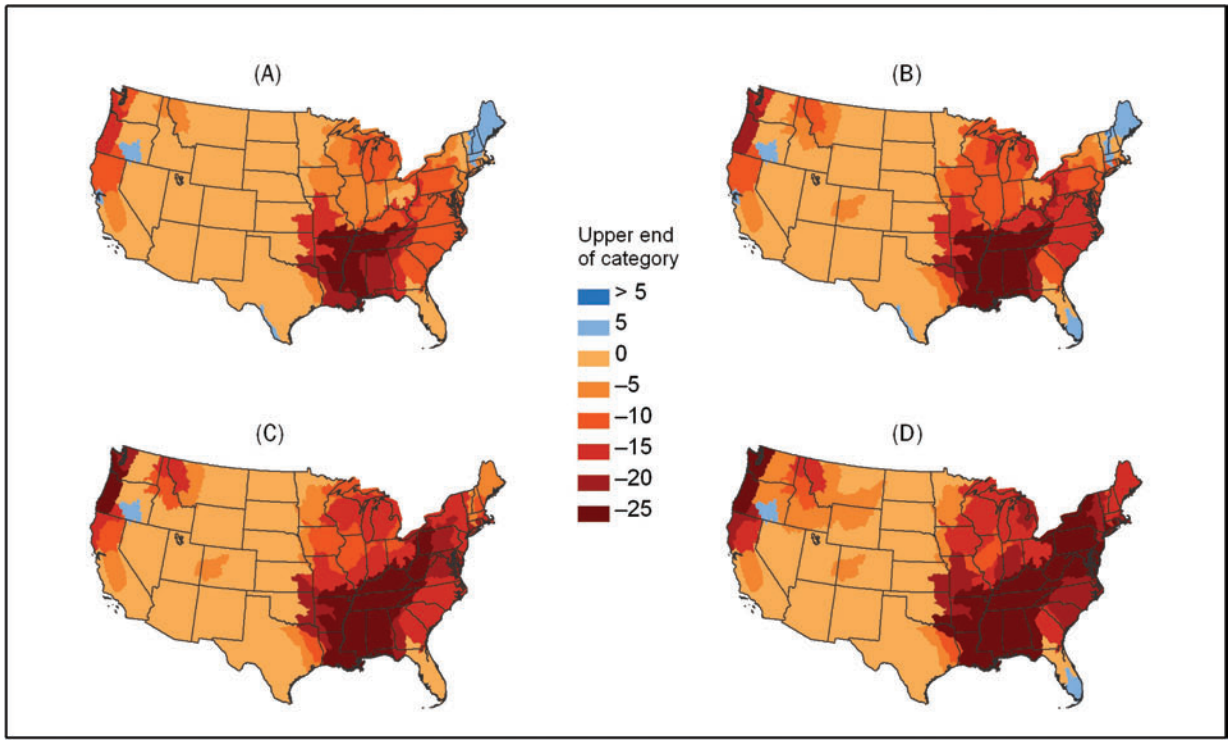

Figure 3.26. Change from current conditions in mean water yield (cm/yr) with the A2-MIROC future for: (A) 2020; (B) 2040; (C) 2060; (D) 2080.

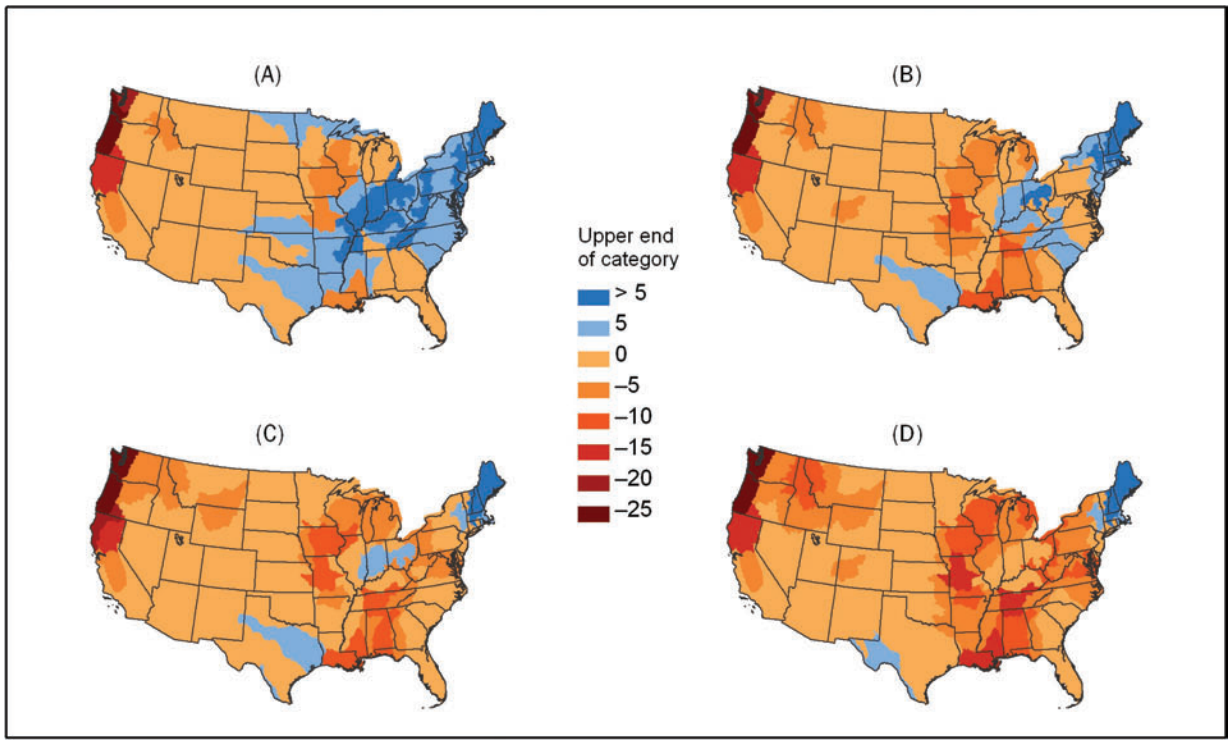

Figure 3.27. Change from current conditions in mean water yield (cm/yr) with the B2-CGCM future for: (A) 2020; (B) 2040; (C) 2060; (D) 2080.

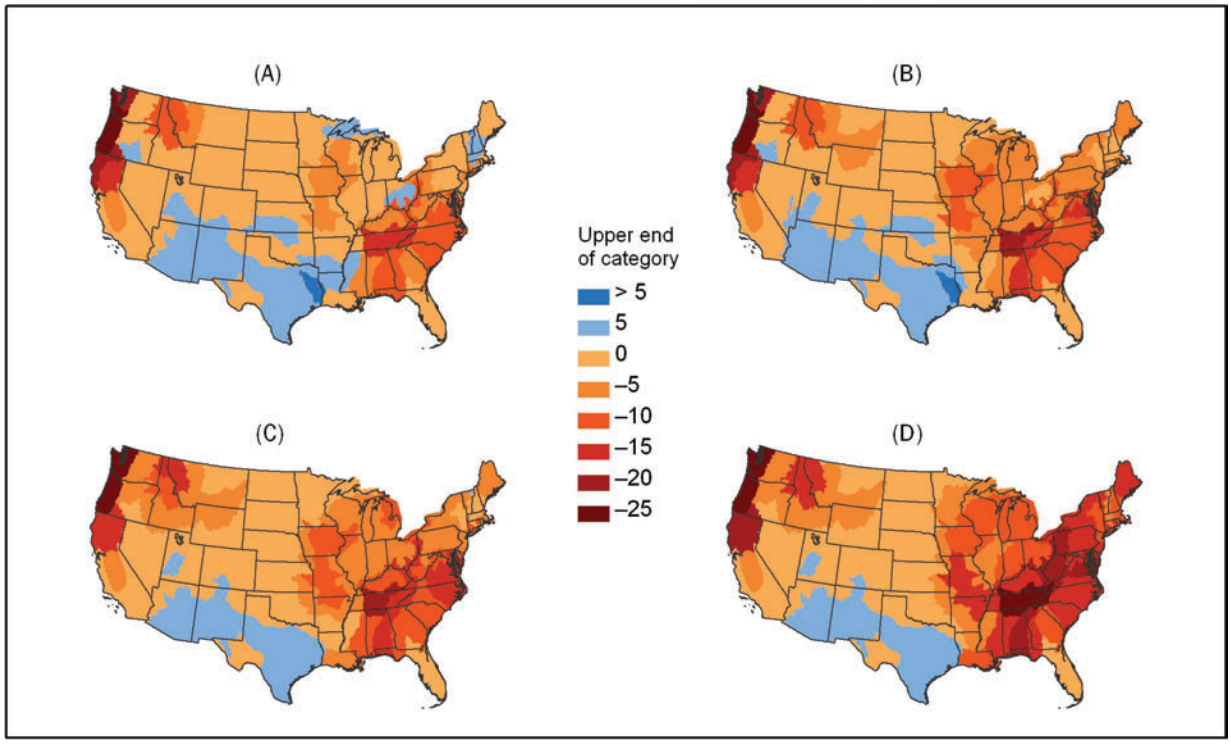

Figure 3.28. Change from current conditions in mean water yield (cm/yr) with the B2-CSIRO future for: (A) 2020; (B) 2040; (C) 2060; (D) 2080.

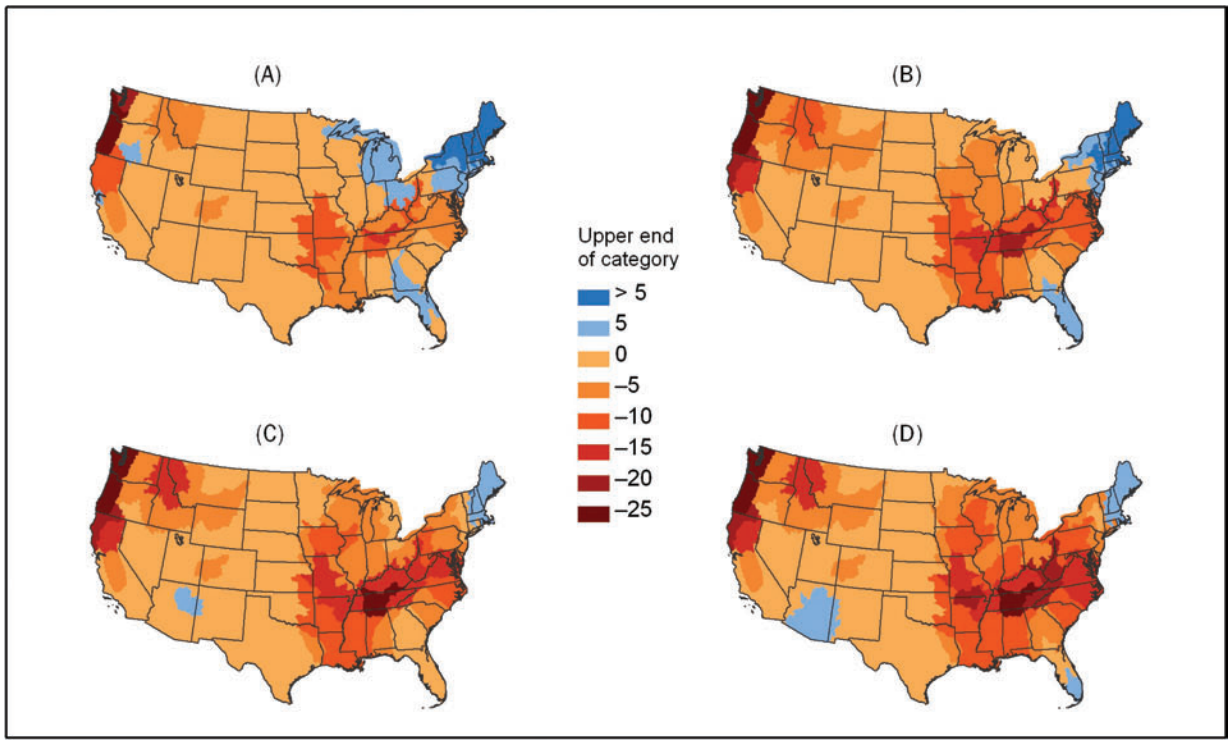

Figure 3.29. Change from current conditions in mean water yield (cm/yr) with the B2-HADN future for: (A) 2020; (B) 2040; (C) 2060; (D) 2080.

Knowing only the changes in the mean values of precipitation and potential evapotranspiration may not, by itself, suffice to indicate the direction of the change in yield. In some circumstances, in fact, the higher moments of the distribution functions of precipitation and potential evapotranspiration strongly affect the distribution function of yield, leading to some apparently counterintuitive results. This is the case in the Lower Colorado River Basin, where an increase in yield (of over 20% by 2060) is projected for the A1B-CGCM future despite a projected decrease in precipitation and increase in potential evapotranspiration. This large percentage increase is caused by the increases in the variance of both predicted precipitation and potential evapotranspiration. As a result of a larger variance of the climatic forcing, in fact, the distribution of extreme events can be affected so as to cause an increase rather than a decrease in average water yield. A larger variance in precipitation, for example, produces extreme events with annual water yield considerably larger than the mean (especially where the mean yield is close to zero), whereas the driest years can never produce a negative water yield (the lowest feasible water yield is zero). Thus, although most future years in the Lower Colorado River Basin are projected to be drier than past years, the overall average is expected to increase due to those few instances of particularly large water yield. This situation, therefore, is likely to occur is in arid climates as a consequence of the highly skewed distributions of precipitation and water yield. However, note that although the percentage increases in yield projected for the Lower Colorado River Basin may be large, their absolute value is extremely small and corresponds to only a fraction of a centimeter.

The substantial decreases in annual yield that our model projects for much of the United States are the result of many methodological decisions, most importantly the selection of GCM models, the downscaling approach that we relied on, the yield model we adopted, and the potential evapotranspiration model we used. We cannot be sure that other models or approaches would not produce quite different results. With that in mind, given that temperatures have been rising in the United States in recent years, it is reasonable to ask whether streamflow has been declining, as recent past streamflow declines would be in concert with our projections. Two recent papers suggest that it has. First, Krakauer and Fung (2008) found for the United States as a whole that although the long-term trend from 1925-1994 in annual streamflow is upward, that trend is very sensitive to an unusual period of heavy precipitation around 1970. Further, the trend since 1994 is downward, though non-significant. Based on an analysis comparing past streamflow trends with trends in temperature and atmospheric CO_2 concentration, the authors concluded that "the overall effect of greenhouse warming has probably been to reduce streamflow" (Krakauer and Fung 2008: 973). Second, for the Northwest, Luce and Holden (2009) found that mean and median annual streamflow over the period 1948-2006 has generally been decreasing. More work is needed to fully understand recent trends in U.S. streamflow and how they have been affected by climatic change, but these recent results are not in opposition to our projections.[9]

Chapter 4: The U.S. Water Supply Network

4.1 Overview

Water supply, the amount of water available for use at a given time and place, depends not only on water yield but also on the ability to store water for later use and on any diversions into or out of the basin. If basins are inter-connected via natural or artificial flow paths, they form a network that must be modeled as a unit in order to measure the water supply of any one basin. Thus, estimating water supply of a given basin requires an accounting of all water yield, storage, and diversion that occurs not only in that basin but also in any basin within the network. As explained in Chapter 1, supply and demand were estimated for 98 ASRs covering the contiguous United States.

The following sections describe the structure of the water networks existing within the United States at the ASR level, the storage capacity and evaporation of reservoirs in the ASRs, the classes of water use, and the set of rules adopted for the network simulation.

4.2 Network Structure

Networks are characterized as systems of nodes connected by links. Each ASR, as well as each demand, in-stream flow constraint, storage capacity, and network sink (representing outflow beyond the ASRs), is represented by a node. Natural and artificial water routes connecting ASRs are represented by directional links. Links are also used to connect ASR nodes to storage, in-stream flow, and demand nodes (Figure 4.1).

The in-stream flow constraint of an ASR was computed as a percentage of natural flow. The natural flow of a downstream ASR is the sum of the water yield produced in that ASR and in all upstream ASRs. We modeled the in-stream flow constraint by simply removing from each ASR an amount of flow equal to the required percentage times the water yield of the ASR. The sum of the removals across naturally connected ASRs equals the in-stream flow constraint of the more downstream ASR.

ASRs were considered linked, that is, part of the same network, if they were connected by either a natural flow path (upstream to downstream river flow) or an artificial diversion (via a canal, tunnel, or other constructed conveyance). An artificial connection between ASRs is called a trans-ASR diversion. Of the 98 ASRs, 83 are part of multi-ASR networks and the remaining 15 are unconnected. The unconnected ASRs drain to the sea, Mexico, or Canada or are closed basins. Three multi-ASR networks were delineated, one with 69 ASRs that includes most of the central and western United States, one with 10 ASRs in the Northeast, and one with 4 ASRs in the Southeast (Figure 4.2).

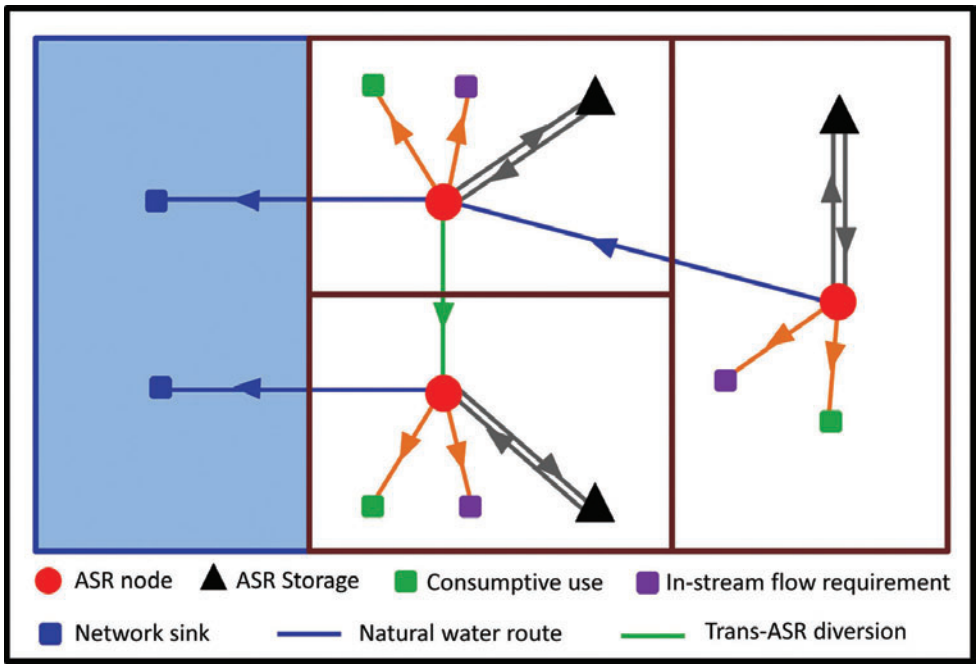

Figure 4.1. Schematization of a network containing three ASRs and including both natural and artificial water routes.

Figure 4.2. Water networks across the contiguous United States at the ASR level. Natural links are indicated with blue lines, artificial links (trans-ASR diversions) are indicated with green lines. The majenta line shows the delivery to Mexico.

4.3 Reservoir Storage Capacity and Evaporation

To estimate reservoir storage capacity of the ASRs, we began with the National Inventory of Dams (NID) (U.S. Army Corps of Engineers 2009). The NID contains data on many thousands of reservoirs, most of which are quite small. To keep the task manageable, we included only reservoirs with a normal surface area of at least 5 km^2, resulting in 1243 reservoirs. We further removed reservoirs that were for flood control only, were mining tailings ponds, or that stored power plant cooling water. In addition, we independently checked reservoirs that had an unusual normal surface area-to-storage volume ratio, searching for information online or via phone calls to responsible individuals, and revised those values as needed. The checking process resulted in the removal of several reservoirs that were found to have a normal surface area below 5 km^2. Finally, we added one reservoir that was not on the list. The final list included 1196 reservoirs. We revised the surface area of 13 of the 1196 reservoirs and the storage volume of 44 reservoirs. Of the 1196 reservoirs, 499 have a storage capacity of less than 50,000 acre-ft and 75 have a storage capacity of over 1 million acre-ft (Figure 4.3).

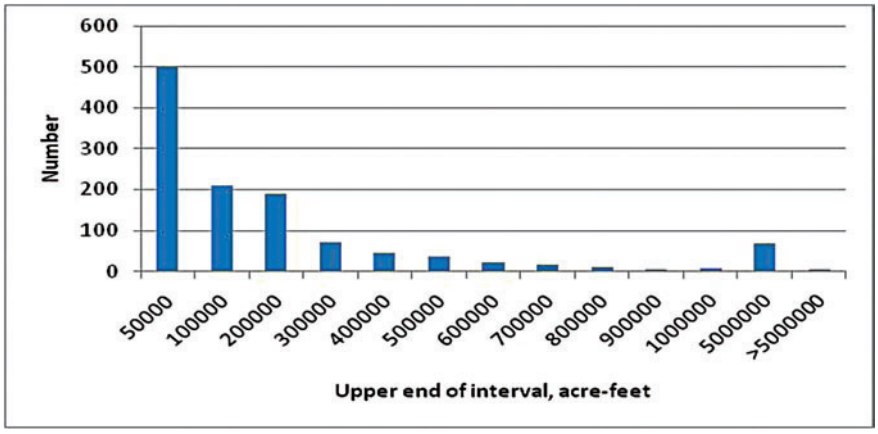

Figure 4.3. Storage volume size distribution of 1196 reservoirs.

Normal storage capacities were then aggregated at the ASR level such that the storage volume of each ASR is the sum all of the storage volumes (among the final 1196 reservoirs) that fall within the ASR borders. Normal storage volumes of the ASRs vary from 0 (ASR 1602) to over 40 million acre-ft (ASR 1005). Thirteen ASRs have at least 10 million acre-ft of storage (Table 4.1).

The amount of stored water lost to evaporation in a given year was estimated by computing a surface area corresponding to the known storage volume and then multiplying that area by an evaporation rate. Because we aggregated reservoirs within an ASR and therefore lost details specific to each reservoir, global relationships were needed.

The basic approach used to determine ASR reservoir surface area was to develop regional area-to-volume relations for four large groups of ASRs. The groups were formed as groups of WRRs whose reservoirs exhibited relatively distinct area-to-volume relations. The groups ranged from those tending to have relatively shallow reservoirs to those tending to have relatively deep reservoirs (Figure 4.4). Area-to-volume relations were determined for each group by regressing normal surface area on normal storage volume across all reservoirs in the group.

Table 4.1. Normal surface areas and storage volumes of the ASRs.

ASR	Number of reservoirs	Surface area (km^2)	Storage volume (acre-feet)	Storage volume (hm^3)
101	53	2,983	9,161,932	11,301
102	11	303	339,694	419
103	1	14	114,000	141
104	4	280	1,450,200	1,789
105	14	270	1,069,773	1,320
106	1	7	3,500	4
201	14	271	1,914,887	2,362
202	9	100	880,684	1,086
203	6	70	950,208	1,172
204	11	184	1,533,703	1,892
205	8	108	731,648	902
206	1	7	33,700	42
207	8	337	4,763,164	5,875
301	9	441	2,635,134	3,250
302	12	2,295	10,745,641	13,255
303	14	2,024	13,326,110	16,437
304	12	228	498,205	615
305	1	15	33,324	41
306	10	781	4,450,780	5,490
307	15	847	5,292,915	6,529
308	14	400	2,521,472	3,110
309	2	145	387,538	478
401	7	185	374,031	461
402	7	1,049	2,361,175	2,912
404	11	185	255,805	316
405	8	108	105,470	130
406	1	5	17,780	22
407	1	18	69,500	86
408	17	1,711	4,910,008	6,056
501	14	199	1,198,789	1,479
502	22	610	3,481,610	4,294
503	13	123	540,130	666
504	5	44	399,690	493
505	18	615	3,601,434	4,442
506	16	185	781,314	964
507	9	875	6,347,200	7,829
601	20	758	6,560,611	8,092
602	8	1,250	5,422,900	6,689
701	19	1,161	1,272,053	1,569
702	30	1,036	2,597,039	3,203
703	18	950	1,867,580	2,304
704	16	490	1,576,975	1,945
705	9	378	1,293,851	1,596
801	4	214	803,180	991
802	27	970	4,875,232	6,014
803	6	60	85,600	106
901	27	1,567	3,115,572	3,843
1001	5	194	617,306	761
1002	11	445	4,658,098	5,746
1003	3	397	15,502,400	19,122

(continued)

Table 4.1 (Continued)

ASR	Number of reservoirs	Surface area (km^2)	Storage volume (acre-feet)	Storage volume (hm^3)
1004	7	269	3,059,354	3,774
1005	13	2,663	40,713,453	50,219
1006	4	646	4,232,535	5,221
1007	28	1,114	6,489,080	8,004
1008	6	63	365,996	451
1009	1	29	144,600	178
1010	18	722	3,191,245	3,936
1011	10	500	2,926,538	3,610
1101	6	694	10,585,000	13,056
1102	12	179	1,311,262	1,617
1103	8	239	1,098,580	1,355
1104	34	1,256	4,982,058	6,145
1105	17	729	4,309,899	5,316
1106	16	667	2,849,744	3,515
1107	41	1,688	6,626,673	8,174
1201	17	5,143	23,303,728	28,745
1202	28	1,524	8,222,684	10,143
1203	31	651	3,819,774	4,712
1204	19	643	4,206,219	5,188
1205	10	582	2,286,848	2,821
1302	9	516	5,729,860	7,068
1303	2	391	3,692,180	4,554
1304	3	114	310,384	383
1305	3	479	2,698,340	3,328
1401	13	375	5,631,191	6,946
1402	10	191	3,095,031	3,818
1403	4	730	28,874,500	35,616
1501	0	0	0	0
1502	5	1,029	30,508,313	37,631
1503	12	205	3,251,572	4,011
1601	6	93	774,780	956
1602	0	0	0	0
1603	4	88	260,800	322
1604	7	607	1,587,300	1,958
1701	15	1,220	11,989,814	14,789
1702	26	1,694	19,047,780	23,495
1703	36	1,426	12,754,945	15,733
1704	7	223	5,520,957	6,810
1705	20	325	6,208,326	7,658
1706	9	340	3,320,425	4,096
1707	4	61	85,190	105
1801	9	634	4,295,705	5,299
1802	31	1,454	23,556,700	29,057
1803	31	1,358	23,171,777	28,582
1804	4	46	663,983	819
1805	4	74	1,051,550	1,297
1806	12	108	2,273,358	2,804
1807	2	30	199,870	247
Total	1196	61,703	472,810,446	583,202

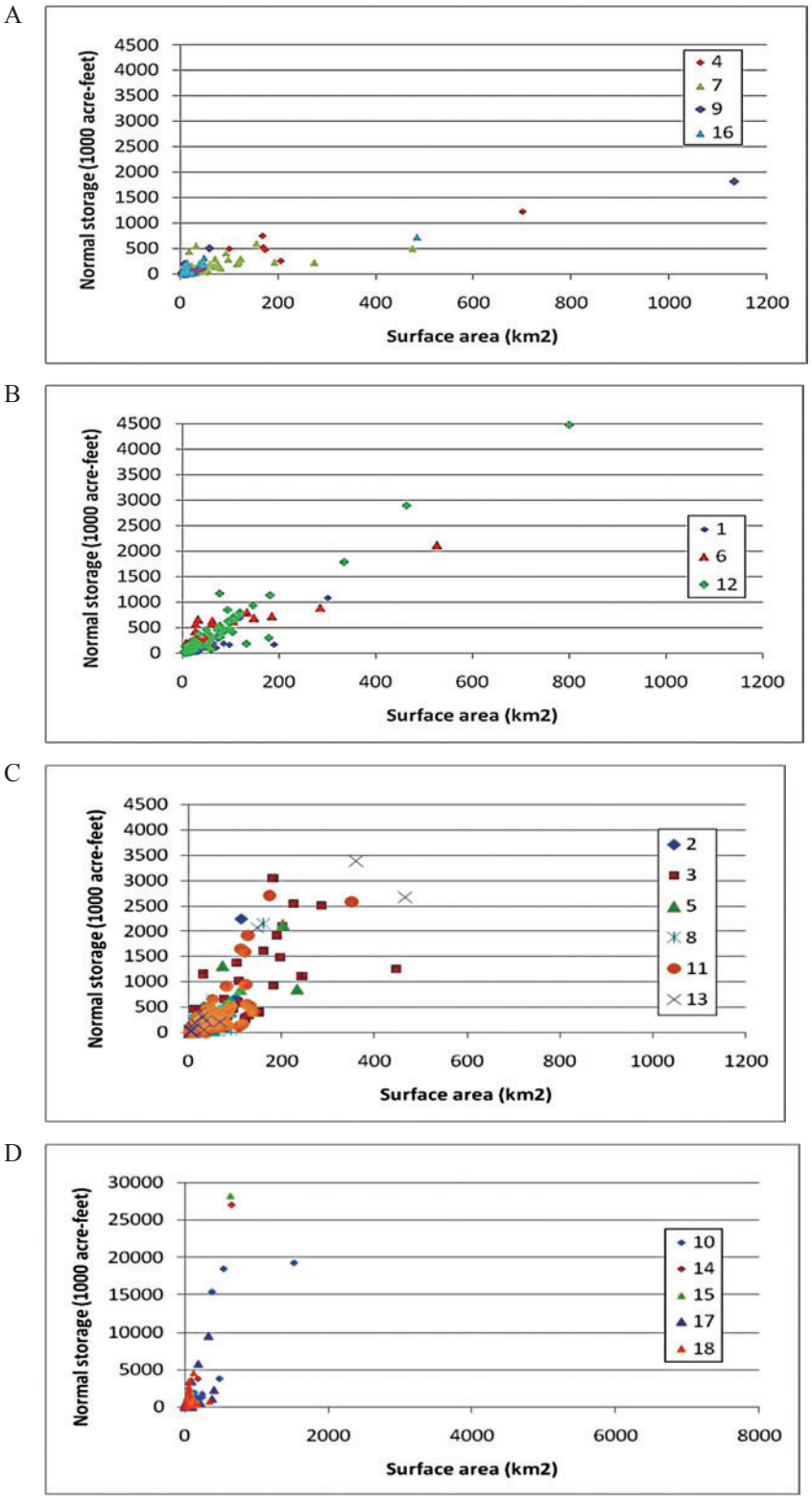

Figure 4.4. Reservoir area-to-volume relationships for groups of WRRs: (A) shallow; (B) medium group 1; (C) medium group 2: (D) deep.

For all regressions, the constant was fixed at zero, producing the slope coefficients listed in Table 4.2. All ASRs in a group were assigned the area-to-volume relation of its group. Individual evaporation rates for each ASR were set equal to the mean 1953-2005 potential evapotranspiration rate from a wet surface of all cells within the ASR.[10]

A separate approach was used for ASRs 1404 and 1503, in which Lakes Powell and Mead, respectively, make up nearly all of the storage capacity. Detailed surface area-to-storage relations were available for these reservoirs (Figure 4.5), as were average evaporation rates (Table 4.3).

Table 4.2. Reservoir categories characterization across the 18 WRRs.

Group	Description	WRRs	Slope coefficient
1	Shallow	4, 7, 9, 16	0.39660
2	Medium 1	1, 6, 12	0.14481
3	Medium2	2, 3, 5, 8, 11, 13	0.09032
4	Deep (without Powell and Mead)	10, 14, 15, 17, 18	0.03868
4	Deep (with Powell and Mead)	10, 14, 15, 17, 18	0.02777

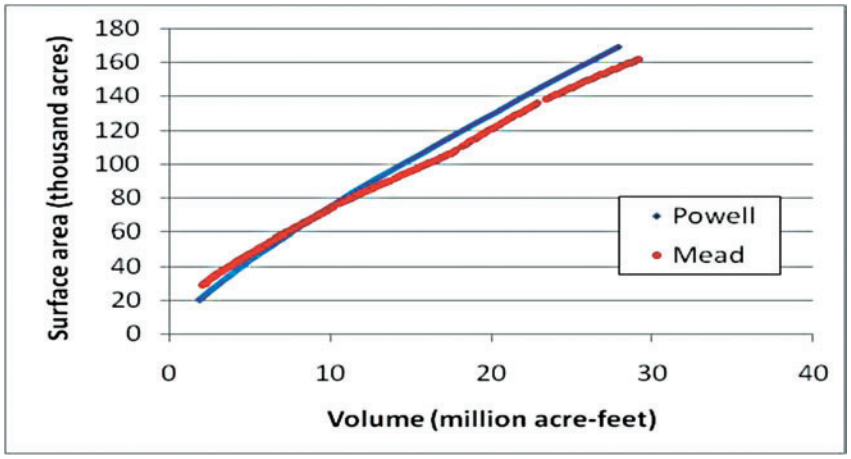

Figure 4.5. Surface area-to-storage relationships for Lakes Powell and Mead.

Table 4.3. Surface area-to-storage regression results for Lakes Powell and Mead and evaporation rates.

	Intercept (km^2)	Slope (km^2 /Mm^3)	Evaporation rate (m/yr)
Powell	59	0.01881	1.21
Mead	91	0.01613	1.98

4.4 Water Use Classes

Three classes of water use were included in the network simulations: in-stream flow requirements, trans-ASR diversions, and consumptive uses. Each of these classes was individually examined for each ASR, as explained in the following sections.

4.4.1 In-Stream Flow Requirements

In-stream flow requirements reflect the desire to leave some water in the stream for wildlife, fish, recreational activities, and aesthetic concerns. Ideally, the determination of a required minimum in-stream flow would be addressed locally in order to consider properly the biological and environmental characteristics of each ecosystem (Tharme 2003). Careful consideration of local stream characteristics is unrealistic at the ASR scale and beyond the scope of this study. In place of a more locally specified minimum flow, we adopted the general guideline provided by Tennant (1976) and specified the in-stream flow requirement as 10% of the average streamflow. Average streamflow was computed as the average total yield over the years 1953-1985. This constant amount was applied on an annual basis to both current and future conditions without adjusting for shifts in the average water yield due to potential climate changes.

4.4.2 Trans-ASR Diversions

Trans-basin diversions, which move water across basin divides, are common throughout the United States and especially common in arid regions. Typically, the amount of water diverted reflects long-standing legal agreements that specify the operating rules used to determine the diversion amount in a given year. Diversion amounts generally vary from year to year about a long-term average amount. Of course, the operating rules may also change over time. Because the operating rules differ from one diversion to the next and are not easily available, and because of the large number of such diversions, we adopted a simple procedure for including trans-ASR diversions in the network simulations, setting each trans-ASR diversion equal to a constant amount computed from data on past diversions.

Most of the information regarding water diversions was taken from two publications of the USGS regarding, respectively, the western (Petsch 1985) and the eastern (Mooty and Jeffcoat 1986) United States. These publications report on transfers between four-digit basins for 1982 and any prior years back to 1973, if available. From these data, we computed the average diversion across years 1980-1982. Information from these two sources was supplemented by more recent information for California (California Department of Water Resources 1998), Colorado (Colorado Water Conservation Board 1998, 2010; Litke and Appel 1989), the Lower Colorado River Basin (International Boundary and Water Commission 2004), and other locations from miscellaneous sources. Data for inter-basin transfers were aggregated at the ASR level in order to obtain an updated dataset of trans-ASR water diversions (Table 4.4). The trans-ASR diversion amount was held constant across all simulation years.

Table 4.4. Trans-ASR diversions.

ASR			
From	To	Acre-feet	$m^3 / 10^3$
102	103	899	1,109
104	105	1,084	1,337
105	102	580	716
201	202	1,474,267	1,818,427
201	207	56,900	70,183
202	104	617	761
203	201	898,170	1,107,844
204	203	44,311	54,655
204	408	635,644	784,033
206	205	213	263
301	205	6,702	8,267
301	302	12	15
306	303	67,345	83,066
307	306	8,350	10,299
307	308	11,550	14,246
309	308	100,000	123,345
402	401	1,617	1,994
404	704	2,231,913	2,752,943
408	201	7,860	9,695
501	502	23,314	28,757
502	506	63	78
502	601	1,077	1,328
503	502	4,142	5,109
505	506	101	125
506	503	1,477	1,822
507	505	662	817
507	601	508	627
602	308	3,300	4,070
602	507	492	607
702	402	3,620	4,465
801	602	43	53
801	1104	23,195	28,610
803	802	12,589	15,528
1008	1009	41,400	51,065
1009	703	83	102
1010	1011	697	859
1011	703	617	761
1011	704	309	381
1011	1101	11,607	14,317
1101	1104	7,720	9,523
1102	1007	20,000	24,669
1103	1010	169	208
1103	1104	23	28
1201	803	65,000	80,174
1201	1107	9,397	11,591
1302	1102	834	1,029
1401	1007	7,727	9,530

(continued)

Table 4.4. (Continued).

ASR			
From	To	Acre-feet	$m^3 / 10^3$
1401	1601	80,153	98,865
1402	1007	357,453	440,899
1402	1102	143,454	176,943
1402	1302	1,156	1,426
1402	1403	130,509	160,975
1403	1302	93,479	115,301
1501	1503	8,860	10,928
1502	1503	1,906,977	2,352,152
1502	1806	4,441,333	5,478,142
1503	1806	0	0
1502	8599 [a]	1,500,000	1,850,168
1503	8599	124,927	154,091
1603	1601	724	893
1604	1802	4,233	5,222
1702	1703	1,700	2,097
1703	1601	1,233	1,521
1704	1703	6,323	7,799
1801	1705	21,833	26,930
1801	1802	879,000	1,084,199
1801	1804	33,000	40,704
1802	1803	3,896,000	4,805,503
1802	1804	317,000	391,002
1802	1806	1,571,000	1,937,743
1802	1807	80,000	98,676
1803	1804	616,000	759,802
1803	1805	28,000	34,536
1803	1806	0	0
1807	1806	360,000	444,040

[a] Mexico

4.4.3 Consumptive use

Estimates of desired consumptive water use, also called water demand herein, were determined by ASR for past years (1985-2005) based on data from the USGS and for future years based on projections of water use drivers and rates of water withdrawal per unit of driver. Estimates of water demand were computed for the following five categories of final water use: domestic and public, industrial and commercial, thermoelectric, agricultural irrigation, and livestock and aquaculture. For simulation purposes, the estimates of the five categories were summed, providing an aggregate estimate of water demand. A full description of the estimation of water demand is found in Chapter 5.

4.5 Water Use Priorities

In the simulation of water allocation for the water networks, the three classes of water use were assigned distinct priorities that determine the order in which the classes are satisfied. In times of water abundance, the priorities have no practical impact as all uses are met, but in times of water shortage, the priorities determine whether uses are met, partially met, or not met.

Note that the five categories of consumptive water use were treated as a block and thus were assigned equal priority. Because of this simplification, we were unable to distinguish among the water use categories in time of shortage and cannot estimate how the shortage would affect each separate category. Although, in reality, the different water use categories may not suffer equally in times of shortage—the effect of shortage in a given ASR would actually reflect the distribution of water rights or existing water allocation rules—fully accounting for local water allocation arrangements was beyond the scope of this national study.

The three classes of water use were assigned priorities in the following order: in-stream flow requirements, trans-ASR diversions, and consumptive uses. Reservoir storage was given the next lower priority. This order of priority guarantees a minimal amount of water for environment and ecosystem needs before any other needs are met and satisfies major water diversion agreements before meeting local demands or storing water for future use.

Note that water uses belonging to the same class were assigned the same level of priority irrespective of their position in the network. For example, the in-stream flow constraint was satisfied in all ASRs within a network before other use classes were met in any ASR of the network. Thus, spatial position within a network (e.g., upstream versus downstream) had no effect on the priority with which uses were satisfied.

4.6 Network Simulation

Simulation of water allocation within each network was performed using the MODSIM (Labadie and others 1984) network simulation package. Network simulation provides annual values of water flows in any network link, storage levels for each ASR, amount of water lost due to reservoir evaporation, and amount of water assigned to each water use class.

The various aspects, assumptions, specifications, etc., of the network simulations that have been previously described, which allow simulation of water allocation within each network, are summarized here:

- Each ASR represents a node in the water network.
- Annual total water yield is accumulated over the entire ASR and is considered as a water input at the ASR node.
- Annual water supply for a given ASR is the sum of the annual water yield, water inflow from upstream ASRs, net water received from other ASRs via trans-ASR diversions, and water previously stored in the ASR.

- Water uses were grouped into three classes: in-stream flow requirements, trans-ASR diversions, and consumptive uses.
- Each water use class was assigned a different priority in the following order: in-stream flow requirements, trans-ASR diversions, and consumptive use.
- If ASR water yield plus contributions from upstream are insufficient to meet the requests of the three water classes in the ASR, water stored in the ASR is used, if available, irrespective of the location of the reservoirs and demands within the ASR.
- Any water in an ASR not needed to satisfy the within-ASR, diversion, or downstream requests of the three water classes is stored up to the total available storage capacity.
- Water that cannot be stored in the most downstream ASR is released to a network sink (an ocean, Mexico, or Canada).
- Water loss due to reservoir evaporation is estimated by assigning to each reservoir an area-volume relationship and multiplying aggregate reservoir surface area by an annual potential evaporation rate for the ASR.

Modeling demand and supply at the ASR level will fail to realistically represent conditions in some localized areas within an ASR. Perhaps the most likely instance of this scale-dependent failure is where a major demand area is located in the upper reaches of an ASR. Such a location would, in the absence of pumping water uphill, place the area upstream of the bulk of the water supply of the ASR, although in the simulation the full supply of the ASR would be available to meet demands within the ASR.

Chapter 5: Water Demand

5.1 Introduction

One approach to modeling future water demand is to estimate economic demand functions of future water use. Having such demand functions for every water basin, along with projections of water supply, we could solve for the amount of water that would be used. However, estimating demand functions for all relevant basins would be a large and complex undertaking and is beyond the scope of the current study. To the contrary, we attempt to limit complexity so that the underlying assumptions are relatively few and their impact on the results is transparent. Specifically, we project future water use under the assumption that water supply will be no more limiting to future use than it was to recent growth in use. We use the term "demand" to indicate the projections of desired future use, mindful that the projections are not economic estimates of demand as the term is used by economists. This approach is in keeping with our overall objective in this assessment, which is not to predict actual water use but rather to show where shortages are likely to occur in the absence of either new sources of supply or alterations in the normal progression of water demand.

The approach to projecting demand relies on estimating future water withdrawal rates (e.g., domestic withdrawal per person) by extrapolating from past trends in those rates and applying those future rates to estimates of the number of water using units (e.g., people). The estimates of withdrawal are then multiplied by consumptive use proportions to yield estimates of the amount of water consumed. It is projected consumptive use, also called demand, that is compared with water supply to indicate the vulnerability to water shortage.

Because past trends in water withdrawal rates reflect trends in factors affecting those rates (e.g., water yield and population), extrapolation of those past trends in withdrawal rates requires the assumption that the trends in factors affecting the rates will continue into the future. To the extent that future trends in such factors are different from those of the recent past (e.g., if water yields diminish in response to anomalous climatic changes), the projections of future water use will fail to equal actual use. Nevertheless, the projections serve the purpose pursued here, that of indicating where shortages are likely to occur in the absence of mitigation or adaptation.

Large-scale projections of water use in the United States have been attempted several times with little agreement (Table 5.1). Projections from the 1960s and early 1970s failed to notice, or sufficiently account for, the improving efficiency in industrial and thermoelectric water use that we now know was occurring as far back as 1960, and thus grossly over-estimated future water withdrawals. By the time of the Water Resource Council's 1978 projection (Table 5.1), ample data on the recent efficiency gains were available. However, the Council actually under-estimated year 2000 withdrawals, largely due to being overly optimistic about further improvements in water use efficiency in the manufacturing, thermoelectric, and irrigation sectors and under-estimating population growth. In 1989, Guldin erred in the other direction, over-estimating year 2000 withdrawals despite under-estimating future population, largely because he assumed no further gains in water use efficiency beyond those already achieved by 1985.[11] If the objective of projecting future use is to show what will happen if past trends

Table 5.1. Projections of U.S. water withdrawals for three future years based on medium or best guess assumptions, compared with actual withdrawals in year 2000, in bgd.[a]

	2000	2020	2040
Senate Select Committee (1961)	888		
Water Resources Council (1968)	804	1368	
Wollman and Bonem (1971)	563	897	
National Water Commission (1973)	1000	1425 [b]	
Water Resources Council (1978)	306		
Guldin (1989)	385	461	527
Brown (1999)	342	350	364
Actual (Hutson et al. 2004)	345		

[a] These estimates are for the 50 states, not just the contiguous 48 states.
[b] Midpoint of range reported.

continue unabated, rather than what will actually happen, these past efforts cannot be faulted for failing to more accurately estimate future use. Nevertheless, projections that fail to reflect past trends and how those trends are gradually changing are less than ideal tools for analyzing future possibilities.

By the late 1990s when Brown (1999 and 2000) projected future water use, a 35-year record of changes in the efficiency of water use provided a rich historical base for projections. Brown's projections for 2020 and 2040 (Table 5.1) are considerably below earlier projections (though not necessarily below what the Water Resources Council in 1978 would have projected if their projections had extended that far into the future). In light of expected further gains in water use efficiency, especially in the industrial, thermoelectric, and agricultural sectors, Brown's projections indicated a 10% increase in nationwide withdrawals by 2040 despite a 41% increase in population.

We now have a 45-year historical record from which to gage trends in water withdrawal rates and thus a better than ever opportunity to produce projections that realistically represent past trends. Using that record, this study projects future water use (both withdrawal and consumptive use) in the United States to 2090 by extending past trends in use in light of expected changes in major drivers of that use. This was first done assuming no change in future climate and then for three alternative future climates each modeled using three different GCMs (Table 2.3). These projections were made for the 98 ASRs comprising the contiguous United States (Figure 1.1).

5.2 Overview of the Methods

As previously mentioned, the approach taken here to project future water use relies, by and large, on extrapolation of past trends in water withdrawal rates and projections of drivers of water use. Considerable effort was devoted to estimating the effects of climate change and future liquid fuel energy goals on future water use. This overview is followed by sections on

each of the major components of the methods. Further details on the methods are presented in Appendix A.

The methods employed for projecting U.S. water withdrawals, with some exceptions, follow those of Brown (2000). In general, water withdrawal (W) for a given water use category and future year was estimated as:

$$W = U \cdot \Phi \tag{5.1}$$

where U is number of demand units such as a person for domestic use or an irrigated acre for agricultural use, and Φ is withdrawal per demand unit. Consumptive use (C) was then estimated by multiplying the estimate of withdrawal by a consumptive use proportion (γ) and adding future consumptive use attributable to climatic or other changes that is not reflected in data on past levels of water use (ΔC):

$$C = W \cdot \gamma + \Delta C \tag{5.2}$$

Estimates of future numbers of demand units (U) are grounded in data obtained from other sources when available (e.g., population), but are developed herein when necessary (e.g., irrigated acres). Estimates of withdrawal rates (Φ) are developed herein by extrapolation of past trends. Consumptive use proportions (γ) are based on data from the U.S. Geological Survey (USGS). Finally, estimates of future effects not captured by extrapolation of past trends rely heavily on projections of climate variables and energy development from other sources.

Knowledge of past trends is our most important asset in projecting how the future is likely to unfold. At a large spatial scale, water withdrawal rates in most cases have changed gradually, rather than abruptly, presenting orderly trends. Extrapolation is an accepted approach for projecting future conditions when the past trend has been orderly and in the absence of detailed knowledge of the underlying mechanisms affecting change or adequate data to model those mechanisms (Wilmoth 1998).

Past trends in the rates of water withdrawal (Φ), in most cases, have been nonlinear, with the rate of change gradually diminishing. Extrapolation of past trends in Φ was accomplished by applying an annual growth rate (g) based on data from recent years and a corresponding decay in that growth rate (d). The decay rate was chosen to attenuate the trend, leading gradually toward a hypothesized equilibrium level (which is not necessarily reached by 2090). Given a five-year time step for projecting withdrawals, the extrapolation procedure for a given year (Y) and Water Resource Region (WRR) is as follows:

$$\Phi_{WRR,Y} = \Phi_{WRR,Y-5}\left(1 + g_{DIV}\left(1 + d_{DIV}\right)^{Y-LDY}\right)^{5} \tag{5.3}$$

where LDY is the last year for which withdrawal data were available (typically 2005) and DIV is a major division of the United States, either the eastern portion or the western portion.[12] g and d typically were computed for major divisions of the United States rather than for each WRR because past trends for individual WRRs, as estimated using withdrawal data from the USGS circulars, are somewhat erratic. The annual growth factor (g) was computed from all or part of the record from 1985 to 2005.[13]

Estimates of water withdrawal and consumptive use were computed for all ASRs, but the factors used to produce those estimates (e.g., Φ or γ) were typically estimated at a larger spatial scale because data for ASRs are sometimes erratic—perhaps because of annual weather fluctuations or errors in estimation—so that they do not appear to support estimation at the smaller scale. Factors Φ and γ were estimated by WRR and applied to ASRs within the WRR. Similarly, *g* and *d* were estimated for eastern (specified as WRRs 1-9) and western (WRRs 10-18) divisions of the United States and typically applied to all ASRs within the division.

Water use was projected for six water use categories, also called water use sectors (Table 5.2). Total population was used directly as a factor in estimating future withdrawals for five of the water use categories and indirectly as a determinant of the sixth category, irrigated agriculture. In addition, electricity consumption was used to estimate thermoelectric water withdrawals, and irrigated acres were used to estimate future irrigation withdrawals. Still other factors were used to bridge the gap from *U* to Φ. For industrial and commercial water use, income per person was used to link population to withdrawal per dollar of income; for thermoelectric use, electricity consumption per person was used to link population to electricity use (with additional computations to account for the amount of total electricity supply provided at other than freshwater thermal plants).

To summarize, consumptive water use in an ASR in a given year (*Y*) was estimated as:

$$C_{ASR,Y} = C^{DP}_{ASR,Y} + C^{IC}_{ASR,Y} + C^{TF}_{ASR,Y} + C^{IR}_{ASR,Y} + C^{LS}_{ASR,Y} + C^{AQ}_{ASR,Y} \quad (5.4)$$

Table 5.2. Non-climatic factors used to project annual freshwater withdrawal.

Water use sector	Factor
Domestic and public (DP)	Population Withdrawal / person
Industrial and commercial (IC)	Population Dollars of income / person Withdrawal / dollar of income
Thermoelectric (TF)	Population Total electricity use / person Fresh thermoelectric production / total electricity production Withdrawal / fresh thermoelectric kWh produced
Irrigation (IR)	Acres irrigated Withdrawal / acre
Livestock (LS)	Population Withdrawal / person
Aquaculture (AQ)	Population Withdrawal / person

As will be seen in subsequent sections, the future water use estimates in the domestic and public (DP), freshwater thermoelectric (TF), and irrigation (IR) sectors are supplemented by effects of climate change on water use, and future use in the industrial and commercial (IC) sector is supplemented by water required to respond to renewable fuel goals.

Past shifts in Φ trends have occurred largely as a result of either legislation (e.g., the Energy Policy Act of 1992 and the Clean Water Act of 1972) or resource limitations (e.g., the shift of water away from irrigation in the West as new sources of supply became scarce as competition from other sectors grew). Of course, shifts are facilitated by technological innovation (e.g., the improving capacity for water reuse in the industrial sector and the shift from flood to sprinkler irrigation). Past trends reflect these shifts, but extrapolation of past trends will fail to reflect future shifts caused by unforeseen perturbations. In this study, we attempted to anticipate future climatic shifts by examining alternative future climates that may result from increasing levels of GHGs, but no attempt was made to anticipate perturbations from other sources, such as new legislation. Rather, to reiterate an earlier point, it is the purpose of this analysis, when combined with estimates of future supply, to point to the likelihood of, or need for, such perturbations.

The following methodological sections describe: (1) the USGS withdrawal data; (2) major drivers of water use, some of which vary by climate scenario; (3) past and projected water withdrawal rates assuming a constant climate; (4) effects on future water use of liquid fuel production; (5) effects on future water use of climate change; and (6) estimation of consumptive water use factors. Following the methods, we summarize the results.

5.3 USGS Water Use Data

Future freshwater use, both withdrawal (surface and ground water together) and consumptive use, were projected based most importantly on withdrawal data for 1960-2005 and consumptive use data for 1985-1995 from the USGS. The USGS compiled water use data quinquennially for the period 1960-2005 and presented findings in the following circulars: MacKichan and Kammerer (1961), Murray (1968), Murray and Reeves (1972, 1977), Solley and others (1983; 1988; 1993, 1998), Hutson and others (2004), and Kenny and others (2009). These USGS reports represent the only consistent effort to periodically document water use for the entire nation.[14] The circulars cover in-stream use at hydroelectric plants; withdrawals to off-stream users; and, for all but the year 2000 and 2005 estimates, consumptive use (pre-1985 estimates of consumptive use are not used herein). The circulars report estimated water use from three principal sources: ground water, fresh surface water, and saline water.

The procedures used by the USGS to report on water use have changed over the years. For the period 1960-1980, the circulars estimated water use for states and WRRs. For the period 1985-1995, the circulars (or the data available with the circulars) estimated water use for counties (and therefore states) and eight-digit watersheds (and therefore WRRs). However, beginning with the year 2000 circular, reporting by watershed or WRR was discontinued—forcing studies focused on watersheds, like this one, to adapt county data to watershed boundaries.

Likewise, the variables for which water use was reported have changed over the years. In 1985, the USGS adopted more detailed water use categories, and then in 2000, some of those new categories were discontinued and others were changed. To obtain a minimum number of consistent categories for the entire 1960-2005 period, the finer distinctions introduced in 1985 were not used. Further, self supplies (water withdrawn by the user) and public supplies (water delivered by a municipality or water company) were combined, as the source of supply was not an important distinction in this study; the sum is called a "withdrawal" herein. We are concerned only with freshwater, not saline water. Thus, the following categories were chosen: (1) domestic and public (public-supplied and self-supplied; DP), (2) industrial and commercial (public-supplied and self-supplied) and mining (self-supplied; IC), (3) freshwater thermoelectric power (public-supplied and self-supplied; TF), (4) irrigation (self-supplied; IR), (5) livestock (self-supplied; LS), and (6) aquaculture (self-supplied; AQ) (when the LS and AQ categories are combined for presentation, the joint category is labeled LA). The "public" in "domestic and public" refers to use in government offices, public parks, and fire fighting, and to losses in the public supply distribution system. "Irrigation" consists mainly of crop irrigation but also includes self-supplied irrigation of parks, golf courses, turf farms, and other large irrigated landscape areas when not included as part of public or industrial and commercial water use.

The source and scale of the data used to estimate the factors listed in Table 5.2 are summarized in Table 5.3. Data for 1960-1980 were summarized by WRR only, based on the USGS circular data; no attempt was made to examine withdrawals at the ASR level for this early period. For 1985-1995, data from the USGS circulars at the eight-digit basin level allowed easy summation to the ASR and WRR levels. For years 2000 and 2005, county-level water use estimates were allocated to ASRs (and thus to the WRRs) using procedures described in Appendix A. Φ and γ were computed by WRR rather than by ASR because, as previously mentioned, trends in Φ and γ for individual ASRs were often erratic and difficult to interpret.

5.4 Principal Socioeconomic and Climatic Drivers of Water Use

The major socioeconomic drives of water use for the approach adopted here are population, income (as a measure of economic growth), electricity consumption, and irrigated acres (Table 5.2). The climatic drivers are temperature, precipitation, and potential evapotranspiration. Trends and projections in these drivers are described in the following subsections.

5.4.1 Population

The A1B scenario most clearly represents a continuation of business as usual in U.S. population growth. Because the IPCC emission scenarios were developed in the late 1990s, they do not incorporate the 2000 U.S. census. Thus, the U.S. Census Bureau's (2004) national moderate population projection to 2050 was accepted as an update of the original A1B scenario for population. The Census Bureau projection expects a higher population than the original A1B scenario, for which the 1990 census was the most recently available. The Census Bureau projection was then extended to 2090, and the IPCC population projections for scenarios A2 and B2 were updated based on the difference between the original A1B scenario and the Census Bureau projection (Zarnoch and others 2008).

Table 5.3. Source and scale of data used for projecting future freshwater use.[a]

Variable	Estimates for years (at five-year intervals):			
	1960-1980	1985-1995	2000-2005	2010-2090
Water withdrawal, all uses	By WRR from USGS[b]	By HUC8 from USGS[d]	By county from USGS	Must be estimated
Consumptive use proportion, all uses	Not used[c]	By WRR from USGS	Must be estimated	Must be estimated
Population	By WRR from USGS	By county from USGS[e]	By census tract from Census Bureau	By county from Zarnoch et al. (2008)
Personal income (2006 $)	By county from BEA	By county from BEA	By county from BEA	By county from Torgerson (2007) and population
Electrical energy produced at thermoelectric plants	Not available	By HUC8 from USGS	Must be estimated	Must be estimated
Electrical energy produced at hydroelectric plants	Not available	By HUC8 from USGS	Must be estimated	Must be estimated
Water withdrawal thermal saltwater plants	Not available	By HUC8 from USGS	Not needed	Not needed
Acres irrigated	By WRR from USGS	By HUC8 from USGS	By county from USGS	Must be estimated
Temperature			PRISM	Downscaled GCM estimates
Precipitation			PRISM	Downscaled GCM estimates
Potential evapotranspiration			Computed from temperature	Computed from temperature

Notes:
[a] In some cases data are available at a finer geographical scale than listed here (for example, the USGS estimated consumptive use by HUC8 for 1985-1995). Listed here is the spatial scale at which the data were used. In some cases an aggregate estimate applied to all basins within the aggregation.
[b] In all cases "from USGS" refers to the USGS water use circulars or to the publically-available data supporting those circulars.
[c] Data are available for WRRs from the USGS, but these data are not used.
[d] To avoid apparent problems with the 1985 HUC8 estimates of livestock withdrawal, the county data for livestock withdrawal was used for 1985-1995.
[e] The 1985 and to a lesser extent the 1990 data by HUC8 from USGS are questionable (there are odd differences with the 1995 data). The apparent problem with the HUC8 population data was avoided by using the USGS county data and applying the year 2000 census tract assignments of counties to ASRs to estimate ASR population.

The U.S. population rose from 177 million people in 1960 to 280 million in 2000 along a nearly linear trend (Figure 2.1). The updated A1B scenario assumes a continuation of that past linear trend, with population reaching 444 million people in 2060.[15] As the linear trend implies, the growth rate is gradually declining. For example, the average annual growth rate was 1.16% from 1960 to 2000 and is projected to be 0.87% from 2000 to 2020, 0.77% from 2020 to 2040, and 0.66% from 2040 to 2060. Scenario A2 anticipates a higher rate of population growth, with population reaching 504 million people in 2060. Scenario B2, however, anticipates slower population growth, with population reaching 396 million people in 2060. The projected populations of the three scenarios begin diverging significantly in about 2030 (Figure 2.1). The projected average annual growth rates from 2000 to 2060 are 0.77%, 0.97%, and 0.57% for scenarios A1B, A2, and B2, respectively.

County-level population projections for the three scenarios were prepared by Zarnoch and others (2008). Briefly, their procedure was to disaggregate the national projections for the three scenarios to the county level for the years 2010 to 2030 based on county shares computed from the projections of county population to 2030 provided by Woods&Poole Economics (2007) and then extend the county-level projections to 2060 based on estimates of prior (2020 to 2030) county-level population growth rates, with the sums of the county estimates constrained to equal the national projections. The county-level projections relate to the U.S. Census Bureau projection of national population (essentially, the A1B scenario). Of course, applying the county shares from the A1B scenario to the other two scenarios requires the assumption of proportional county-level population change across scenarios. The projections were extended to 2090 using the population growth rates implied by the IPCC projections for the United States for the three scenarios.

To allocate county population estimates to ASRs, the Water Resources Council (1978) simply assigned each county to an ASR, a procedure that introduced error because county boundaries rarely coincide with watershed boundaries.[16] Because population tends to be concentrated in unevenly distributed urban areas, allocating county population estimates to ASRs based on area-weighting at the county level is also problematic. To allocate estimates of county population to ASRs, year 2000 census tract data were used. Given the 78,918 census tracts in the 48 contiguous states, there are 387 census tracts per ASR on average, allowing for a fairly accurate apportionment of population to ASRs. Specifically, county population estimates for 2005-2090 were assigned to ASRs based on the proportions (z) of a county's population located in each ASR in year 2000 as follows:

$$\rho_{ASR,Y} = \sum_{j} \left[\rho_{j,Y} \cdot z_{ASR,j,2000} \right] \tag{5.5}$$

where ρ is population and j indicates county.[17] z was computed from year 2000 census tract data using a simple area-weighted procedure for tracts spanning ASR boundaries.[18] Of course, the further into the future the ρs are applied, the less accurate they become because population growth will not occur uniformly across all census tracts.

5.4.2 Income

As with population, the economic growth projections of the IPCC scenarios, having been developed in the late 1990s, are somewhat dated. To estimate future disposable personal income (DPI) for the A1B scenario, which is assumed to represent a business as usual future, the original IPCC A1B economic growth projection was replaced with one based on more recent U.S. information and modeling assumptions. The procedure for accomplishing this began with a national-level estimate of DPI for 2006 from the Bureau of Economic Analysis, to which were applied estimates of future growth rates estimated for the 2010 RPA Assessment by the Economic Research Service (Torgerson 2007). Those annual rates, of 2.9% for years 2006 to 2017 and 2.1% for years 2018 to 2060 (in real terms), were produced by runs of a standard macroeconomic model of the U.S. economy, and incorporate assumptions about interest rates, inflation, growth of the labor force, international trade, and technological change, among other things. The A2 and B2 projections of DPI were then estimated as proportions of the A1B projection, with the proportions set equal to the proportional differences in Gross Domestic Product (GDP) across the three scenarios as provided by the IPCC (the IPCC did not estimate future personal income). These estimates of DPI were converted to personal income assuming that DPI is 89% of PI.

Personal income in the United States rose from about $3.5 to $10.5 trillion from 1960 to 2000 in 2006 dollars (Figure 2.2), which translates to an annual growth rate over those 45 years of 2.50% (the growth rate was 2.40% from 1960 to 1980 and 2.86% from 1980 to 2000). Scenario A1B assumes the future growth rates previously listed (initially 2.9% and then 2.1%), yielding an overall average growth rate of 2.24% per annum for the 55-year period from 2005 to 2060, with total personal income reaching $35.8 trillion in 2060 (Figure 2.2). Scenario A2 anticipates lower future growth (1.80% per year on average), resulting in total personal income of $28.1 trillion in 2060, whereas scenario B2 exhibits an initial high growth rate that then diminishes substantially for an overall average growth rate of 1.49% from 2000 to 2060 and a final total personal income in 2060 of $23.8 trillion. The projections were extended to 2090 using the per-capita income growth rates implied by the IPCC projections for the United States.

County-level DPI projections were derived using the national-level DPI projection and the county-level population projection, discussed in the previous section, in combination with county-level 2006 per-capita personal income (PCPI) figures. The procedure was to compute the county share of national personal income based on 2006 data and multiply that proportional share by the national projection of DPI for the given year, as follows:

$$DPI_{j,Y} = \frac{\rho_{j,Y} \cdot PCPI_{j,2006}}{\sum_{j}\left(\rho_{j,Y} \cdot PCPI_{j,2006}\right)} DPI_{US,Y} \qquad (5.6)$$

where ρ is population, j indicates county, and $DPI_{US,Y}$ is personal income in the United States in year Y. This procedure implicitly assumes that both the relative per-capita income levels between counties and their relative tax rates (and thus the difference between personal income and disposable income) remain constant throughout the projection period.

To allocate county DPI to ASRs, the 2000 census tract information was used as previously explained for population.

5.4.3 Electric Energy

Future freshwater use in the electric energy sector depends most importantly on how much electricity will be produced at freshwater thermoelectric plants. The basic approach used here to project electricity output at freshwater thermoelectric plants was to estimate total consumption of electricity and then determine the portion of that consumption that is likely to be supplied at other than freshwater thermoelectric plants, the difference being the projected production at freshwater thermoelectric plants. An underlying assumption is that total national production equals consumption, although this equality need not hold at the ASR scale.

The procedure begins with a national-level projection of total per-capita electricity consumption, which is applied to each WRR. Application of the national rate of growth in per-capita consumption to the WRRs allows computation of electricity production in each WRR to reflect projected population growth in the WRR while still conforming to the overall expected change in per-capita electricity use. The base (year 2005) per-capita production rate that the growth rate is applied to differs considerably across WRRs, reflecting factors such as the location of major thermoelectric or hydroelectric plants, and how demand from heavy industry is distributed across the WRRs. Thus, this approach assumes that WRRs that produce a disproportionate share of the U.S. electricity supply will continue to do so. The WRR totals for a given future year were then allocated to ASRs within a WRR based on the proportion of thermoelectric withdrawal in the WRR that occurred in the ASR in 1995 (1995 being the last year for which the USGS released thermoelectric withdrawal data by eight-digit basin).

In order to maintain comparability between estimates of energy production and water use in that production, we use the energy production estimates from the USGS water use circulars rather than those from the Department of Energy.[19] The USGS data show that per-capita electric energy use in the United States rose from 4244 kWh per year in 1960 to 11,792 in 2005.[20] The growth in per-capita electricity use appears to have occurred in three stages, each of about 15 years in length (Figure 5.1). From 1960 to 1975, per-capita electric energy use rose at an average annual rate of 5.4%; from 1975 to 1990, it rose at an average annual rate of 1.2%;

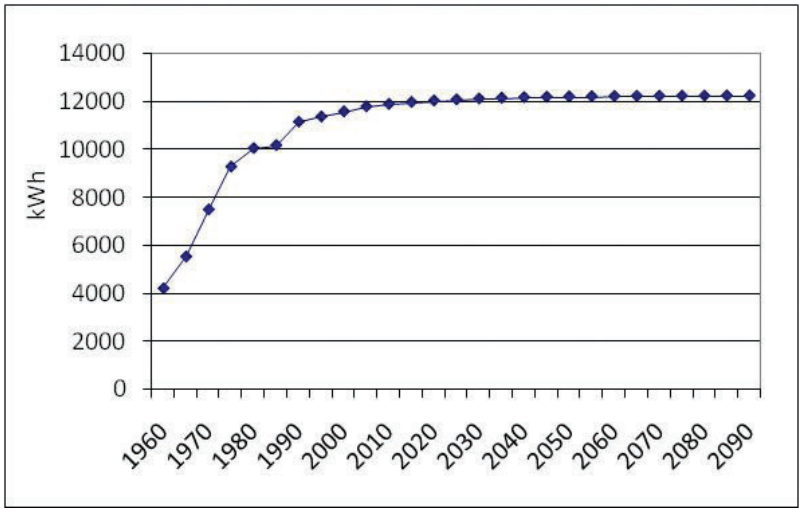

Figure 5.1. Annual electricity consumption per capita.

and from 1990 to 2005, it rose at an average annual rate of 0.37%. The gradually decreasing growth rate is assumed to result from improvement in the energy efficiency of electric appliances and the gradual loss of manufacturing plants in the United States. In keeping with this decreasing trend, future total electric energy use was modeled using equation 5.3 with *g* set at the 1990-2005 annual growth rate of 0.0037 and a decay rate (*d*) of -0.05 (Table 5.4). Per-capita annual electricity use is thus projected to rise from 11792 in 2005 to 12245 in 2060, by which time the growth rate will have dropped nearly to zero (Figure 5.1), for an average annual growth rate of 0.10% from 2005 to 2035 and of 0.02% from 2035 to 2060.[21]

Electricity is produced at freshwater thermoelectric, saltwater thermoelectric, and hydroelectric plants, and at a variety of other plants using renewable energy sources, including solar, wind, and geothermal plants, and plants burning wood and other biomass or municipal waste. From 1960 to 2005, there was relatively little growth in production at hydroelectric and other renewable plants, such that production at thermoelectric plants grew at an impressive rate in response to population growth and the increasing per-capita use rate (Figure 5.2; note that Figure 5.2 is for the entire United States, not just the contiguous states). However, production at other (non-hydroelectric) renewable plants is expected to grow rapidly in the near future. Projections of future electricity production in the United States to 2035 at hydroelectric and other renewable plants were taken from the Energy Information Administration's Annual Energy Outlook (EIA 2010).[22] Production at hydroelectric plants is projected to remain

Table 5.4. Driving factor extrapolation coefficients.

	Electricity consumption per capita	Other renewable electricity production	Irrigated area
Eastern DIV			
G	0.0037	0.0265	0.0253
D	-0.0500	-0.0300	-0.0350[a]
Western DIV			
G	0.0037	0.0265	-0.0021
D	-0.0500	-0.0300	-0.0100[b]

[a] WRRs 3, 8, and 9 set at -0.09, -0.08, and -0.07, respectively.
[b] WRR 10 set at -0.05.

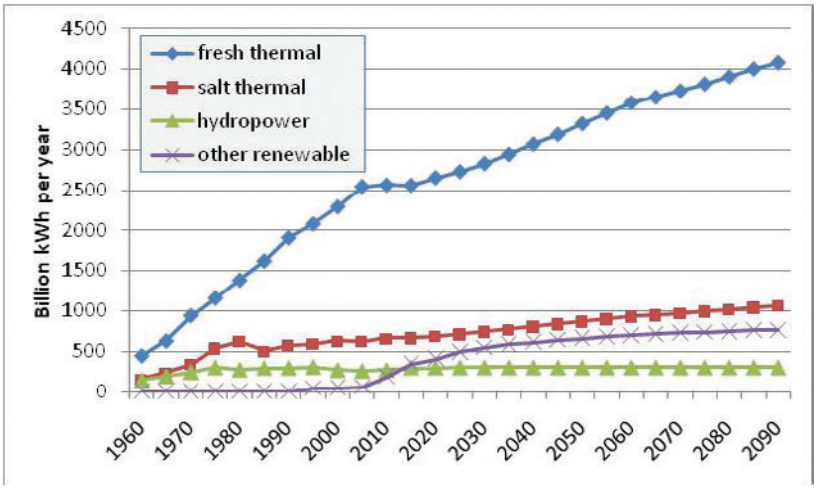

Figure 5.2. Past and projected annual U.S. electricity production.

roughly at its current level into the future, as the modest additions to capacity serve only to replace losses, but production at other renewable plants is expected to rise sharply, from 61 billion kWh in 2005 to 589 billion kWh in 2035 (Figure 5.2).[23] Projections beyond 2035 at other renewable plants are intended to extend the EIA projected trends, and were implemented by extrapolation using equation 5.3 with the growth rate *g* set at 0.0265 (reflecting 2.65%, the average annual rate of the EIA projection from 2015 and 2035) and *d* set at -0.03 (Table 5.4). With this extrapolation, U.S. production at other renewable plants reaches 763 billion kWh in 2060 (Figure 5.2).

The difference between total electricity production and production at hydroelectric and other renewable plants determines the production at thermal plants. The proportion of future thermal production that will occur at freshwater (as opposed to saltwater) plants was assumed to remain at the average proportion for years 2000 and 2005, as estimated from the USGS water use data. Given these assumptions, electricity production at freshwater thermoelectric plants is projected to remain fairly flat from 2005 to 2015 (in response to the depressed economy and the rapid growth in production at other renewable plants) and then grow along a nearly linear projection to 2060, assuming the A1B population projection (Figure 5.2). This electricity projection translates to an average annual growth rate of 0.72% from 2015 to 2060.[24]

5.4.4 Irrigated Area

Nationally, irrigated area grew rapidly (at an average annual growth rate of 1.6%) from 1960 to 1980, was relatively stable from 1980 to 1995, and took another jump from 1995 to 2000. However, a closer look reveals a geographical difference in irrigated area trends (Figure 5.3). Irrigated area in the arid and semi-arid western states (WRRs 10-18), where most irrigation occurs, grew at an average annual rate of 1.5% from 1960 to 1980, then dropped at an average annual rate of 0.55% from 1980 to 1995, with little net change between 1995 and 2005. The drop occurred as farmers sold some of their land or water to cities, industries, and

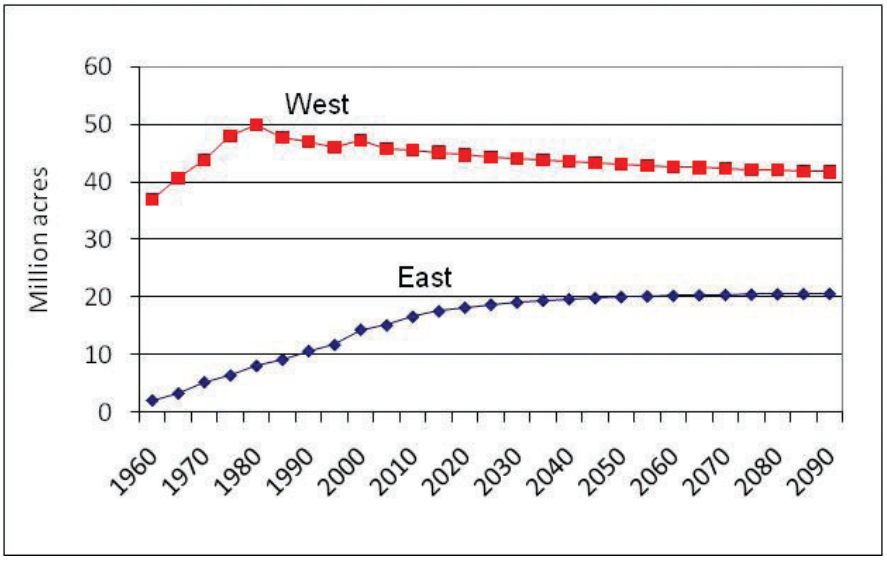

Figure 5.3. U.S. irrigated area.

rural domestic users, and as pumping costs, crop prices, and Government incentive programs caused marginal lands to be removed from irrigation. Meanwhile, irrigated area in the eastern states (WRRs 1-9) grew continuously from 1960 to 2005, at an average annual rate of 4.5%, as farmers moved to rely more on irrigation water to supplement precipitation during dry times in order to reduce variability in yields and product quality (Moore and others 1990).[25]

Projecting irrigated area is complicated by the sheer number of factors that affect agricultural area in general and irrigated area in particular.[26] Agricultural area is affected by population growth (as increases in population both increase demand for crops and, via urban expansion, decrease the supply of arable land), crop yield per unit area (and thus by genetic and other technological improvements), international markets, Federal agricultural policies and related subsidies, and pests and disease, among other factors. Irrigated area is further affected by energy prices (via their effect on pumping costs), irrigation technologies, in-stream flow concerns, and precipitation variations. In addition, irrigated area responds to the fact that irrigation is generally a lower-valued use of water at the margin than most other uses—most of the recent water trades in the Western states, for example, have been from agriculture to municipal and industrial uses (Brown 2006)—so that withdrawals for irrigation are partially a function of water use in the more highly valued uses.

In light of the difficulty of accounting for all these factors, irrigated area was projected by extrapolating from past trends using the coefficients listed in Table 5.4. Irrigated area in the West is projected to continue the downward trend begun in the early 1980s, dropping from 45.8 million acres in 2005 to 42.4 million acres in 2060, for an average annual decline of 0.14% (Figure 5.3). In the East, irrigated area is projected to continue to increase, at a decreasing rate, from 15.2 million acres in 2005 to 20.3 million acres in 2060, for an average annual increase of 0.50%. Total irrigated area is projected to peak in 2040 at 62.6 million acres and drop to 62.3 million acres in 2060. These projections do not include the effects of meeting the recently established renewable fuel standards. As seen below, meeting those goals would increase irrigated area slightly.

5.5 Water Withdrawal Rates: Trends and Projections

The water withdrawal rates (Φ) described in this section include domestic and public withdrawal per capita, industrial and commercial withdrawal per dollar of income, thermoelectric withdrawal per kWh of electricity produced, irrigation withdrawal per irrigated acre, and livestock and aquaculture withdrawals per capita (Table 5.2).

To provide some context for considering trends in withdrawal per unit of water use driver, let us first examine total withdrawals as reported in the USGS circulars. Combining across all water use sectors, total U.S. withdrawals rose by 72% from 1960 to 1980, from 215 to 369 billion gallons per day (bgd), but have remained relatively constant since then, rising slowly from 332 bgd in 1985 to 349 bgd in 2000 and then dropping slightly to 347 bgd in 2005. The small change in total withdrawals during the past 20 years is remarkable in light of the fact that U.S. population rose during that period by 25% (from 236 million to 294 million).

These trends in total withdrawal—rapid rise followed by relative stability—are not shared by all water use categories. As seen in Figure 5.4, which shows withdrawal levels by sector from

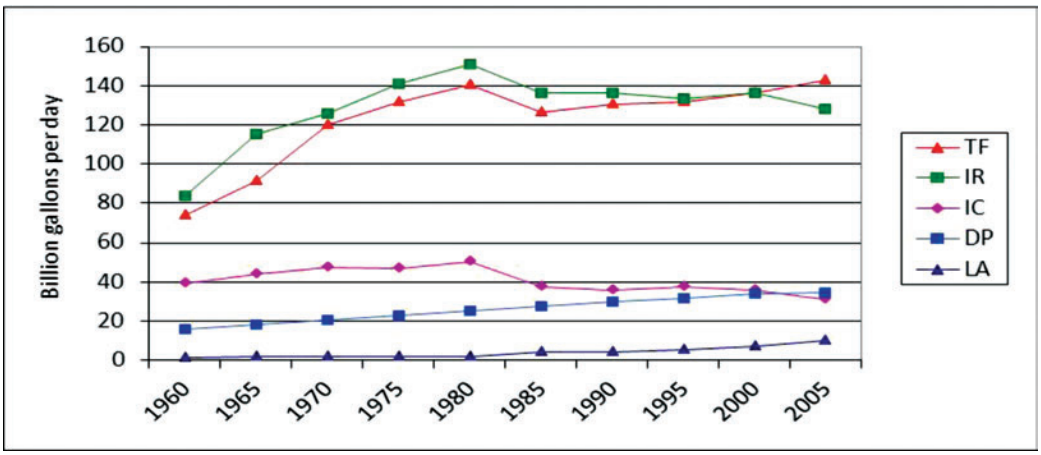

Figure 5.4. Past U.S. withdrawals.

the USGS circulars (with some rearrangements to maintain consistent water use categories over time), the rapid rise from 1960 to 1980 was due mainly to irrigation and thermoelectric uses. Meanwhile, the relative stability from 1985 to 2005 is attributable not only to the ending of the rapid rise in irrigation and thermoelectric withdrawals but also to the fact that declines in irrigation and industrial and commercial uses roughly balanced increases in thermoelectric, domestic and public, and livestock uses.[27]

The thermoelectric and agricultural sectors have consistently dominated national withdrawals, each with annual levels of roughly 130 bgd since 1985 (Figure 5.4). The IC and DP sectors form an intermediate group, with annual withdrawals ranging from about 30 to 37 bgd from 1990 to 2005. Finally, livestock and aquaculture withdrawals together reached 10 bgd in 2005, with recent increases largely attributable to growth in aquaculture. Interestingly, from 2000 to 2005 the thermoelectric and irrigation sectors switched places, with the thermoelectric sector passing the irrigation sector for the first time. Similarly, the IC and DP sectors switched places, with the DP sector passing the IC sector for the first time.

The trends in aggregate withdrawals sometimes belie the trends in withdrawal rates that underlie the aggregate withdrawals. As seen in the following subsections, total withdrawals may be rising although withdrawal rates are dropping. Findings are discussed here for the United States as a whole and separately for the East and West, based on rates computed at the WRR scale.

5.5.1 Domestic and Public Use

During most of the latter half of the Twentieth Century, U.S. average per-capita domestic and public water withdrawals steadily increased, from 89 gallons per day in 1960 to 122 in 1990. However, since 1990, the nationwide withdrawal rate has fluctuated between 118 and 122 gallons per day with the most recent change being a decrease from 121 gallons in 2000 to 118 in 2005 (Table 5.5).

Table 5.5. Average water withdrawal rates and electricity consumption for the United States [a].

Year	Φ^{DP} (g/p/d)	Φ^{IC} (g/$1000/d)	Φ^{TF} (g/kWh)	Φ^{IR} (depth in feet)	Φ^{LS} (g/p/d)	Φ^{AQ} (g/p/d)	E^{ρ} (kWh/p/d)
1960	89.6	11.3	60.5	2.40			11.6
1965	96.6	9.6	53.2	2.94			15.2
1970	102.8	11.0	46.6	2.87			20.6
1975	106.9	9.5	41.5	2.91			25.5
1980	112.3	9.0	37.0	2.91			27.6
1985	117.4	5.7	28.5	2.68			27.9
1990	121.8	4.8	25.0	2.64	9.0	9.1	30.6
1995	118.8	4.6	23.1	2.59	8.6	12.1	31.2
2000	121.2	3.6	21.7	2.48	8.2	17.8	31.7
2005	118.5	3.0	20.5	2.36	7.2	27.4	32.3
2010	117.5	2.7	19.1	2.32	7.0	31.3	32.6
2020	114.2	2.0	16.9	2.23	6.4	40.3	33.0
2030	111.9	1.7	15.3	2.16	6.0	45.5	33.2
2040	110.4	1.5	14.1	2.11	5.8	48.7	33.3
2050	109.3	1.4	13.1	2.08	5.6	50.7	33.4
2060	108.6	1.3	12.4	2.05	5.5	52.0	33.5
2070	107.8	1.2	11.9	2.03	5.5	52.6	33.5
2080	107.2	1.2	11.5	2.01	5.4	52.9	33.5
2090	106.8	1.2	11.2	2.00	5.4	53.1	33.5

[a] E^{ρ} is for the entire U.S., not just the coterminous U.S.

The increasing per-capita water use from 1960 to 1990 may be largely attributable to a decrease in average household size (Schefter 1990). People per household (i.e., per occupied housing unit) decreased from 3.4 in 1960 to 2.7 in 1995. Because a certain minimum level of water use per household is largely unrelated to household size, especially use for lawn and garden watering, per-capita use rises as household size drops. Other factors that contributed to the increase in per-capita water use are the conversion of older or rural households to complete plumbing, and the growing adoption of water-using appliances such as dishwashers, washing machines, swimming pools, and lawn sprinkler systems. These changes are consistent with the increasing real incomes and decreasing real domestic water prices that were experienced in many areas of the United States over the 1960-1990 period (Schefter 1990).

The leveling off of the per-capita domestic and public withdrawal rate may be the result of conservation education programs, the expansion of water metering to previously unmetered taps, and the use of more efficient plumbing fixtures in newer homes and renovations—in part pursuant to water use provisions of the Energy Policy Act of 1992 (public law 102-486)—plus the completion of the conversion to modern plumbing and the dwindling of the drop in household size (Brown 1999).

The leveling-off in U.S. domestic and public per-capita water withdrawals over the 1990-2005 period (Table 5.5) is mainly a Western phenomenon (Figure 5.5). In the East, withdrawal per person peaked in 1995 at 106 gallons per day and then dropped to 103 in 2000 and 99 in 2005 (Table 5.6). The drop from 1995 to 2005 translates to a growth rate of -0.66% per year. In the West, the trend in the withdrawal rate is still uncertain, as it has fluctuated in the vicinity of 150 gallons per day from 1985 to 2005, without clear indication that

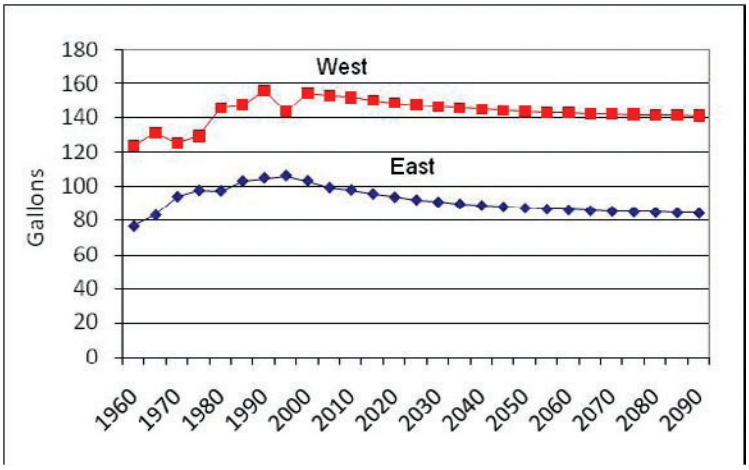

Figure 5.5. Domestic and public withdrawal per capita per day.

Table 5.6. Average water withdrawal rates across WRRs 1-9.

Year	Φ^{DP} (g/p/d)	Φ^{IC} (g/$1000/d)	Φ^{TF} (g/kWh)	Φ^{IR} (depth in feet)	Φ^{LS} (g/p/d)	Φ^{AQ} (g/p/d)
1960	76.9	12.8		1.01		
1965	83.2	11.0		1.87		
1970	94.0	12.8		1.29		
1975	97.6	10.9		1.48		
1980	97.4	10.1		1.76		
1985	102.9	6.6	34.8	1.28		
1990	104.7	5.4	30.8	1.39	4.8	8.6
1995	106.0	5.0	28.1	1.37	4.8	8.2
2000	103.1	4.0	26.0	1.41	4.4	10.1
2005	99.2	3.5	24.4	1.33	4.3	19.0
2010	97.9	3.1	22.9	1.34	4.3	20.4
2020	93.8	2.4	20.4	1.33	4.1	27.0
2030	90.9	2.1	18.6	1.32	4.0	31.9
2040	88.8	1.8	17.2	1.31	3.9	35.3
2050	87.3	1.7	16.2	1.31	3.9	37.6
2060	86.2	1.6	15.4	1.30	3.9	39.2
2070	85.4	1.5	14.8	1.30	3.9	40.1
2080	84.8	1.5	14.3	1.29	3.8	40.6
2090	84.3	1.5	13.9	1.29	3.8	40.9

it will continue on the slight downward trend observed from 2000 to 2005 (Table 5.7). The drop from 2000 to 2005 translates to an annual growth rate of -0.21%. Based on the more obvious recent downward trend in the East, it is assumed here that the rate in the West will continue to decline. The growth rate (g) for the East (-0.0066) was based on the change from 1995 to 2005, but the growth rate for the West was set at -0.0035, a level in between the Eastern rate and the recent (2000-2005) Western rate, based on the expectation of continuing conservation efforts in the West. Decay rates (d) were chosen, as previously explained, to gradually diminish the rate of change (Table 5.8). The resulting water withdrawal rates through 2090 are shown in Figure 5.5 and listed in Tables 5.6 and 5.7.

Table 5.7. Average water withdrawal rates across WRRs 10-18.

Year	Φ^{DP} (g/p/d)	Φ^{IC} (g/$1000/d)	Φ^{TF} (g/kWh)	Φ^{IR} (depth in feet)	Φ^{LS} (g/p/d)	Φ^{AQ} (g/p/d)
1960	124.0	7.6		2.48		
1965	131.1	6.1		3.02		
1970	125.2	6.4		3.06		
1975	129.5	6.2		3.10		
1980	145.9	6.6		3.10		
1985	147.7	3.9	13.6	2.95		
1990	156.1	3.4	12.3	2.93	17.3	9.9
1995	143.7	3.8	12.1	2.91	16.0	19.7
2000	155.0	2.9	11.8	2.80	15.4	32.3
2005	153.4	2.1	11.0	2.70	12.5	42.7
2010	152.1	1.9	10.3	2.68	11.9	50.4
2020	148.9	1.3	9.3	2.59	10.2	62.9
2030	146.7	1.1	8.5	2.52	9.3	68.0
2040	145.0	0.9	7.9	2.47	8.7	70.0
2050	143.8	0.8	7.4	2.43	8.3	71.0
2060	142.9	0.8	7.0	2.40	8.0	71.6
2070	142.1	0.8	6.9	2.38	7.9	71.7
2080	141.6	0.7	6.7	2.36	7.8	71.7
2090	141.2	0.7	6.6	2.35	7.7	71.7

Table 5.8. Water withdrawal rate extrapolation coefficients.

	DP	*IC*	*TF*	*IR*	*LS*	*AQ*
Eastern DIV						
g	-0.0066	-0.0369	-0.0176	0.0000	-0.0069	0.0540
d	-0.0300	-0.0350	-0.0200	0.0000	-0.0400	-0.0500
Western DIV						
g	-0.0035	-0.0578	-0.0106	-0.0044	-0.0218	0.0804
d	-0.0300	-0.0420	-0.0200	-0.0250	-0.0400	-0.1000

5.5.2 Industrial and Commercial Use

Because of the great variety of outputs of the industrial and commercial sectors, relating water use to units of physical output is unrealistic. Instead, an economic measure of total output, personal income, was used. In year 2006 dollars, withdrawal per day per $1000 of total personal income in the United States declined steadily from 11 gallons in 1970 to about 3 gallons in 2005 (Table 5.5). The drop in withdrawal per dollar of income is largely attributable to changes in the type and quantity of industrial and commercial outputs, such as a shift from water intensive manufacturing and other heavy industrial activity to service oriented businesses, and to enhanced efficiency of water use. Efficiency improved in response to such factors as environmental pollution legislation (e.g., the Clean Water Act of 1972 and its amendments), which regulated discharges and thereby encouraged reductions in withdrawals (made possible by modifying production process and recycling withdrawn water), and technological advances facilitating recycling (David 1990). Most recent data show that the rate of decrease in water withdrawal per dollar of income has slackened somewhat (Figure 5.6).[28]

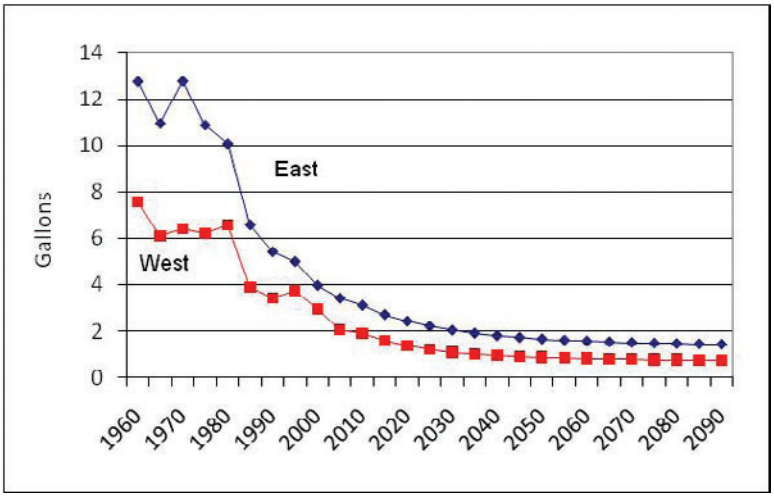

Figure 5.6. Industrial and commercial withdrawal per $1000 of income (2006 $).

The 2005 industrial and commercial withdrawal rates were 3.5 gallons per day per $1000 of income in the East and 2.1 gallons in the West, again in 2006 dollars (Tables 5.6 and 5.7). The larger rate in the East is attributable to the greater water availability and the greater prevalence of heavy manufacturing than in the West. From 1995 to 2005, the withdrawal rate in the East changed at an average rate of -3.7% per year, whereas the change in the West was -5.8% per year (Table 5.8). The reasons for past declines—loss of heavy manufacturing plants and ever-present environmental concerns—are likely to continue to play a role, suggesting that recent past trends are a good indication of future changes. It is assumed here that the rate from 1995 to 2005 will remain in place but will be attenuated gradually as the use rate approaches a minimum needed for operations. The resulting water withdrawal rates through 2090 are shown in Figure 5.6 and listed in Tables 5.6 and 5.7.

5.5.3 Thermoelectric Use

About 90% of the electric energy produced in the United States is generated at thermoelectric power plants, most of which use heat from nuclear fission or burning of fossil fuels (principally coal, natural gas, and oil) to produce steam to turn turbines (EIA 2009b). These plants require large amounts of water for condensing steam as it leaves the turbines, plus some additional water for equipment cooling and emissions scrubbing. Most plants use either a once-through or closed-loop cooling system.[29] In a once-through system, a large volume of water is withdrawn (usually from a river if the plant uses freshwater), used for condensing steam and other purposes, and returned to the source (at a higher temperature). Less than 5% of the withdrawn water evaporates (EIA 2009b; Feeley and others 2008). Once-through systems were once the preferred design, but few such plants have been built in recent decades because of concerns about water use, and they now account for only about 43% of total thermoelectric generating capacity in the United States (Feeley and others 2008). Closed-loop systems withdraw much less water than once-through systems and recycle that water, sending the condensed and cooling water to a cooling tower or pond for later reuse. Some water is evaporated

during each cycle, causing consumptive use per kWh produced at closed-loop plants to be 5 to 10 times greater than at once-through plants (Feeley and others 2008; Hoffman and others 2004). Closed-loop plants now account for about 56% of thermoelectric generating capacity.

Water withdrawals at U.S. thermoelectric plants rose rapidly from 1960 to 1980, but total withdrawals have risen much more slowly since 1985 (Figure 5.4). In contrast to the slow rise in total freshwater thermoelectric withdrawals from 1985 to 2005 (0.6% per year), electricity production at freshwater thermoelectric plants has risen at the much higher rate of 2.3% per year. Consequently, freshwater withdrawal per kWh produced (Φ^{TF}) has fallen in the United States, from 29 gallons in 1985 to 20 in 2005, for an annual rate of change of -1.6%. The improving efficiency of water withdrawals has occurred largely by greater reuse of withdrawn water, made possible by the aforementioned shift from once-through to recirculating plants.

Water withdrawal rates differ markedly between the East and West. The 2005 thermoelectric withdrawal rate was 24.4 gallons per kWh in the East but only 11.0 in the West (Tables 5.6 and 5.7).[30] The rates differ because recycling is much more common in the West, largely because of greater water scarcity. As seen in Figure 5.7, the water withdrawal rate in the East has been falling at a declining rate. For example, the annual rate of change was -2.4% from 1985 to 1990 and -1.3% from 2000 to 2005. Not as obvious in Figure 5.7, the rate of decline in the West has also been changing, from -1.9% from 1985 to 1990 to -1.3% from 2000 to 2005.

The reasons for past declines—especially the movement from once-through to recycling plants—are likely to continue to play a role, suggesting that recent past trends are a good indication of future changes. It is assumed here that the rate from 1985 to 2005 will carry on into the future, but be gradually attenuated, in keeping with recent declines in the growth rate. The decay rate would necessarily be greater in the West, which has already reduced withdrawals per kWh to a low level, than in the East where significant improvements are still possible (Table 5.8). The resulting water withdrawal rates through 2090 are shown in Figure 5.7 and listed in Tables 5.6 and 5.7.

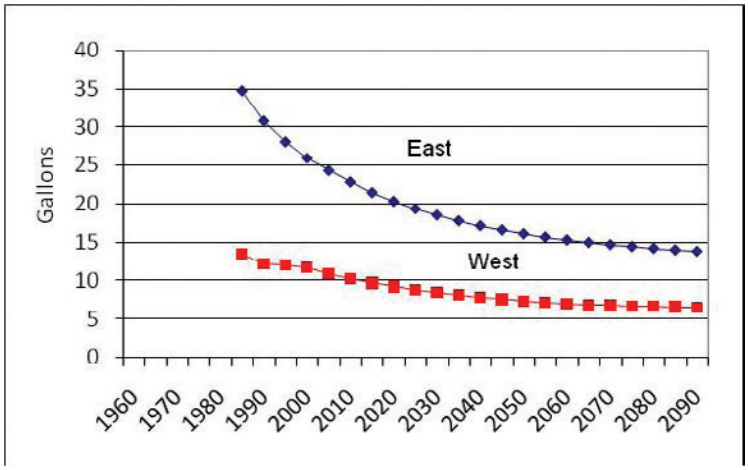

Figure 5.7. Thermoelectric withdrawal per kWh produced.

5.5.4 Irrigation

Withdrawals for U.S. irrigation increased dramatically from 1960 to 1980, then declined in 1985, followed by a period of little change from 1985 to 2000 and then another significant drop from 2000 to 2005 (Figure 5.4). The 1985-2000 period of stability in total withdrawals occurred as total irrigated area rose from 57 million acres in 1985 to nearly 62 million acres in 2000. Consequently, the overall water withdrawal rate (the annual irrigation depth) dropped from 2.68 ft to 2.48 ft during that period. However, to understand these trends one must look separately at the East and West.

Since 1985, irrigation depth in the East has been roughly constant at about 1.35 ft, whereas irrigation depth in the West has fallen from 3.10 ft in 1980 to 2.70 ft in 2005 for an annual growth rate of -0.55%. The drop in withdrawal rate in the West may be a response to such factors as the waning of the era of publicly funded dam and canal construction, higher prices for water from publicly funded projects, increasing ground water pumping lifts, and improved irrigation technology (Moore and others 1990).

Withdrawal per acre can vary considerably from year to year at the WRR level because of weather. Thus, time trends of withdrawal per acre at the WRR level are often erratic. To avoid this regional phenomenon, future changes in irrigation rates are based on the 1985 to 2005 rate of change in the East and West using the extrapolation factors listed in Table 5.8. In the West, withdrawal per acre was thus projected to continue falling as it did from 1985 to 2005, reaching 2.40 ft in 2060 (Table 5.6). In the East, future withdrawal per unit area was assumed to remain constant at the mean 1985-2005 rate and reach 1.30 ft per acre in 2060 (Table 5.7).[31]

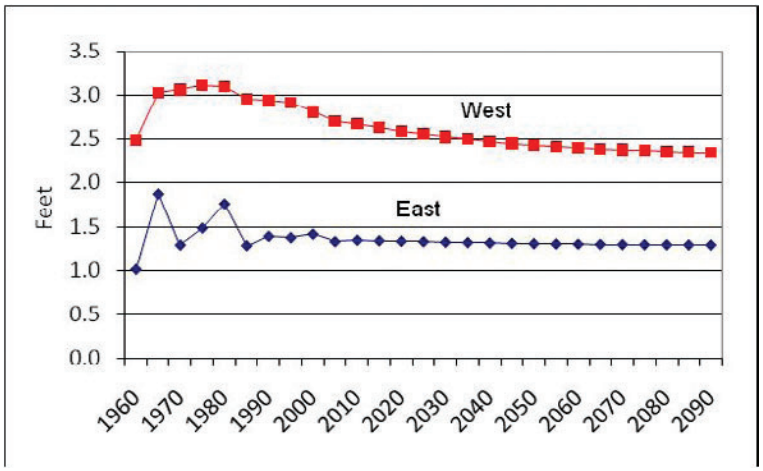

Figure 5.8. Annual irrigation withdrawal per irrigated acre.

5.5.5 Livestock and Aquaculture

The USGS's livestock water use category consisted solely of use by terrestrial animals (or "stock"—principally cattle, hogs, sheep, and poultry) until 1985 when "animal specialties" (consisting largely of aquaculture, including fish farming and fish hatcheries) were moved from the industrial to the livestock category. U.S. livestock withdrawals gradually increased

from 1.6 bgd in 1960 to 2.1 bgd in 1980 in response to increasing animal numbers and then more than doubled in 1985 (to 4.5 bgd) when animal specialties were added (Figure 5.4).

Water use by terrestrial animals has been estimated by the USGS largely based on numbers of animals served, with different animal species assigned their respective average water requirements. Use of water at fish farms was typically estimated based on pond area and estimates of evaporation, seepage, and refresh rate. Estimates of future stock numbers and pond areas were not available for projecting future livestock water use. Human population was used as the demand unit based on the assumption that population is an underlying determinant of demand for livestock and fish products.

Livestock withdrawal per capita has been dropping at least since 1990 (when the USGS data first allow clear separation between livestock and aquaculture), presumably because of improved efficiency of water use and changing consumer tastes. From 1990 to 2005, daily per-capita withdrawals dropped from 17.3 to 12.5 gallons in the West and from 4.8 to 4.3 gallons in the East (Figure 5.9). Using extrapolation with the coefficients listed in Table 5.8, withdrawal rates are projected to reach 3.9 gallons per capita per day in the East (Table 5.6) and 8.0 in the West (Table 5.7) in 2060.

Aquaculture withdrawal per capita consistently rose from 1990 to 2005 as aquaculture has become ever more prevalent. In the West, daily per-capita withdrawals rose from 9.9 gallons in 1990 to 42.7 in 2005 (Table 5.7); and in the East, the rate increased from 8.6 to 19.0 gallons over the same time period (Table 5.6, Figure 5.10).[32] Using extrapolation with the coefficients listed in Table 5.8, withdrawal rates are projected to reach 72 gallons per capita per day in the West (Table 5.7) and 39 in the East (Table 5.6) in 2060.

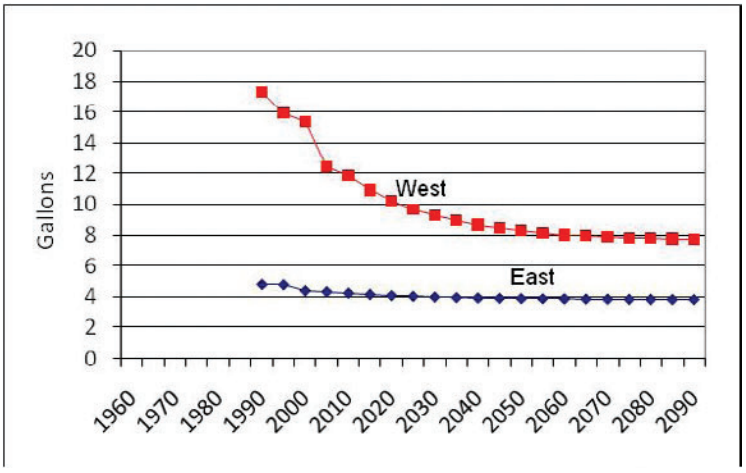

Figure 5.9. Livestock withdrawal per capita per day.

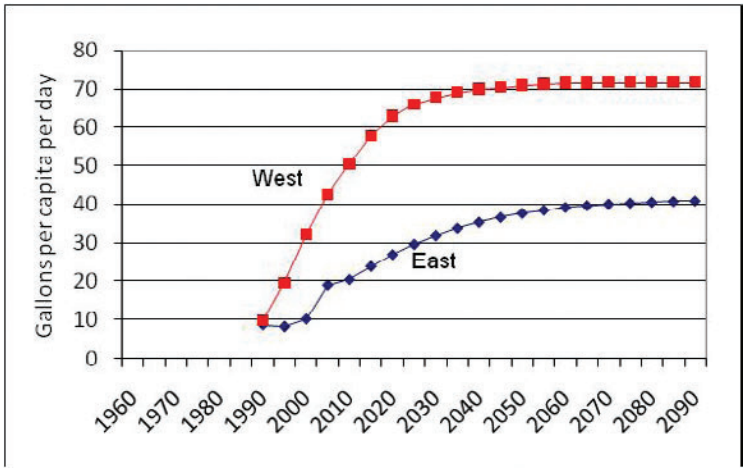

Figure 5.10. Aquaculture withdrawal per capita per day.

5.6 Future Effects of New Developments in Liquid Energy Production

In the effort to decrease U.S. reliance on petroleum, many changes in liquid fuel production are expected in the coming years, most notably a rapid increase in biofuel production. In addition, there is the possibility of shale oil exploitation. Because processing of liquid fuels from biomass and other non-traditional sources is a relatively new industry, future water use in this sector is not represented in industrial water use projections based on past water use, and thus must be computed separately.[33]

Consumptive water use in processing biofuels and producing liquid fuel from coal (CTL), ΔC^{IC}, was estimated for a given ASR and year as follows:

$$\Delta C^{IC}_{ASR,Y} = F_{ASR,Y} \cdot \Phi^{FP}_{Y} \tag{5.7}$$

where F is the annual volume of fuel produced and Φ^{FP} is the rate of consumptive water use per unit of fuel produced. As indicated, water for fuel processing falls within the IC water use category. F is measured in gallons of fuel produced per year, and Φ is measured in gallons of consumptive water use per gallon of fuel produced, so that ΔC^{IC} is in gallons of consumptive water use per year.

We first look at processing of biofuels and coal-to-liquid fuel, then consider water needs for irrigating crops used to produce biofuels, and finally examine oil shale issues.

5.6.1 Liquid Fuel Processing

Domestic production of biofuels has increased rapidly in recent years, rising from 4 billion gallons in 2005 to 10 billion in 2008, and is expected to continue growing for many years (EIA 2010: Table 11). The 2008 total consists of ethanol (91.5%), biodiesel (7%), and other biomass-derived fuels (1.5%).

Domestic production of ethanol is projected by the EIA (2010) to reach 28 billion gallons in 2035 (the most recent projections extend only to 2035). Most ethanol in the United States currently comes from corn, but other sources, which include cellulose, are expected to surpass corn as an ethanol source in the future. The Energy Independence and Security Act of 2007 (EISA) sets the goal that by 2022, transportation fuels consumed in the United States will contain 36 billion gallons of renewable fuels per year and no more than 15 billion gallons will be from corn-based ethanol. The EIA projections do not separate corn-based ethanol from cellulosic and other ethanols. We base the apportionment of total ethanol production to ethanol feedstocks on the EISA goals for the proportion of biofuels that will come from corn ethanol. Using this approach, domestic production of corn-based ethanol is projected to peak in 2014 at 13.8 billion gallons per year and then drop slightly in 2015, remaining at 13.2 billion gallons per year to 2035 (Figure 5.11). Production of non-corn ethanol (mainly cellulosic ethanol) is projected to increase consistently and at a heightened rate after 2030. By 2035, ethanol is projected to be 46% corn-based and 54% non-corn-based.

Production of biodiesel is projected by the EIA to gradually increase but remain a relatively minor component of the biofuel portfolio (Figure 5.11). Other biomass-derived liquid fuels—which the EIA defines to include pyrolysis oils, biomass-derived Fischer-Tropsch liquids, and renewable feed stocks used for the production of green diesel and gasoline—are projected by the EIA to increase slowly at first but become increasingly important after 2020, reaching nearly 10 billion gallons per year in 2035.

Of other sources of domestically produced liquid fuel alternatives to petroleum, production of liquids from coal is the primary single source listed by the EIA.[34] CTL fuel production is projected by the EIA to begin in 2011 and then gradually increase, reaching about 4 billion gallons per year in 2035.

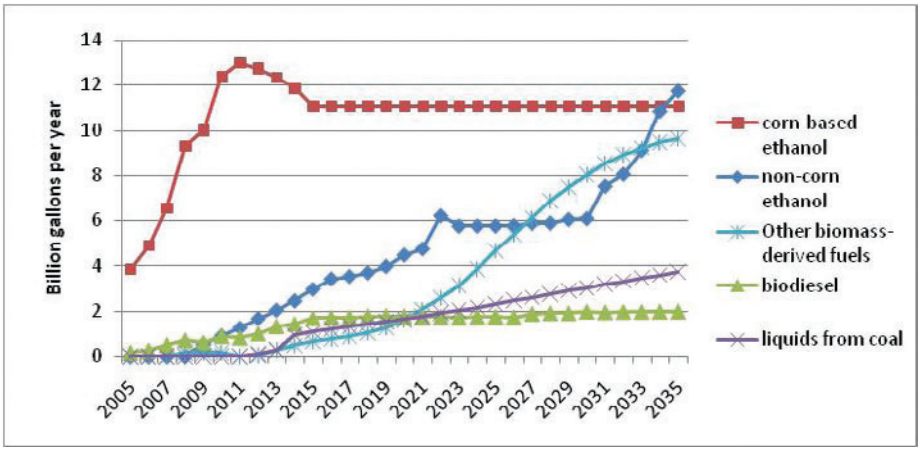

Figure 5.11. Non-petroleum liquid fuels produced in the United States from the EIA.

5.6.2 Water Use in Liquid Fuel Processing (Φ^{FP})

The principal use of water in biofuel production occurs in the irrigated field (GAO 2009) (discussed in the next section). However, significant quantities of water are used in biofuel and CTL processing. First, consider corn-based ethanol. Consumptive water use in corn ethanol processing has been dropping (Elcock 2010; Schnoor and others 2008). Expressed as the ratio of gallons of water to gallon of fuel produced, consumptive water use dropped from 3.5-6.0 gallons only a few years ago (King and Webber 2008) to 4 gallons in 2005 (Schnoor and others 2008), to 3 gallons more recently, and some further improvements are expected (Wu and others 2009). We assume that consumptive water use in ethanol processing will gradually drop from 4 gallons per gallon in 2005 to 3 in 2010, to 2 in 2030, with no improvements thereafter. King and Webber (2008) reported that the ratio of water withdrawal to consumptive use is about 2.

Pate and others (2007) reported that consumptive water use in processing biodiesel is about 1 gallon per gallon of biodiesel, and King and Webber (2008) reported a range from 0.28 to 0.58 gallons per gallon (assuming a fuel efficiency of 28.2 mpg). We use a constant value of 0.58 gallons of water per gallon of biodiesel. King and Webber (2008) reported that the ratio of water withdrawal to consumptive use is about 4.5.

For processing cellulosic ethanol, Aden (2007) suggested a range from 2 to 6 gallons of water per gallon of ethanol, which is within the range reported for corn ethanol. We assume that the corn ethanol consumption factors described above apply to cellulosic ethanol and other biomass-derived fuels.

Estimates of water use in production of CTL fuel vary. The National Energy Technology Laboratory (NETL) (Chan and others 2006) reported a range of 5 to 7.3 gallons of water per gallon of fuel depending on the type of coal used (see also Elcock 2010), King and Webber (2008) reported a range from 3.9 to 11.9 (assuming a fuel efficiency of 20.5 mpg for diesel fuel), and Höök and Akellett (2009) reported a value of 5.7 gallons of water per gallon of fuel. Expecting some efficiency improvements in the future, we use a rate that declines linearly from 6 gallons of water per gallon of fuel in 2005 to 4 gallons in 2030, with no further improvements. We assume that the ratio of water withdrawal to consumptive use is 2 for CTL fuel.

Assuming the above estimates of water use and given the fuel production levels of Figure 5.11, total consumptive use across all non-petroleum liquid fuel types is thus projected to grow from 42 million gallons per day (mgd) in 2005 to 119 mgd in 2010, 165 in 2020, 202 in 2030, and 253 in 2035. For the period from 2005 to 2035 this increase translates to an average annual growth rate of 6.1%. Projections for the individual fuel types are shown in Figure 5.12. Moving beyond 2035, lower growth rates were assumed (Figure 5.12). Combining across fuel types, total consumptive use was projected to reach 334 mgd in 2060. The rise from 2035 to 2060 translates to an average annual growth rate of 1.1%.

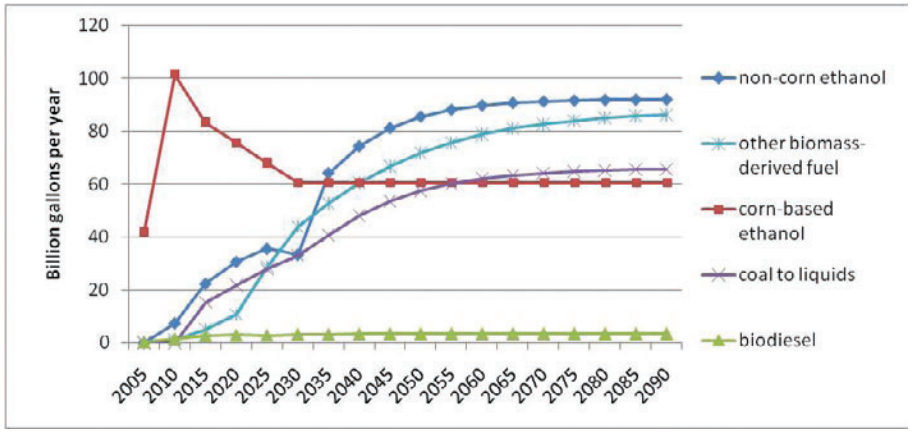

Figure 5.12. Consumptive use for processing non-petroleum liquid fuels.

5.6.3 Apportioning Future Liquid Fuel Processing Among ASRs

Total U.S. water use in liquid fuel processing was apportioned to individual ASRs based on the assumption that biofuels and CTL will be processed near where the feed stock or coal is found (grown, mined, or otherwise gathered). First of all, this implies that corn-based ethanol would be processed near where the corn is grown. We used state-level data from the National Agricultural Statistics Service (NASS) on volumes of corn harvested in 2008 and 2009 to determine where most corn was recently grown, selecting the 21 states that harvested at least 500,000 acres, which accounts for 96% of the total corn harvest (Table 5.9). The total amount of water used in corn-based ethanol processing was apportioned to ASRs within those 21 states in proportion to harvested area assuming an equal assignment to all ASRs within a state.

Table 5.9. Crop harvest and coal production by state.

Corn		Soybeans		Coal	
State	Acres/10^3	State	Acres/10^3	State	Tons/10^6
CO	1000	AR	3260	AL	20
IL	11850	IL	9235	CO	34
IN	5460	IN	5435	IL	33
IO	13100	IO	9600	IN	35
KS	3745	KS	3450	KY	118
KY	1135	KY	1400	MT	44
LA	560	LA	945	ND	30
MI	2120	MI	1940	NM	25
MN	7175	MN	7045	OH	24
MO	2785	MO	5165	PA	65
MS	698	MS	1995	TX	40
NC	815	NC	1720	UT	24
ND	2025	ND	3815	VA	25
NE	8700	NE	4810	WV	156
NY	618	OH	4505	WY	461
OH	3130	SD	4125		
PA	900	TN	1495		
SD	4550	VA	570		
TN	610	WI	1605		
TX	1995	SC	550		
WI	2905				
Total	75875		72665		1135

Biodiesel is produced from plant oils, principally soybean oil. We assumed that biodiesel would be processed near where soybeans were recently grown. NASS state-level data on volumes of soybeans harvested in 2008 and 2009 were used to determine where most soybean was grown, focusing on the 20 states that harvested at least 500,000 acres, which accounts for 96% of the total harvest (Table 5.9). The total water use in biodiesel processing was apportioned to ASRs within those 20 states in proportion to harvested area assuming an equal assignment to all ASRs with in a state.

For non-corn ethanol and other biomass-derived fuels, we assumed that cellulose and other feed stock would be generally available, and thus that these fuels would be produced in all ASRs in proportion to the population of the ASR.

For coal to liquid fuel, we assumed that processing would occur near where most coal is mined. We used state-level data from the EIA on volumes of coal produced in 2007 and 2008 to determine where most coal was produced, selecting the 15 states that produced at least 10 million tons per year, which accounts for 98% of the total production (Table 5.9). The total water use in CTL processing was apportioned to ASRs in proportion to coal volumes within those 15 states based on the locations of major coal deposits within the states.

5.6.4 Irrigation of Feed Stock for Biofuels

Increased demand for crops (principally corn and soybeans) to meet biofuel production goals is likely to bring additional agricultural land into production. Malcolm and others (2009) estimated for year 2015 the change in planted area attributable to production of 15 billion gallons of biofuels. The 15 billion gallon level is approximately equal to the combined production of corn-based ethanol and biodiesel that we project for 2010 and beyond (Figure 5.12). Malcolm and others estimated the effect on crop area of biofuel production as the difference between a scenario where the renewable fuel standard goal was met by 2015 and a business as usual (that is, in the absence of the renewable fuel standard) scenario. Their estimates (from their Table 3) were reported for 10 farm production regions, which are each groups of states. The percentage increases in planted acres by region are listed in Table 5.10.

Table 5.10. Increase in planted crop area attributable to meeting the renewable fuel standard goals.

Farm region	Percent increase
Northeast	0.68
Lake states	1.27
Corn belt	1.09
Northern Plains	3.07
Appalachia	2.21
Southeast	5.17
Delta	3.45
Southern Plains	0.39
Mountain	0.00
Pacific	1.30
U.S. total	1.56

The Malcolm and others (2009: Table 4) modeling results show some shifts in planted area for all major crops, with corn and soybean area increasing more than the area of other crops is decreasing. As Malcolm and others indicate, some of the additional planted area will be irrigated. We applied the estimated net percentage area increases to our irrigated areas for the ASRs within a region, applying a given farm production region's percentage to all ASRs that fall within the region, as follows:

$$A_{ASR,Y}^{RFS} = A_{ASR,Y} \cdot \frac{Z_{ASR}}{100} \tag{5.8}$$

where $A_{ASR,Y}^{RFS}$ is additional acres for a given year (Y) and ASR attributable to meeting the renewable fuel standard, $Z_{ASR,Y}$ is acres without meeting the renewable fuel standard, and Z_{ASR} is the percentage change in planted acres. This approach assumes that irrigated and non-irrigated acres will be added in proportion to the current distribution between these two agricultural situations, and that the percentage increases in net agricultural area of entire farm production regions apply to all ASRs within a farm production region.

5.6.5 Oil Shale

The United States has vast oil shale resources, with major deposits located in or near northwestern Colorado (including northeast Utah and southwest Wyoming), eastern Oklahoma, Michigan, and the Ohio River valley (from Tennessee to western Pennsylvania).[35] The richest deposits occur in the Green River Formation in and near northwest Colorado. This area is thought to contain up to 1 million barrels of oil equivalent per acre of surface area, for a total of roughly 1.5 trillion barrels, which is more than the entire world's proven petroleum reserves (Bartis and others 2005). Technologies for exploiting oil shale deposits and producing oil from those deposits are now being developed and tested, but no commercial facilities exist in the United States. Current estimates of future production costs range from $70 to $100 per barrel of oil equivalent in 2007 dollars.

Water availability and quality are both major considerations in exploiting oil shale deposits (Bartis and others 2005). This is especially so in the Green River Formation, which lies within the Upper Colorado River Basin where water resources are already stretched. Early estimates of consumptive water use in oil shade development ranged from 2 to 5 gallons of water per gallon of oil, with a ratio of 3:1 used by the U.S. Water Resources Council in 1981 (as reported by Bartis and others 2005). Newer technologies may lower the water requirement considerably (Bartis and others 2005), but, as the Government Accountability Office recently reported, estimates of the water requirement vary widely and that requirement will depend on the technology that is ultimately adopted (GAO 2011).

A recent GAO report concluded that it is not yet possible to predict future levels of oil shale production (GAO 2010). The EIA expects that no commercial project will begin construction before 2017, with no commercial production before 2023,[36] and the 2010 EIA projections (EIA 2010) do not include oil shale.[37] Lacking estimates of future production levels and given the uncertainty about when or whether oil shale deposits will be developed, we do not include oil shale as a future water use in this analysis.

5.7 Climate Change Effects

The emissions scenarios have implications for temperature, precipitation, and other climatic variables, which will in turn affect desired water use. For example, higher temperatures will induce increases in demand for air conditioning and thus additional electricity production at thermoelectric plants, and a decrease in precipitation would add to the need for irrigation. These effects are summarized below.

5.7.1 Effects on Crop Irrigation

The net irrigation amount per unit area (Φ_{net}^{IR}) is often defined as:

$$\begin{aligned} \Phi_{net}^{IR} &= k_c\, ETp - P' \quad \text{if } k_c\, ETp > P' \\ \Phi_{net}^{IR} &= 0 \qquad\qquad\quad \text{otherwise} \end{aligned} \tag{5.9}$$

where k_c is a crop specific dimensionless constant, ETp is potential evapotranspiration, and P' is effective precipitation (Döll 2002).[38] k_cETp represents crop water demand and P' is the part of that demand that does not need to be met by irrigation. In this formulation, it is assumed that irrigation fully meets crop water demand, and thus that water will not be a limiting factor in plant growth. Because some irrigation water may be returned to the stream, withdrawal may exceed Φ_{net}^{IR}. Gross irrigation amount per unit area (Φ_{gross}^{IR}) is defined as:

$$\Phi_{gross}^{IR} = \Phi_{net}^{IR} / \gamma \tag{5.10}$$

where γ is irrigation efficiency computed as irrigation consumptive use divided by irrigation withdrawal.

In this study, we are not differentiating among crops, so k_c is set to 1 for convenience. In addition, equation 5.9 does not take CO_2 concentration into account. However, CO_2 concentrations are rising and will continue to rise, and CO_2 concentration is known to affect plant water use. Amending equation 5.9 with these considerations in mind, the change in Φ_{net}^{IR} with a change in climate ($\Delta\Phi_{net}^{IR}$), equal to ΔC^{IR} (the irrigation component of ΔC in equation 5.2), for the situation where precipitation is inadequate to satisfy crop water demand, is then:

$$\begin{aligned} \Delta C^{IR} = \Delta\Phi_{net}^{IR} &= \Phi_{net,2}^{IR} - \Phi_{net,1}^{IR} \\ &= \left(ETp_2 - P_2'\right) - \left(ETp_1 - P_1'\right) - \varphi\left(ETp_2 - ETp_1\right) \\ &= (1-\varphi)\left(ETp_2 - ETp_1\right) + \left(P_1' - P_2'\right) \end{aligned} \tag{5.11}$$

where 1 and 2 indicate time before and after some change in CO_2 and climate, respectively, and φ is the proportional change in ETp caused by the change in CO_2 concentration. We consider the three terms of ΔC^{IR}, each representing one of the three identified influences on irrigation requirement, in the following subsections.

5.7.1.1 The precipitation effect

P' is the portion of precipitation (P) that is useable by plants. The P'/P proportion depends on the precipitation rate and the ability of the soil to hold additional water (which in turn depends on soil moisture, texture, and depth) and is difficult to determine for a given point in space and time, especially when being modeled at a regional scale. We use a simple approximation,

the USDA Soil Conservation Method as described by Smith (1992: 21) (see also Döll 2002) where, in terms of monthly mean depth in centimeters:

$$\begin{aligned} P' &= P(12.5 - 0.2P)/12.5 \quad \text{for } P < 25 \text{ cm/month} \\ P' &= 12.5 + 0.1P \qquad\qquad\quad \text{for } P \geq 25 \text{ cm/month} \end{aligned} \tag{5.12}$$

Accordingly, the proportion of a change in P that is available to meet crop water demands varies linearly with P from 1.0 at very low monthly P to 0.2 at P approaching 25 cm per month, and is then constant at 0.1 cm at P of 25 cm or greater.

The change in P' for a discrete change in P from P_1 to P_2 of equation 5.11 is given by:

$$\begin{aligned} P_1' - P_2' &= (P_1 - P_2) + 0.016\left(P_2^2 - P_1^2\right) \quad \text{for } P_1 < 25 \text{ cm/month} \\ P_1' - P_2' &= 0.1\,(P_1 - P_2) \qquad\qquad\qquad\quad \text{for } P_1 \geq 25 \text{ cm/month} \end{aligned} \tag{5.13}$$

For implementation of this approach to estimating P', we assume a six-month growing season (April to September) and compute monthly P as the mean monthly P over the growing season (thus, for convenience, we are assuming that monthly P is evenly distributed across the months of the growing season). Across the ASRs, the maximum monthly P in 2005 (the base year for computing precipitation changes) is about 18 cm. Thus, $\Delta P'/\Delta P$ remains within the range from 0.45 to 1.

Computation of ΔC^{IR} has relied on several simplifying assumptions, in addition to those underlying projections of irrigated area, including the following two. First, changes (increases or decreases) in variability of rainfall will not affect irrigation (thus, we are ignoring the possibility that if variability increases and dry times, as well as wet times, are more extreme or longer than in the past, irrigation demand will increase). Second, changes in growing season and plant maturity time of annual plants that may occur with temperature increases will not cause a change in irrigation volume.

5.7.1.2 The ETp effect

Rising temperatures increase transpiration by increasing the vapor pressure deficit at the leaf surface, and also elevate evaporation of water from the soil. These effects are approximated by the estimated change in *ETp*, the computation of which is described in Chapter 2. To get a rough idea of the potential effect of *ETp* increases on crop water demand, consider that average *ETp* across the nine futures for the United States for a six-month growing season (April-September) is projected to increase from 5.6 mm/d in 2005 to 6.5 mm/d in 2060—a 16% increase, equivalent to 17 cm over the six-month growing season. Assuming, as previously mentioned, that irrigation fully meets crop water demand, irrigation would be needed to make up this deficit, all else equal.

5.7.1.3 The direct CO_2 effect

Most of the research on the direct effect of increasing CO_2 on crops has focused on crop yields, but some of this work has included estimates of the effect on crop water use. Early experiments occurred in enclosures such as greenhouses, where plants were typically grown in pots. These studies showed substantial increases in crop water use efficiency (WUE, total biomass per unit of water transpired), but concerns were raised about the applicability of the

results to the field, where conditions regarding water availability, temperature, pests, vapor pressure deficit, ozone levels, and other factors are more variable (Unsworth and Hogsett 1996). More recent experiments use the free-air CO_2 enrichment (FACE) approach, where extra CO_2 is piped to outdoor plots of roughly 100 m^2 located within a larger cultivated field. In these experiments, increasing CO_2 has also been found to increase crop WUE, although not to the same extent as in the enclosure studies.[39]

As shown by both sets of experiments, the effect on WUE varies by crop type and furthermore by individual crop. C_3 crops (e.g., wheat, barley, rice, soybeans, cotton, potatoes, and cool season grasses such as blue grass) differ from C_4 crops (e.g., corn, sorghum, most millets, and Bermuda and other warm season grasses) in the efficiency with which they fix carbon and also in the biomass response to increasing CO_2, with C_3 crops showing a greater biomass response per unit area.[40] Producing additional biomass requires water and thus diminishes, to some extent, the water savings per unit area that would otherwise occur as WUE improves (Allen and others 1996; Leakey 2009; Leakey and others 2006, 2009; Van de Geijn and Goudriaan 1996). Because of this difference between C_3 and C_4 plants, the effects of CO_2 increases on plant water use tend to be greater for C_4 plants. However, as seen in Table 5.11, FACE experiments indicate a range of results among both C_3 and C_4 plants. The range in effect on plant evapotranspiration for C_3 species is thought to depend at least partly on the strength of the biomass response to elevated CO_2 (Kimball and Bernacchi 2006: Figure 17.3).

Considerable uncertainty remains about the effects of CO_2 increases on plant water use. Few FACE studies have been completed, and replications are needed to increase confidence in the findings. Further, the FACE experiments that have imposed elevated CO_2 levels have not simultaneously imposed an increase in ambient temperature, and the joint effects of CO_2 and temperature increases in field conditions are not known precisely.[41] In addition, the large-scale implications of the findings are not well understood (Allen and others 1996; Unsworth and Hogsett 1996). For example, there is the possibility that, at the regional scale (such as for a large planted field), if plants transpire less because of increased CO_2, the surrounding air becomes drier than it would otherwise be, increasing the water vapor concentration gradient between the leaves and the over-passing air and encouraging additional transpiration (Jarvis and McNaughton 1986). FACE studies have been too small to test for or observe such an effect.

Table 5.11. Approximate change in crop ET per unit area with CO2 at about 550 ppm versus the ambient level (350-375 ppm) in FACE experiments with ample water and N (Leakey and others 2006, 2009).

Crop	Percent change
Cotton (C_3)	0
Wheat (C_3)	-5
Rice (C_3)	-9
Maize (C_4)	-10
Soybean (C_3)	-12
Sorghum (C_4)	-13

Given this uncertainty, we cannot have confidence in any specific projection of plant water use. The approach taken here is to model plant water use in two extremes: no direct CO_2 effect and a large direct CO_2 effect. In the first case, $\varphi = 0$. In the other case, we assume a 10% reduction in plant water use of all crops for an increase in CO_2 from 360 ppm (roughly the average ambient CO_2 concentration when the FACE experiments were performed) and 550 ppm (roughly the average future CO_2 level used in the experiments).[42] In this second case, $\varphi = 0.1$. Further, we assume a linear relation between CO_2 and percent reduction in plant water use, from 0% at 360 ppm to 10% at 550 ppm and on from there. To get a rough idea of the impact of this effect, consider that the average CO_2 concentration change from 2005 to 2060 across the three scenarios used here, an increase from 379 to 552 ppm, would result in a reduction in plant water use of about 9%—less than the 16% increase in plant water use from the average *ETp* effect reported above for the same period. Of course, the *ETp* and direct CO_2 effects are site specific, so the difference between the two effects will vary spatially in any given year. Further, the direct CO_2 effect varies by scenario and the *ETp* effect varies by scenario and by GCM, so these averages give only a rough idea of the net change in plant water use for a specific scenario, GCM, location, and year.[43]

5.7.2 Effects on Landscape Irrigation

Landscaping involves a mixture of plants—perennials such as grass, forbs, shrubs, and trees, and annuals such as flowers and vegetables—that may differ widely in their water use requirements. As temperatures increase, the growing season may lengthen for some species (e.g., grass) and shorten for others (e.g., vegetables). The additional biomass production that is expected with higher CO_2 levels may be unnecessary and thus consciously avoided for some species (e.g., grass), resulting in water savings, but may be welcomed for others (flowers and vegetables).[44] This complex situation makes the effects of temperature, precipitation, and CO_2 changes on overall landscaping water use even more difficult to predict than for agricultural crops.

Unlike with agricultural irrigation, we lack large-scale data on area irrigated for landscape watering, so we cannot compute irrigation depth and are left seeking an indirect approach to estimate the effect of changing precipitation or *ETp* on DP withdrawal. The approach adopted here is to use the past relation of per-capita withdrawal to precipitation or *ETp*, estimated from variation across space, to indicate the future change in per-capita withdrawal with changing precipitation or *ETp*. The relation of per-capita withdrawal to *P'* or *ETp* was estimated using year 2005 withdrawal, population, and weather data. The analyses were performed at the WRR level, which allows for sufficient aggregation to provide reliable estimates of seasonal outdoor per-capita DP water use. The estimated withdrawal change per unit change in *P'* or *ETp* (η) was then multiplied by the future changes in *P'* or *ETp* to estimate future change in per-capita DP withdrawal.[45]

Generally, the total change in DP consumptive use with climate change (ΔC^{DP}) is the sum of three effects:

$$\Delta C^{DP} = \Delta C^{DP,P'} + \Delta C^{DP,ET_P} + \Delta C^{DP,CO_2} \quad (5.14)$$

The procedures for estimating the three effects are explained more fully in the following subsections.

5.7.2.1 The Precipitation Effect

The effect of a change in effective P (P') on domestic and public (DP) consumptive water use ($\Delta C^{DP,P'}$) in gallon-days (gallons per day for a year) for a given basin was modeled as a change in per-capita water use times population and calculated as follows:

$$\Delta C^{DP,P'} = \rho \cdot \eta^{P} \cdot \Delta P' \cdot \gamma^{DP} \tag{5.15}$$

where ρ is human population, η^{P} is the change in DP gallons per capita per day withdrawn for a 1 cm change in P' from 2005 to some future year, $\Delta P'$ is the change in P' from 2005 to the future year, and γ^{DP} is the portion of withdrawal that is consumptively used.

The factor η^{P} accounts for the effect of P' on per-capita landscape irrigation needs and for the conversion from P' measured in cm to water use measured in gallons per capita per day (gcd). η^{P} was computed by regressing annual per-capita DP water withdrawal used outdoors in gcd on mean growing season (April-September) P' in cm. Because the USGS withdrawal data are annual totals that do not distinguish between indoor and outdoor use, a procedure was needed to isolate outdoor use. The procedure used here was to estimate the proportion of annual delivery that is used each month, and assume that water use in the winter is completely for indoor use. Specifically, the proportion of annual withdrawal that is used outdoors (ω) per person per day for the WRRs was estimated as follows:

$$\omega = \frac{\Phi^{DP} - 12b}{\Phi^{DP}} = 1 - \frac{12b}{\Phi^{DP}} \tag{5.16}$$

where Φ^{DP} is annual DP withdrawal for 2005 in gcd computed from USGS water withdrawal and population estimates (Kenny and others 2009) and b is mean monthly proportion of annual withdrawal occurring in January and February, with water use during January and February assumed to be used totally indoors. The percentage of annual water withdrawal that occurs in these two months was based on a survey of 232 cities across the United States, each providing from one to four recent years of monthly water delivery data (see Appendix B for details). Growing season precipitation for the regression was estimated from PRISM data (Daly and others 1994) as mean April to September precipitation for 10 recent years spanning the period represented by most of the city monthly delivery data. Growing season P' was then estimated using equation 5.12. The analysis was performed at the WRR scale. The data are summarized in Table 5.12.

The data used in the regression are plotted in Figure 5.13. The slope of the regression line, -1.415, gives η^{P}, the change in gcd for a 1 cm increase in growing season P' ($R^2 = 0.85$). Equation 5.15 was applied at the ASR level, with η^{P} constant for all ASRs.

Table 5.12. Data for estimating η.

WRR	DP withdrawal (gcd)	Proportion of withdrawal used outdoors (ω)	DP withdrawal used outdoors (gcd)	Mean effective *P* April-Sept. (cm)	Mean *ETp* (cm)
1	85.5	0.07	6.2	48.3	79.2
2	97.7	0.03	3.2	50.5	99.6
3	108.3	0.12	13.4	58.9	136.3
4	86.1	0.10	8.6	44.4	80.8
5	83.6	0.08	6.5	52.9	104.9
6	92.0	0.08	6.9	57.4	118.5
7	95.4	0.17	16.7	49.6	91.0
8	124.4	0.14	17.0	58.9	132.9
9	86.9	0.14	12.1	37.1	77.2
10	126.9	0.33	42.2	34.7	115.0
11	119.6	0.28	33.2	43.0	140.7
12	165.7	0.21	34.8	42.2	156.3
13	192.7	0.26	49.2	23.1	180.6
14	154.7	0.44	67.5	17.7	138.9
15	173.6	0.32	56.1	14.2	228.1
16	183.1	0.48	88.2	14.1	157.0
17	124.7	0.34	42.4	24.9	104.0
18	156.7	0.44	68.6	9.9	177.2

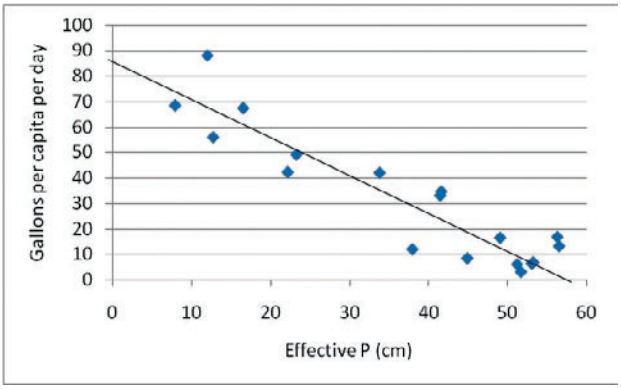

Figure 5.13. Variation in 2005 annual outdoor DP withdrawal with precipitation for WRRs.

5.7.2.2 The ETp effect

The procedure for estimating the change in DP water use for a change in *ETp* is similar to that used for a change in precipitation. The effect of a change in *ETp* on consumptive use in gallon-days for a given basin ($\Delta C^{DP,ETp}$) was modeled as a change in per-capita water use times population as follows:

$$\Delta C^{DP,ETp} = \rho \cdot \eta^{ETp} \cdot \Delta ETp \cdot \gamma^{DP} \qquad (5.17)$$

where η^{ETp} is the change in DP gallons per capita per day withdrawn for a 1 cm change in *ETp* from 2005 to some future year. ρ and γ are described in equation 5.15, and ΔETp is the change from 2005 to the future year.

The factor η^{ETp} accounts for the effect of *ETp* on per-capita landscape irrigation needs and for the conversion from *ETp* measured in cm to water use measured in gcd. η^{ETp} was computed by regressing annual per-capita DP water withdrawal in gcd on mean annual *ETp* in cm.[46] Annual DP withdrawal per person per day for WRRs was computed from USGS water withdrawal and population estimates (Kenny and others 2009). Annual *ETp* was estimated from PRISM temperature data. The analysis was performed at the WRR scale. The data are summarized in Table 5.12.

The data used in the regression are plotted in Figure 5.14. The slope of the regression line, 0.778, gives η^{ETp}, the change in gcd for a 1 cm increase in annual *ETp* ($R^2 = 0.73$). Equation 5.17 was applied at the ASR scale, with η_{ETp} constant for all ASRs.

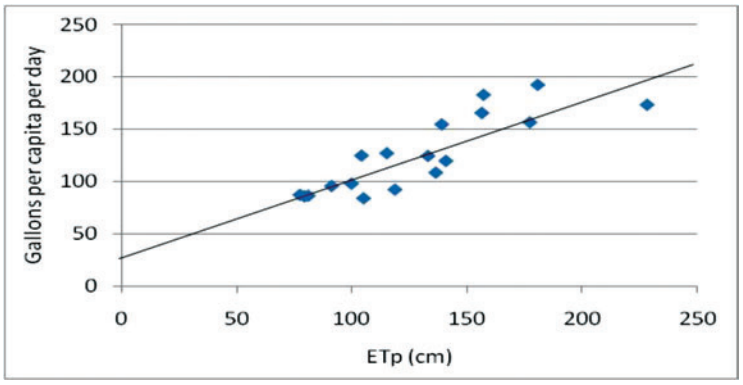

Figure 5.14. Variation in 2005 annual outdoor DP withdrawal with ETp for WRRs.

5.7.2.3 The direct CO_2 effect

Finally, the direct effect of CO_2 concentration on irrigation water requirement for a given basin ($\Delta C^{DP,CO_2}$) was computed as a change in outdoor per-capita DP water withdrawal as follows:

$$\Delta C^{DP,CO_2} = -\rho \cdot \Phi^{DP} \cdot \omega \cdot \varphi \cdot \gamma^{DP} \tag{5.18}$$

where Φ^{DP} is DP withdrawal for a given year, ω is the proportion of that withdrawal that occurs outdoors from equation 5.16, and φ is the proportion change in outdoor water use due to an increase in CO_2 from current levels, as previously explained.

5.7.3 Effects on Thermoelectric Water Use

Most energy uses require only small amounts of water. For example, heating houses with natural gas and powering vehicles with gasoline do not require large water inputs.[47] However, thermoelectric power plants (mainly fossil fuel and nuclear plants) use large quantities of water. The primary impact of climate change on thermoelectric energy production is expected to be the effect of temperature increases on space cooling, although areas where electricity is used for heating may also be affected. Of course, the impact will be smaller where hydroelectricity is prevalent, such as in the State of Washington.[48]

The change in thermoelectric water use needed to accommodate the increase in space cooling with a rise in temperature (ΔC^{TF}) is computed here by introducing a multiplier M to represent the effect of the temperature increase on the per-capita electricity consumption rate (E^{ρ}). The change in C^{TH} with a change in temperature is then total thermoelectric production with the temperature increase minus total production absent the temperature increase:

$$\begin{aligned}\Delta C^{TF} &= \left(\rho \cdot E^{\rho} \cdot M - E^{non-TF}\right)\Phi^{TF}\,\gamma^{TF} - \left(\rho \cdot E^{\rho} - E^{non-TF}\right)\Phi^{TF}\gamma^{TF} \\ &= \rho \cdot E^{\rho}\left(M-1\right)\Phi^{TF}\gamma^{TF}\end{aligned} \tag{5.19}$$

where ρ is population, E^{ρ} is electricity consumption per capita in kWhs, $E^{non\text{-}TF}$ is the number of kWh produced at non-freshwater thermoelectric plants, Φ^{TF} is the amount of water withdrawn per kWh produced at thermoelectric plants, and γ^{TF} is the proportion of withdrawal that is consumptively used. Non-thermoelectric plants include hydroelectric, wind, solar, and other non-thermal plants in addition to saltwater thermoelectric plants.[49] See Appendix A for more detail.

As characterized by Sailor and Pavlova (2003), there are both short-term and long-term effects of temperature increases on electricity used for space cooling. In the short term, residents and businesses decide on a daily basis whether or not to use their air conditioners, and in the long term, people without air conditioners decide whether or not to purchase them. Most commercial establishments and office buildings have air conditioning units already, so we assume that only short-term effects are relevant to the commercial sector, but for the residential sector, both short-term and long-term effects are relevant. Thus, we estimate factors for the short-term effect (M^{ST}) and the combined effect (M^{ST+LT}). These estimates are performed at the WRR level because the limited data available on the effects of temperature on electricity use did not justify producing estimates at the ASR level.

Both short-term and long-term effects of temperature on E^{ρ} vary across the United States (Sailor 2001; Sailor and Pavlova 2003). Short-term effects vary spatially due to differences in climate (e.g., temperature, humidity, and wind) and available energy sources.[50] Long-term effects vary because air conditioning is already common in some warm areas (market saturation exceeds 90% in parts of the southern United States) and becomes increasingly less common as one moves north. Opportunities for increasing market saturation are greater in areas not already relying heavily on air conditioning.

Because of regional differences, studies that have applied consistent methods over a mixture of conditions are most useful for estimating large-scale impacts.[51] For short-term effects, we extended the results of Sailor (2001), who estimated the percentage increase in residential and

commercial electricity consumption for different levels of annual temperature increase for eight states scattered across the United States. Combining residential and commercial uses, we expanded Sailor's estimates to all states using data on past (1971-2000) temperatures, and developed state-specific nonlinear regression equations expressing the percent change in E^{ρ} as a function of change in temperature (T).[52] These state-level relations were matched to WRRs based on the proportion of a WRR falling in respective states. The equations for short-term effects are of the form:

$$M^{ST} = \left(\Delta T\, x_1 + \Delta T^2\, x_2\right)/100 \tag{5.20}$$

where ΔT is the change in annual temperature in degrees Celsius and M^{ST} is the proportion increase in electricity consumption due to short-term effects.[53] The coefficients for the WRRs are listed in Table 5.13. Results for a selection of WRRs are shown in Figure 5.15. As expected, the short-term effect is greatest in the Southeast (WRR 3) and relatively low in New England (WRR 1).

To our knowledge, Sailor and Pavlova (2003) provided the only readily available analysis of long-term effects of temperature change on electricity consumption in the United States. The authors estimated the short-term and long-term changes in residential electricity consumption for 12 cities located in four different states (California, New York, Ohio, and Texas). From this information, we estimated the ratio of total percent increase to short-term percent increase.[54] The ratios for the 12 cities were extended to the 18 WRRs by selecting the cities or groups of cities that were considered most representative of the WRRs.[55] The resulting ratios (x_3) are listed in Table 5.13. As seen in the table, the long-term effect is very small in southern, hotter

Table 5.13. Coefficients for computation of the change in thermoelectric energy production with climate change.

	Residential		Commercial		
WRR	x1	x2	x1	x2	x3
1	0.14	0.02	0.59	0.04	2.63
2	0.63	0.11	0.90	0.06	1.62
3	3.05	0.45	1.71	0.12	1.06
4	0.26	0.07	0.72	0.06	1.90
5	0.76	0.16	1.04	0.08	1.67
6	1.62	0.28	1.28	0.09	1.36
7	0.54	0.10	0.71	0.05	1.90
8	2.29	0.40	1.49	0.11	1.06
9	0.09	0.01	0.35	0.03	2.12
10	0.27	0.05	0.68	0.05	1.36
11	1.49	0.23	1.14	0.08	1.36
12	2.36	0.22	1.01	0.07	1.06
13	1.63	0.19	1.03	0.08	1.06
14	0.09	0.01	0.73	0.05	1.67
15	2.10	0.36	1.43	0.10	1.06
16	0.19	0.03	0.83	0.06	1.47
17	-1.12	0.08	0.29	0.09	2.33
18	1.59	0.23	2.16	0.12	1.63

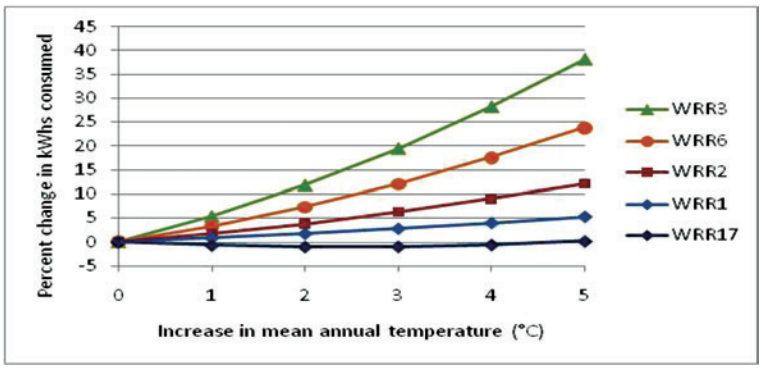

Figure 5.15. Short-term response of annual per-capita electricity consumption to temperature increase for a few WRRs.

areas (e.g., WRRs 3, 13, 14, and 15) and rises progressively as one moves north, with the exception of WRR 17, which includes the State of Washington and is therefore a special case.

The combined (short-term plus long-term) proportional increase in electricity consumption with a change in temperature is:

$$M^{ST+LT} = x_3 M^{ST} \tag{5.21}$$

The combined effects are shown for a sampling of WRRs in Figure 5.16. Comparison of Figures 5.15 and 5.16 shows the impact of adding the long-term effect.

As mentioned, M^{ST} applies to commercial uses and M^{ST+LT} applies to residential uses. Industrial electricity consumption is much less sensitive to temperature than are residential and commercial uses, and is ignored here.[56] The residential and commercial sectors consume 37% and 36% of U.S. electricity production, respectively (EIA 2009a: Table A-8). Assuming that these proportions apply in all WRRs, the multiplier (M) for change in C^{TF} due to a temperature change is:

$$M = 1 + 0.36 M^{ST} + 0.37 M^{ST+LT} \tag{5.22}$$

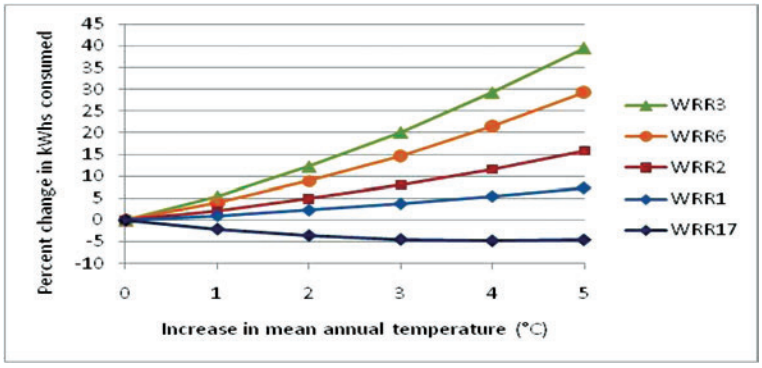

Figure 5.16. Short- plus long-term response of annual per-capita electricity consumption to temperature increase for a few WRRs.

5.8 Consumptive Use Proportions

Estimates of the proportion of withdrawals that were consumptively used for the period 1960-1995, computed from USGS withdrawal and consumptive use estimates, typically show no obvious trend at the WRR level.[57] The year-to-year variations in consumptive use proportion may reflect weather conditions or the particular methods used at various times and locations. On the assumptions that the more recent estimates are both the more accurate and more likely to represent current conditions, but that an estimate for any one year may represent unusual conditions, consumptive use rates (γ) for years beginning in 2000 were, with the exception of aquaculture, based on the two most recent estimates, those for 1990 and 1995 (Table 5.14).[58]

Consumptive use rates for aquaculture computed from the USGS data were highly variable across WRRs, ranging from 0.0 to 1.0 with no obvious spatial relations. For example, the rates were 0.90 in WRR 1 but 0.10 in WRR 2, and 1.0 in WRR 12 but 0.19 in WRR 13. Consumptive use rates depend in part on the aquaculture process used. Raceways, for which the rate is probably below 0.01, are often used with fish such as trout that require water of high oxygen content. Otherwise, ponds are used, and the rate at which water is moved though the ponds depends on water availability, the fish species, and the extent to which the water is cleaned and reused. Among the few estimates of consumptive use rates we found in the literature, Schaffer (2009) reported a rate of 0.05 for Ohio and Indiana; Boyd and Gross (2000) reported a rate of 0.09 for four aquaculture ponds in Alabama; and Boyd and others (no date) suggested average rates of 0.2 for watershed ponds (ponds created by dams placed across a small valley), 0.36 for annually drained embankment ponds, and 0.58 for undrained embankment ponds. These rates are lower than the more extreme rates estimated from the USGS circulars. Where the estimates based on the data from the circulars were judged to be too high, we used rates that reflect the above cited literature and expectation for raceways.

Table 5.14. Consumptive use proportions by WRR, in most cases estimated as the average of the USGS estimates for 1990 and 1995.

WRR		DP	IC	TF	IR	LS	AQ
1	New England	0.12	0.10	0.01	0.99	0.83	0.05
2	Mid-Atlantic	0.08	0.10	0.02	0.77	0.86	0.05
3	South Atlantic-Gulf	0.20	0.13	0.02	0.68	1.00	0.30
4	Great Lakes	0.07	0.09	0.02	0.94	0.87	0.05
5	Ohio	0.10	0.16	0.04	0.90	0.90	0.05
6	Tennessee	0.12	0.11	0.00	0.85	1.00	0.02
7	Upper Mississippi	0.31	0.13	0.03	0.93	0.92	0.20
8	Lower Mississippi	0.38	0.10	0.03	0.73	1.00	0.40
9	Souris-Red-Rainy	0.29	0.17	0.01	0.89	1.00	0.20
10	Missouri	0.31	0.24	0.02	0.53	1.00	0.20
11	Arkansas-White-Red	0.33	0.17	0.04	0.81	1.00	0.30
12	Texas-Gulf	0.35	0.39	0.04	0.93	0.99	0.40
13	Rio Grande	0.38	0.57	0.81	0.50	0.97	0.20
14	Upper Colorado	0.30	0.35	0.95	0.35	0.92	0.01
15	Lower Colorado	0.43	0.62	0.97	0.61	1.00	0.20
16	Great Basin	0.34	0.45	1.00	0.57	0.65	0.20
17	Pacific Northwest	0.13	0.07	0.05	0.40	0.70	0.01
18	California	0.23	0.20	0.04	0.80	1.00	0.20

The base estimates of γ for all six water uses differ substantially across the WRRs (Table 5.14). In the East, γ is high (0.7 or above) for IR and LS uses and much lower (generally below 0.2) for the other four uses. However, there is much greater variability among the WRRs in the West, which is mainly a response to the diversity of climates across the West. For example, consider thermoelectric water use, where γ is below 0.1 in most WRRs but 0.8 or higher in the four driest WRRs of the West. Unlike in the other WRRs, once-through power plants in these four WRRs are very uncommon. Once-through plants withdraw a large amount of water but consume very little of that water, whereas recirculating plants generally withdraw only enough to replenish the amount consumptively used. The relation between withdrawal and consumptive use is reflected in the correlation between γ^{TF} and Φ^{TF}, which is -0.80. This difference in technologies is also seen in irrigation—γ^{IR} is generally high in the East where flood irrigation is uncommon and return flow is therefore a lower percentage of withdrawal, and closer to 0.5 in the West where flood irrigation has been common. In agriculture, the corresponding correlation between γ^{IR} and Φ^{IR} is -0.73, indicating a strong negative relation between withdrawal per acre and consumptive use proportion.[59]

Looking in more detail at the consumptive use proportions, first for domestic and public use, we see that the WRRs fall roughly into three groups, one with γ^{DP} less than 0.1 (WRRs 1, 2, 4, 5, 6, and 17), one with γ^{DP} of about 0.2 (WRRs 3 and 18), and a third group with γ^{DP} of from 0.3 to 0.4 (WRRs 7-16) (Table 5.14). The variation among the groups reflects the prevalence of landscape irrigation, although other factors may also play a role. For industrial and commercial use, the WRRs fall roughly into four groups—one with γ^{DP} of about 0.1 (WRRs 1-8 and 17), one with γ^{DP} of about 0.2 (WRRs 9-11 and 18), one with γ^{DP} of about 0.4 (WRRs 12, 14, and 6), and a fourth group with γ^{DP} of about 0.6 (WRRs 13 and 15). Prevalence of landscape irrigation may partially explain the variation across groups, but industry type would also play a role. As previously mentioned, for thermoelectric use the WRRs fall into two groups, one with γ^{TF} less than 0.05 (WRRs 1-12, 17, and 18) and one with γ^{TF} above 0.8 (WRRs 13-16), based largely on the cooling technologies used. For agricultural irrigation, the WRRs fall roughly into two groups, one with γ^{IR} of from 0.3 to 0.6 (WRRs 13-17) and the other with γ^{IR} of from 0.7 to 1 (WRRs 1-9, 11, 12, and 18), with the difference between groups largely reflecting the differences in prevalence of flood versus more efficient irrigation technologies. Finally, for livestock, the WRRs fall into two groups, one with γ^{LS} above 0.80 (WRRs 1-15 and 18) and the other with γ^{LS} of from 0.65 to 0.70 (WRRs 16 and 17). The reason that return flow is higher than elsewhere in WRRs 16 and 17 is not apparent.

Consumptive use rates for years past 1995 were assumed to remain at the levels listed in Table 5.14 for all but thermoelectric use nationwide and agriculture in the West. TF and IR rates in the West were allowed to change to reflect the gradual shift expected from once-through to recirculating plants in thermoelectric cooling and from flood to sprinkler irrigation in the West.

Future consumptive use at thermoelectric plants is based on a recent study of future water needs in the thermoelectric sector (NETL 2008). Their Case 2, which Feely and others (2008) suggest is the more likely case of the five presented in the NETL study, assumes that additions to generating capacity will be freshwater wet recirculating plants and that retirements will be proportional to current water source and cooling system conditions. Projections of future

withdrawals and consumptive use for Case 2 (NETL 2008: Table ES-1) were used to estimate an implicit rate of increase in consumptive use proportion of 1.09% per year. This rate is applied to all WRRs without a decay factor.

The rate of increase in future irrigation consumptive use in western WRRs was estimated based on the increase for the West as a whole from 0.54 in 1980 to 0.59 in 1995, which is equivalent to a 0.63% annual increase, as computed from the USGS water use data. Equation 3 was used with each western WRR to extend the base rate into the future with *g* set to 0.0063 and *d* set to -0.04. Using this approach, the average rate in the West increased from 0.59 in 1995 to 0.69 in 2060 (with rates for individual WRRs of course reflecting their base rates).

5.9 Results

Results described here are for the United States and for WRRs and ASRs. Results are presented first for water required to meet the renewable fuel standard (RFS) goals, assuming the A1B scenario future population and income levels but no climate change. Those water amounts are included in all subsequent results about the effects of future changes in population, income, and climate.

5.9.1 RFS Goals

For the United States, meeting the RFS goals is expected to increase consumptive use by 1.3% above what would otherwise occur in 2005. This percentage increase is projected to diminish to about 0.9% by 2025 as the production of corn ethanol decreases and production of liquid fuels from other sources increases, and then increase slightly thereafter, reaching 1.0% in 2060 as production of liquid fuels from other renewable sources continues to increase. The IR sector accounts for the bulk of the consumptive use attributable to meeting the RFS goals, with the remainder assigned to the IC sector (Figure 5.17). The percentage of the total RFS consumptive use attributable to irrigation decreases from 92% in 2010 to 83% in 2025. With irrigation of crops (mainly corn and soybeans) for ethanol and biodiesel stabilized at about the 2025 level and liquid fuel production from other sources gradually increasing, the proportion of the consumptive use attributable to irrigation gradually diminishes from 83% in 2025 to 74% by 2060.

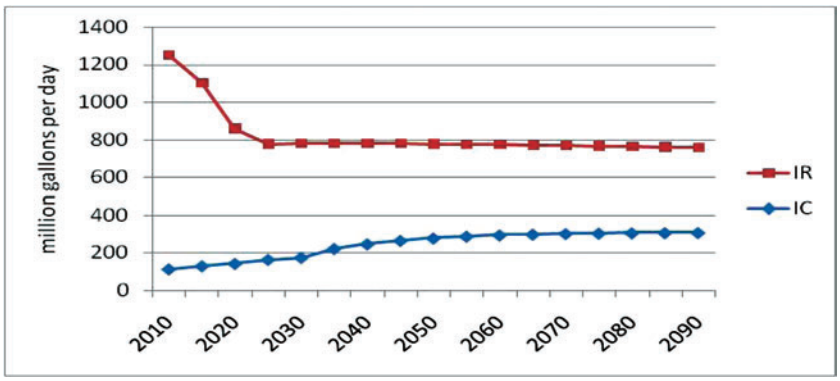

Figure 5.17. Projected change in U.S. consumptive use attributable to meeting the renewable fuel standards, assuming scenario A1B future population and income.

The impacts of meeting the RFS goals on water use are unevenly distributed across the United States. To examine the distribution among WRRs, consider year 2030 after the irrigation impact has stabilized. In 2030, four WRRs (3, 8, 10, and 18) are projected to account for 75% of the total consumptive use attributable to the RFS goals (Table 5.15). Looking only at the IC sector, 57% of the projected consumptive use in 2030 occurs in the East, largely because of the greater demand and available biomass (Table 5.15).

Table 5.15. Projected increase in consumptive use in 2030 (mgd) attributable to meeting the RFS goals, assuming the A1B future population and income.

WRR		IC	IR
1	New England	3	1
2	Mid-Atlantic	13	3
3	South Atlantic-Gulf	15	126
4	Great Lakes	10	4
5	Ohio	24	2
6	Tennessee	2	1
7	Upper Mississippi	29	6
8	Lower Mississippi	3	205
9	Souris-Red-Rainy	2	2
10	Missouri	32	158
11	Arkansas-White-Red	5	67
12	Texas-Gulf	8	10
13	Rio Grande	1	1
14	Upper Colorado	9	0
15	Lower Colorado	3	0
16	Great Basin	1	0
17	Pacific Northwest	3	37
18	California	10	161
Total		174	782

5.9.2 Future Water Use Assuming No Change in Climate

Future U.S. water use was projected for three alternative specifications of future population and income corresponding to the A1B, A2, and B2 scenarios. Results for the A1B scenario are described here in some detail, as this scenario incorporates the U.S. Census Bureau's 2000 projection of the most likely future population levels. Results for the other two scenarios are then compared with those of the A1B scenario.

5.9.2.1 The A1B scenario—business as usual

For the United States as a whole, assuming the A1B population and income projections and no climate effects, little change in withdrawals or consumptive use is projected over the next 50 years. Withdrawals for the A1B scenario are projected to drop gradually from 347 bgd in 2005 to 332 bgd in 2025 and increase gradually thereafter, reaching 357 bgd in 2060, for a net increase from 2005 to 2060 of about 3% (Figure 5.18). Consumptive use is projected to increase gradually and consistently from 100 bgd in 2005 to 110 bgd in 2060 (Figure 5.18).[60] Consumptive use is expected to grow at a higher rate than withdrawals largely because of the move to more efficient use of withdrawals, especially in the IC, TF, and IR sectors.[61]

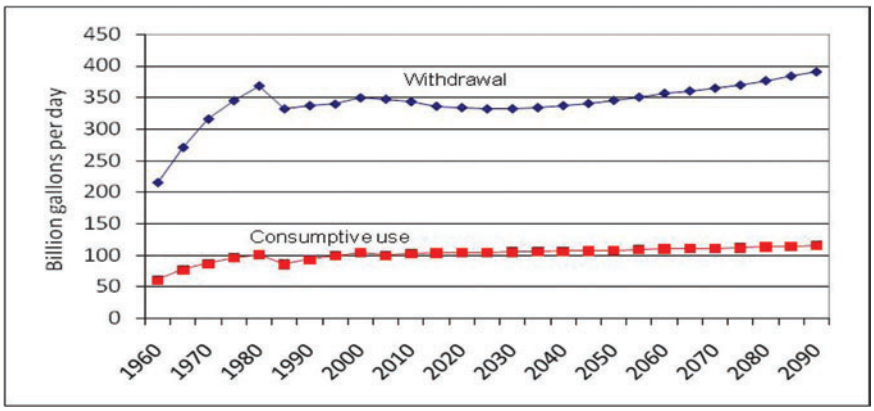

Figure 5.18. Past and projected annual U.S. water use, scenario A1B population and income, no future change in climate.

As seen in Figure 5.19, the projected decrease in withdrawals over the next 20 years or so is attributable largely to the TF and IR water use categories. The largest decrease in withdrawals occurs in the TF category as a result of the continuing declines in the withdrawal rates (Φ^{TF}) (as some once-through plants are gradually retired and recirculating plants are added to meet the growing demand for electricity) and the dramatic increase in electricity production at renewable (e.g., wind and solar) plants. The drop in withdrawals at thermoelectric plants is projected to bottom out in 2035 as the increase in production at other renewable plants diminishes to the point where it no longer compensates fully for the increasing demand for electricity. The drop in U.S. irrigation withdrawals occurs because the reduction in withdrawal rate (Φ^{IR}) and the drop in irrigated area in the West more than compensates for the increase in irrigated area in the East.

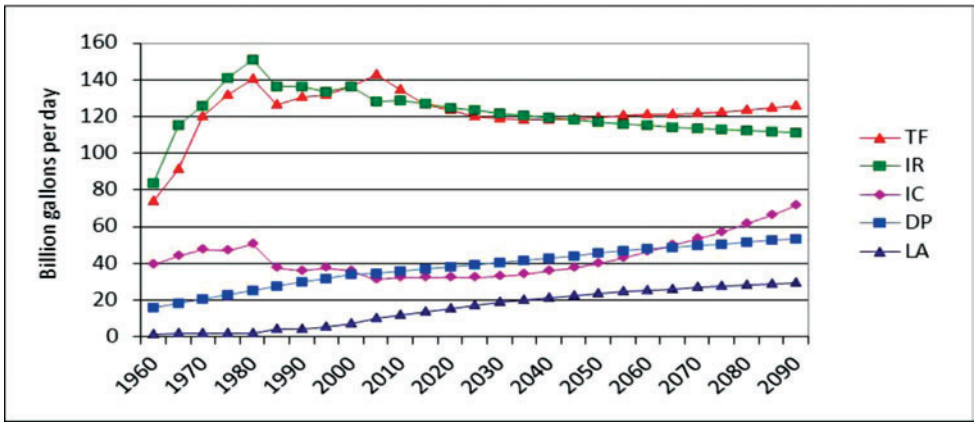

Figure 5.19. Past and projected annual U.S. withdrawals by water use type, scenario A1B population and income, no future change in climate.

In contrast to the decreases in TF and IR withdrawals, total withdrawals in the DP and LA categories are projected to rise continuously, and withdrawals in the IC sector are projected to remain nearly constant for about two decades and then rise. The increases in the DP and IC sectors occur because the projected decrease in withdrawal rates (Φ) are insufficient to compensate for the increases in population and income. Finally, LA withdrawals are projected to increase because of increasing population and income and a lack of projected change in withdrawal rates (Φ) in livestock and aquaculture.

Over the next 50 years, aggregate consumptive use in the United States is projected to remain steady in irrigation and increase in the other four water use sectors (Figures 5.20 and 5.21). The relatively constant trend in IR consumptive use occurs as the slight increase in the proportion consumptively used (γ) roughly balances the decrease in withdrawal. The rise in consumptive use in the DP and IC sectors occurs as a direct response to the rise in withdrawals, as the proportion consumptively used was not projected to change. The rise in the TF category occurs because of the increasing demand for electricity (as previously mentioned, this demand is met without increases in withdrawals because of the retirement of some once-through thermoelectric plants and the addition of recirculating plants).

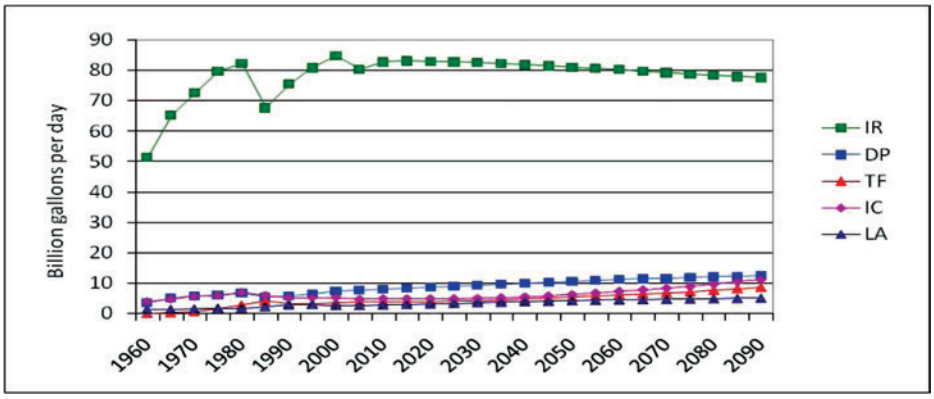

Figure 5.20. Past and projected annual U.S. consumptive use by water use type, scenario A1B population and income, no future change in climate.

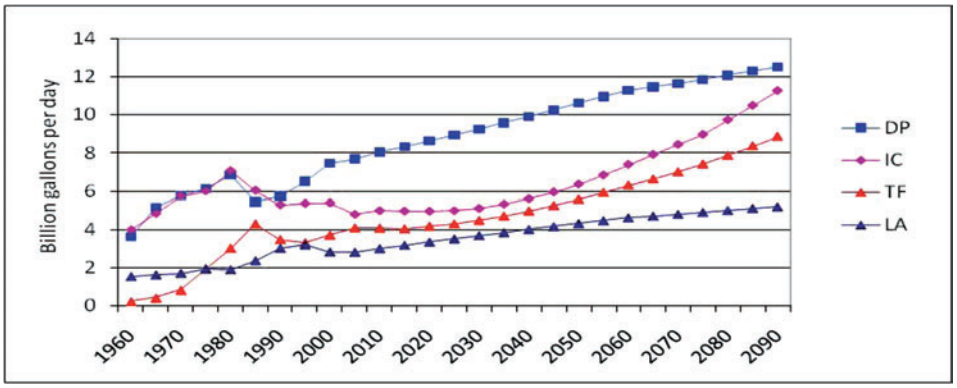

Figure 5.21. Past and projected annual U.S. consumptive use for the four use types of lower use amount, scenario A1B population and income, no future change in climate.

5.9.2.2 The A2 and B2 scenarios

Consistent with expectations given the relative levels of population (Figure 2.1) and income (Figure 2.2) among the three scenarios and the importance of population in the projection methods, projected withdrawals and consumptive use of the A1B scenario fall in between the levels of the A2 and B2 scenarios. In comparison with the projected aggregate change in withdrawals in the United States with the A1B scenario of about 3% from 2005 to 2060, the changes with the A2 and B2 scenarios are 8% and -9%, respectively (Figure 5.22). Withdrawals with the A2 scenario follow a similar path to those of the A1B scenario, reaching a minimum in 2025 and then rising continuously thereafter. However, the B2 scenario withdrawals decrease until 2045 and rise only slightly thereafter. Under this scenario, the effect of the continuously rising withdrawals of the DP and LA sectors eventually (in 2045) outweighs the effect of the continuously declining TF and IR withdrawals, with IC withdrawals changing little and thus having little effect on the changing slope of the total withdrawal curve.

As previously indicated, U.S. consumptive use with the A1B scenario is projected to increase by about 10% from 2005 to 2060. Comparable changes for the A2 and B2 scenarios are 12% and 5%, respectively (Figure 5.23). Consumptive use is largely a matter of irrigation. As modeled here, irrigated area does not vary by scenario such that consumptive use does not vary much among the scenarios.

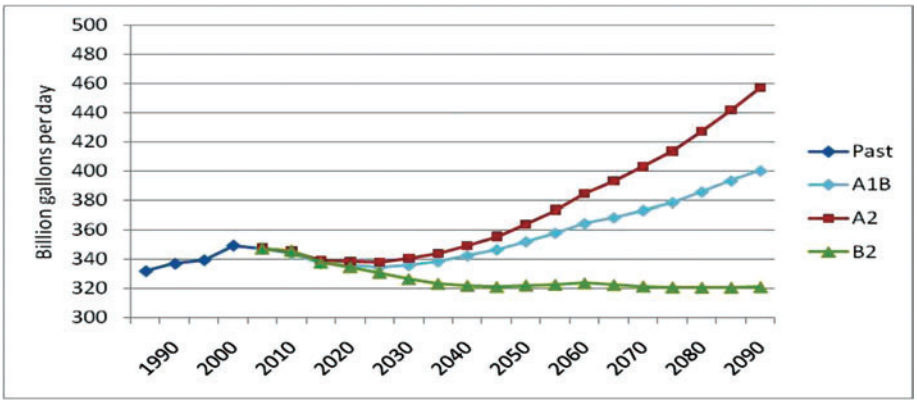

Figure 5.22. Past and projected U.S. withdrawals assuming no future change in climate and projected population and income for three scenarios.

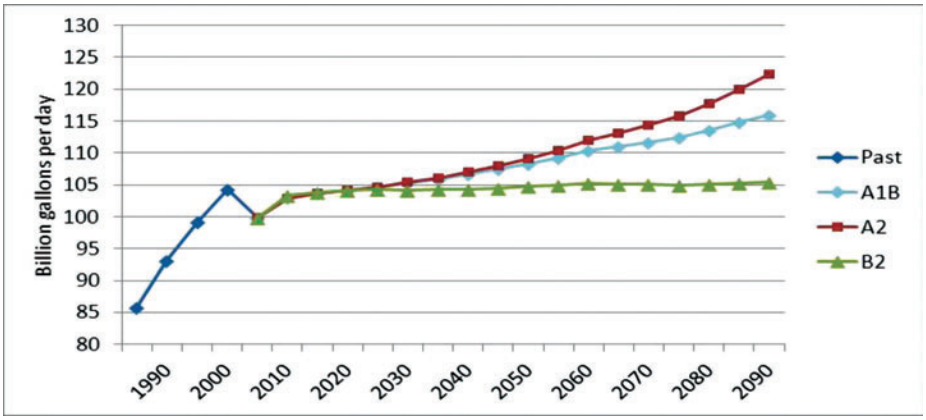

Figure 5.23. Past and projected U.S. consumptive use assuming no future change in climate and projected population and income for three scenarios.

5.9.2.3 Future water use by WRR and ASR

Projected changes in water use over the next 50 years vary widely across WRRs. Figures 5.24 and 5.25 show percent change from 2005 to 2060 in withdrawals and consumptive use, respectively. Withdrawals are projected to increase in some WRRs and decrease in others (Figure 5.24). The large percentage increases shown for some WRRs occur for various reasons. For example, the increases in WRR 3 are primarily due to increases in the DP, IC, and IR water use sectors; in WRR 8, the increase is largely due to increases in the IR sector; in WRR 15, the increase largely reflects the expansion of the DP sector in response to population growth; in WRR 9, the increase is attributable largely to changes in the IR and AQ categories; and in WRR 17, the AQ sector is largely responsible for the large increase. Some other WRRs show large decreases in withdrawal, and again the reasons vary across WRRs. For example, the decreases in WRRs 4 and 5 are attributable to reductions in the TF sector, where increases in production of renewable energy allow production at thermoelectric plants to remain relatively steady while efficiency (γ^{TH}) simultaneously improves. The decreases in withdrawals in WRRs 13 and 14 are caused largely by reductions in IR water use.

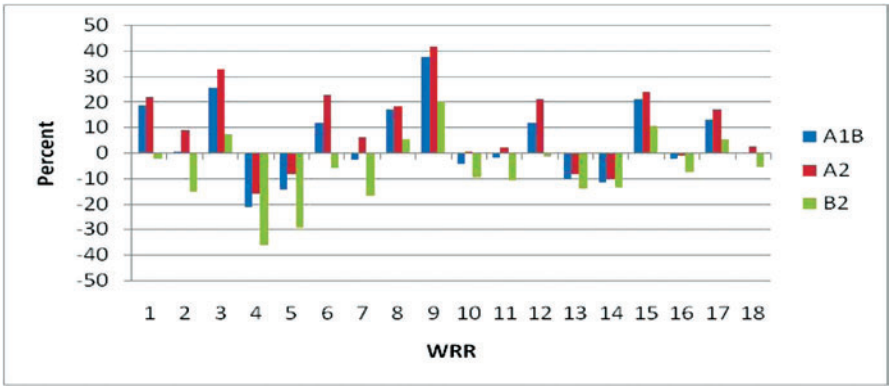

Figure 5.24. Change in withdrawal from 2005 to 2060 by WRR assuming no future change in climate and projected population and income for three scenarios.

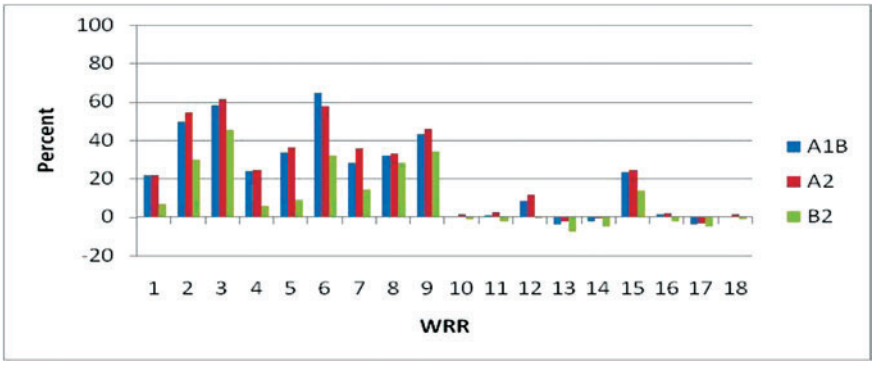

Figure 5.25. Change in consumptive use from 2005 to 2060 by WRR assuming no future change in climate and projected population and income for three scenarios.

Percent changes in consumptive use (Figure 5.25) present a different picture from percent changes in withdrawals. Consumptive use is projected to increase substantially in eastern WRRs but not in western WRRs, with the exception of WRR 15. In the East, consumptive use increases in all six water use categories. In the West, decreases in the IR sector tend to balance out increases in the other categories except for WRR 15 where increases in DP use overwhelm the IR decreases. The dichotomy between the East and West in consumptive use results mainly from the way irrigation—for which consumptive use proportion (γ) is relatively high—is modeled. Recall that, based on past trends, irrigated area is projected to increase in the East and decrease in the West.

Also noteworthy in Figures 5.24 and 5.25 are the differences among the three scenarios. As expected, water use with the low population growth B2 scenario is consistently and substantially lower than with the other two scenarios. And water use with the A2 scenario is nearly always, though moderately, higher than that of the A1B scenario.

Under the A1B scenario, consumptive use is projected to decrease in 25 ASRs and increase from 2005 to 2060 by up to 25% in 27 WRRs, by from 25% to 50% in 31 ASRs, and by over 50% in the remaining 15 ASRs (Figure 5.26). Decreases, which tend to be less than 10%,

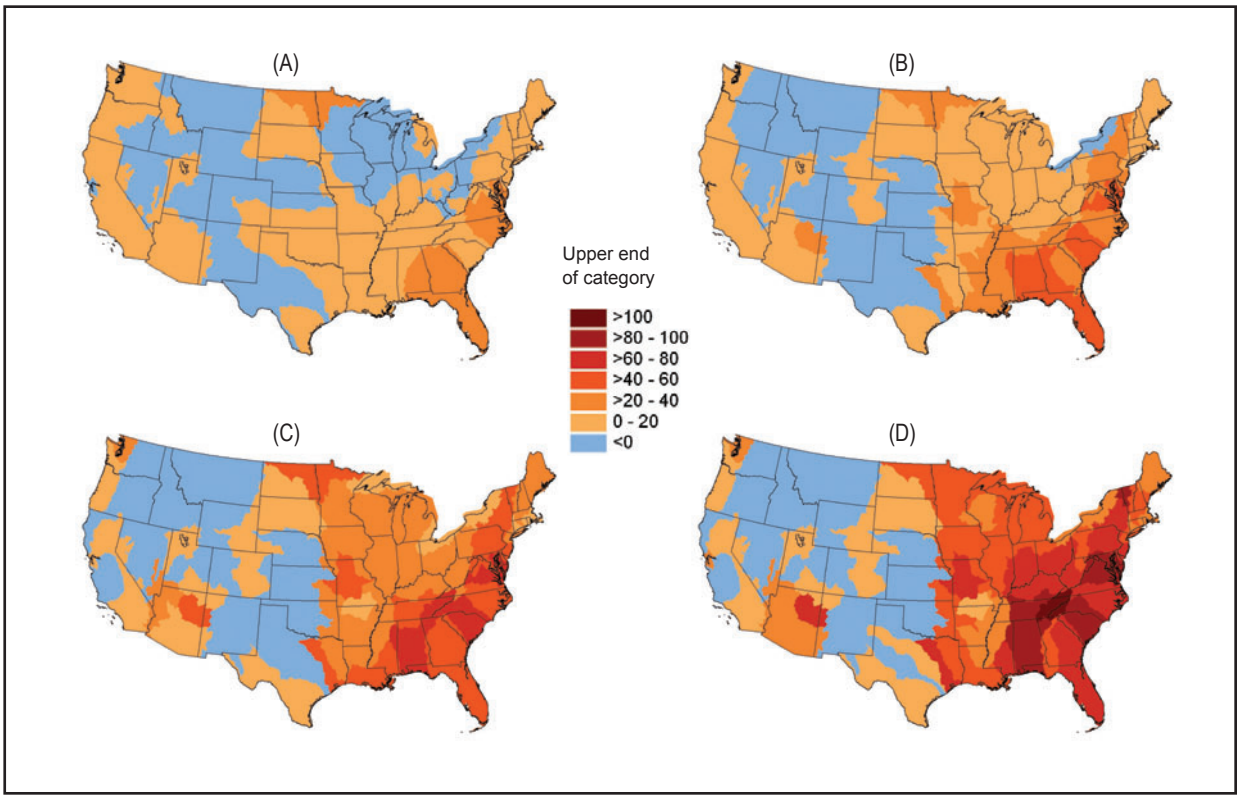

Figure 5.26. Change in projected annual consumptive use for the A1B scenario assuming no future climate change—percent change from 2005 to (A) 2020, (B) 2040, (C) 2060, and (D) 2080.

are concentrated in the West and reflect mainly the gradually decreasing irrigated acreage and withdrawal rate. The greatest increases occur in the Southeast and Mid-Atlantic regions. Patterns of change for the A2 scenario (Figure 5.27) and B2 scenario (Figure 5.28) are similar to those of the A1B scenario. These projections, while not as extreme as one might expect given the large expected population increases, ignore climate change. As seen in the next section, climate change has the potential to more dramatically alter projected water use.

5.9.3 Future Water Use Under a Changing Climate

The separate effects of changes in temperature, precipitation, potential evapotranspiration (ETp), and CO_2 are first presented, followed by the combined effects. Then, we present the results for the nine alternative futures, which incorporate both socioeconomic and climate effects. Finally, the major results are extended to 2090. As will be seen, the projected climate effects are heavily dependent on estimates of future ETp, and thus on the model we used to estimate ETp (see Chapter 2).

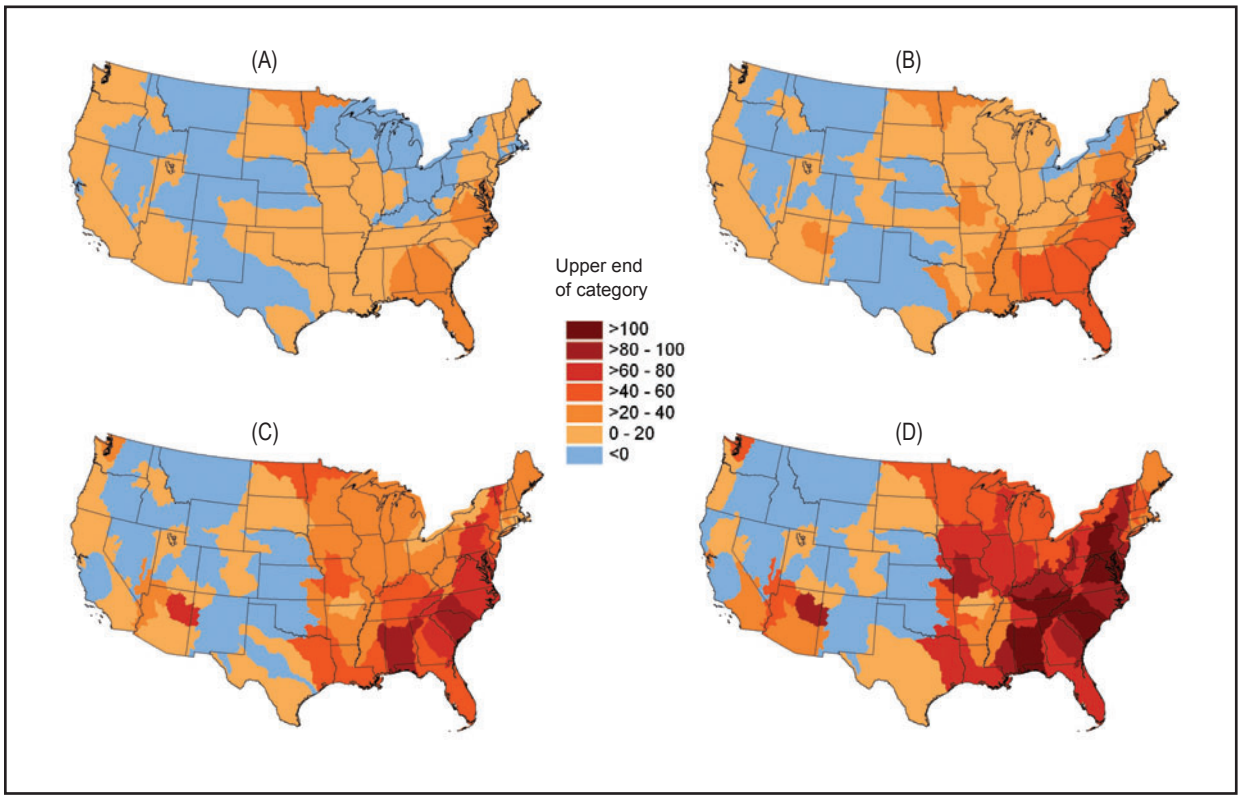

Figure 5.27. Change in projected annual consumptive use for the A2 scenario assuming no future climate change—percent change from 2005 to (A) 2020, (B) 2040, (C) 2060, and (D) 2080.

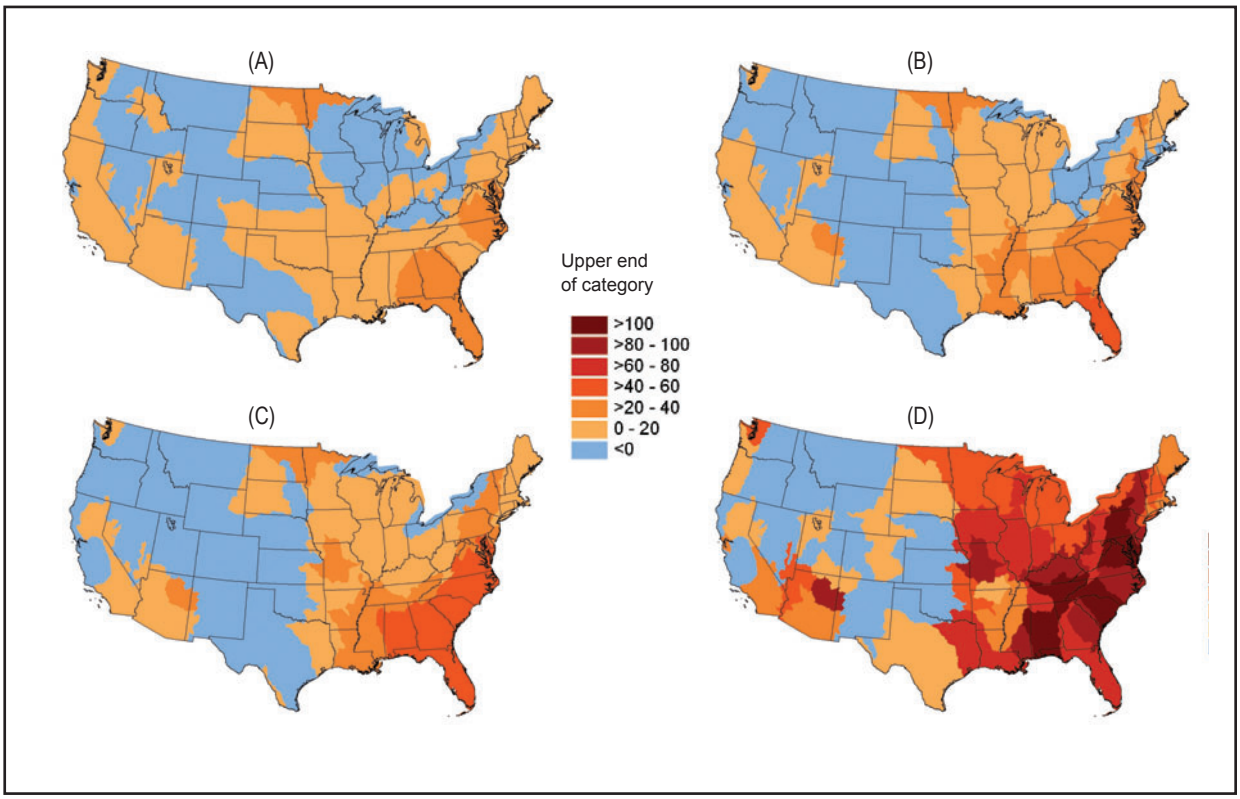

Figure 5.28. Change in projected annual consumptive use for the B2 scenario assuming no future climate change—percent change from 2005 to (A) 2020, (B) 2040, (C) 2060, and (D) 2080.

5.9.3.1 Climate effects

The projected changes in water use attributable to climate change were computed by comparing projected total water use in a given future year assuming no future change in climate with projected total water use for that year if the climate were to change. This was done separately for temperature, precipitation, ETp assuming no direct CO_2 effect, and for ETp with a corresponding direct CO_2 effect.

The magnitudes of the different climate effects vary by alternative future. To give a general notion of the magnitude of the effects, Figures 5.29 and 5.30 depict the effects in percentage terms averaged across the nine futures.[62] The temperature effect is minimal, the precipitation effect is small, and the ETp effect is quite large, even if mitigated by the direct CO_2 effect. The temperature effect is due to increasing water use at thermoelectric plants to accommodate the increase in electricity use to meet space cooling demands. Because the consumptive use proportion for thermoelectric withdrawals (γ^{TF}) is relatively low in most WRRs, the temperature effect on consumptive use is correspondingly low (typically below 0.5%). The precipitation effect is due to the change in agricultural irrigation and landscape watering that occurs as precipitation varies above or below the historical average. The precipitation effect on consumptive use is typically below 5%.

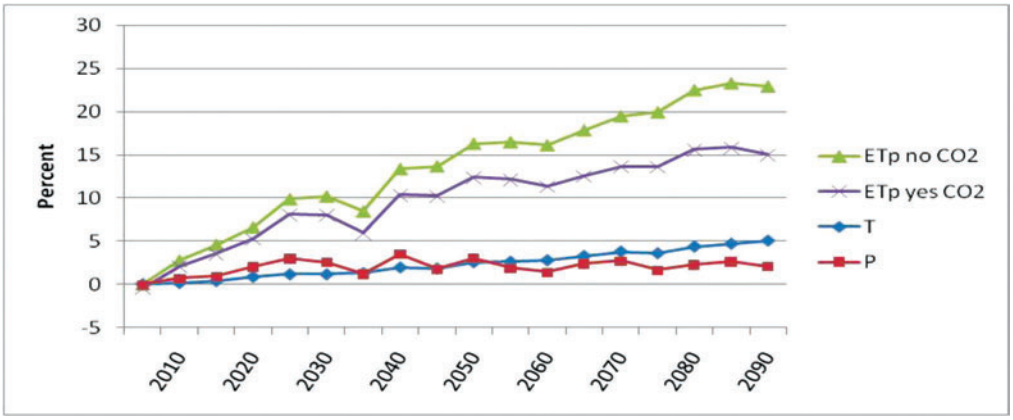

Figure 5.29. Separate climate change effects on projected total annual U.S. withdrawal, averaged over the nine alternative futures (percent change from a future with no climate change to the climate change future).

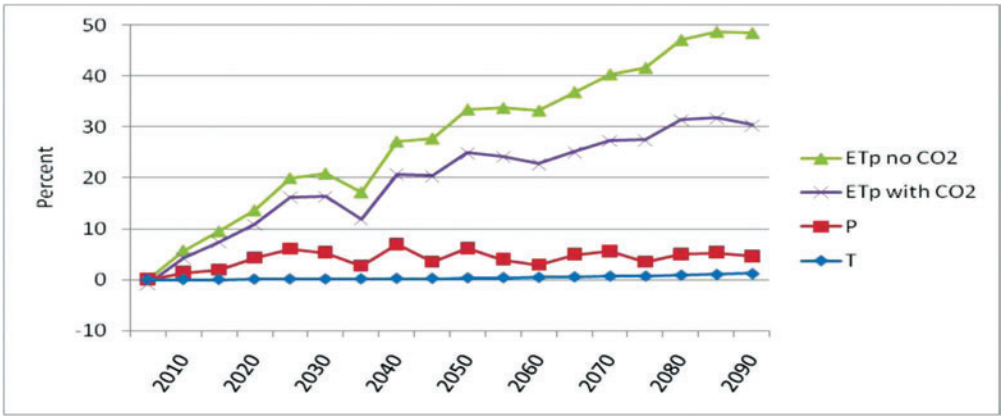

Figure 5.30. Separate climate change effects on projected total annual U.S. consumptive use, averaged over the nine alternative futures (percent change from a future with no climate change to the climate change future).

The ETp effect is due to change in irrigation and landscape watering as plant water demand responds to changes in ETp. By 2060, the ETp effect (that is, the change in water use attributable to climate change, all else equal) reaches 16% for withdrawal and 33% for consumptive use. The ETp effect is reduced by roughly one-fourth when the direct CO_2 effect is also included. Recall that the direct CO_2 effect modeled here is more or less an upper bound of what is currently understood to be the potential direct CO_2 effect.

Again averaging across the nine scenario-GCM alternative futures, the combined (temperature, precipitation, and ETp) effect of a changing climate is to increase aggregate consumptive use in the United States in year 2060, as compared to a constant climate, by 25% (when the direct CO_2 effect is included) to about 35% (excluding the direct CO_2 effect) (Figure 5.31). The fluctuations over time shown in Figures 5.29-5.31 occur largely because of cyclical patterns in the GCM projections of temperature and precipitation.[63] Despite these fluctuations, the overall trend is inexorably upward as ETp rises in response to rising temperatures.

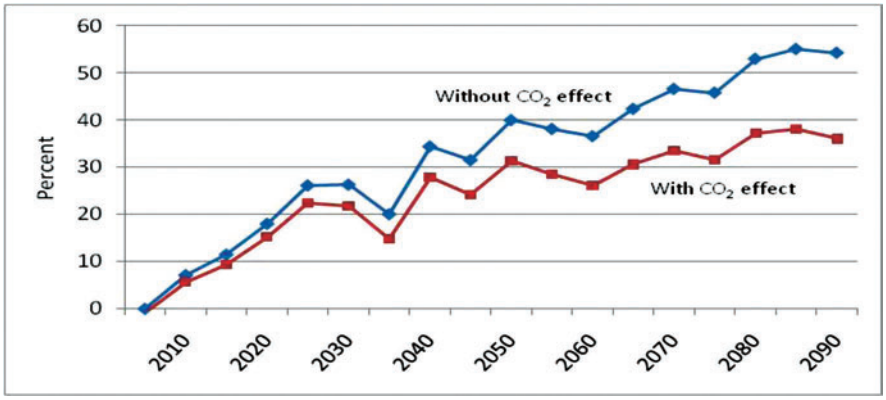

Figure 5.31. Combined (T, P, and ETp) effect of climate change on projected total annual U.S. consumptive use for an average of the nine alternative futures (percent change from the future with no climate change to the climate change future).

As seen in Figure 5.31, climate change has the potential to significantly raise projected water use above the levels that would occur if only population and income were changing. What Figure 5.31 masks is the variation in the effect of climate change on future water use across the scenarios, across the GCMs within a scenario, and across space. This variation is examined next, for the combined (temperature, precipitation, and ETp) climate effect, ignoring the direct CO_2 effect.

Percent changes in projected withdrawals in 2060 attributable to climate change are relatively modest in most of the eastern WRRs (Figure 5.32), largely because the water use categories most affected by climate change (DP and IR) account for little of total withdrawals (for example, in 2005, DP and IR withdrawals across WRRs 1-9 were each 10% of total withdrawal, whereas 65% of total withdrawal occurred in the TF sector).[64] In contrast, in the West, the DP and IR water use categories account for the large majority of total withdrawals (in 2005, DP and IR withdrawals across WRRs 10-18 were 10% and 68%, respectively, of total withdrawal), causing withdrawals in the West to be more sensitive to projected climate change.

In contrast to withdrawals, percent changes in projected consumptive use in 2060 are more evenly spread across the United States (Figure 5.33). However, significant differences remain among individual WRRs. For example, for the A1B scenario modeled using the CGCM GCM, the change in consumptive use varies from -14% for WRR 10 to 36% for WRR 8, with the change exceeding 10% in 15 WRRs and 20% in 5 WRRs. Similarly, for the A1B scenario modeled using the CSIRO GCM, the change in consumptive use varies from 11% for WRR 15 to 106% for WRR 9, with the change exceeding 20% in 16 WRRs and 30% in nine WRRs. The percent changes are even greater for the MIROC GCM. Comparing scenarios, we see that the percent changes are generally (though not always) higher with the A2 scenario and lower with the B2 scenario than with the A1B scenario for respective GCMs (Figure 5.33). Differences among GCMs for a given scenario of course reflect differences in projections of temperature, precipitation, and ETp.

A1B

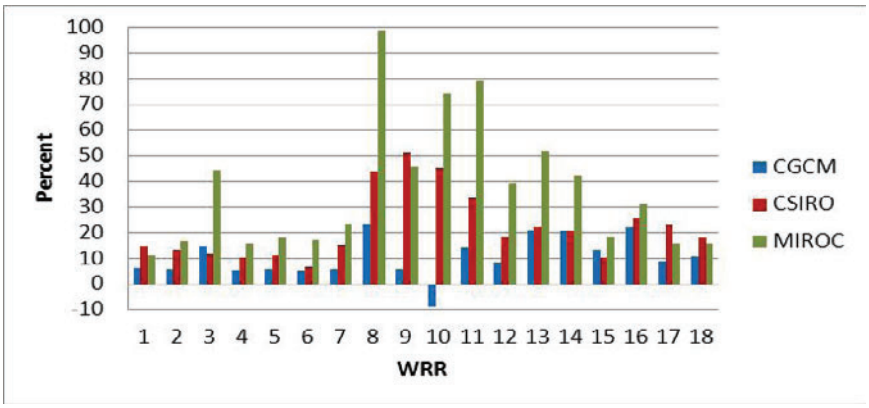

A2

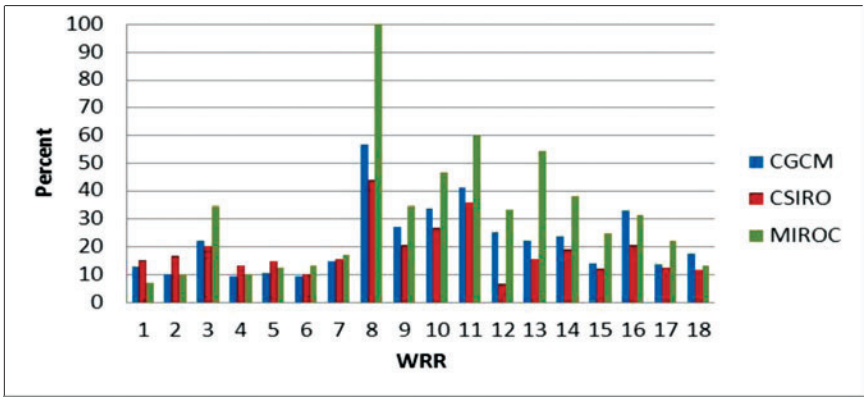

B2

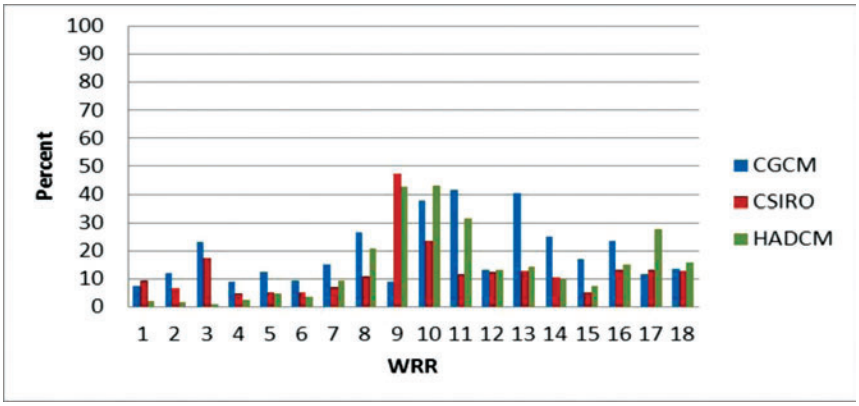

Figure 5.32. Effect of climate change on projected total annual withdrawal by WRR (percent change in 2060 from the constant climate future to the climate change future, no direct CO_2 effect).

A1B

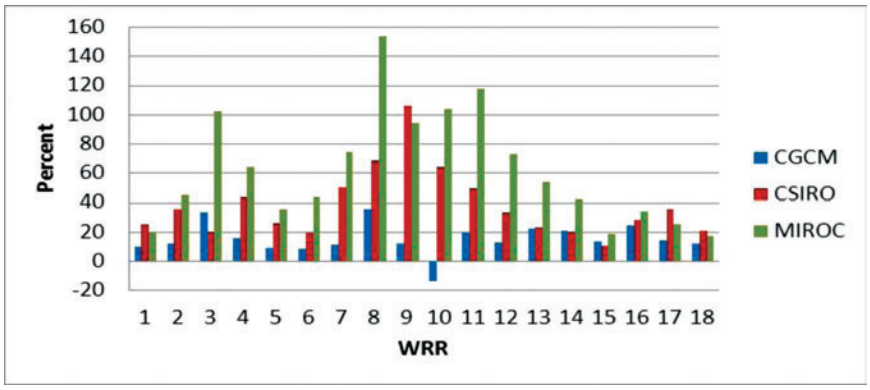

A2

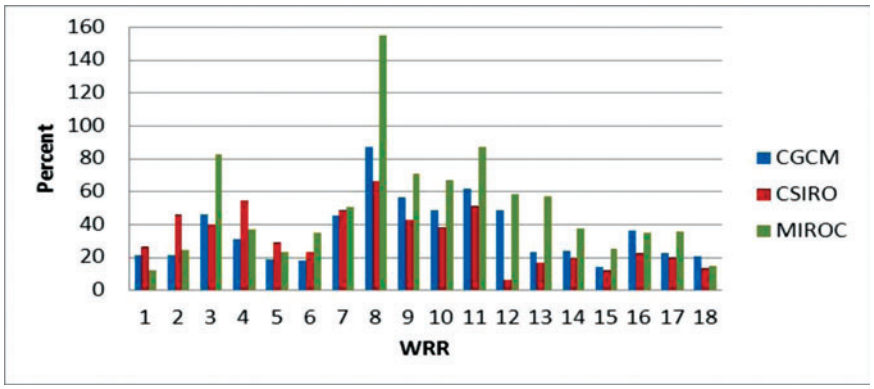

B2

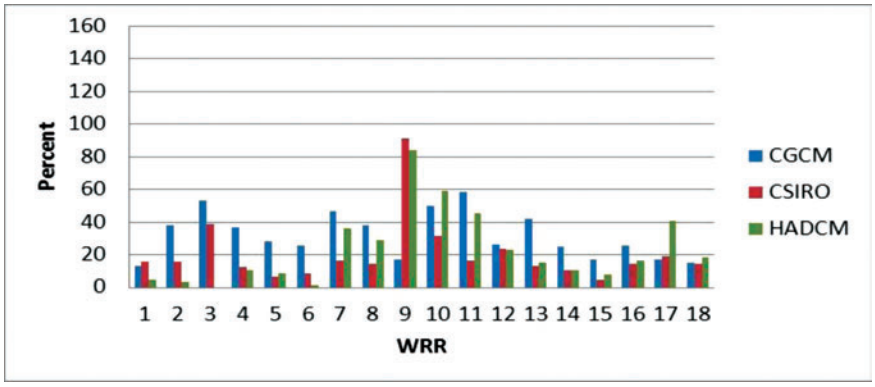

Figure 5.33. Effect of climate change on projected total annual consumptive use by WRR (percent change in 2060 from the constant climate future to the climate change future, no direct CO_2 effect).

The climate change effects for 2060 shown in Figures 5.32 and 5.33 provide a general picture of the effect of climate change on withdrawals and consumptive use, but change for any one year (or five-year interval, as shown in the figures) may be misleading, for it may not represent the long-term trend. A good example of this possibility is WRR 10 modeled using the CGCM GCM, where withdrawal and consumptive use under climate change actually decrease compared with a constant climate (Figures 5.32 and 5.33). This occurs because growing season precipitation in WRR 10 is unusually high in year 2060, at 6.3 cm above the 2005 level. In comparison, the increase above 2005 growing season precipitation is only 1.6 cm in 2050 and 0.5 cm in 2070.

5.9.3.2 Projected water use

We now combine the population and income effects with the climate change effects to compute projected future water use for the nine alternative futures, looking first at the United States as a whole. For withdrawals, projections for 2060 vary from 354 bgd with the B2-CSIRO future to 493 bgd with the A2-MIROC future, compared with 357 assuming the A1B population and income projection and no change in climate (Figure 5.34). And for consumptive use, projections for 2060 vary from 125 bgd with the B2-CSIRO future to 186 bgd with the A1B-MIROC future, compared with 110 assuming the A1B population and income projection and a constant climate (Figure 5.35).

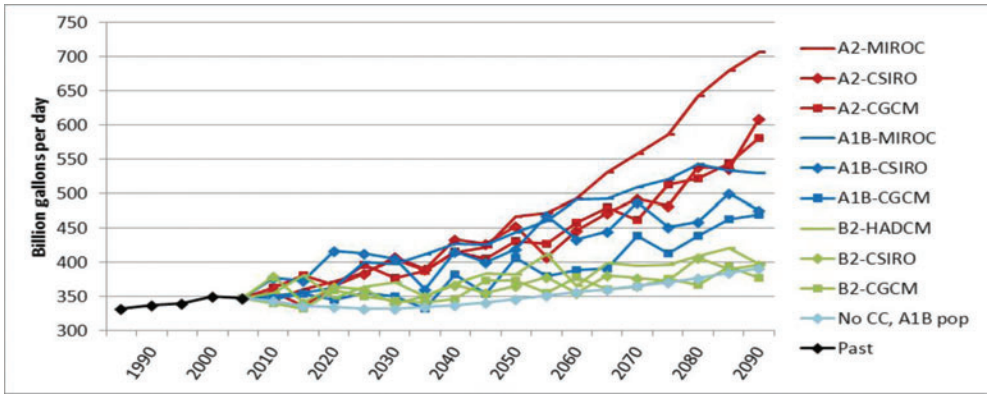

Figure 5.34. Past and projected U.S. withdrawal for alternative futures, with no direct CO_2 effect.

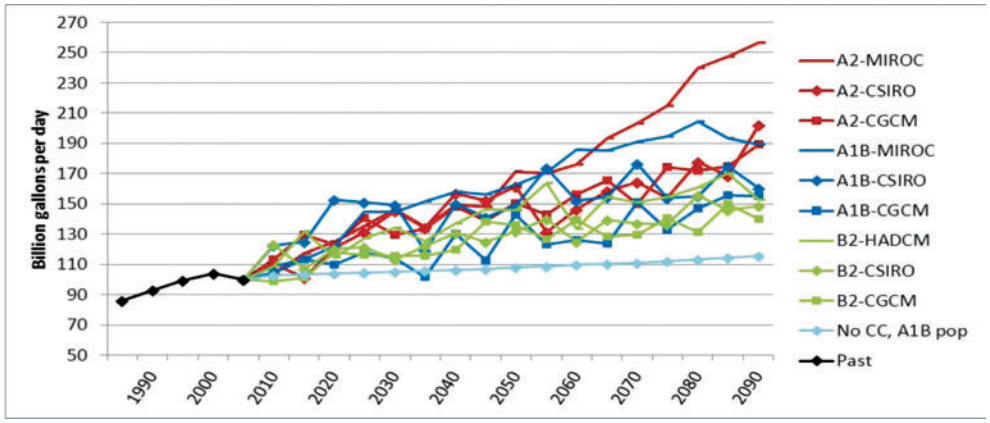

Figure 5.35. Past and projected U.S. consumptive use for alternative futures, with no direct CO_2 effect.

Projected water use varies considerably across GCMs for a given scenario (Figures 5.34 and 5.35). The greatest variation occurs with the A1B scenario, where for 2060, for example, projected consumptive use varies from 126 bgd with the CGCM GCM to 186 bgd with the MIROC GCM. This variation is a direct result of differences in projected temperature and precipitation. For 2060, the MIROC GCM predicts the highest temperatures (Figure 2.4) and lowest precipitation levels (Figure 2.3), and the CGCM GCM predicts the highest precipitation levels.

There is no way to know the extent to which the GCMs used in this study capture the range in future climate for a given emission scenario, or the extent to which an average across the three GCMs for a given scenario represents a central tendency for that scenario. Nevertheless, it is instructive to view results for the three scenarios when results of the three GCMs per scenario are averaged, for such averaging shows more clearly the relative relations among the three scenarios. For withdrawal (Figure 5.36) and also largely for consumptive use (Figure 5.37), the A1B and A2 scenarios do not differ much in projected water use through 2060, whereas projected use with the B2 scenario is much lower. Consumptive use is projected to increase from 2005 to 2060 by 55%, 60%, and 33% with the A1B, A2, and B2 scenarios, respectively, assuming no direct CO_2 effect.

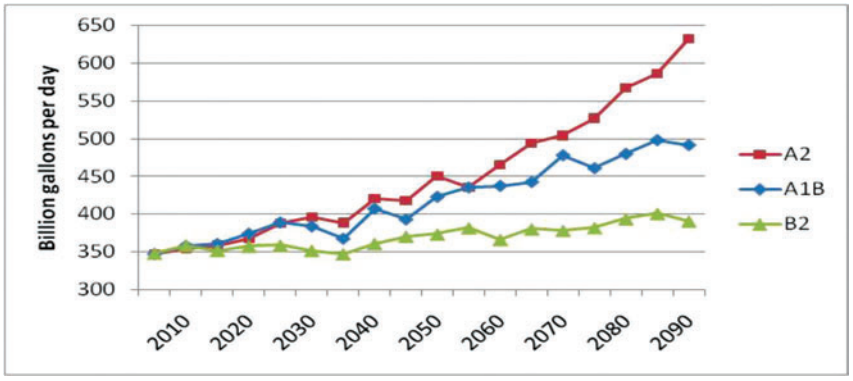

Figure 5.36. Projected U.S. withdrawals for three scenarios, averaging across three GCMs per scenario, with climate change but no direct CO_2 effect.

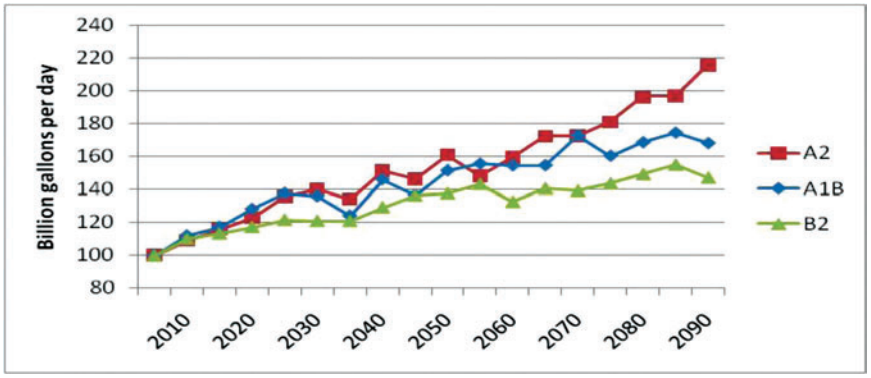

Figure 5.37. Projected U.S. consumptive use for three scenarios, averaging across three GCMs per scenario, with climate change but no direct CO_2 effect.

As expected given the information we presented about the separate socioeconomic and climate effects, there is wide variation across space in projections of future water use. Focusing first on the change from 2005 to 2060, taking the A1B-CGCM future as an example, consumptive use is projected to decrease in four ASRs, increase by more than 25% in 59 ASRs, and increase by more than 50% in 29 WRRs (Figure 5.38). The projected changes with the A1B scenario tend to be greater when the CSIRO or MIROC GCMs is used, with the changes in consumptive use reaching well above 100% in some cases (Figures 5.39 and 5.40).

The purview of the 2010 RPA Assessment is to 2060, but the most dramatic climate effects are expected in the latter half of the century. The projections were extended to 2090 by growing population and income in all ASRs using growth rates for years beyond 2060 specified by the IPCC and by applying the methods described previously for estimating the other factors used to project water withdrawal and consumptive use.

As seen in Figures 5.38-5.46, projected consumptive use in the United States beyond 2060 continues to grow at roughly the prior rate with most futures, except for the two MIROC-based projections, which show much higher use levels. As described earlier, the MIROC model expects a much drier future than do the other models. Aggregate U.S. consumptive use in 2090 is projected to be 115 bgd with the A1B scenario assuming no change in climate. Averaging across GCMs for a given scenario, 2080 consumptive use is projected to be 168, 216, and 147 bgd with the A1B, A2, and B2 scenarios, respectively.

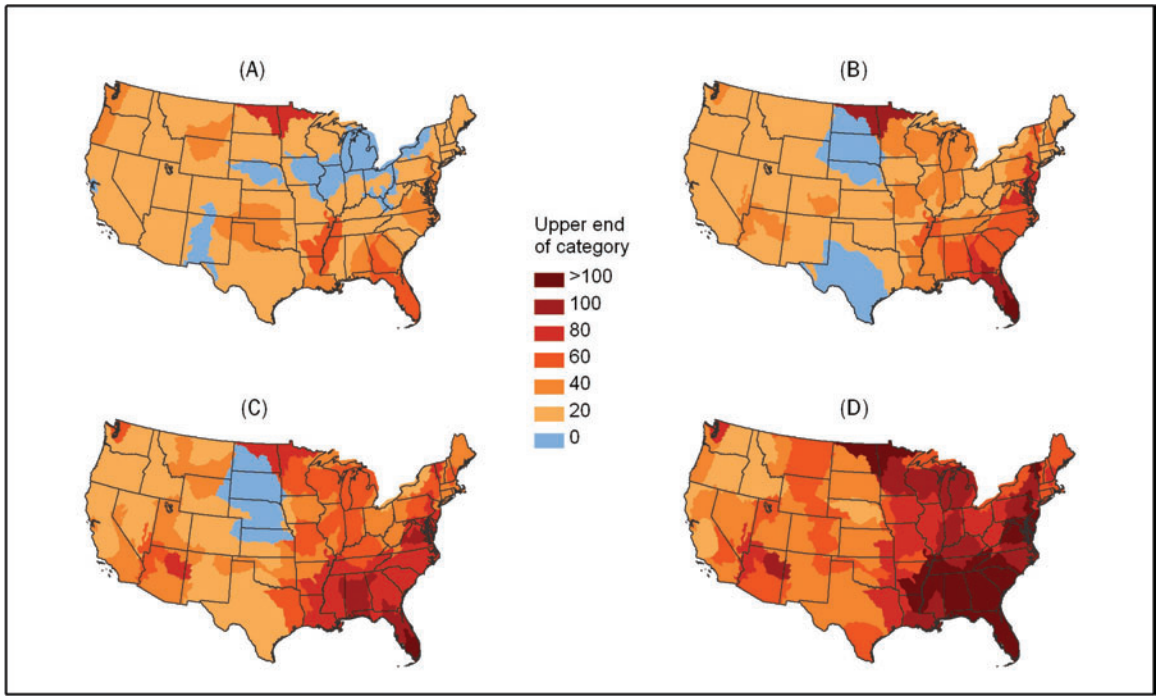

Figure 5.38. Change in projected annual consumptive use for the A1B-CGCM future (with climate change but no direct CO_2 effect)—percent change from 2005 to (A) 2020, (B) 2040, (C) 2060, and (D) 2080.

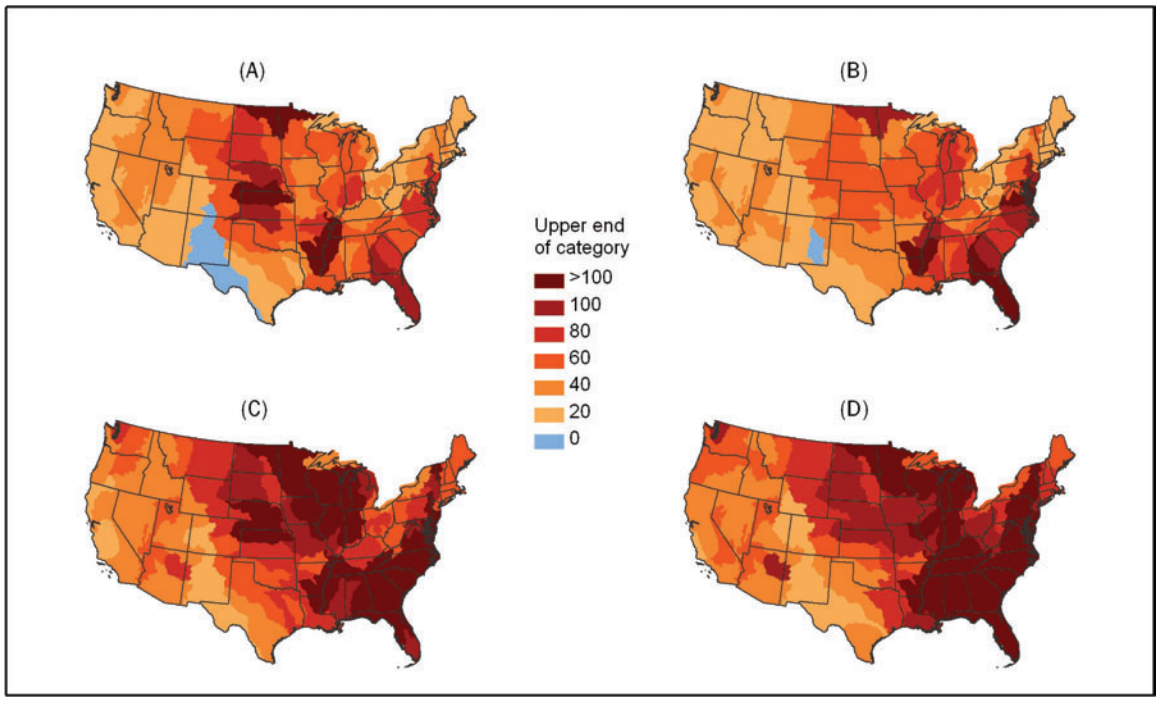

Figure 5.39. Change in projected annual consumptive use for the A1B-CSIRO future (with climate change but no direct CO_2 effect)—percent change from 2005 to (A) 2020, (B) 2040, (C) 2060, and (D) 2080.

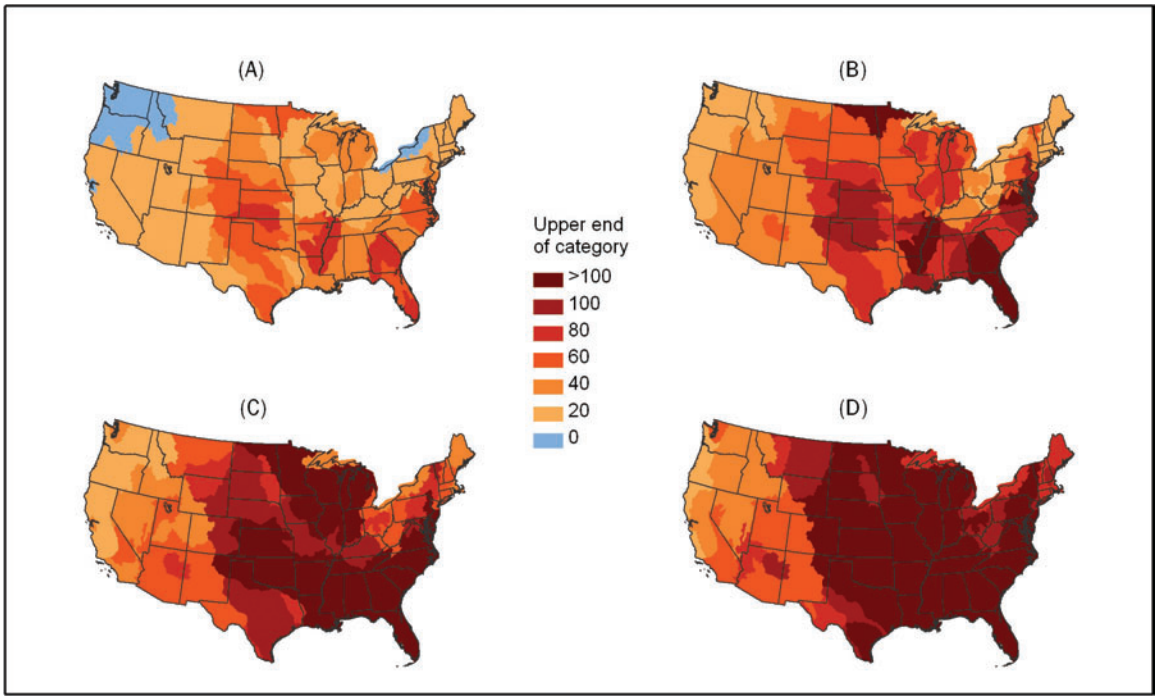

Figure 5.40. Change in projected annual consumptive use for the A1B-MIROC future (with climate change but no direct CO_2 effect)—percent change from 2005 to (A) 2020, (B) 2040, (C) 2060, and (D) 2080.

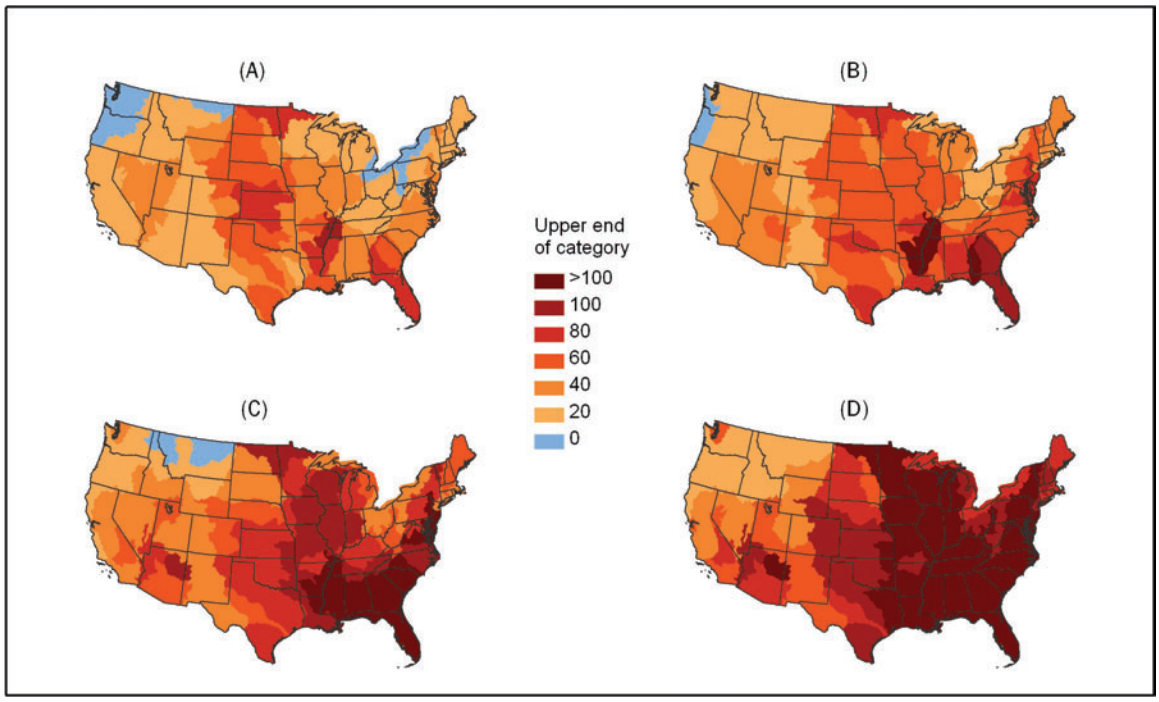

Figure 5.41. Change in projected annual consumptive use for the A2-CGCM future (with climate change but no direct CO_2 effect)—percent change from 2005 to (A) 2020, (B) 2040, (C) 2060, and (D) 2080.

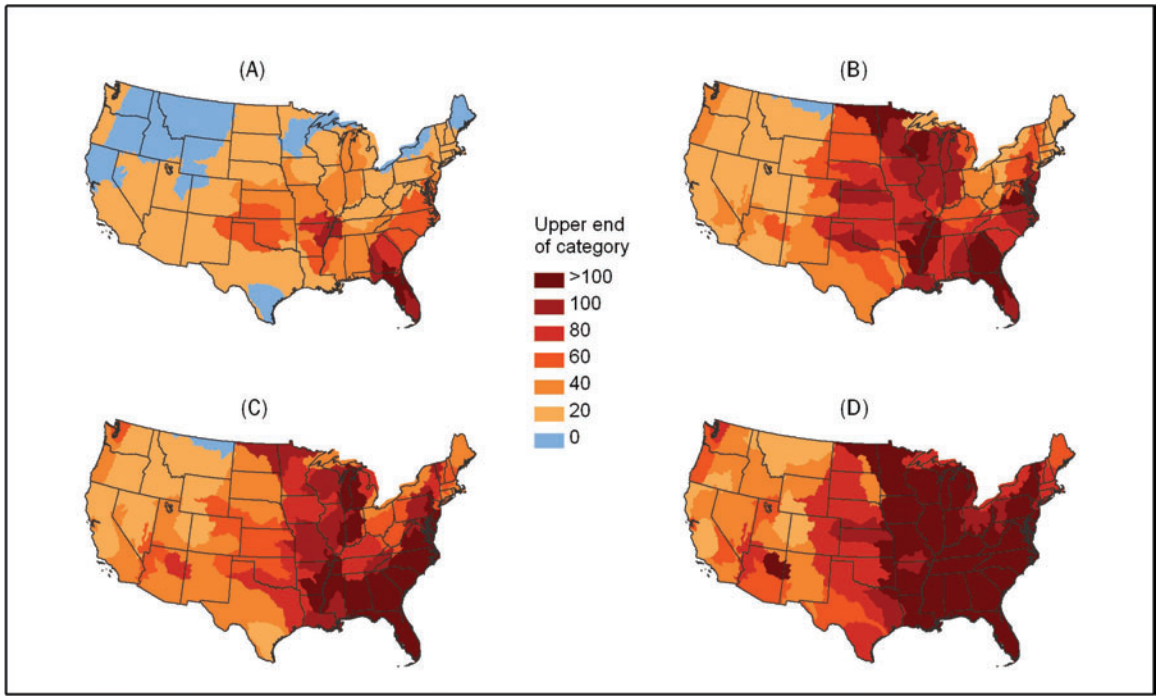

Figure 5.42. Change in projected annual consumptive use for the A2-CSIRO future (with climate change but no direct CO_2 effect)—percent change from 2005 to (A) 2020, (B) 2040, (C) 2060, and (D) 2080.

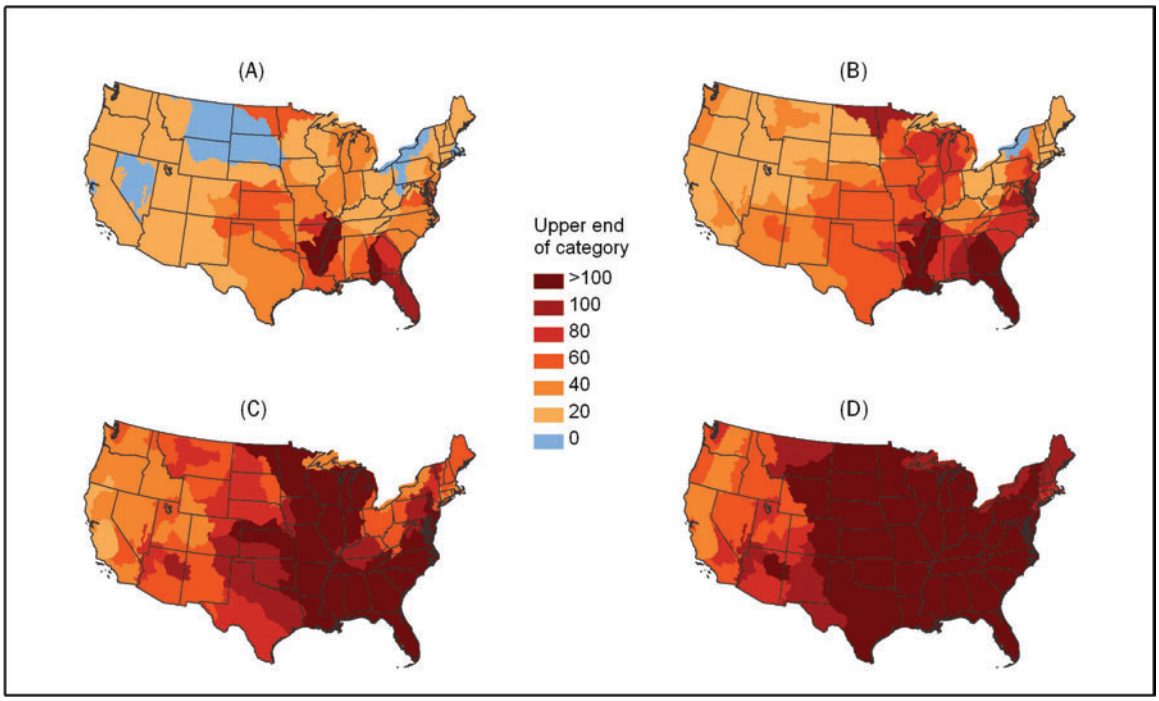

Figure 5.43. Change in projected annual consumptive use for the A2-MIROC future (with climate change but no direct CO_2 effect)—percent change from 2005 to (A) 2020, (B) 2040, (C) 2060, and (D) 2080.

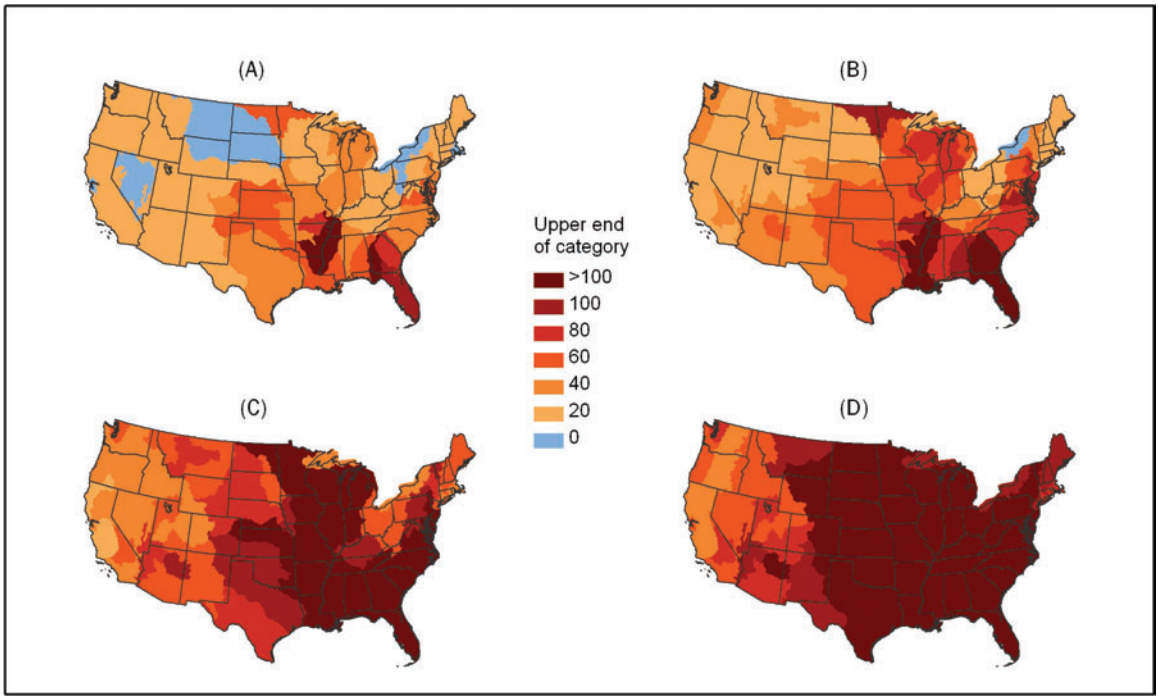

Figure 5.44. Change in projected annual consumptive use for the B2-CGCM future (with climate change but no direct CO_2 effect)—percent change from 2005 to (A) 2020, (B) 2040, (C) 2060, and (D) 2080.

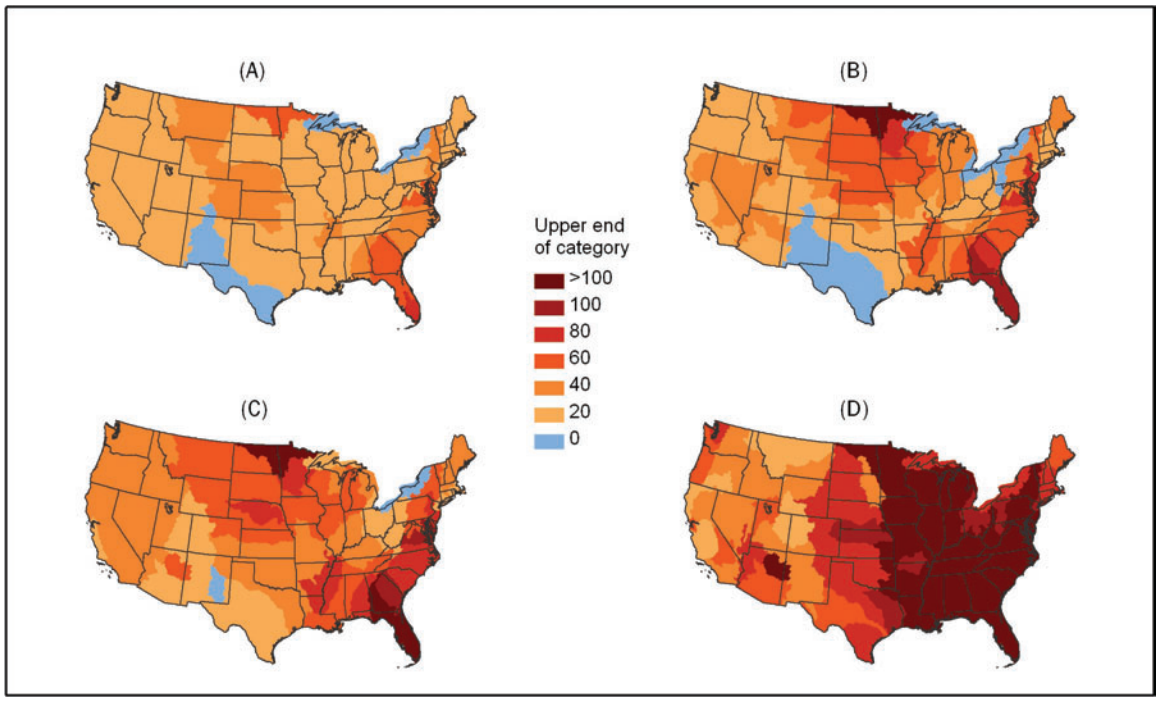

Figure 5.45. Change in projected annual consumptive use for the B2-CSIRO future (with climate change but no direct CO_2 effect)—percent change from 2005 to (A) 2020, (B) 2040, (C) 2060, and (D) 2080.

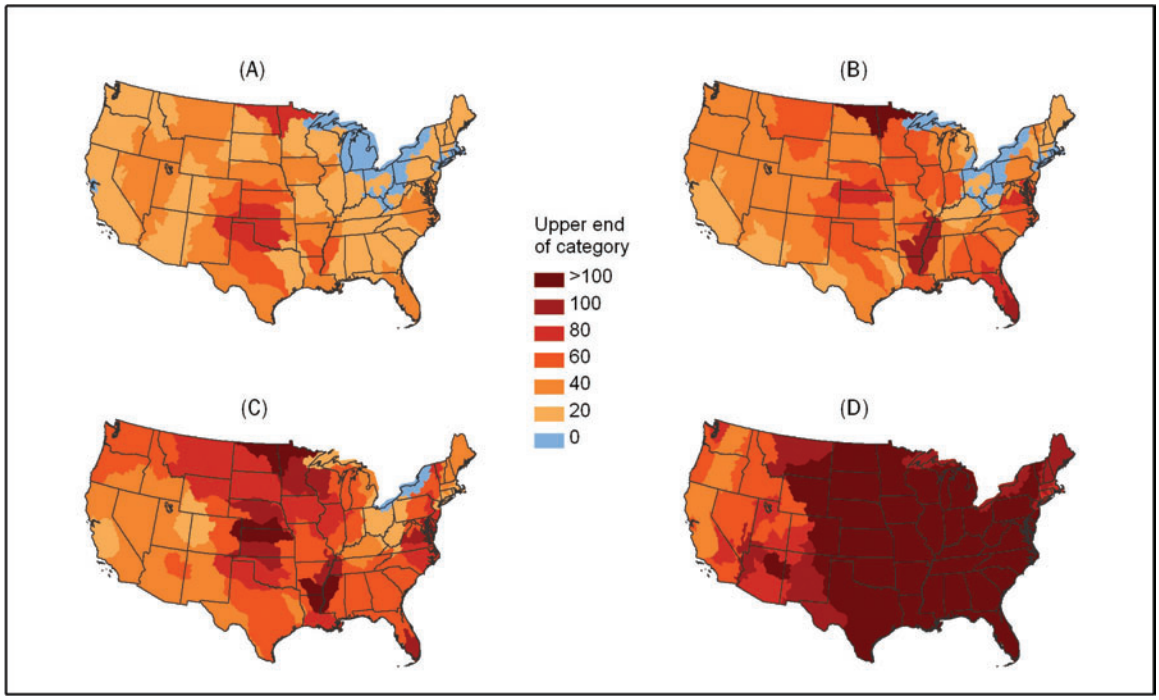

Figure 5.46. Change in projected annual consumptive use for the B2-HADN future (with climate change but no direct CO_2 effect)—percent change from 2005 to (A) 2020, (B) 2040, (C) 2060, and (D) 2080.

By far, the greatest projected consumptive use in 2080 (240 mgd) occurs with the A2-MIROC future as a result of a much lower precipitation estimate than that of the other futures and also the highest mean temperature among the futures.

5.10 Summary

Despite an expected large increase in population, over the next 50 years total water withdrawals in the United States are projected to remain remarkably close to current levels assuming no future climate change. Given the A1B scenario, which incorporates the moderate prediction for future population, U.S. withdrawals are projected to increase from 2005 to 2060 by 3% and consumptive use by about 10% despite a 51% increase in population. This hopeful projection occurs largely because of expected future gains in water use efficiency and reductions in irrigated area in the West. However, climate change may significantly alter water demands. Again assuming the A1B scenario, water withdrawals under climate change are projected to increase over the next 50 years by 12% to 41%, and consumptive use is projected to increase by 26% to 86%, depending on which GCM is used to simulate climate for the A1B scenario. The MIROC GCM predicts the highest temperatures and lowest precipitation levels of the three models for 2060 and accounts for the upper ends of these two ranges. The CGCM GCM predicts the lowest temperatures and accounts for the lower ends of the ranges.

The projections generally indicate that total consumptive use will increase more in the East than in the West, which is perhaps unexpected given that populations in the West are growing faster than those in much of the East. The principal reason is that, in line with recent past changes, irrigated area is projected to decline in the West but grow in the East. Because agricultural irrigation accounts for most of consumptive use in the West, total consumptive use is very sensitive to irrigated area changes.

These projections and the GCM output on which the projected effects of climate change rely are educated guesses. The wide ranges highlight the uncertainty about the effects of increases in GHGs on temperature and precipitation. Although we cannot be sure that the ranges reported here span the full extent of the future possibilities, it is notable that with all nine alternative futures, the long-term effects of climate change are always to increase water demands. Further, the principal effect is that of increasing temperature on plant water demand, not that of increasing temperature on electricity demand or of changing precipitation. Increasing precipitation in some locations ameliorates the effect of temperature increases, but precipitation increases, where they occur, are insufficient to balance out the temperature effect.

Aside from the estimates of future climate variables, perhaps the most critical assumption made for projecting future water use is about future irrigated area because irrigation accounts for the bulk of consumptive use and because irrigation requirements are more sensitive than the other water use sectors to climate change. Although recent trends in irrigated area provide some basis for extrapolation, unexpected changes in world markets could easily alter the trajectory. Additional effort should be allotted to improving the estimates of future irrigated area.

Chapter 6: Vulnerability Assessment

6.1 Overview

Vulnerability, defined as the probability of water shortage, was assessed at the ASR level for current and future climatic and socio-economic conditions. A shortage occurs whenever the water supply of an ASR is insufficient to meet the demand.

Vulnerability for both current and future conditions was evaluated by simulating water allocation within the water networks of the United States. Individual water network simulations were performed for the nine alternative futures at the annual time step. Each simulation started in 1953 and proceeded to year 2090. Vulnerability was measured for five 20-year time periods within the 1953-2090 time span. Current vulnerability was estimated as the probability of shortage for the period 1986-2005. Future vulnerability was estimated for four 20-year periods centered at 2020, 2040, 2060 and 2080. Because years 1953-1985 served to initialize the simulations, results for those years were ignored.

Our probabilistic approach to vulnerability is explained in the next section. The subsequent two sections present the results for current and projected future climatic and socio-economic conditions.

6.2 Vulnerability: Definition and Approach

In general, the vulnerability of a system is a function of the extent to which it can be stressed by external hazards. The definition of vulnerability, however, is subject to considerable discussion (Blaikie and others 1994; Kelly and Adger 2000). In its fourth assessment, the Intergovernmental Panel on Climate Change (IPCC) defined vulnerability as "the degree to which these systems are susceptible to, and unable to cope with, adverse impacts" (Schneider and others 2007). While this definition seems to be widely accepted, it is difficult to implement in practice, in part because "susceptible to… adverse impacts" lacks a precise definition. In assessments of water resources, many studies have resorted to estimating the potential impact of future climatic and socio-economic scenarios by projecting the values of a set of water stress indicators (Postel 2000; Vörösmarty and others 2005; Weib and Alcamo 2011).

In agreement with the IPCC definition, we observe that, conceptually, the vulnerability of a system is a function of its ability to respond to (i.e., cope with or adapt to) inherently variable stressors. However, modeling the ability to respond to stresses—via, for example, construction of new reservoirs or alteration of allocation priorities—is a step beyond our goals in this assessment. Rather, we seek to measure the likelihood that adaptation will be needed and to objectively address the uncertainty about the stressors affecting the system. In particular, we estimate vulnerability as the probability that a critical system threshold, itself a function of both the capacity and the stressors of the system, will be crossed (Kochendorfer and Ramirez 1996). In the context of the U.S. water supply system, this definition translates into evaluating the probability that, at a given time and place, water demand exceeds water supply. In other words, we define vulnerability as the probability of shortage:

$$V = \Pr[S < D] = \Pr[S - D < 0] \tag{6.1}$$

where S is water supply and D is water demand. In general, supply is defined as:

$$S = P - E + I + Q_{div} \tag{6.2}$$

where P is precipitation, E is actual evapotranspiration, I is the input from upstream and from reservoir storage, and Q_{div} is the net trans-basin diversion (the difference between diversions into and diversions out of the ASR).[65]

Setting Z equal to S - D, equation (6.1) can be rewritten as:

$$V = \Pr[Z < 0] = \frac{1}{\sqrt{2\pi\sigma_Z^2}} \cdot \int_{-\infty}^{0} e^{\frac{(z-\mu_Z)^2}{2\sigma_Z^2}}\, dz \tag{6.3}$$

where $\mu_Z = \mu_S - \mu_D$, $\sigma_Z^2 = \sigma_S^2 + \sigma_D^2 - 2\,\mathrm{cov}(S, D)$, and μ_S and μ_D, σ_S and σ_D, and *cov(S, D)* are the mean (μ), standard deviation (σ), and covariance of water supply and water demand.

Equation 6.3 is the exact expression for vulnerability in the case of correlated normally distributed S and D. Or, in the case of non-Gaussian variables, it corresponds to a First Order Second Moment approximation.

Carrying out the integral of equation 6.3 yields,

$$V(\mu_S, \mu_D, \sigma_Z) = \frac{1}{2} + \frac{1}{2} erf\left[\frac{-\mu_S + \mu_D}{\sqrt{2\sigma_Z^2}}\right] \tag{6.4}$$

where *erf()* is the Gauss error function.[66]

Therefore, as is clear from equation 6.4, the vulnerability of water supply to shortage as defined in equation 6.1 is a function of the mean, standard deviation, and covariance of water supply and water demand, that is, μ_S, μ_D, σ_S, σ_D, and *cov(S, D)*. We may then express the total change in vulnerability, *dV*, as a function of the individual contributions of changes in each of those variables as follows:

$$dV = \frac{\partial V}{\partial \mu_S} d\mu_S + \frac{\partial V}{\partial \mu_D} d\mu_D + \frac{\partial V}{\partial \sigma_S} d\sigma_S + \frac{\partial V}{\partial \sigma_D} d\sigma_D + \frac{\partial V}{\partial\, \mathrm{cov}(S, D)} d\,\mathrm{cov}(S, D) \tag{6.5}$$

Each of the five terms of equation 6.5 represents the total change in vulnerability resulting from the changes in μ_S, μ_D, σ_S, σ_D, and *cov(S, D)*. As equation 6.5 makes clear, the total change in vulnerability depends not only on the actual changes in demand and supply but also on the sensitivity of vulnerability to unit changes in demand and supply.

The partial derivatives appearing in equation 6.5 are obtained by differentiating equation 6.4 with respect to μ_S, μ_D, σ_S, σ_D, and *cov(S, D)*, as seen in equations 6.6-6.10:

$$\frac{\partial V}{\partial \mu_S} = -\frac{1}{\sqrt{2\pi\sigma_Z^2}} \cdot e^{\frac{(-\mu_S + \mu_D)^2}{2\sigma_Z^2}} \tag{6.6}$$

$$\frac{\partial V}{\partial \mu_D} = -\frac{1}{\sqrt{2\pi\sigma_Z^2}} \cdot e^{\frac{(-\mu_S+\mu_D)^2}{2\sigma_Z^2}} \tag{6.7}$$

$$\frac{\partial V}{\partial \sigma_S} = -\frac{\sigma_S \cdot (-\mu_S+\mu_D)}{\sqrt{2\pi(\sigma_Z^2)^3}} \cdot e^{\frac{(-\mu_S+\mu_D)^2}{2\sigma_Z^2}} \tag{6.8}$$

$$\frac{\partial V}{\partial \sigma_D} = -\frac{\sigma_D \cdot (-\mu_S+\mu_D)}{\sqrt{2\pi(\sigma_Z^2)^3}} \cdot e^{\frac{(-\mu_S+\mu_D)^2}{2\sigma_Z^2}} \tag{6.9}$$

$$\frac{\partial V}{\partial \operatorname{cov}(S,D)} = \frac{(-\mu_S+\mu_D)}{\sqrt{2\pi(\sigma_Z^2)^3}} \cdot e^{\frac{(-\mu_S+\mu_D)^2}{2\sigma_Z^2}} \tag{6.10}$$

Although not included here for brevity, the above analysis can be easily extended to define changes in vulnerability as a function of changes in the probabilistic characteristics of P, E, I, and Q_{div}, explicitly.[67]

The vulnerability estimates are based on the results of multi-year simulations of water allocation and routing within ASR networks. Each ASR network was simulated for a total of 138 years, from 1953 to 2090. To begin a simulation, reservoirs in 1953 were set as half full. A flat value of water demand, corresponding to the demand in 1985, was used for the first 33 years. The first 33 years of simulation were considered transient and discarded for any vulnerability estimation purposes.

Distribution functions of precipitation, temperature, and potential evapotranspiration for the period 1986-2090 thus were used as input to the water balance model to determine the PDF of water yield. Water demands, as previously mentioned, are also characterized by a stochastic component. The annual consumptive use of a given ASR is dependent, in part, on the amount of precipitation as well as on temperature and potential evapotranspiration. PDFs of water supply and water demand, therefore, are correlated because they both derive from the climatic input (precipitation, temperature, and potential evapotranspiration).

6.3 Current Vulnerability of U.S. Water Supply to Shortage

Water allocation within the simulated networks for the period 1986-2005 allows us to compute vulnerability estimates for the current condition. However, more important than providing an estimate of the current probability of shortage, the analysis of the current condition provides the benchmark to which future estimates of vulnerability can be compared.

Estimates of μ_S, μ_D, σ_S, σ_D, and *cov(S, D)* for the current period for each ASR were computed from the annual values of S and D produced by the network simulations. For example, μ_S for a given ASR is the mean of the 20 years (1986-2005) of S_i from the multi-year simulation.

Recalling that water surplus, Z, was defined as the difference between water supply and water demand, vulnerability is the probability that the water surplus is zero or negative. By simply looking at the first moments of the water surplus PDF, one notices that vulnerability increases as the mean of the surplus μ_z decreases and as its variance σ^2_z increases.[68]

The water supply system for much of the larger Southwest—including parts of California and of the Great Plains and parts of the eastern plains of Colorado and southern Wyoming—is vulnerable under current hydro-climatic and socio-economic conditions (Figure 6.1[A]). However, only a few areas show vulnerability values exceeding 0.1 at the ASR scale, and they tend to be those that rely heavily on mining of groundwater.

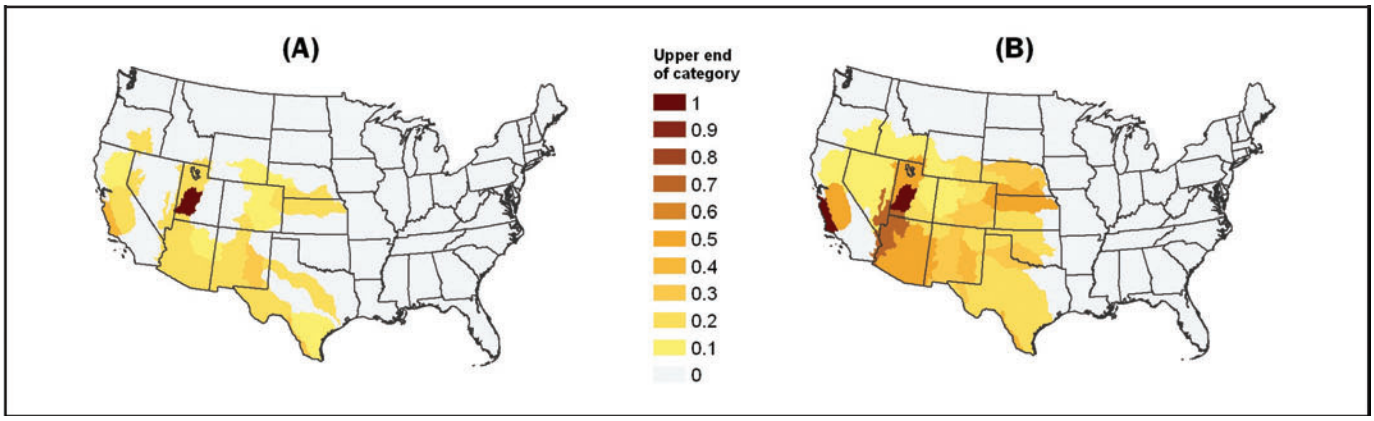

Figure 6.1. Vulnerability (probability of shortage) for: (A) current period; (B) as projected for the A1B-CGCM future for 2060.

6.4 Future Vulnerability of U.S. Water Supply to Shortage

Future vulnerability was evaluated for each of the nine alternative futures for the target 20-year periods centered at 2020, 2040, 2060, and 2080.

6.4.1 Sensitivity of Vulnerability to Changes in Drivers with the CGCM-A1B Future

Understanding how a given location responds to potential changes in climatic and socio-economic conditions is essential for future water management planning. As previously explained, future changes in vulnerability of water supply to shortage are a function not only of the magnitude of the changes in future supply and demand, but also of the sensitivity of vulnerability to unit changes in supply and demand. In turn, those sensitivities are functions of the means, variances, and covariances of *P, E,* and *D* (equation 6.5).

The sensitivity of vulnerability to changes in supply ($\partial V / \partial \mu_S$), that is, the change in vulnerability per unit change in mean supply (μ_S), for the A1B-CGCM scenario (Figure 6.2[A]) is greatest in portions of the Southwest where vulnerability is greatest (Figure 6.1[A]). The negative values in Figure 6.2(A) indicate that as supply increases vulnerability decreases. A similar behavior occurs with respect to changes in mean demand, μ_D, but with opposite sign (Figure 6.2[B]). Therefore, these areas, in addition to being quite vulnerable under the current conditions, are more prone to large changes in vulnerability for the same change in *S* and *D*. In other words, these areas are vulnerable because their mean surplus, μ_Z, is close to zero and because they are more sensitive to unit changes in mean surplus.

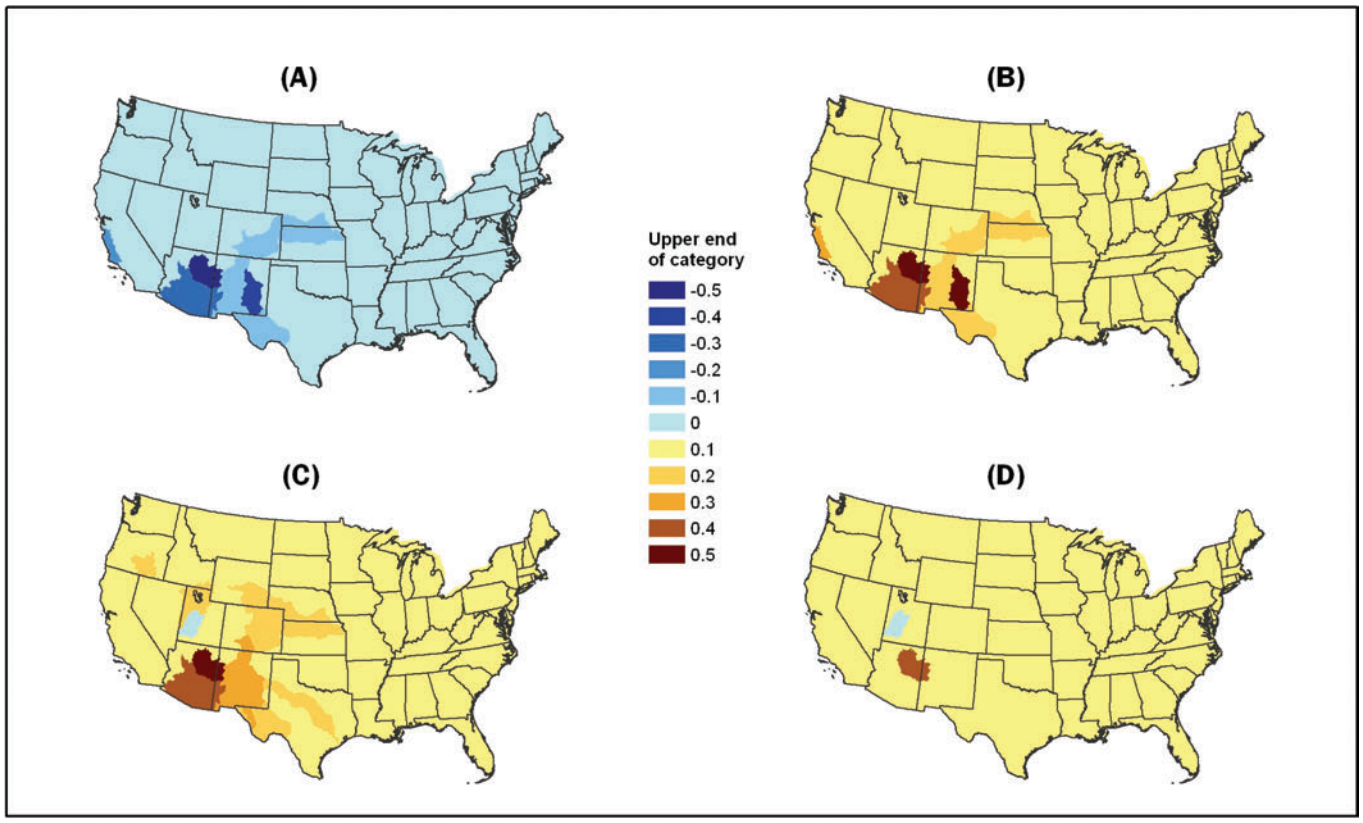

Figure 6.2. Current sensitivity of vulnerability for A1B-CGCM to unit changes in: (A) mean water supply; (B) mean water demand; (C) standard deviation of water supply; (D) standard deviation of water demand.

As indicated, it is not only changes in the means of the drivers that affect vulnerability but also changes in their variances and co-variances. For the A1B-CGCM scenario, as the variance of supply (σ_S) increases so does the vulnerability of water supply to shortage ($\partial V / \partial \sigma_S$) over nearly all of the United States (Figure 6.2[C]). Similar behavior is observed with respect to changes in the variance of demand (Figure 6.2[D]).

6.4.2 Changes in Supply and Demand with the CGCM-A1B Future

As seen in Figure 6.1, vulnerability is projected to increase substantially in the larger Southwest from the current period to the 20-year period centered at 2060 assuming the A1B-CGCM future. This increase in vulnerability results from corresponding changes in water supply and demand. As seen in Figure 6.3(A and B), vulnerability increases because of a combination of decreases in mean supply and increases in mean demand. Among the 29 ASRs for which vulnerability is projected to increase (Figure 6.1), the decrease in mean supply is greater than the increase in mean demand in about one-half of the ASRs. The ASRs where the reverse is true are scattered among the WRRs of the larger Southwest.

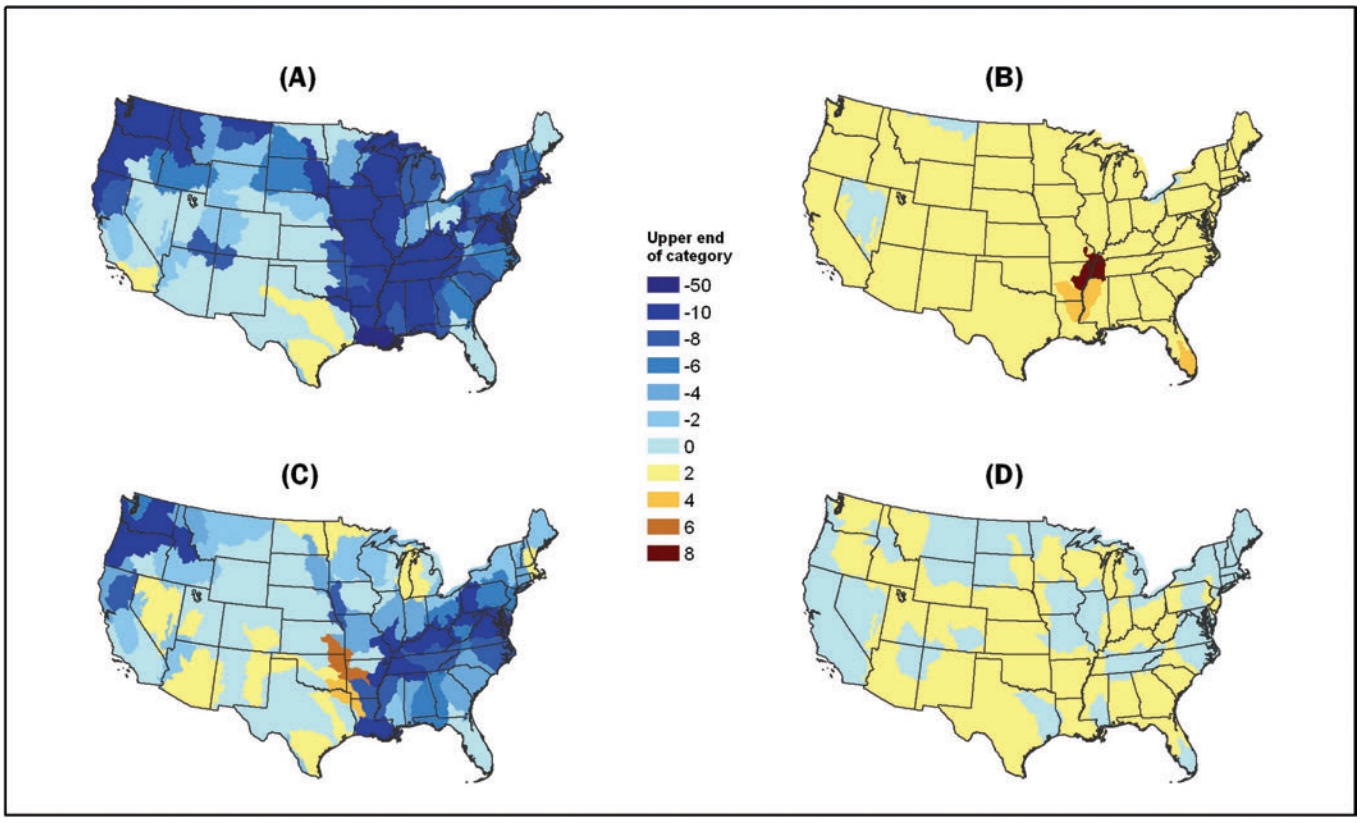

Figure 6.3. Change from the current period to 2060 for the A1B-CGCM future (in cm) in: (A) mean water supply; (B) mean water demand; (C) standard deviation of water supply; (D) standard deviation of water demand.

The variance of supply is projected to decrease from the current to the 2060 period with the A1B-CGCM future in most ASRs. A decreasing variance would tend to ameliorate the effect of a decreasing mean. Most ARSs where the variance is projected to increase are in the larger Southwest (Figure 6.3[C]). Among the 29 ASRs for which vulnerability is projected to increase, the variance of supply is projected to decrease in 21. In contrast, the variance of demand is projected to increase in most ASRs (Figure 6.3[D]), and among the 29 ASRs for which vulnerability is projected to increase, the variance of demand is projected to increase in 21.

6.4.3 Effect of Changes in Supply and Demand with the A1B-CGCM Future

The effects of changes in supply or demand on resulting changes in vulnerability are each a combination of changes in the mean and the standard deviation. The effects of changes in the mean and standard deviation of supply are represented by the first and third terms of equation 6.5, respectively, and the effects of changes in the mean and standard deviation of demand are represented by the second and fourth terms of equation 6.5, respectively.

As seen in Figure 6.4(A and B), assuming the A1B-CGCM future, the changes from the current period to 2060 in the mean of supply and the mean of demand both tend to increase vulnerability in nearly all ASRs. The changes in the variance of supply, however, tend to decrease vulnerability in most ASRs (Figure 6.4[C]), whereas the changes in the variance of demand are more site-specific, tending to increase vulnerability in roughly half of the ASRs and decrease vulnerability elsewhere (Figure 6.4[D]).

The combined effects of changes in the mean and the standard deviation of supply for the A1B-CGCM future are shown in Figure 6.5(A), again for changes from the current period to the 2060 period. Changes in the mean and variance of supply lead by 2060 to increases in vulnerability over much of the western two-thirds of the United States; exceptions include many of the ASRs along the Pacific coast and a few ASRs in the Southwest and Minnesota. The greatest effects are seen in the lower Colorado River basin and in northern Utah.

The combined effects of changes in the mean and standard deviation of demand for A1B-CGCM are shown in Figure 6.5(B). Unlike in the case of supply, the combined effects of changes in the mean and standard deviation of demand are projected to nearly always increase future vulnerability; exceptions include parts of the Great Basin and the southern tip of California. The effect of demand change is largest in southern Arizona. The increases in demand in many areas of the East are insufficient to result in much shortage at the ASR scale.

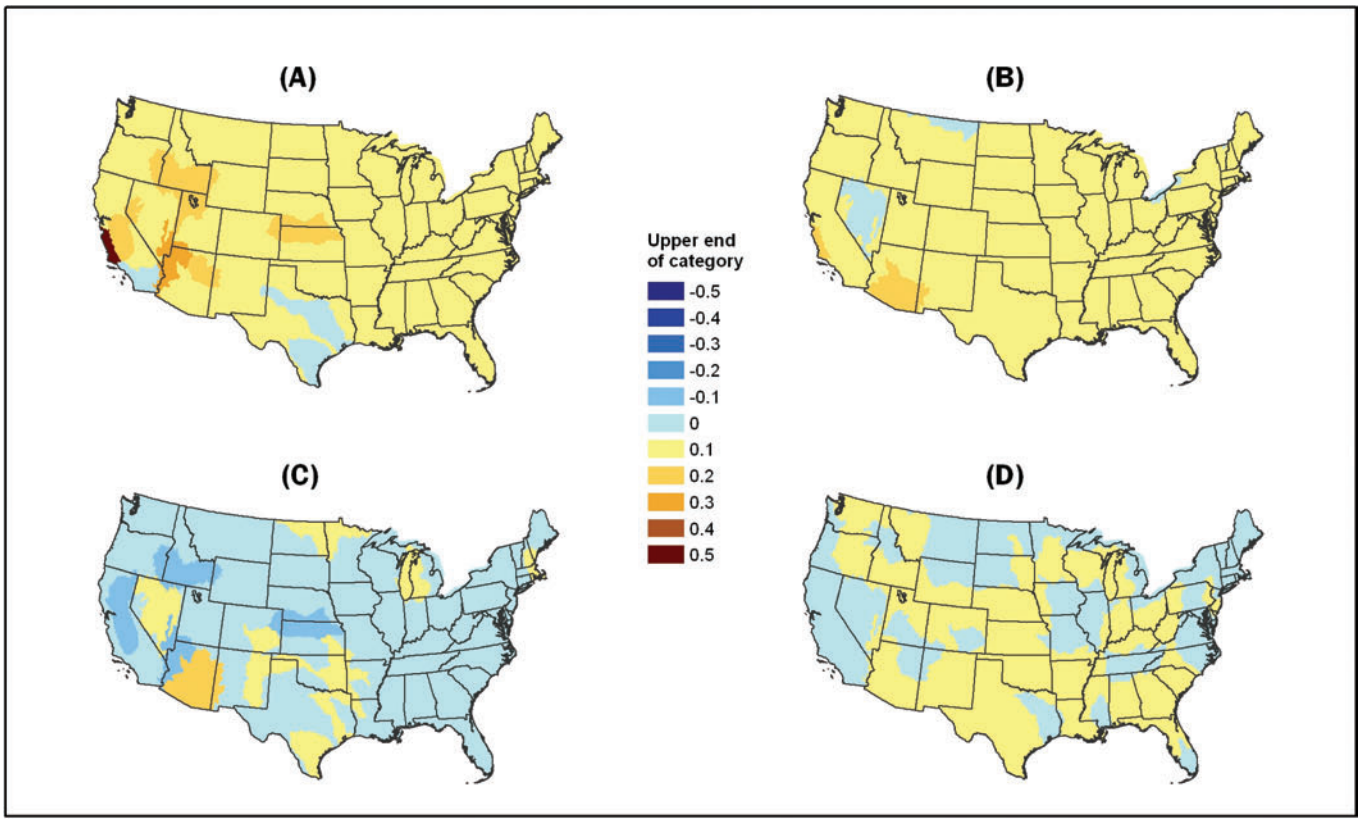

Figure 6.4. Change in vulnerability from the current period to 2060 for the A1B-CGCM future resulting from the change in: (A) mean water supply; (B) mean water demand; (C) standard deviation of water supply; (D) standard deviation of water demand.

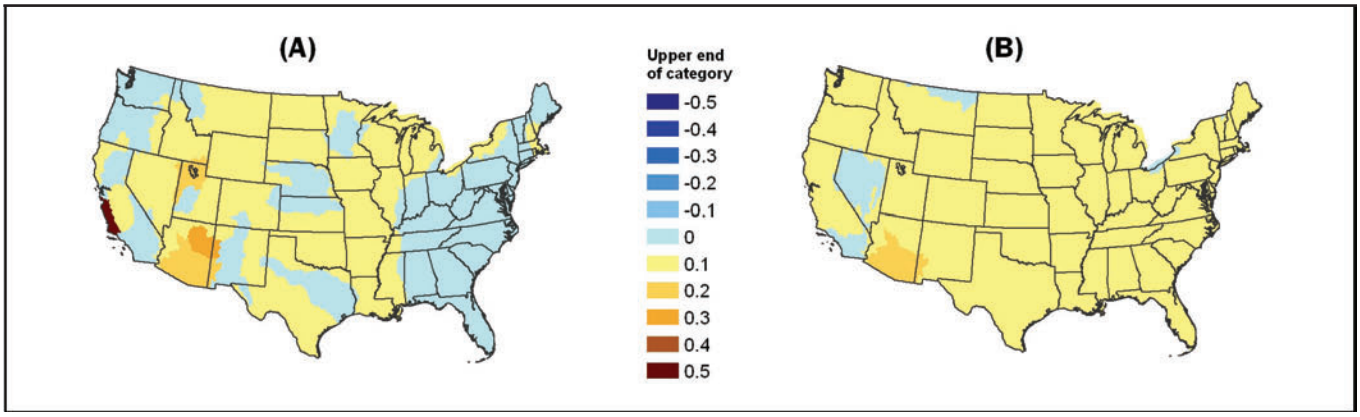

Figure 6.5. Change in vulnerability from the current period to 2060 for the A1B-CGCM future resulting from the change in: (A) mean and standard deviation of water supply; (B) mean and standard deviation of water demand.

In most locations where decreases in supply cause substantial increases in vulnerability (for example, central coastal California, northern Utah, and much of Arizona), future increases in vulnerability will depend more on changes in supply than on changes in demand (Figure 6.5). However, in the many locations where changes in supply are projected to decrease vulnerability, future increases in vulnerability will depend on changes in demand.

6.4.4 Vulnerability Under the A1B-CGCM Future

Changes in future vulnerability reflect changes in the probability distribution functions of supply and demand. Figure 6.6 shows the levels of vulnerability predicted for the A1B-CGCM future for the periods 2020, 2040, 2060, and 2080. The southwestern United States and the Great Plains, where shortages are more likely, are also the areas expected to face the greatest

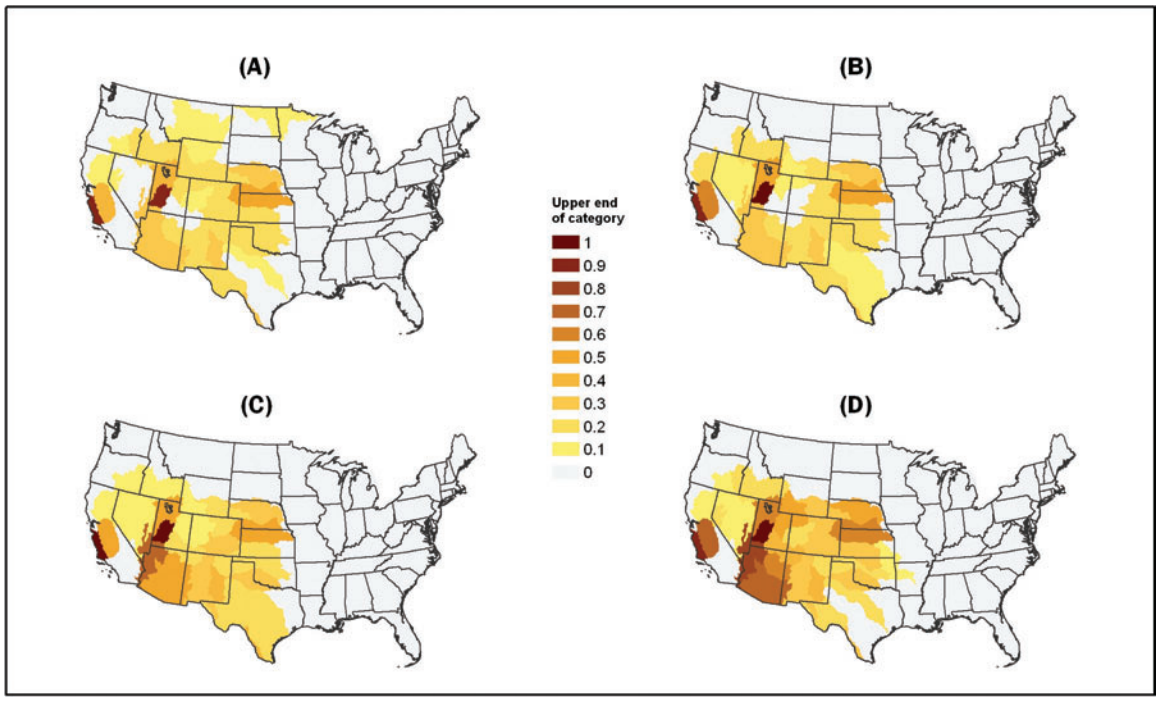

Figure 6.6. Projected vulnerability for the A1B-CGCM future for: (A) 2020; (B) 2040; (C) 2060; (D) 2080.

levels of vulnerability. Dramatic increases in vulnerability are projected over much of the Twenty-First Century for the lower Colorado River Basin, the central Great Plains, central California, and parts of the Great Basin. Large increases are also expected in the Rio Grande basin and Texas.

6.4.5 Change in Vulnerability by Scenario and GCM

The A1B-CGCM future represents only one possible future set of hydro-climatic and socio-economic conditions. Analyzing alternative scenarios and utilizing alternative CGMs is one way to characterize the uncertainty that exists about the vulnerability projections. Figures 6.7 through 6.14 present estimates for future vulnerability projected for the other eight alternative futures. Those maps show pictures of the future broadly similar to that of the A1B-CGCM future (Figure 6.6). In particular, consistent increases in vulnerability are projected for all nine futures, predominantly in the larger Southwest (including part of California plus the central and southern Great Plains).[69] However, the magnitude of those increases can vary considerably among the alternative futures, as does the areal extent of the most vulnerable areas.

The CGCM model generally projects the less dramatic increases in vulnerability. The CSIRO model projects the largest increases in vulnerability in the eastern United States, as shown by comparing its projections with those of the other GCMs for corresponding scenarios. The MIROC model (as well as the HADN for the B2 scenario), on the other hand, projects the largest increases in vulnerability in the Great Plains, in the southern central United States, and in the Colorado River Basin.

Among scenarios, the largest increases in vulnerability generally are found with A2, but several are also found with A1B.[70]

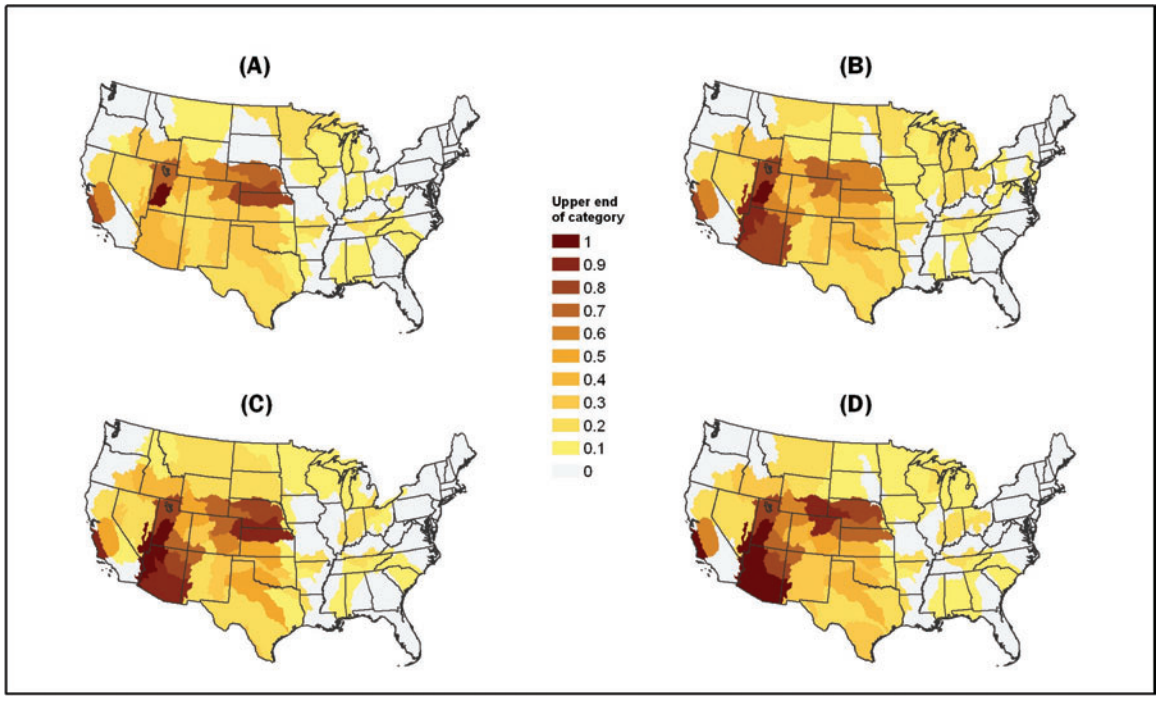

Figure 6.7. Projected vulnerability for the A1B-CSIRO future for: (A) 2020; (B) 2040; (C) 2060; (D) 2080.

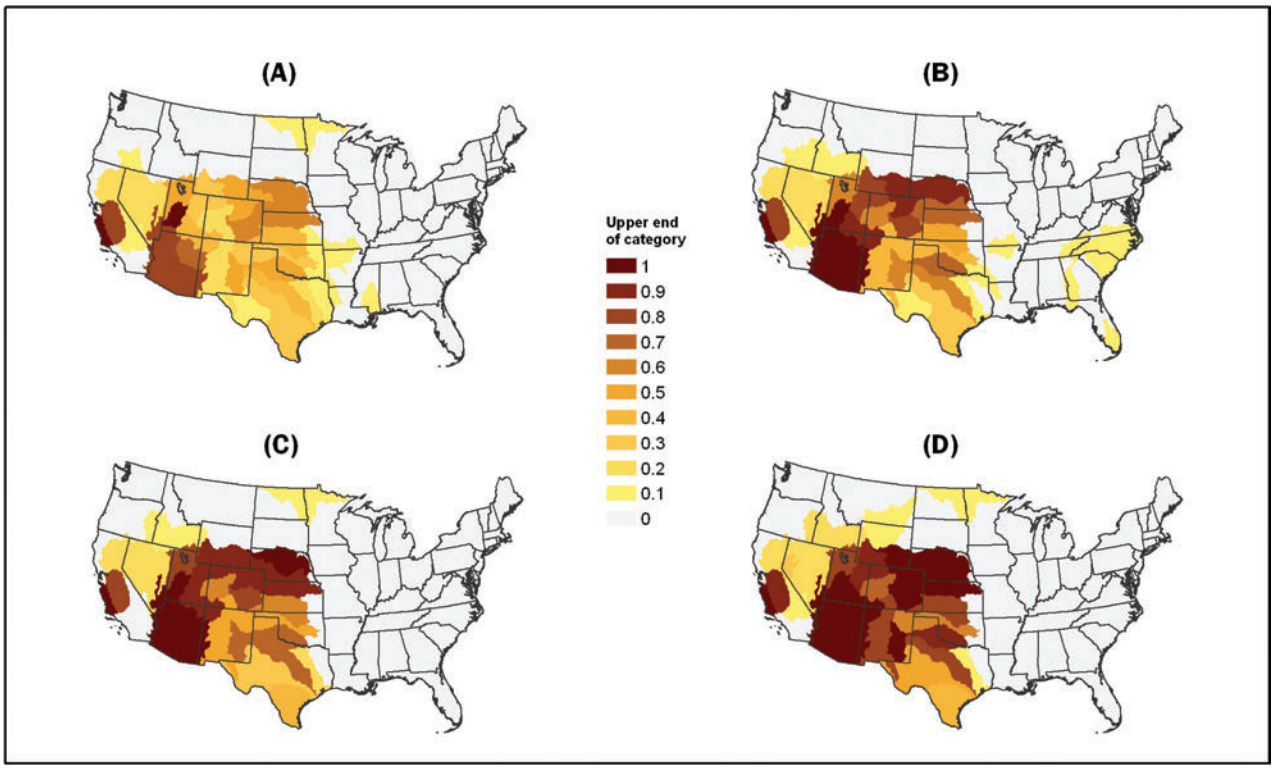

Figure 6.8. Projected vulnerability for the A1B-MIROC future for: (A) 2020; (B) 2040; (C) 2060; (D) 2080.

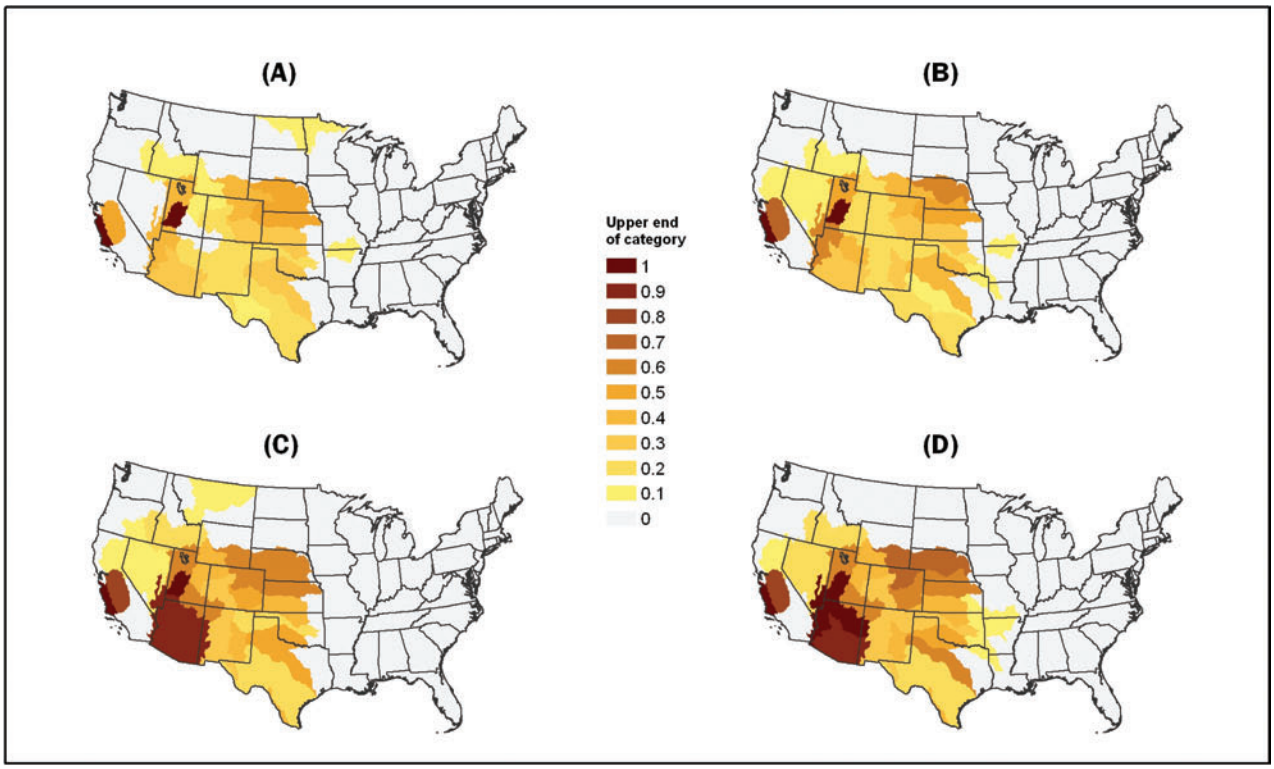

Figure 6.9. Projected vulnerability for the A2-CGCM future for: (A) 2020; (B) 2040; (C) 2060; (D) 2080.

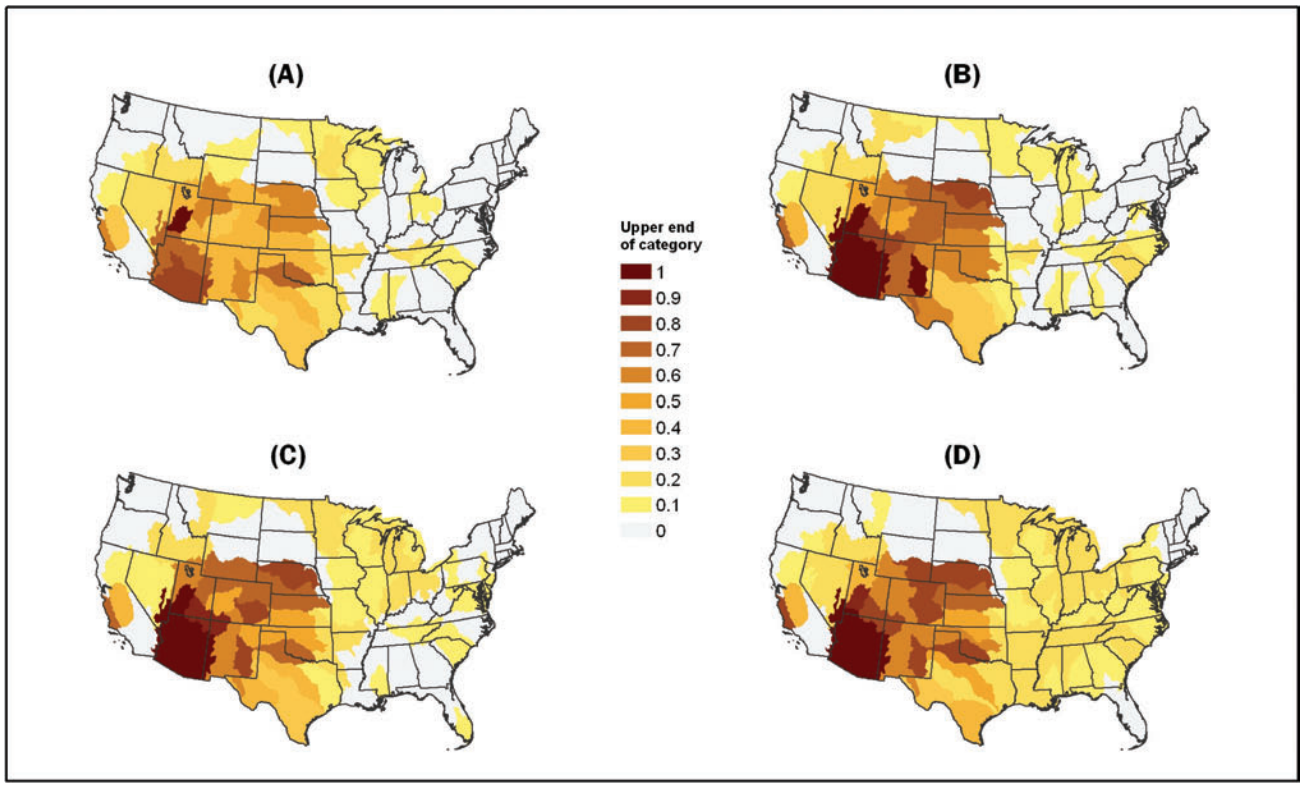

Figure 6.10. Projected vulnerability for the A2-CSIRO future for: (A) 2020; (B) 2040; (C) 2060; (D) 2080.

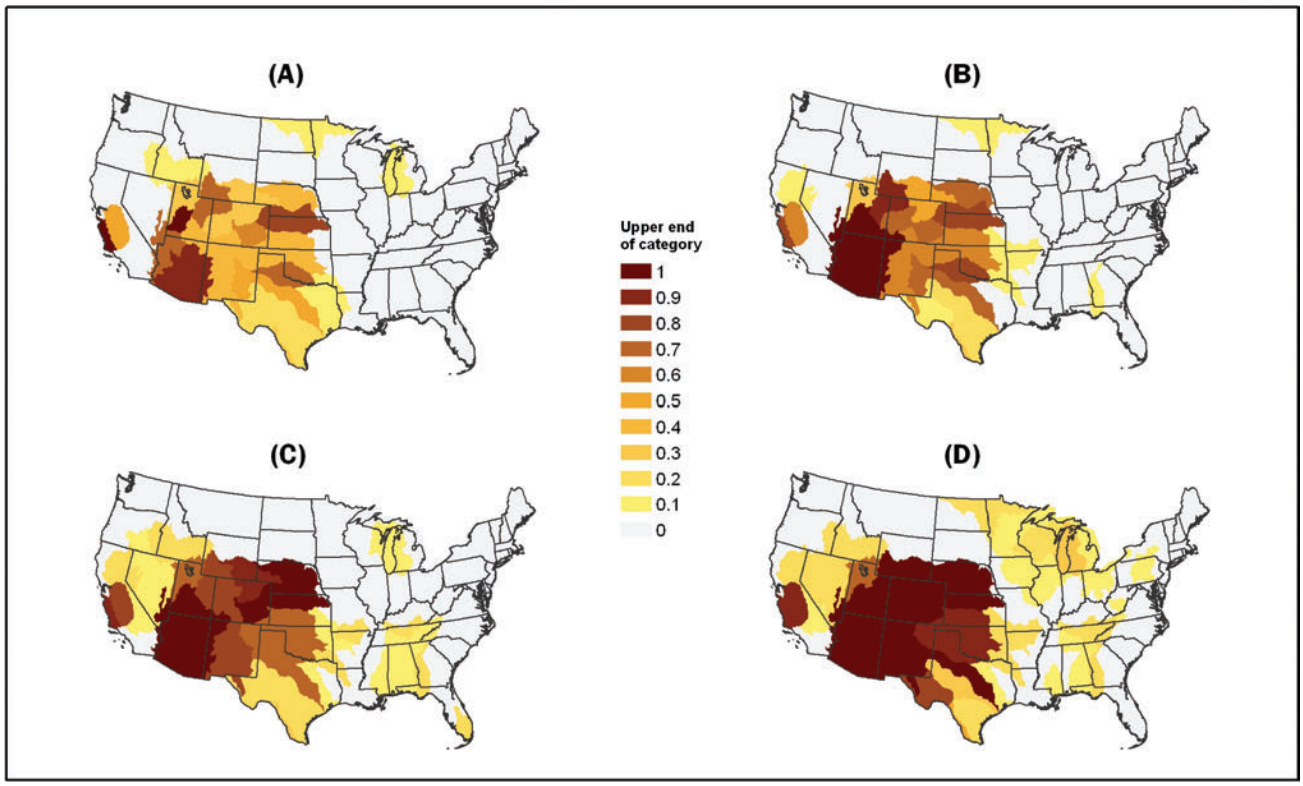

Figure 6.11. Projected vulnerability for the A2-MIROC future for: (A) 2020; (B) 2040; (C) 2060; (D) 2080.

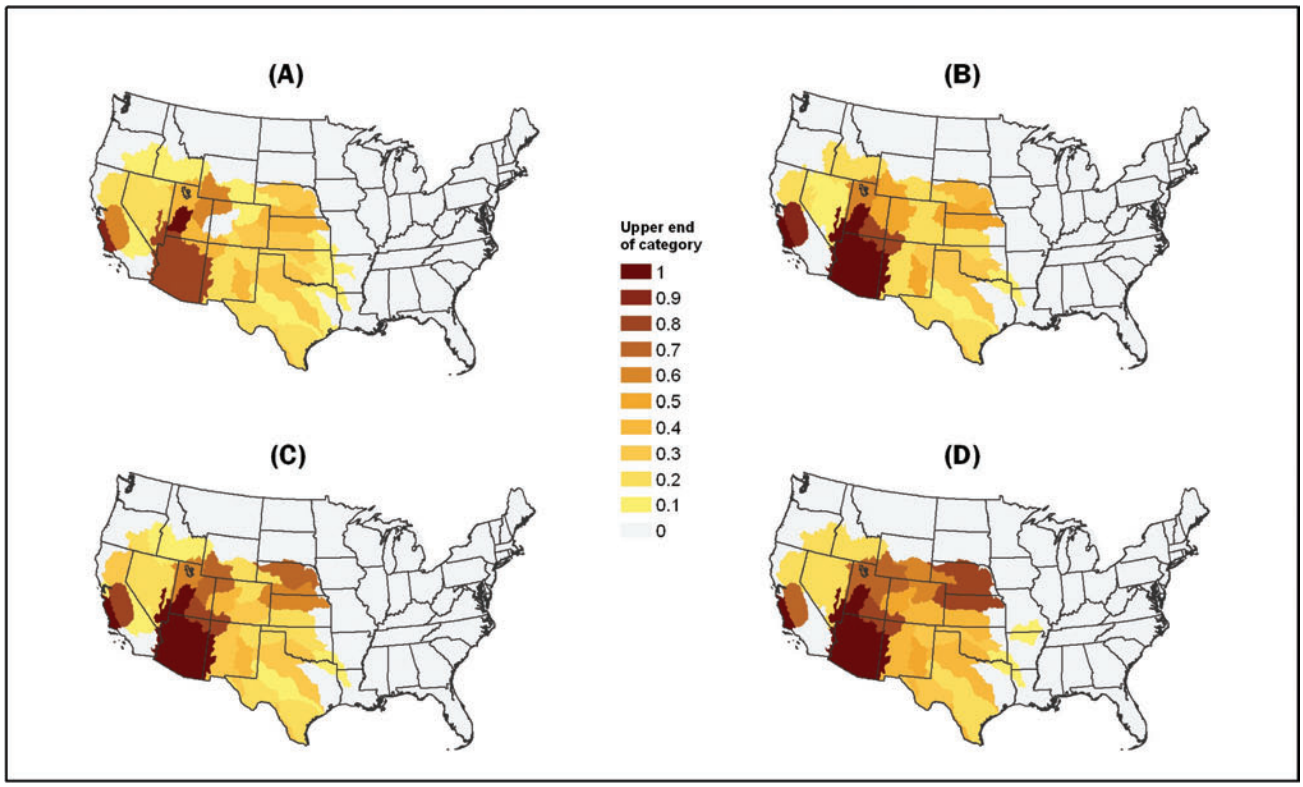

Figure 6.12. Projected vulnerability for the B2-CGCM future for: (A) 2020; (B) 2040; (C) 2060; (D) 2080.

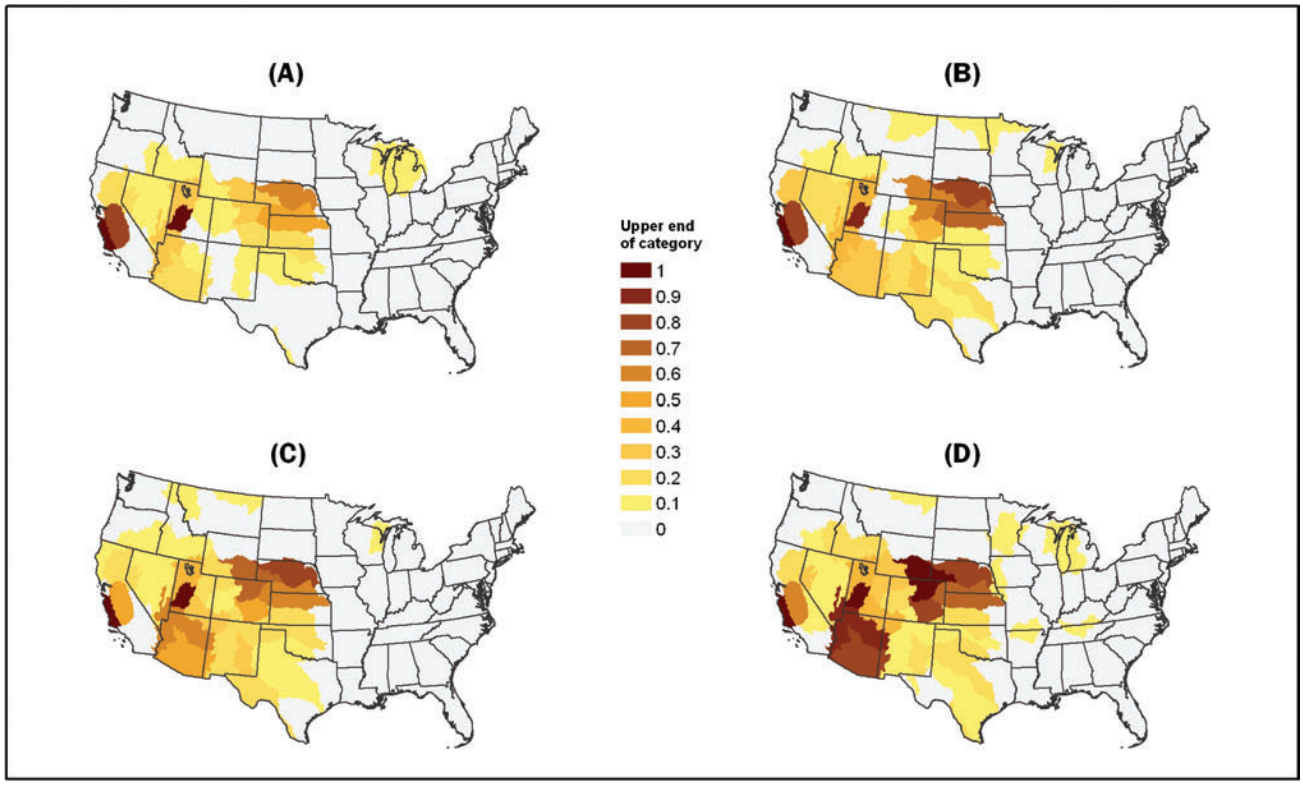

Figure 6.13. Projected vulnerability for the B2-CSIRO future for: (A) 2020; (B) 2040; (C) 2060; (D) 2080.

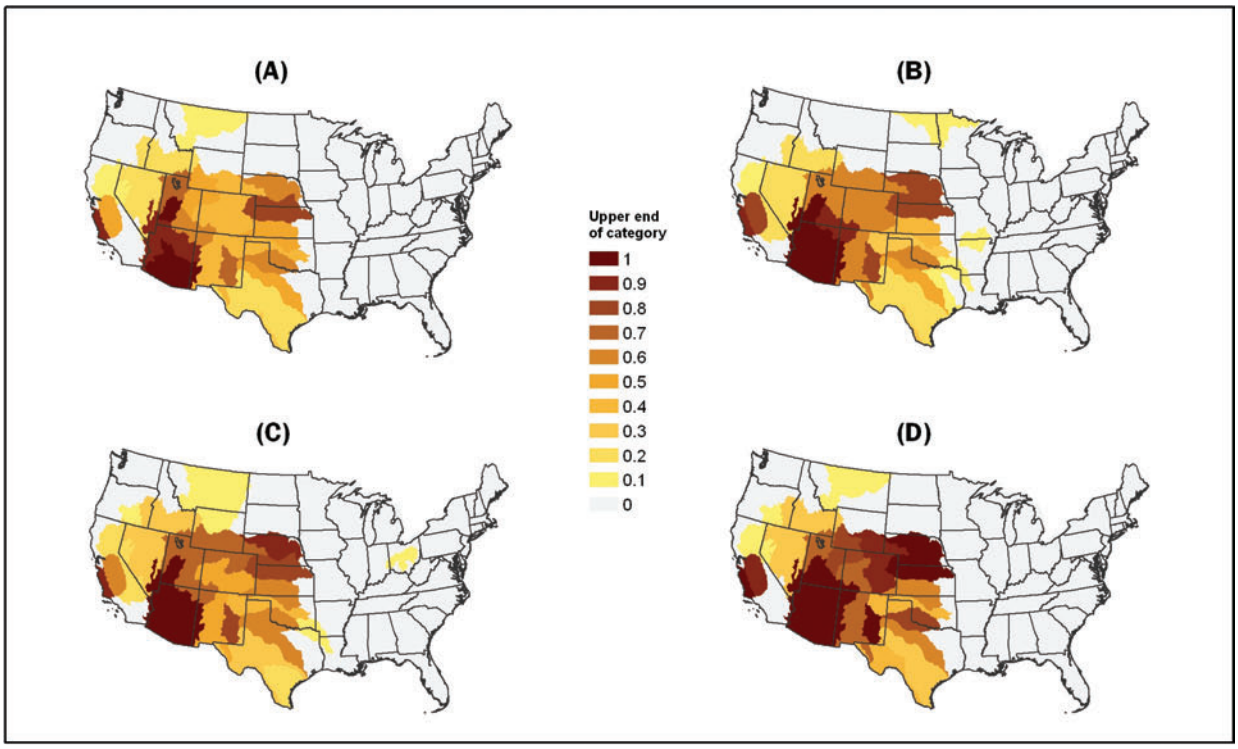

Figure 6.14. Projected vulnerability for the B2-HADN future for: (A) 2020; (B) 2040; (C) 2060; (D) 2080.

6.5 Future Reservoir Storage Levels

Projected storage volume as a proportion of storage capacity is highly variable across the ASRs. For example, consider the six representative trajectories for one of the nine futures, A2-CGCM, shown in Figure 6.15. Each graph in the figure plots storage levels from 1986 to 2090.[71] The trajectories, of course, reflect the priorities explained in Chapter 4, which place reservoir storage at a lower priority than diversions or minimum in-stream flows.

Analysis of ASR storage volume trajectories indicates whether additional aggregate storage capacity could help alleviate aggregate ASR shortages. From the standpoint of water supply—thus ignoring recreation, hydropower production, and other possible reservoir management objectives—an addition to storage capacity could help alleviate water shortages only if demands are not completely met. If demands are given a higher priority than storage and storage never falls to zero, the reservoir is always able to satisfy the demands placed upon it. Based on the simulated storage levels, this is the case for the majority of ASRs (subject to the caveats described later). For the A2-CGCM future, in the eastern ASRs, annual storage levels never reach zero storage. ASR 307 (Figure 6.15[A]), covering much of eastern Alabama, is typical of this situation. In these eastern ASRs, reservoir storage capacity is typically a small percentage of annual yield and storage volume only occasionally drops below maximum capacity. Western ASRs show much more variety in storage levels, but even here storage levels in 33 of the 48 ASRs with any storage capacity never reach zero volume. ASR 1302 (Figure 6.15[D]), containing the Rio Grande, is typical of these ASRs, where storage volume is quite variable but does not drop to zero during the simulation period.

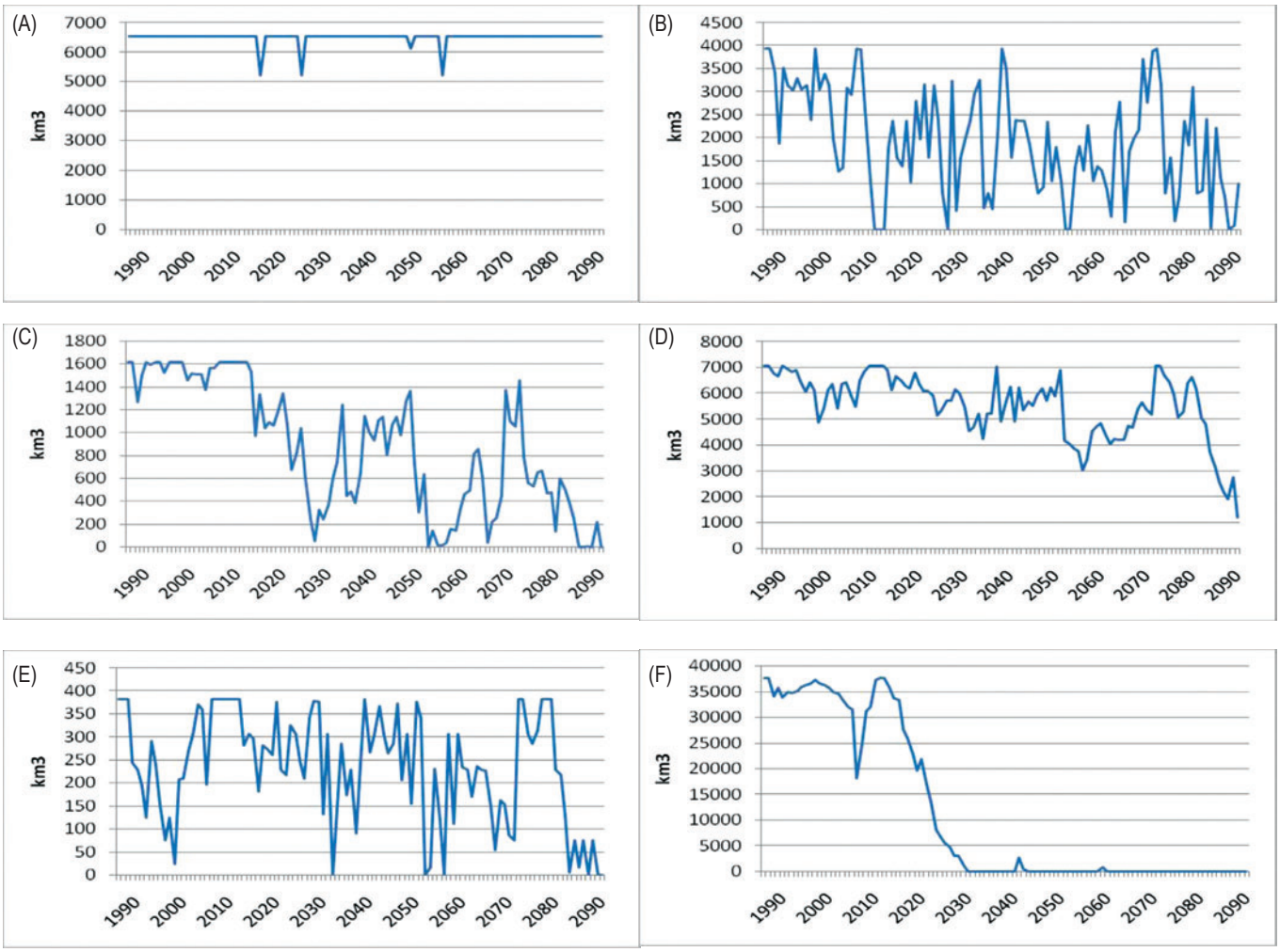

Figure 6.15. Reservoir storage volumes for A2-CGCM of six ASRs: (A) 307, (B) 1010, (C) 1102, (D) 1302; (E) 1304; (F) 1502.

In 10 of the remaining 15 ASRs, where reservoir storage reaches zero, an addition to storage capacity may not have helped much because once storage volume drops to zero, it never again returns to capacity, as depicted by the storage trajectory of ASR 1102 (Figure 6.15 [C]) in southeastern Colorado. Additional storage capacity might have postponed the drop to zero storage volume but would not have enhanced deliveries much thereafter. An extreme version of this situation is that of ASR 1502 (Figure 6.15[F]) along the lower Colorado River and including Lake Mead and four other reservoirs, where once the storage level reaches zero, it rarely rises much above that (this occurs also in ASR 1403, which includes Lake Powell in the Upper Colorado Basin).

In the remaining 5 of the 16 ASRs where storage volume reaches zero, storage volume does thereafter reach capacity during the simulation period. These ASRs are more promising locations for major storage additions because, according to the simulations, there were numerous times when additional storage capacity would have allowed additional storage and therefore smaller subsequent shortages. ASR 1010 (Figure 6.15[B]) along the Nebraska-Kansas border and ASR 1304 (Figure 6.15[E]) in southeastern New Mexico are examples of this situation.

In summary, when analyzed at the ASR spatial scale and annual time scale, reservoir capacity is typically not found to limit deliveries to consumptive uses. In only a few western ASRs does storage volume fall to zero, and only some of those ASRs would have benefited much from increased storage capacity. In the others, those where storage volume drops gradually to zero and never returns thereafter to full capacity, water shortages are largely due to demand-supply imbalance. This is most dramatically so in ASRs 1403 and 1502, which contain huge reservoirs that once empty tend to remain so, but is also true in some other ASRs for which significant vulnerability is projected but storage levels never recover to capacity. Note, however, that these results apply to aggregate ASR storage and do not preclude the possibility of useful additions to storage in selected upstream locations. Further, these results are for the A2-CGCM future; findings differ somewhat with the other futures.

6.6 Caveats

Using different scenarios of future socioeconomic conditions and related GHG emissions is one way to highlight the uncertainty that exists about future population, climate, and other basic drivers of water supply and demand. As seen in various graphs presented in earlier chapters, the scenarios differ considerably, especially in the latter half of the century. However, even if we were sure about socioeconomic conditions, much uncertainty would remain about future water yield, supply, and demand, and thus about the resulting estimates of vulnerability. Projections of vulnerability and its components rely on data that are potentially subject to some error in measurement and on models that undoubtedly fail to fully characterize reality. Some of this uncertainty becomes apparent when comparing output from different GCMs for a given scenario. Comparison of the temperature and precipitation projections of the different GCMs we used shows that although there is reasonable agreement about future temperatures, there is much disagreement about future precipitation. This disagreement is apparent even if one looks at U.S. averages, and it becomes more dramatic at the regional scale.

Except for temperature and precipitation estimates, we did not use multiple models to estimate future quantities. For example, we used only one water yield model, and as input to that model, used only one approach to estimate potential evapotranspiration. Further, only one downscaling model was used. Similarly on the demand side, we used only one approach to estimate the effect of a changing climate on water use in a given water sector, and we relied on old data on most trans-basin diversions. The fact that we used single approaches to estimate such quantities should not suggest that alternative approaches are not feasible or that the estimates are not subject to potential error.

Because the downscaled climate data we used covered only temperature and precipitation, options for estimating potential evapotranspiration were limited and may have produced overestimates, potentially resulting in overestimates of projected shortages.

Vulnerability is a scale-dependent property, and our estimates of vulnerability apply only to the spatial and temporal scales of the analysis. This assessment has been carried out at the ASR spatial scale. Some localized, within-ASR areas that are known to have faced shortages in the past are not revealed as areas of shortage at the ASR scale. This is most likely for

areas located in the upper reaches of an ASR, which places them upstream of the bulk of the available water supply in the ASR, as in the case of Atlanta (Feldman 2009; Georgakakos and others 2010).

Similarly, this assessment was carried out at an annual time scale. Because of the annual time step of the simulations, our analysis ignores the possibility of intra-annual shortages, which could occur even in ASRs that have no shortages at the annual time step. In other words, our analysis could have failed to capture seasonal vulnerabilities. Also because of the annual time step, the analysis could not address flooding issues.

Our estimates of vulnerability reflect a greatly simplified set of rules for reservoir operations, wherein all consumptive use demands were met in the current year once the in-stream flow constraint was satisfied. We have ignored the many existing operating procedures at the various reservoirs across the country. Some of these procedures, such as those aimed at flood control, might tend to exacerbate vulnerability compared with our simple rules, whereas others, especially those that incorporate forecasting, might help to lessen vulnerability.

Chapter 7: Conclusions

Vulnerability was evaluated, for each of 98 basins that make up the coterminous United States, as the probability that water supply is insufficient to meet demand. Current and future water supplies were estimated as local freshwater yield plus the contribution of reservoir releases, inflow from upstream, and water transfers. Demands were estimated as desired consumptive use based on projections of water use drivers and extension of trends in rates of water withdrawal per unit of driver. The analyses were completed for nine separate possible futures corresponding to three emissions scenarios and to different GCMs used to project the climate of those scenarios.

In agreement with other large-scale assessments (Hurd and others 1999), our findings show that the Southwest and central and southern Great Plains are the more vulnerable areas to future climatic and socio-economic changes. In addition, this analysis adds to that prior work in several ways including an accounting for reservoir storage, trans-basin diversions and routing of water among basins, a more comprehensive effort to project future desired water use, and a probabilistic approach to vulnerability.

The distribution of increase in projected vulnerability (i.e., in probability of shortage) is highly skewed. Averaging across the nine alternative futures, 75 ASRs are projected to face an increase in vulnerability of less than 0.1, 16 ASRs are projected to face in increase in vulnerability of from 0.1 to 0.5, and seven ASRs are projected to face an increase in vulnerability above 0.5. All ASRs with a projected increase in vulnerability greater than 0.1 are in the West. The ASRs with a projected increase in vulnerability greater than 0.5 are located in WRRs 10, 14, and 15.

Contrary to a prior global scale conclusion (Vörösmarty and others 2000) and in concert with a recent U.S. study (Roy and others 2012), we find that in some ASRs future increases in the vulnerability of the water supply depends more on reductions in water yield than on growth in water demand. This is supported by the fact that water use has leveled off in recent years as irrigated area in the West has diminished and withdrawal rates in nearly all sectors have dropped. Moreover, although climate change is expected to increase water demand, future reductions in withdrawal rates will mitigate that impact so that overall increases in desired water use in some ASRs are expected to be modest in comparison with the effect of climatic changes on water supply.

The findings of this analysis assume no major modifications to the physical structure of U.S. water networks, and reflect the very simple reservoir operating rules we employed. In addition, in-stream flow requirements and trans-ASR diversions were set constant, thereby ignoring possible future changes in surface water redistribution. Indeed, it was the purpose of this assessment to point to those locations where adaptation will be most needed. Options for avoiding shortages include enlarged trans-basin diversion capacity, within-basin water transfers, forward-looking reservoir operating rules, conjunctive management of surface reservoir storage and groundwater storage, and enhanced water conservation efforts. Because about 80% of the total consumptive use is currently in agriculture, and most water transfers that now occur are from agriculture to other sectors (Brown 2006), additional transfers from agriculture are likely.

A traditional option for avoiding shortages is to increase reservoir storage. However, our simulations at the ASR scale show that only a few areas in the West would benefit from additional storage. In other locations storage levels either do not drop to zero or, if reservoirs do empty they never recover. This latter situation is most dramatically demonstrated along the Colorado River, where storage levels in the ASRs containing Lakes Powell and Mead are projected to drop to zero and only occasionally thereafter add rather small amounts of storage before emptying again. Thus, major increases in reservoir storage capacity do not appear to be a successful adaptation strategy in many of the most vulnerable regions. It is important to note, however, that these results apply to aggregate ASR storage, and do not preclude the possibility of useful additions to storage in selected upstream locations.

Literature Cited

Abu Rizaiza, Omar S. 1991. Residential water usage: a case study of the major cities of the western region of Saudi Arabia. Water Resources Research 27(5): 667-671.

Aden, Andy. 2007. Water usage for current and future ethanol production, Southwest Hydrology 6: 22-23. Tucson, AZ: University of Arizona.

Allen, L. Hartwell, Jr.; Baker, Jeff T.; Boote, Ken J. 1996. The CO_2 fertilization effect: higher carbohydrate production and retention as biomass and seed yield. In: Bazzaz, Fakhri; Sombroek, Wim, eds. Global climate change and agricultural production: direct and indirect effects of changing hydrological, pedological and plant physiological processes. Rome, Italy: Food and Agriculture Organization of the United Nations.

Amato, Anthony D.; Ruth, Matthias; Kirshen, Paul; Horwitz, James. 2005. Regional energy demand responses to climate change: methodology and application to the Commonwealth of Massachusetts. Climatic Change 71(1-2): 175-201.

Averyt, Kristen; Fisher, Jeremy; Huber-Lee, Annette; [and others]. 2011. Freshwater use by U.S. power plants: electricity's thirst for a precious resource. Cambridge, MA: Energy and Water in a Warming World Initiative, Union of Concerned Scientists.

Barnett, T. P.; Pierce, D. W. 2008. When will Lake Mead go dry? Water Resources Research 45.

Bartis, James T.; LaTourrette, Tom; Dixon, Lloyd; Peterson, D. J.; Cecchine, Gary. 2005. Oil shale development in the United States. Santa Monica, CA: Rand Corporation.

Bedard, Roger J.; Previsic, Mirko; Polagye, Brian L. 2009. Marine energy: how much development potential is there? Hydro Review 28(4).

Blaikie, P.; Cannon, T.; Davis, I.; Wisner, B. 1994. At Risk: Natural Hazards, People's Vulnerability, and Disasters. London: Routledge.

Boyd, C. E.; Gross, A. 2000. Water use and conservation for inland aquaculture ponds. Fisheries Management and Ecology 7: 55-63.

Boyd, Claude E.; Lim, Chhorn; Queiroz, Julio; [and others]. no date. Best management practices for responsible aquaculture. U.S. Agency for International Development.

Brooks, R. H.; Corey, A. T. 1966. Properties of porous media affecting fluid flow. Journal of Irrigation and Drainage Engineering-ASCE IR2: 61-88.

Brown, Thomas C. 1999. Past and future water use in the United States. General Technical Report RMRS-39. Fort Collins, Colorado: Rocky Mountain Research Station.

Brown, Thomas C. 2000. Projecting U.S. freshwater withdrawals. Water Resources Research 36(3): 769-780.

Brown, Thomas C. 2006. Trends in water market activity and price in the western U.S. Water Resources Research 42: W09402.

Brutsaert, Wilfried H. 1967. Some methods of calculating unsaturated permeability. Trasaction of the ASAE (400-404).

California Department of Water Resources. 1998. California Water Plan Update. Bulletin 160-98. Sacramento, CA: California Department of Water Resources.

Chan, Melissa; Duda, John; Forbes, Sarah; Vagnetti, Robert; McIlvried, Howard. 2006. Emerging issues for fossil energy and water—investigation of water issues related to coal mining, coal to liquids, oil shale, and carbon capture and sequestration. DOE/NETL-2006-1233: National Energy Technology Laboratory, U.S. Department of Energy.

Colorado Water Conservation Board. 1998. River Basin Facts. Colorado Division of Water Resources Available: http://cwcb.state.co.us/Home/RiverBasinFacts.

Colorado Water Conservation Board. 2010. CDSS memoranda. Colorado Division of Water Resources. Available: http://cdss.state.co.us/DNN/.

Cooley, Heather; Fulton, Julian; Gleick, Peter H. 2011. Water for energy: future water needs for electricity in the Intermountain West. Oakland, CA: Pacific Institute.

Daly, C.; Neilson, R. P.; Phillips, D. L. 1994. A statistical-topographic model for mapping climatological precipitation over mountainous terrain. Journal of Applied Meteorology 33(2): 140-158.

David, Elizabeth L. 1990. Manufacturing and mining water use in the United States, 1954-83. In: Carr, Jerry E.; Chase, Edith B.; Paulson, Richard W.; Moody, David W., eds. National water summary 1987: hydrologic events and water supply and use. Denver, CO: U.S. Geological Survey, Water-Supply Paper 2350: 81-92.

Döll, Petra. 2002. Impact of climate change and variability on irrigation requirements: a global perspective. Climatic Change 54: 269-293.

Eagleson, P. S. 1978a. Climate, soil, and vegetation. 1. Introduction to water-balance dynamics. Water Resources Research 14(5): 705-712.

Eagleson, P. S. 1978b. Climate, soil, and vegetation. 2. Distribution of annual precipitation derived from observed storm sequences. Water Resources Research 14(5): 713-721.

Eagleson, P. S. 1978c. Climate, soil, and vegetation. 3. Simplified model of soil-moisture movement in liquid-phase. Water Resources Research 14(5): 722-730.

Eagleson, P. S. 1978d. Climate, soil, and vegetation. 4. Expected value of annual evapotranspiration. Water Resources Research 14(5): 731-739.

Eagleson, P. S. 1978e. Climate, soil, and vegetation. 5. Derived distribution of storm surface runoff. Water Resources Research 14(5): 741-748.

Eagleson, P. S. 1978f. Climate, soil, and vegetation. 6. Dynamics of annual water-balance. Water Resources Research 14(5): 749-764.

Eagleson, P. S. 1978g. Climate, soil, and vegetation. 7. Derived distribution of annual water yield. Water Resources Research 14(5): 765-776.

Energy Information Administration [EIA]. 2009a. Annual energy outlook 2009. DOE/EIA-0383(2009). Washington, DC: Energy Information Administration, U.S. Department of Energy.

Energy Information Administration [EIA]. 2009b. Annual energy review 2008. DOE/EIA-0384(2008). Washington, DC: Energy Information Administration, U.S. Department of Energy.

Energy Information Administration [EIA]. 2010. Annual energy outlook 2010. DOE/EIA-0383(2010). Washington, DC: Energy Information Administration, U.S. Department of Energy.

Elcock, Deborah. 2010. Future U.S. water consumption: the role of energy production. Journal of the American Water Resources Association 46(3): 447-460.

Elkhafif, Mahmoud A. T. 1996. An iterative approach for weather-correcting energy consumption data. Energy Economics 18(3): 221-230.

Feeley, Thomas J.; Skone, Timothy J.; Stiegal, Gary J.; [and others]. 2008. Water: a critical resource in the thermoelectric power industry. Energy 33(1): 1-11.

Feldman, David L. 2009. Preventing the repetition: or, what Los Angeles' experience in water management can teach Atlanta about urban water disputes. Water Resources Research 45: W04422.

Franco, Guido; Sanstad, Alan H. 2008. Climate change and electricity demand in California. Climatic Change 87(supplement 1): 139-151.

Government Accountability Office [GAO]. 2009. Energy-water nexus: many uncertainties remain about national and regional effects of increased biofuel production on water resources. GAO-10-116. Washington, DC: U.S. Government Accountability Office.

Government Accountability Office [GAO]. 2010. Energy-water nexus: a better and coordinated understanding of water resources could help mitigate the impacts of potential oil shale development. GAO-11-35. Washington, DC: U.S. Government Accountability Office.

Government Accountability Office [GAO]. 2011. Energy development and water use: impacts of potential oil shale development on water resources. GAO-11-929T. Washington, DC: U.S. Government Accountability Office.

Georgakakos, Aris; Zhang, Feng; Yao, Huaming. 2010. Climate variability and change assessment for the ACF River Basin, southeast US. Technical Report GWRI/22010-TR1. Atlanta, GA: Georgia Water Resources Institute, Georgia Institute of Technology.

Gillilan, David M.; Brown, Thomas C. 1997. Instream Flow Protection: Seeking a Balance in Western Water Use. Washington, DC: Island Press. 417 p.

Guldin, Richard W. 1989. An analysis of the water situation in the United States: 1989-2040. Gen. Tech. Rep. RM-177. Fort Collins, Colorado: Rocky Mountain Forest and Range Experiment Station, U.S. Forest Service.

Hobbins, Michael T.; Ramirez, Jorge A.; Brown, Thomas C.; Claessens, Lodevicus H. J. M. 2001. The complementary relationship in estimation of regional evapotranspiration: the complementary relationship areal evapotranspiration and advection-aridity models. Water Resources Research 37(5): 1367-1387.

Hoffman, Jeffrey; Forbes, Sarah; Feeley, Thomas. 2004. Estimating freshwater needs to meet 2025 electricity generating capacity forecasts. National Energy Technology Laboratory, U.S. Department of Energy.

Höök, M.; Aleklett, K. 2009. A review on coal to liquid fuels and its coal consumption. International Journal of Energy Research 34(10): 839-932.

Hurd, B.; Leary, N.; Jones, R.; Smith, J. 1999. Relative regional vulnerability of water resources to climate change. Journal of the American Water Resources Association 35: 1399-1409.

Hutson, Susan S.; Barber, Nancy L.; Kenny, Joan F.; [and others]. 2004. Estimated use of water in the United States in 2000. Circular 1268. Reston, VA: U.S. Geological Survey.

International Boundary and Water Commission. 2004. Flow of the Colorado River and other Western Boundary Streams and Related Data. Western Water Bulletin 2004: U.S. Department of State.

Jarvis, P. G.; McNaughton, K. G. 1986. Stomatal control of transpiration: scaling up from leaf to region. Advances in Ecological Research 15: 1-49.

Joyce, Linda A.; Price, David T; McKenney, Daniel W.; [and others]. 2011. High resolution interpolation of climate scenarios for the coterminous USA and Alaska derived from general circulation model simulations. General Technical Report RMRS-GTR-263. Fort Collins, CO: Rocky Mountain Research Station, U.S. Forest Service. Available: http://www.fs.fed.us/rm/pubs/rmrs_gtr263.html.

Joyce, Linda A.; Price, David T.; Coulson, David P.; [and others]. In press. Projecting climate change in the United States: a technical document supporting the Forest Service 2010 RPA Assessment. General Technical Report RMRS-GTR-xxx. Fort Collins, CO: Rocky Mountain Research Station, U.S. Forest Service.

Kelly, P. M.; Adger, W. N. 2000. Theory and practice in assessing vulnerability to climate change and facilitating adaptation. Climatic Change 47(4): 325-352.

Kenny, Joan F.; Barber, Nancy L.; Hutson, Susan S.; [and others]. 2009. Estimated use of water in the United States in 2005. Circular 1344. Reston, VA: U.S. Geological Survey.

Kimball, B. A.; Bernacchi, C. J. 2006. Evapotranspiration, canopy temperature, and plant water relations. In: Nosberger, J.; Long, S. P.; Norby, R. J.; Stitt, M.; Hendrey, G. R.; Blum, H., eds. Managed ecosystems and CO_2: Case studies, processes, and perspectives, Vol. 187. Berlin: Springer-Verlag: 311-324.

King, Carey W.; Webber, Michael E. 2008. Water intensity of transportation. Environmental Science and Technology 42(21): 7866-7872.

Kittel, T.G.F.; Rosenbloom, N.A.; Painter, T.H.; [and others]. 1996. The VEMAP Phase I Database: an integrated input dataset for ecosystem and vegetation modeling for the conterminous United States. Available: http://www.cgd.ucar.edu/vemap/users_guide. html.

Kittel, T.G.F.; Rosenbloom, N.A.; Painter, T.H.; Schimel, D.S.; VEMAP Modeling Participants. 1995. The VEMAP integrated database for modeling United States ecosystem/vegetation sensitivity to climate change. Journal of Biogeography 22(4-5): 857-862.

Kochendorfer, John P. 2005. A Monthly, Two-Soil-Layer Statistical-Dynamical Water Balance Model for Ecohydrologically Focused Climate Impact Assessments. Colorado State University, Fort Collins. 287 p.

Kochendorfer, John P.; Ramirez, Jorge A. 1996. Integrated hydrological/ecological/economic modeling for examining the vulnerability of water resources to climate change. Paper presented at the North American Water and Environment Congress 1996—ASCE, New York.

Krakauer, N. Y.; Fung, I. 2008. Is streamflow increasing? Trends in the coterminous United States. Hydrology and Earth System Sciences Discussions 5: 785-810.

Krug, William R.; Gebert, Warren A.; Graczyk, David J. 1989. Preparation of average annual runoff map of the United States, 1951-80. Open-file Report 87-535. Madison, WI: U.S. Geological Survey.

Labadie, J. W.; Pineda, A. M.; Bode, D. A. 1984. Network analysis of raw water supplies under complex water rights and exchanges: Documentation for Program MODSIM3. Fort Collins, CO: Colorado Water Resources Institute, Colorado State University.

Le Pen, Yannick; Sévi, Benoît. 2010. What trends in energy efficiencies? Evidence from a robust test. Energy Economics 32: 702-708.

Leakey, Andrew D. B. 2009. Rising atmospheric carbon dioxide concentration and the future of C_4 crops for food and fuel. Proceedings of the Royal Society B (Biological Sciences).

Leakey, Andrew D. B.; Ainsworth, Elizabeth A.; Bernacchi, Carl J.; [and others]. 2009. Elevated CO_2 effects on plant carbon, nitrogen, and water relations: six important lessons from FACE. Journal of Experimental Botany 60(10): 2859-2876.

Leakey, Andrew D. B.; Uribelarrea, Martin; Ainsworth, Elizabeth A.; [and others]. 2006. Photosynthesis, productivity, and yield of maize are not affected by open-air elevation of CO_2 concentration in the absence of drought. Plant Physiology 140: 779-790.

Linacre, E. T. 1977. A simple formula for estimating evaporation rates in various climates using temperature data alone. Agricultural Meteorology 18: 409-424.

Lins, Harry F.; Slack, James R. 2005. Seasonal and regional characteristics of U.S. streamflow trends in the United States from 1940 to 1999. Physical Geography 26(6): 489-501.

Litke, D.W.; Appel, C.L. 1989. Estimated use of water in Colorado, 1985. Water-Resources Investigations Report 88-4101. Denver, CO: U.S. Geological Survey.

Luce, C. H.; Holden, Z. A. 2009. Declining annual streamflow distributions in the Pacific Northwest United States, 1948-2006. Geophysical Research Letters 36.

MacKichan, K. A.; Kammerer, J. C. 1961. Estimated use of water in the United States, 1960. Circular 456. Washington, DC: U.S. Geological Survey.

Macknick, Jordan; Newmark, Robin; Heath, Garvin; Hallett, K. C. 2011. A review of operational water consumption and withdrawal factors for electricity generating technologies. Technical Report NREL/TP-6A20-50900. Golden, CO: National Renewable Energy Laboratory.

Malcolm, Scott A.; Aillery, Marcel; Weinberg, Marcia. 2009. Ethanol and a changing agricultural landscape. Economic Research Report 86. Washington, DC: Economic Research Service, U.S. Department of Agriculture.

McKenney, D.; Price, D.; Papadapol, P.; Siltanen, M.; Lawrence, K. 2006. High-resolution climate change scenarios for North America. Frontline Technical Note 107. Sault Ste. Marie, Ontario: Great Lakes Forestry Centre, Canadian Forestry Service.

McMahon, James E.; Price, Sarah K. 2011. Water and energy interactions. Annual Review of Environment and Resources 36: 163-191.

Moore, Michael R.; Crosswhite, William M.; Hostetler, John E. 1990. Agricultural Water Use in the United States, 1950-85. In: Carr, J. E.; Chase, E. B.; Paulson, R. W.; Moody, D. W., eds. National Water Summary 1987—Hydrologic Events and Water Supply and Use, 2350 ed. Washington, DC: U.S. Geological Survey: 93-108.

Mooty, Will S.; Jeffcoat, Hillary H. 1986. Inventory of interbasin transfers of water in the eastern United States. Open-File Report 86-148. Tuscaloosa, AL: U.S. Geological Survey.

Murray, C. Richard. 1968. Estimated use of water in the United States, 1965. Circular 556. Washington, DC: U.S. Geological Survey.

Murray, C. Richard; Reeves, E. Bodette. 1972. Estimated use of water in the United States in 1970. Circular 676. Washington, DC: U.S. Geological Survey.

Murray, C. Richard; Reeves, E. Bodette. 1977. Estimated use of water in the United States in 1975. Circular 765. Arlington, VA: U.S. Geological Survey.

Musial, W. 2008. Status of Wave and Tidal Power Technologies for the United States. Technical Report NREL/TP-500-43240: National Renewable Energy Lab.

Nakicenovic, Nebojsa; Alcamo, Joseph; Davis, Gerald; [and others]. 2000. Emissions Scenarios: A Special Report of Working Group III of the Intergovernmental Panel on Climate Change. Cambridge, UK: Cambridge University Press. Available: http://www.grida.no/climate/ipcc/emission/index.htm.

National Water Commission. 1973. Water policies for the future: final report to the Congress of the United States by the National Water Commission. Washington, DC: U.S. Government Printing Office.

NETL. 2008. Estimating freshwater needs to meet future thermoelectric generation requirements. DOE/NETL 400/2008/1339: National Energy Technology Laboratory, Department of Energy.

Pate, R.; Hightower, M.; Cameron, C.; Einfeld, W. 2007. Overview of energy-water interdependencies and the emerging energy demands on water resources. SAND 2007-1349C. Los Alamos, NM: Sandia National Laboratories.

Petsch, Harold E., Jr. 1985. Inventory of interbasin transfers of water in the western conterminous United States. Open-File Report 85-166. Lakewood, CO: U.S. Geological Survey.

Phillip, J. R. 1969. The theory of infiltration. In: Chow, V. T., ed. Advances in Hydroscience, Vol. 5. New York: Academic: 215-296.

Postel, Sandra L. 2000. Entering an era of water scarcity: the challenge ahead. Ecological applications 10(4): 941-948.

Price, David T.; McKenney, D. W.; Papadopol, P.; Logan, T.; Hutchinson, M. F. 2006. High-resolution climate change scenarios for North America. Frontline Technical Note 107. Sault Ste. Marie, ON: Canadian Forestry Service.

Rajagopalan, B.; Nowak, K.; Prairie, J.; [and others]. 2009. Water Supply Risk on the Colorado River: Can Management Mitigate? Water Resources Research 45.

Roy, Sujoy B.; Chen, Limin; Girvetz, Evan H.; [and others]. 2012. Projecting water withdrawal and supply for future decades in the U.S. under climate change scenarios. Environmental Science and Technology 46: 2545-2556.

Ruth, Matthias; Lin, Ai-Chen. 2006. Regional energy demand and adaptations to climate change: methodology and application to the state of Maryland, USA. Energy Policy 34(17): 2820-2833.

Sailor, D. J.; Pavlova, A. A. 2003. Air conditioning market saturation and long-term response of residential cooling energy demand to climate change. Energy 28(9): 941-951.

Sailor, David J. 2001. Relating residential and commercial sector electricity loads to climate--evaluating state level sensitivities and vulnerabilities. Energy 26(7): 645-657.

Sailor, David J.; Muñoz, J. Ricardo. 1997. Sensitivity of electricity and natural gas consumption to climate in the U.S.A.—methodology and results for eight states. Energy 22(10): 987-998.

Schefter, John E. 1990. Domestic water use in the United States, 1960-85. In Carr, Jerry E.; Chase, Edith B.; Paulson, Richard W.; Moody, David W., eds. National Water Summary 1987--Hydrologic Events and Water Supply and Use. Washington, DC: U.S. Geological Survey: 71-80.

Schneider, S.H.; Semenov, S.; Patwardhan, A.; [and others]. 2007. Assessing key vulnerabilities and the risk from climate change. In: Parry, M.L.; Canziani, O.F.; Palutikof, J.P.; Linden, P.J. van der; Hanson, C.E., eds. Climate change 2007: impacts, adaptation and vulnerability. Contribution of Working Group II to the Fourth Assessment Report of the Intergovernmental Panel on Climate Change. Cambridge, UK: Cambridge University Press: 779-810.

Schnoor, Jerald L.; Doering, Otto C., III; Entekhabi, Dara; [and others]. 2008. Water implications of biofuels production in the United States. Washington, DC: National Research Council. 76 p.

Scott, Michael J.; Dirks, James A.; Cort, Katherine A. 2008. The value of energy efficiency programs for US residential and commercial buildings in a warmer world. Mitigation and Adaptation Strategies for Global Change 13(4): 307-339.

Senate Select Committee on National Water Resources. 1961. Report of the Select Committee on National Water Resources pursuant to Senate Resolution 48, 86th Congress, together with supplemental and individual views. Senate Report 29: U.S. 87th Congress, 1st session. Washington, DC.

Shaffer, Kimberly H. 2009. Variations in withdrawal, return flow, and consumptive use of water in Ohio and Indiana, with selected data from Wisconsin, 1999-2004. Scientific Investigations Report 2009-5096. Reston, VA: U.S. Geological Survey.

Slack, J. R.; Landwehr, J. M. 1992. Hydro-climatic data network (HCDN): A U. S. Geological Survey streamflow data set for the United States for the study of climate variations, 1874-1988. Open-File Report 92-129: U.S. Geologic Survey.

Smith, Martin. 1992. CROPWAT: a computer program for irrigation planning and management. Irrigation and Drainage Paper 46. Rome, Italy: FAO.

Solley, Wayne B.; Chase, Edith B.; Mann, William B., IV. 1983. Estimated use of water in the United States in 1980. Circular 1001. Alexandria, VA: U.S. Geological Survey.

Solley, Wayne B.; Merk, Charles F.; Pierce, Robert R. 1988. Estimated use of water in the United States in 1985. Circular 1004. Denver, CO: U.S. Geological Survey.

Solley, Wayne B.; Pierce, Robert R.; Perlman, Howard A. 1993. Estimated use of water in the United States in 1990. Circular 1081. Denver, CO: U.S. Geological Survey.

Solley, Wayne B.; Pierce, Robert R.; Perlman, Howard A. 1998. Estimated use of water in the United States in 1995. Circular 1200. Denver, CO: U.S. Geological Survey.

Solomon, Susan; Plattner, Gian-Kasper; Knutti, Reto; Friedlingstein, Pierre. 2009. Irreversile climate change due to carbon dioxide emissions. Proceedings of the National Academy of Sciences 106(6): 1704-1709.

Tennant, Donald Leroy. 1976. Instream flow regimens for fish, wildlife, recreation and related environmental resources. Fisheries 1(4).

Tharme, R. E. 2003. A global perspective on environmental flow assessment: emerging trends in the development and application of environmental flwo methodologies for rivers. River Research and Applications 19(5-6): 397-441.

Torgerson, David. 2007. U.S. marcoeconomic projections to 2060. Washington, DC: Economic Research Service.

Tubiello, Francesco N.; Soussana, Jean-François; Howden, S. Mark. 2007. Crop and pasture response to climate change. PNAS 104(50): 19686-19690.

U.S. Army Corps of Engineers. 2009. National inventory of dams. Now available at: https://nid.usace.army.mil.

U.S. Bureau of Census. 2004. U.S. interim projections by age, sex, race, and Hispanic origin: 2000-2050. Available: http://www.census.gov/population/www.projections/usinterimproj/ [Released March 18, 2004].

USDA Forest Service. 2012. Future scenarios and assumptions: a technical document supporting the Forest Service 2010 RPA Assessment. Gen. Tech. Rep. RMRS-GTR-272. Fort Collins, CO: U.S. Department of Agriculture, Forest Service, Rocky Mountain Research Station. 34 p.

U.S. Department of Agriculture, Forest Service. 2012. Future of America's forest and rangelands: Forest Service 2010 Resources Planning Act assessment. Gen. Tech. Rep. WO-87. Washington, DC. 198 p.

U.S. Water Resources Council. 1968. The nation's water resources. Washington, DC: U.S. Government Printing Office.

U.S. Water Resources Council. 1978. The nation's water resources 1975-2000. Washington, DC: U.S. Government Printing Office.

Unsworth, Michael H.; Hogsett, William E. 1996. Combined effects of changing CO_2, temperature, UV-B radiation and O_3 on crop growth. In: Bazzaz, Fakhri; Sombroek, Wim, eds. Global climate change and agricultural production: direct and indirect effects of changing hydrological, pedological and plant physiological processes. Rome, Italy: Food and Agriculture Organization of the United Nations.

Van de Geijn, Siebe C.; Goudriaan, Jan. 1996. The effects of elevated CO_2 and temperature on transpiration and crop water use. In: Bazzaz, Fakhri; Sombroek, Wim, eds. Global climage change and agricultural production: direct and indirect effects of changing hydrological, pedological and plant physiological processes. Rome, Italy: Food and Agriculture Organization of the United Nations.

Vörösmarty, C. J.; Douglas, E. M.; Green, P. A.; Revenga, C. 2005. Geospatial indicators of emerging water stress: an application to Africa. Ambio 34(3).

Vörösmarty, C. J.; Green, P.; Salisbury, J.; Lammers, R.B. 2000. Global water resources: vulnerability from climate change and population growth. Science 289: 284-288.

Weib, M.; Alcamo, J. 2011. A systematic approach to assessing the sensitivity and vulnerability of water availability to climate change in Europe. Water Resources Research 47.

Wilmoth, J. R. 1998. The future of human longevity: a demographer's perspective. Science 280: 395-397.

Wollman, N.; Bonem, G. W. 1971. The outlook for water quality, quantity, and national growth. Baltimore, MD: John Hopkins University Press.

Woods&Poole Economics. 2007. Complete economic and demographic data source. Available: http://www.woodsandpoole.com/.

Wu, May; Mintz, Marianne; Wang, Michael; Arora, Salil. 2009. Water consumption in the production of ethanol and petroleum gasoline. Environmental Management 44(5): 981-997.

Zarnoch, Stanley J.; Cordell, H. Ken; Betz, Carter J.; Langner, Linda. 2008. Projecting county-level populations under three climate change future scenarios for the 2010 RPA Assessment. Athens, GA: Internet Research Information Series (IRIS). Available: http://warnell.forestry.uga.edu/nrrt/nsre/IrisReports.html.

Endnotes

[1] If one were to use our projections to predict what *will* happen, the viability of the projections would be quite good for the near term but would deteriorate the farther one looked into the future because any errors in our projections would likely become more serious the farther into the future one looked and because adaptation will gradually occur in response to rising shortages, altering future conditions.

[2] We made some minor changes in some of the Water Resource Council's ASRs, combining some and dividing others, in part to assure that the ASRs do not span WRR boundaries or divide the standard four-digit basins. The following changes were made: (1) a new ASR was created with the part of the Council's ASR 106 that was in WRR 2; (2) the new ASR 404 contains areas around eastern and southwestern Lake Michigan (in the Council's version, the eastern and southwestern portions were separate as ASRs 403 and 404); (3) the new ASR 1303 includes all of four-digit basin 1304 (in the Council's version, four-digit basin 1304 was split between ASRs 1303 and 1305); (4) the new ASR 1302 contains the upper and middle Rio Grande (the Council had the upper and middle Rio Grande as separate ASRs 1301 and 1302); and (5) the new ASR 1503 includes all of four-digit basin 1507 (in the Council's version, four-digit basin 1507 was split between ASRs 1502 and 1503). These changes reduced the number of ASRs from the 99 of the Water Resources Council to the current 98.

[3] Water treatment and subsequent reuse (also called recycling) is becoming a viable option for increasing supply without increasing withdrawals from the raw water source. Note that although reuse does not require new withdrawals, it does add to consumptive use. We do not account for water reuse in this assessment, and thus will overestimate total withdrawal to the extent that new demand is met with recycled water, but our estimates of consumptive use will remain viable because water reuse adds to consumptive use just as would a new withdrawal.

[4] The adjustment in T of the second step removed a large positive bias in estimated potential evapotranspiration. The magnitude of the bias was remarkably consistent across all scenario-GCM combinations, ranging from 1.52 mm/day for A1B-CSIRO to 1.95 mm/day for B2-CSIRO.

[5] The assumption that hydrologic fluxes are in equilibrium with the climate implies that in the long-term mean sense, mean carryover storage is zero. This does not preclude positive year-by-year carryover storage and does not imply that the climate is stationary.

[6] Restricting the test basin calibration data to years before 1995 was a matter of convenience as it allowed us to take advantage of our previous research (e.g., Hobbins and others 2001).

[7] For this calibration procedure, only the transpiration efficiency coefficient was assumed to be constant, not the vegetation coverage itself. Although changes in climate are assumed not to affect the maximum rate of plant transpiration, the actual vegetative coverage projected for future years may change in response to the changes in the climatic drivers.

[8] This decision was only reached after initially developing a procedure to infer changes in the storm statistics spatial field from the changes in the total monthly precipitation field. However, the accuracy of the projections of storm statistics was difficult to estimate, and we concluded that the potential gain in yield estimation would be offset by the further source of uncertainty that such estimation would introduce.

[9] A recent study by Lins and Slack (2005) concluded, based on streamflow data for years 1940-1999, that median daily streamflows have been increasing in parts of most eastern WRRs and also in the Missouri, Arkansas-White-Red, and Texas-Gulf WRRs. Because median annual flows may be decreasing even though median daily flows are increasing, this result is not directly relevant to the current study. Nevertheless, the findings raise questions about past flows that should be carefully addressed.

[10] Evaporation rates are kept constant for all simulations (they are not altered to reflect the impact of climate change on evaporation rates).

[11] Guldin's projections were produced as part of the U.S. Forest Service's periodic national Water Assessment. The agency's Water Assessment is one of several periodic assessments of demand and supply of renewable natural resources completed pursuant to the Renewable Resources Planning Act (RPA) of 1974, as mentioned in Chapter 1.

[12] For example, the year 2015 estimate is based on the year 2010 estimate and the year 2020 estimate is based on the 2015 estimate. An exception is that the prior period ($Y-5$) estimate for the first projected year (2010) was generally computed as an average of estimates from two prior years rather than just the value for year 2005. For example, the prior year estimate for estimating the year 2010 value for per-capita domestic and public withdrawal was a weighted mean of the estimates for years 2000 and 2005, with year 2005 receiving twice the weight of year 2000. This procedure was used to lessen the impact of potentially incorrect single-year estimates.

[13] Data from years before 1985 were not used in computing the growth rate because the USGS changed its water use data procedures beginning in 1985, resulting in some apparent discontinuities, and because, we assume, the USGS gradually improved its methodology over the years, making the more recent estimates more reliable. In addition, data from early estimates in the 1985-2005 record are not used to compute g if the trend in the early years appeared to be inconsistent with the trend of more recent years.

[14]An important limitation of the approach used here is that the USGS water withdrawal estimates were sometimes based on assumed relations with other, more easily measured variables, such as population or irrigated acres, rather than actual measures of water diversion or delivery. The degree of reliance on assumed relations of withdrawal to other variables varied by water use category, USGS state office, and year. Any such reliance compromises independent efforts using the USGS data to discover what factors affected water use. Thus, only to the extent that the assumed relations were accurately specified do the USGS data provide a basis for describing the relations of past use to factors affecting that use and for projecting future water use.

[15] The population of the full 50 states was 178 million in 1960, 282 million in 2000, and is projected for the A1B scenario to be 446 million in 2060.

[16] Our analysis of the year 2000 census tract data showed that assigning whole counties to ASRs results in estimates of ASR population that differ across the ASRs by a median of 7% from the area-weighted census-tract-based assignment we employed.

[17] $\rho_{ASR,j}$ is a 98 (for ASRs) by 3114 (for counties) matrix. $z_{j,Y}$ is a 3114 (for counties) by 16 (for years 1985-2060 in five-year intervals) matrix.

[18] The area weighting procedure for allocating year 2000 population of census tracts that spanned ASR boundaries was accomplished using $\rho_{ASR,j}$, a 98 (for ASRs) by 3114 (for counties) matrix.

[19] The per-capita electricity production rates reported by the USGS are lower than those reported by the Energy Information Administration (EIA) in their Annual Energy Outlook reports. For example, the 2005 EIA per-capita electricity production rate was about 13,500 kWh per person per year, nearly 15% higher than the 11,792 estimate reported here based on the USGS data. This difference reflects the lower thermal generation reported by the USGS. In recent years, the USGS has not been including plants using water from public supplies, nor some small plants using groundwater (Susan Hutson, personal communication; USGS 2009). These latter plants, called merchant plants, tend to be privately held gas or oil turbine plants used for peaking power, many of which have been built in the past 10-15 years. The merchant plants are recirculating plants, and thus do not add greatly to total withdrawals.

[20] It is common to compute energy efficiencies in terms of economic units (e.g., GDP) rather than population units (Le Pen and Sévi 2010). We use population rather than economic units because population is assumed to be more accurately measured and projected than GDP.

[21] EIA measures of total electricity generation per capita show a significant drop for the years 2007 to 2009. The EIA projection (EIA 2010) shows a partial recovery from this drop from 2010 to 2012 followed by a gradual increase from 2013 to 2035 at an average annual growth rate of 0.10%.

[22] The EIA projection ignores the potential for hydrokinetic energy. According to Bedard and others (2009), there is substantial potential for producing electricity using hydrokinetic energy in the United States. Although most of the potential is in Alaska, there is potential in the coterminous United States for wave and tidal energy along the West Coast and along the north Atlantic, for ocean current energy in Florida, and for river kinetic energy in some major rivers including the Columbia and Mississippi. Conservatively, the total potential that could be developed in the coterminous Untied States may exceed 84 GWh of capacity, or about 2% of projected total consumption for 2030. We follow the EIA's lead in ignoring this potential.

[23] See the EIA report (EIA 2010) for the breakdown of this total among wind, solar, and the other sources of renewable electric energy.

[24] The methods for projecting fresh thermoelectric withdrawals are more complicated than those for the other water uses. A more thorough explanation is found in Appendix A. It should be noted, however, that to accurately project future development of thermoelectric production, the methodology would need to be considerably more robust, employing detailed models of the energy sector and extensive knowledge of industry growth plans.

[25] The separation of the coterminous United States into these two divisions fairly accurately describes trends in irrigated area but may mask localized trends that run counter to the division-level trends.

[26] Agriculture accounts for the bulk of irrigated acres, but self-supplied irrigation of parks, golf courses, and similar landscapes are also included in this category, further complicating the picture.

[27] The unusual drop from 1980 to 1985 in IC, TF, and IR water uses was due partly to (1) above average rainfall in 1985, which lessened the need for irrigation withdrawals, (2) an economic slowdown and reduction in commodity prices, (3) higher ground water pumping costs as lifts had continued to increase, and (4) improved efficiency in water use (Solley and others 1988). However, the drop was also partially attributable to the improved process for amassing the water use data that was initiated by the USGS for the 1985 report, indicating that earlier estimates may be too high (Brown 1999; Solley and others 1988).

[28] The sharp drop in water withdrawal rate from 1980 to 1985 shown in Figure 5.6 and Table 5.5 is partly attributable to the USGS move of "animal specialties" (aquaculture) from the industrial and commercial category to the livestock water use category beginning in 1985. About 2.3 of the 13-bgd drop in total withdrawal from 1980 to 1985 in the coterminous United States was attributable to this change of categories.

[29] Dry cooling (air cooled) systems also exist but are less efficient and make up less than 1% of the thermoelectric generation capacity.

[30] Recent reports (Macknick and others 2011; McMahon and Price 2011) list withdrawal and consumptive use rates for different types of thermoelectric plants. Their estimates are roughly consistent with those established here for regions of the United States. Focusing on consumptive use, Macknick and others reported rates for steam plants, in gallons per kWh, ranging from 0.064-0.4 for once-through plants and from 0.46-2.6 for recirculating plants. Similar rates for combined-cycle plants range from 0.02-0.1 for once-through plants and from 0.13-0.44 for recirculating plants (see also Cooley and others 2011). We estimate consumptive use for the East and West in 2005, based largely on the USGS data, to average 0.48 and 0.55 gal/kWh, respectively. A lower rate would be expected in the East because once-through plants are more common there than in the West (Averyt and others 2011: Figure 3).

[31] In the East, the projected average withdrawal rate drops slightly over time (Table 5.6) despite the lack of change in projected withdrawal rates of the individual WRRs (Table 5.8) because of changes over time in the irrigated areas of the WRRs.

[32] The much different rates in 2005, compared with 1990, reflect differences in the species that are produced and the water management methods used. Trout, for example, need a relatively high dissolved oxygen level and often are raised in raceways, which rely on continual freshwater inputs, as opposed to most warm water fishes, which are commonly grown in ponds with a much lower refresh rate. Note that very little of the water diverted to raceways is consumptively used.

[33] Another recent energy development is the use of hydraulic fracturing in natural gas production. The use of fracturing has greatly increased in the past few year, but considerable uncertainty remains about the full potential of such fracturing (EIA 2010). Amounts of water used per BTU of energy produced tend to be small compared to amounts used in producing most other petroleum-based fuels. We did not attempt to separately estimate water use in hydraulic fracturing for natural gas production and cannot determine the extent to which the expected surge in hydraulic fracturing will result in water use levels exceeding those projected for industrial and commercial water use.

[34] A final minor category, not included here, includes "other blending components, other hydrocarbons, and ethers" (EIA 2010: Table 11).

[35] "Oil shale" is an inaccurate term. The deposits are of kerogen, which can be converted into liquid and gaseous hydrocarbons, including petroleum, and the rock where the kerogen is found is not necessarily shale.

[36] http://www.eia.doe.gov/oiaf/aeo/otheranalysis/aeo_2009analysispapers/oesp.html.

[37] Although not included in EIA's Table 11 on liquid fuel supply, oil shale is included along with other unconventional liquid fuels in an estimate of future unconventional production in Table 21 of the EIA report.

[38] This definition of effective precipitation is different from a commonly used understanding of effective precipitation as the portion of precipitation that produces runoff.

[39] The CO_2 levels with the three scenarios at issue are projected to vary in 2060 from 504 ppm (B2) to 580 ppm (A2), similar to the levels used in the FACE experiments (Table 2.1).

[40] Crop yield increases have been in the range of 10 to 20% for C_3 plants and 0 to 10% for C_4 plants (Tubiello and others 2007). However, accompanying increases in temperature may cause yield decreases, principally because the shortening of the crop life cycle that occurs with temperature increases can lower seed production (Allen and others 1996). These yield decreases perhaps can be avoided by altering planting dates or using improved cultivars.

[41] The importance of temperature is indicated by the fact that the reduction in transpiration per unit leaf area with increased CO_2 has been found to lead to increases in canopy temperature (Kimball and Bernacchi 2006; Leakey 2009), and this plant feedback effect on leaf temperature is thought to have a small negative effect on WUE (Leakey 2009).

[42] The ambient CO_2 concentration when the FACE experiments were performed ranged from about 350 to 375 ppm, depending on when the experiment occurred.

[43] One possibility we are not considering here is that the increase in temperature will lengthen the available growing season and allow some areas to move from a single crop per year to two crops. Such double-cropping would of course roughly double the irrigation water use per unit area. On the other hand, warming is likely to shorten the life cycle of annual plants, consequently shortening the time during which irrigation is needed. Determining the location and extent of the effects, and the extent to which one negates the other in terms of irrigation needs, is beyond the scope of this study.

[44] Grass, which if irrigated probably requires more irrigation than all other landscaping plant groups combined, is typically grown to the desired lushness. Under careful management, if biomass production increased under elevated CO_2, which is likely for cool season (C_4) grasses, irrigation per time period could be cut back. However, an extension of the growing period with temperature rises would increase water use, partially or totally negating any water savings resulting from the CO_2 rise.

[45] This approach is not ideal because it relies on applying a relationship developed across WRRs for a given year to future changes in each WRR (i.e., it relies on spatial variation across WRRs in a given year to estimate temporal effects within a given WRR). Future efforts should search for a way to develop individual relations for each WRR.

[46] η^{ETp} was estimated using annual data rather than growing season data for purely practical reasons; using annual data produced a much more significant relation. Understanding why the relation was best modeled with annual data is left for future study.

[47] In this study, minor energy-related water uses are included in the industrial water use category.

[48] Overall energy use in the United States may decrease as the temperature increases (Scott and others 2008), but electricity use will increase because cooling relies almost entirely on electricity, whereas heating generally relies on other energy sources (mainly natural gas and heating oil). According to the U.S. Department of Energy, in the residential sector, electricity accounts for 7%, 22%, and 100% of the energy used in space heating, water heating, and cooling/lighting, respectively (the corresponding figures for commercial buildings are 9%, 18%, and 100%) (Scott and others 2008: Table 5).

[49] Thermoelectric plants provide the bulk of U.S. electricity production, and also take up the slack when energy from other sources is not available.

[50] Hydroelectricity is typically used for heating in the State of Washington. Because ambient warming lowers heating needs and summer temperatures in Washington are not excessive, the electricity savings in winter are expected to exceed the additional electricity need in summer as temperatures increase (Sailor 2001). Note, however, that although the bulk of electricity used in Washington is from hydroelectric plants, marginal effects may affect thermoelectric plants.

[51] Studies of particular locations (Amato and others 2005; Franco and Sanstad 2008; Ruth and Lin 2006) provide interesting insights about local or regional conditions but may not be useful for large-scale analyses because they employ differing methodologies or omit information that would allow their results to be integrated with those from studies of other locations.

[52] Data for one of the eight states, Louisiana, were not used because the information appeared to be an outlier.

[53] We use annual temperature rather than warm season temperature because Sailor's analysis used annual temperature.

[54] Sailor and Pavlova (2003) provided estimates for a uniform 20% increase in cooling degree days, which they reported corresponds roughly to a 1 °C increase in temperature. We assume that the long-term effect they estimate applies to successive temperature increases.

[55] A more accurate procedure would be to estimate the change in CDD with a given change in temperature on a distributed spatial basis, and then use the changes in CDD to estimate change in market saturation using a relationship provided by Sailor and Pavlova (2003) that captures the nonlinear relation between CDD and saturation. This extension is left for a future revision of our analysis.

[56] EIA data indicate that space conditioning utilizes 58%, 40%, and 6% of residential, commercial, and industrial energy consumption, respectively (Amato and others 2005)—suggesting that energy use in the industrial sector is not very sensitive to temperature changes. Sailor and Munoz (1997) concluded that industrial uses are not sensitive to temperature, and Elkhafif (1996) found some sensitivity in the industrial sector but much less than in the commercial and residential sectors.

[57] The USGS did not estimate consumptive use in 2000 or 2005. Estimating consumptive use is more challenging than estimating withdrawal, especially at large spatial scales. The estimates of consumptive use proportions presented here are tenuous. Research is needed to improve the estimation of consumptive use proportions that can be used with confidence with the USGS water withdrawal estimates.

[58] In some cases, the 1995 estimate was weighted more heavily than the 1990 estimate.

[59] This relation is also seen in the correlation between γ^{IR} and the proportion of all irrigated acres that use flood irrigation as opposed to sprinkler or micro irrigation, which is -0.63 for the average for 1990 and 1995. Consumptive use is higher when more efficient technologies are used.

[60] Brown (2000) projected total withdrawals in the United States to reach 364 bgd in 2040 compared to our projection for 2040 of 337 bgd. The current projection is lower than the earlier projection largely because of water savings at thermoelectric plants. These savings result from expected increases in power produced at other (non-hydro) renewable (e.g., wind, solar, and geothermal) plants—increases that were not considered likely at the end of the 1990s.

[61] If withdrawals decrease while the number of water demand units (U) remains constant or if withdrawals remain constant while U increases, the efficiency of withdrawals (Φ) is improving, which generally implies that the consumptive use proportion (γ) is rising. For example, irrigation withdrawals can decrease although irrigated area remains constant by shifting from flood to sprinkler irrigation, which lowers withdrawal by increasing the proportion of withdrawal that is used by the crops. However, not all withdrawal decreases result from increasing γ. For example, if homeowners convert their lawns to rock gardens, they will use less water outdoors, which will lower both withdrawal and consumptive use.

[62] The estimates of water use at five-year intervals for 2010 to 2090 in these and subsequent figures each reflect five-year averages of the relevant climatic variables. For example, the value for 2060 reflects averages computed over the years 2058 to 2062.

[63] The sharp drop in percent change in consumptive use shown in Figure 5.29 that occurs in 2035 (and to a lesser extent in 2030) occurs because of decreases in T and increases in P in some WRRs, most notably 7, 8, 10, 11, and 12. The effect is greatest in IR withdrawals, which are the most sensitive to changes in T and P.

[64] The exceptions in the East, WRRs 8 and 9, occur partly because TF is relatively unimportant and IR is relatively important in these two WRRs in comparison with the East as a whole (TF accounts for 31% and 21% of 2005 withdrawals in WRRs 8 and 9, and IR accounts for 47% and 27% of withdrawals, respectively). Additionally, precipitation and temperature changes in WRRs 8 and 9 are relatively large for some GCMs.

[65] Unlike P, which is an exogenous input each year, S is an endogenous quantity because it depends on storage and delivery decisions made in response to the priorities determining water allocation within a network. S of an ASR potentially is affected by water stored in that ASR the previous year. And if the ASR is part of a multi-ASR network, S of the ASR potentially also is affected by water previously stored in reservoirs of upstream ASRs. Thus, S can only be obtained as an output of the water routing model. The estimates of S used here follow the specification in equation 6.2, with I to a given downstream ASR in a given year including not only all inflows from upstream (which may include releases from upstream reservoirs) but also releases from reservoirs within the given ASR. Note also that S includes the water that must be used to satisfy the required in-stream flow release from the ASR.

[66] The Gauss error function is also known as the probability integral.

[67] Initially, we implemented an alternative approach to measuring vulnerability that involved creating alternative synthetic traces of water yield and demand. We used a multivariate AR(1) model to generate the synthetic traces based on the statistical properties of the original estimates of precipitation, temperature, potential evapotranspiration, and related water yield. Simulations using those traces provided alternative, statistically identical versions of past and future supply and demand. Combining the supply and demand results of four synthetic traces with those of the original trace provided a total of 100 years of results for each 20-year period of interest. This relatively cumbersome approach provided estimates of vulnerability very similar to those obtained using the approach described here.

[68] Taking into account both effects simultaneously, one may also quantify vulnerability as a function of the ratio of the mean surplus to the corresponding standard deviation, $\beta = \mu_z/\sigma_z$, referred to as the reliability index. The reliability index quantifies in units of the standard deviation how far from shortage a given ASR is.

[69]Recent studies of the Lower Colorado River Basin allow a rough comparison with our results. Rajagopalan and others (2009: alternative A) estimated the probability of depleted reservoirs in about 2060 to be close to 0.5 assuming a 20% reduction in flow, which is roughly equivalent to our water yield estimate. And using somewhat different methods, Barnett and Pierce (2008) estimated a probability of nearly 1.0 for the same future year and percentage reduction in flow. Our estimates of shortage fall between these two prior estimates. For the 2060 period, and averaging across the three GCMs for a given scenario and the three ASRs in the Basin (ASRs 1501, 1502, and 1503), we estimate the probability of shortage occurring in the Lower Colorado River Basin to be 0.61, 0.86, and 0.69 for the A1B, A2, and B2 scenarios, respectively.

[70] Among the 71 ASRs for which one scenario-GCM combination clearly yielded a higher level of vulnerability than for other combinations, the highest level of vulnerability occurred with the A2 scenario in 44 ASRs, with the A1B scenario in 23 ASRs, and with the B2 scenario in four ASRs. Among climate models, the highest level of vulnerability occurred with the CGC model in five ASRs, with the CSIRO model in 40 ASRs, with the MIROC model in 24 ASRs, and with the Hadley model in two ASRs.

[71] The graphs in Figure 6.15 show average storage levels from five alternative simulations, each based on a separate water yield trace that reflects the same basic GCM input (see footnote 67).

United States Department of Agriculture

Forest Service

Rocky Mountain Research Station

General Technical Report RMRS-GTR-295

November 2012